Journal of Shellfish Research, Vol. 37, No. 2, 247–448, 2018.

SCANNING ELECTRON MICROSCOPIC AIDS FOR IDENTIFICATION OF LARVAL AND POST-LARVAL BIVALVES

RICHARD A. LUTZ,[1]* JACOB D. GOODWIN,[1] BRAD S. BALDWIN,[2] GAVIN BURNELL,[3] MICHAEL CASTAGNA,[4] SAMUEL CHAPMAN,[5] AL CHESTNUT,[6] PATRICK DABINETT,[7] CHRIS DAVIS,[5] ARNOLD G. EVERSOLE,[8] S. CYNTHIA FULLER,[1] SCOTT M. GALLAGER,[9] RONALD GOLDBERG,[10] JOY GOODSELL,[1] JUDITH GRASSLE,[1] RICHARD G. GUSTAFSON,[11] HERBERT HIDU,[5] YA-PING HU,[1] DAVID JABLONSKI,[12] SHANNON JOHNSON,[13] VICTOR S. KENNEDY,[14] MARCEL LE PENNEC,[15] ROGER MANN,[16] CARTER NEWELL,[5] ALAN S. POOLEY,[1] ANTONIETO S. TAN,[1] ROBERT C. VRIJENHOEK[13] AND A. PARTRIDGE[17]

[1]*Department of Marine and Coastal Sciences, Rutgers University, 71 Dudley Road, New Brunswick, NJ 08901;* [2]*Department of Biology, 23 Romoda Drive, St. Lawrence University, Canton, NY 13617;* [3]*School of Biological, Earth and Environmental Sciences, University College Cork, North Mall Campus, Distillery Fields, Cork, Ireland T23 N73K;* [4]*Virginia Institute of Marine Science, College of William and Mary, 40 Atlantic Avenue, Wachapreague, VA 23480;* [5]*Ira C. Darling Center, University of Maine, 193 Clarks Cove Road, Walpole, ME 04573;* [6]*Department of Biology, Belhaven College, 1701 N. State Street, Jackson, MS 39202;* [7]*Marine Sciences Research Laboratory, Memorial University of Newfoundland, 230 Elizaabeth Avenue, St. John's, NF A1C 5S7, Canada;* [8]*Department of Aquaculture, Fisheries and Wildlife, 261 Lehotsky Hall, Clemson University, Clemson, SC 29634;* [9]*Woods Hole Oceanographic Institution, 266 Woods Hole Road, Woods Hole, MA 02543;* [10]*Northeast Fisheries Center, National Marine Fisheries Service, Milford Laboratory, 212 Rogers Avenue, Milford, CT 06460;* [11]*Northwest Fisheries Science Center, National Marine Fisheries Service, National Oceanic and Atmospheric Administration, 2725 Montlake Blvd. E., Seattle, WA 98112;* [12]*Department of Geophysical Sciences, University of Chicago, 5734 S. Ellis Ave., Chicago, IL 60637;* [13]*Monterey Bay Aquarium Research Institute, 7700 Sandholdt Road, Moss Landing, CA 95039;* [14]*Chesapeake Biological Laboratory, University of Maryland Center for Environmental Science, 146 Williams Street, Solomons, MD 20688;* [15]*Laboratoire des Sciences de l'Environnement Marin (LEMAR), Institut Universitaire Européen de la Mer, Place Nicolas Copernic, Plouzané 29280, France;* [16]*Virginia Institute of Marine Science, College of William and Mary, 1375 Greate Road, Gloucester Point, VA 23062;* [17]*in a pear tree*

ABSTRACT The identification of bivalve larvae and early postlarvae in plankton and benthic samples has long been a challenge, hampering both basic and applied research efforts in marine, estuarine, and freshwater environments. The usefulness of published optical micrographs of the early life-history stages of bivalves is limited because of the great morphological similarity of the imaged articulated shells, particularly at the early (straight-hinge) developmental stages. While a number of techniques have been refined in recent years and show promise for use in routine identifications of larval and post-larval bivalves (e.g., single-step nested multiplex polymerase chain reaction; *in situ* hybridization protocols through color coding with taxon-specific, dye-labeled DNA probes; coupled fluorescence *in situ* hybridization and cell sorting; and image analysis techniques using species-specific shell birefringence patterns under polarized light), no adequate comprehensive reference source exists that accurately depicts the morphology and morphometry of the shells of larval and post-larval stages of target bivalve species in a consistent format to assist in identification of such stages. To this end, scanning electron micrograph (SEM) sequences are presented of the disarticulated shell valves of laboratory-reared larval and post-larval stages of 56 species of bivalve molluscs from a wide spectrum of marine, estuarine, and freshwater habitats. Emphasis is placed on the usefulness of the morphology and morphometrics of consistently-oriented, disarticulated shell valves and associated hinge structures in discriminating the early life-history stages of these various bivalve species. Although the scanning electron micrograph sequences presented accurately depict the gross morphologies/morphometrics and hinge structures of the disarticulated shell valves of the larvae and/or postlarvae of the 56 species of bivalves, it is important to emphasize that a scanning electron microscope is not necessary to observe even fine hinge structures associated with the early ontogenetic stages of these species. Such structures are readily visible using a wide range of optical compound microscopes equipped with high-intensity reflected light sources, although the disarticulated shell valves must be viewed in several planes of focus to discern the often subtle details seen clearly in the scanning electron micrographs. These morphological characters provide researchers with invaluable aids for the routine identification of the early life-history stages of these species isolated from plankton and benthic samples.

KEY WORDS: bivalve, larvae, postlarvae, identification, scanning electron microscopy

*Corresponding author. E-mail: rlutz@marine.rutgers.edu
DOI: 10.2983/035.037.0202

Downloaded From: https://bioone.org/journals/Journal-of-Shellfish-Research on 25 Feb 2020
Terms of Use: https://bioone.org/terms-of-use Access provided by IFREMER

INTRODUCTION

The identification of bivalve larvae and early postlarvae has been important for many ecological research efforts in marine, estuarine, and freshwater environments for over a century (Stafford 1912, Odhner 1914, Lebour 1938, Werner 1939, Jørgensen 1946, Sullivan 1948, Rees 1950, Miyazaki 1962, Loosanoff & Davis 1963, Newell & Newell 1963, Loosanoff et al. 1966, Le Pennec & Lucas 1970, Chanley & Andrews 1971, de Schweinitz & Lutz 1976, Lutz & Jablonski 1978a, 1978b, 1979, 1981, Jablonski & Lutz 1980, Le Pennec 1980, Lutz et al. 1982a, 1982b, Lutz 1988, 2012, Fuller & Lutz 1989, Kennedy et al. 1989, 1991, Goodsell et al. 1992, Hu et al. 1992, 1993, Lutz & Kennish 1992, Baldwin et al. 1994, Hare et al. 2000, Garland & Zimmer 2002, Tiwari & Gallager 2003a, 2003b, Hendriks et al. 2005, Larsen et al. 2005, 2007, Wang et al. 2006, North et al. 2008, Henzler et al. 2010, Thompson et al. 2012a, 2012b, Malchus & Sartori 2013, Goodwin et al. 2014, 2016a, 2016b). As Hendriks et al. (2005) emphasized, ''Despite the importance of the planktonic larval stage in intertidal bivalves, our understanding of this stage is still insufficient. A major obstacle in the quantification of planktonic larval distributions is the identification of sampled larvae.''

In early efforts to assist with the identification of larval bivalves isolated from plankton samples, Chanley and Andrews (1971) published a key to the larval stages of a number of bivalve species along the east coast of North America based on optical micrographic sequences of articulated shells of laboratory-cultured larval specimens; however, the usefulness of this key is limited because of the great morphological similarity of the imaged articulated shells, particularly at the early (straight-hinge) developmental stages. Although a number of techniques have been refined in recent years and show promise for use in routine identifications of larval and post-larval bivalves (e.g., single-step nested multiplex polymerase chain reaction; *in situ* hybridization protocols through color coding with taxon-specific, dye-labeled DNA probes; coupled fluorescence *in situ* hybridization and cell sorting; and image analysis techniques using species-specific shell birefringence patterns under polarized light; Larsen et al. 2005, 2007, Henzler et al. 2010, Thompson et al. 2012a, 2012b, Goodwin et al. 2014, 2016a, 2016b, 2018), no adequate comprehensive reference source exists that accurately depicts the morphology and morphometry of the shells of larval and post-larval stages of target bivalve species in a consistent format to assist in identification of such stages.

With the aforementioned as background, in this monograph scanning electron micrograph (SEM) sequences of the disarticulated shell valves of laboratory-reared larval and post-larval stages of 56 species of bivalve molluscs from a wide spectrum of aquatic habitats are presented (Table 1). Emphasis is placed on the usefulness of the morphology and morphometrics of consistently-oriented, disarticulated shell valves and associated hinge structures in discriminating the early life-history stages of these species. Most of these species are from environments along the east coast of North America and include most of the commercially important species in this region.

Taxonomic nomenclature was assigned according to the latest ''accepted name'' (or acceptable ''alternate representation'') and associated classification hierarchy in the World Register of Marine Species (www.marinespecies.org).

Over the years, various workers have used both optical and scanning electron microscopy to describe in detail the larval and/or post-larval hinge structures of a number of bivalves and have suggested that such structures may be diagnostic at the generic, or even specific, level (Chanley 1965, 1969, Turner & Johnson 1970, Pascual 1971, 1972, Scheltema 1971, Le Pennec 1973, 1978, 1980, LaBarbera 1975, Boyle & Turner 1976, Culliney & Turner 1976, Dinamani 1976, Le Pennec & Masson 1976, Booth 1977, 1979a, 1979b, Siddall 1977, 1978, Lutz & Jablonski 1978a, 1978b, 1981, Carriker & Palmer 1979, Lutz & Hidu 1979, Chanley & Dinamani 1980, Jablonski & Lutz 1980, Lutz et al. 1982a, 1982b, Redfearn 1982, 1987, Jablonski & Lutz 1983, Ramorino & Campos 1983, Redfearn et al. 1986, Tremblay et al. 1987, Fuller & Lutz 1989, Fuller et al. 1989a, Kennedy et al. 1989, 1991, Hu et al. 1993, Paugam et al. 2006, Wassnig & Southgate 2012). Despite these efforts, much of the morphologic and morphometric data obtained over the years has not been presented in an adequate or sufficiently consistent format to permit unambiguous identification of early life-history stages of bivalves at various taxonomic levels. In recognition of this shortcoming, the SEM sequences of the larval and post-larval stages of a number of the species depicted in this monograph that have been previously published in various journals are presented here in a consistent format, together with other pertinent details related to procurement, preparation, and descriptions of the specimens comprising these sequences (Lutz et al. 1982b, Fuller & Lutz 1989, Fuller et al. 1989b, Kennedy et al. 1989, 1991, Goodsell et al. 1992, Gustafson & Lutz 1992, Hu et al. 1993, Tan et al. 1993). These sequences and pertinent details are included herein, together with a large number of unpublished sequences and associated pertinent details of most of the species in Table 1. The goal is to present a coherent compilation of all 56 species in one single publication to assist in the discrimination of larval and post-larval stages of these species isolated from a variety of aquatic environments.

MATERIALS AND METHODS

Sexually mature adults of 56 species of bivalves were obtained from the sources indicated in Table 1. These adults were induced to spawn (or larvae/juveniles were obtained from spontaneous spawning/release events in the case of certain species with nonplanktotrophic modes of development) using a variety of protocols described by various workers (Loosanoff & Davis 1963, Morse et al. 1977, Lutz et al. 1982a, 1982b, Gibbons & Castagna 1984, Fuller & Lutz 1989, Fuller et al. 1989a, Kennedy et al. 1991, Gustafson & Lutz 1992). The larvae and postlarvae of most of these species were reared using standard hatchery techniques (e.g., techniques described by Loosanoff & Davis 1963, Turner & Johnson 1970, Chanley & Andrews 1971, Castagna 1975, Castagna & Kraeuter 1977). Further specific details concerning the culture of the larvae and postlarvae of a number of these species may be found in Lutz et al. (1982b), Fuller and Lutz (1989), Fuller et al. (1989a), Kennedy et al. (1989), (1991), Goodsell et al. (1992), Gustafson and Lutz (1992), Hu et al. (1993), and Tan et al. (1993).

Cultured larval and post-larval specimens were sampled at frequent intervals (frequency dependent on the growth of organisms since the previous sampling period) and placed in distilled water for 30 min (Calloway & Turner 1979). Immediately

Downloaded From: https://bioone.org/journals/Journal-of-Shellfish-Research on 25 Feb 2020
Terms of Use: https://bioone.org/terms-of-use Access provided by IFREMER

following this treatment, specimens were preserved in 95% ethanol. After various lengths of time (up to 2 months), specimens were removed from the ethanol, rinsed in distilled water, and immersed in a 5% solution of sodium hypochlorite (Rees 1950) for approximately 10 min to facilitate separation of shell valves and removal of soft tissue. After rinsing in distilled water, disarticulated valves were mounted on copper or silver tape (or double-sided sticky tape), coated (under vacuum) with approximately 400 Å of gold–palladium or a combination of gold and carbon, and examined under an ETEC Autoscan scanning electron microscope [or, in the case of *Ostrea stentina* (= *Ostrea equestris*), *Solemya velum* and *Mercenaria campechiensis* specimens, under Hitachi S-540 and JEOL 848 scanning electron microscopes].

Procedures used for accurate documentation of shapes and dimensions of the larval and post-larval shells using scanning electron microscopy were those of Fuller et al. (1989b) and are outlined below.

Before imaging individual larval or post-larval specimens under the scanning electron microscope, great care was taken to adjust the microscope so that *x* and *y* dimensions were equal on a calibration sphere that was approximately the same size as the specimen being photographed. In turn, these adjustments were made at a magnification close to that at which the specimen was to be photographed. The calibration spheres were sand-blasting beads that were selected for roundness by comparing measurements of the diameter on electron micrographs taken at rotations of 0, 45, and 90 degrees (see Fuller et al. 1989b for further details).

The method used for consistent orientation of the disarticulated shell valves, in which each larval or post-larval valve is positioned with points of the hinge and shell margin aligned in a plane normal to the axis of the electron optical system, is described by Fuller et al. (1989b, p. 59) as follows. "Specifically, a disarticulated valve with the interior shell surface visible on the microscope screen is rotated until the anterior and posterior margins are at equal working distances. A digital voltmeter (monitoring the reference voltage of the lens control) is used to measure carefully the differences in working distance when opposite margins of the shell are successively focused at 30,000×. A difference of 1 mV on the meter is equal to a change in working distance of about 0.34 μm. Subsequently, the specimen is tilted perpendicularly to the first axis until the dorsal and ventral margins of the valve also are at the same working distances. A photomicrograph of the shell in this position documents its characteristic shape."

It should be noted that it was necessary to modify the aforementioned procedure to obtain consistent orientations for later post-larval stages of a number of species because of the irregular contours of the shell margins of these stages. In the case of post-larval *Teredo navalis*, for example, orienting the specimens in a manner similar to that described previously was impossible because points along the post-larval shell margin do not lie in a single plane. As articulated by Fuller et al. (1989a, p. 25) concerning *T. navalis*: Throughout the post-larval developmental period, however, points along the dorsoventral margin of the anterior slope (except those at the extreme ventral region) comprise a plane. Thus, consistent orientation of post-larval shells was achieved by positioning specimens such that this plane was perpendicular (Fuller et al.1989a mistakenly indicated "parallel") to the electron optical axis. Additional adjustments were made so that dorsal and ventral condyles were at an equal working distance. Similar adjustments were also used to obtain consistent orientations of post-larval specimens of *Bankia gouldi* (Tan et al. 1993).

The dimensions of the larval and post-larval shells were determined by positioning a flat 400-mesh copper transmission electron microscope grid (on the same specimen mount, near the shell valve) normal to the electron optical axis and photographing this grid at the identical magnification at which the shell valve was photographed. Measurements of the shell dimensions are based on the 63.5-μm grid spacings of the 400-mesh grid, rather than on magnification or scale bar displays on the microscope screen (for further details, see Fuller et al. 1989b).

The numbers depicted above each of the micrographs in Figures 1–195 indicate the maximum linear distance in micrometers measured along any axis of the shell, with a few exceptions. In most cases, this maximum distance represents "shell length" as defined by numerous authors (Fuller & Lutz 1989, Kennedy et al. 1989, 1991, Goodsell et al. 1992, Gustafson & Lutz 1992, Hu et al. 1993), although in the case of the larval stages of certain pholads and teredinids [e.g., *Bankia gouldi* (Tan et al. 1993) (Figs. 69 and 70) and *Teredo navalis* (Fuller et al. 1989a) (Figs. 73 and 74)], this maximum distance represents "shell height." Shell nomenclature of the teredinids is taken from Turner (1966, 1971). The numbers depicted above the larval stages of *Crassostrea gigas*, *Crassostrea virginica*, *Ostrea edulis*, and *Ostrea stentina* (= *Ostrea equestris*) (Figs. 105–123) represent the maximum anteroposterior dimension ("shell length", which in some larval stages of these species is less than or equal to "shell height"; see Hu et al. 1993).

We use the term "provinculum" in the sense of Bernard (1898) and Rees (1950). Provinculum length represents the linear distance between the lateral extremes of the hinge apparatus in larval and early post-larval shells (see Bayne 1976, p. 87, for a diagrammatic illustration of this dimension).

RESULTS AND DISCUSSION

An inability to identify bivalve larvae and postlarvae within planktonic and benthic samples has long hampered both applied and basic research efforts in marine, estuarine, and freshwater environments (Hu et al. 1992). For example, assessing the impact of natural or anthropogenic disturbances (e.g., chemical pollutants, thermal discharges, oil spills, dredge spoil dumping, ocean acidification, discharges of ships' ballast water containing entrained meroplanktonic organisms) on marine ecosystems; predicting recruitment for fisheries management; optimizing the timing of substrate placement for aquaculture; assessing the impact of fluctuations in climatic conditions; and conducting basic environmental surveys all depend on identifying the temporal and spatial abundance of meroplanktonic and/or early post-larval stages of various species. Along these lines, the discovery of planktonic stages of a myriad of invertebrate organisms within the ballast waters of ships traveling between countries has led to concerns regarding potentially severe and irreversible biological conservation impacts of the introduction of invasive aquatic species via the discharge of such ballast waters in areas where the entrained species are not indigenous (Cohen & Carlton 1998, Carlton 1999, Ruiz et al. 2000, Gollasch 2002, Murphy et al. 2002). As Hayes and Hewitt (1998) point out: "The assessment of risk associated with ballast

Downloaded From: https://bioone.org/journals/Journal-of-Shellfish-Research on 25 Feb 2020
Terms of Use: https://bioone.org/terms-of-use Access provided by IFREMER

water discharge depends on reliable knowledge of the identity, viability and quantity of its inhabitants.'' Hence, while this monograph consists predominantly of species from environments along the east coast of North America, a number of bivalve species (e.g., *Arca noae*, *Pecten maximus*, and *Ruditapes philippinarum*) that various individuals collected from waters in the eastern Atlantic and cultured under controlled laboratory conditions have been included in this treatise.

For over a century, workers have attempted to define larval and post-larval morphological characters diagnostic at various systematic levels (for discussions, see Stafford 1912, Odhner 1914, Werner 1939, Rees 1950, Loosanoff & Davis 1963, Chanley & Andrews 1971, Lutz & Hidu 1979, Fuller & Lutz 1989, Hu et al. 1993, Hendriks et al. 2005, Larsen et al. 2007, Goodwin et al. 2014, 2016a, 2016b, 2018). Historically, the larval and early post-larval characteristics generally used in routine plankton and benthic identifications have been shell length, height, and depth, as well as the length of the ''straight-hinge line''; differences in larval shell shape, color, and texture; provinculum length; number and configuration of hinge teeth; and presence or absence of a byssal notch, eyespot, or apical cilia (''apical flagellum'') (Loosanoff et al. 1966, Chanley & Andrews 1971, Turner & Boyle 1975, Chanley & Chanley 1980, Lutz et al. 1982b, Fuller & Lutz 1989, Hu et al. 1993, Tan et al. 1993, Larsen et al. 2007). More recently, a spectrum of image analysis, cell sorting, and genetic techniques has proven useful for the identification of a myriad of larval and post-larval bivalves (Tiwari & Gallager 2003a, 2003b, Hendriks et al. 2005, Larsen et al. 2005, 2007, Henzler et al. 2010, Thompson et al. 2012a, 2012b, Goodwin et al. 2014, 2016a, 2016b, 2018).

The present monograph is designed to provide additional tools for the identification of larval and post-larval bivalve species isolated from planktonic and benthic samples from aquatic environments. To this end, Figures 1–195 depict scanning electron micrographic sequences of the gross shell morphologies, morphometrics, and details of the hinge regions of disarticulated shell valves of a spectrum of larval and post-larval bivalves at various stages of development. These sequences are presented in a manner (i.e., a consistent orientation of imaged specimens) that will facilitate comparison of the shell morphologies and morphometrics of the early life-history stages of these species. The micrographic sequences depict larval and post-larval shell features of species in 47 genera from 25 bivalve families. The morphologies of the larval hinges range from distinctly taxodont dentition in the case of the Arcoidea, Mytiloidea, and Pectinoidea to a lack of prominent denticular structures in the Arcticoidea, Hiatelloidea, Myoidea, and Veneroidea (with the exception of the venerid *Ruditapes philippinarum* that has fairly well-defined hinge teeth along the larval shell provinculum). The morphological features of various ontogenetic stages of the disarticulated larval and post-larval shell valves of many of the species are quite distinct, permitting discrimination at the specific level. Although differences in morphological features among many other taxa are subtle, it is believed that they can be defined, permitting discrimination of bivalve larvae and postlarvae at the levels of subfamily and genus, respectively.

The following sections summarize the utility (as articulated by various authors) of comparing scanning electron micrographs of early ontogenetic stages of species from a spectrum of select families for discrimination of larval and post-larval bivalves at various taxonomic levels.

Veneridae and Arcticidae

From detailed examination and analyses of the SEM sequences of the early life-history stages of five venerids (*Chione cancellata*—Figs. 168–170; *Mercenaria mercenaria*—Figs. 173–175; *Mercenaria campechiensis*—Figs. 176–178; *Mercenaria campechiensis texana*—Figs. 179–181; and *Pitar morrhuanus*—Figs. 186–189), Goodsell et al. (1992) concluded that ''documentation and comparison of scanning electron photomicrographs of larval and post-larval venerids would appear to be a successful aid for identification at the levels of subfamily and genus, respectively.'' As articulated by Lutz et al. (1982b), the sequence of ontogenetic changes in the morphology of the larval hinge apparatus of *Arctica islandica* (Figs. 149 and 150) is remarkably similar to that described and illustrated by Le Pennec (1978, 1980) for various species of venerids. Throughout larval development, the provinculum of *A. islandica* is slightly wedge shaped with the narrower portion toward the posterior region of the shell (Fig. 150). ''Denticles,'' analogous to those described by Le Pennec (1980) along the provinculum of certain venerids, are absent. During the early straight-hinge stage, an elongated ridge (''fold''; Le Pennec, 1980) develops in the left valve along almost the entire length of the anterior half of the provinculum (Figs. 149 and 150). At the anterior extremity of the provinculum of the left valve, there is a slight depression in shells of specimens greater than approximately 170 μm in length. In the right valve, a relatively short projection develops during the early straight-hinge stage along the central region of the provinculum (Fig. 150). This latter projection subsequently develops into the first cardinal tooth (according to the nomenclature of Le Pennec, 1978, 1980), which is readily apparent in the post-larval stages (Figs. 151 and 152) (Lutz et al. 1982b).

No ''primary'' (after Trueman 1950; ''primitive'' of Le Pennec 1980) ligament pits (''fossettes ligamentaire'' of Bernard 1896a) were observed in *Arctica islandica* specimens with shell lengths <200 μm (Fig. 150) or in numerous specimens ranging in length from 200 to 230 μm. Ligament pits, although often very much reduced in size, appeared to be present in all specimens examined with shell lengths >230 μm. Since the classic studies of Bernard in the late nineteenth century (Bernard 1895, 1896a, 1896b, 1897, 1898), numerous workers have commented on the presence of ligaments or ligament pits in ''larval'' specimens (Rees 1950, Ansell 1962, Loosanoff et al. 1966, Chanley & Andrews 1971, Bayne 1976; for further discussion concerning the significance of the presence or absence of ligament pits in the shells of early ontogenetic stages of bivalves, see Lutz et al. 1982b). Lutz and Hidu (1979) suggested that ''primary'' (after Trueman 1950) ligament pits do not form until metamorphosis has been initiated (see also Lutz 1979). It has been further suggested that changes associated with metamorphosis proceed in an orderly fashion (Bayne 1965, 1971, Turner 1976b) and that ''any interruption … in the normal sequence of events affects the ability of the larvae to progress to the next step whether that be the loss of a larval organ or the acquisition of a post-larval one'' (Turner 1976a).

In specimens of *Arctica islandica* examined during the course of preparation of the present monograph,,ligament pits were observed in shells of a number of specimens with larval lengths

Downloaded From: https://bioone.org/journals/Journal-of-Shellfish-Research on 25 Feb 2020
Terms of Use: https://bioone.org/terms-of-use Access provided by IFREMER

ranging between 200 and 230 μm. If, as suggested by Lutz and Hidu (1979, pp. 117–118), development of the primary ligament pit is "one of the first morphological changes that occurs during metamorphosis," it is reasonable to conclude that larvae within this size range are at least capable of metamorphosis (Lutz et al. 1979). Ligament pits were not observed in any *A. islandica* specimens with shell lengths <200 μm (Figure 150) (Lutz et al. 1982b). This observation, when coupled with the fact that no pediveliger larva with a length below 200 μm was found in any of the cultures, strongly suggests that the larvae of this species are not capable of metamorphosing at shell lengths below this size and has implications for determining the size at which most of the species in this monograph are capable of metamorphosing.

After metamorphosis, relatively dramatic changes take place in the morphology of the hinge apparatus of *Arctica islandica*. The sequence of ontogenetic changes photographically illustrated in Figures 151 and 152 is similar to that diagrammatically illustrated by Le Pennec (1978, 1980) in his detailed summary of the development of the heterodont hinge. A close similarity exists between the early post-larval hinge apparatus of *Venus verrucosa* figured by Le Pennec (1980, p. 617) and that of *A. islandica*. At a shell length of approximately 1–2 mm (Figs. 151, 152), the *A. islandica* hinge has acquired many adult characteristics, although it does not attain its definitive form until specimens have reached a shell length of approximately 4 mm (Fig. 12 in Lutz et al. 1982b, p. 761).

Mytilidae

Fuller and Lutz (1989) published scanning electron micrograph sequences of the larvae and postlarvae of six mytilids from the northwestern Atlantic: *Arcuatula papyria* (= *Amygdalum papyrium*) (Figs. 77–80); *Brachidontes exustus* (Figs. 81–84); *Geukensia demissa* (Figs. 85–88); *Ischadium recurvum* (Figs. 89–92); *Modiolus modiolus* (Figs. 97–100); and *Mytilus edulis* (Figs. 101–104). All six species have a long provinculum with taxodont dentition, with provinculum length and number of teeth increasing steadily during the larval period. The bold, comparatively few provincular teeth of *A. papyria* (Fig. 78) and the small, numerous provincular teeth of *M. edulis* (Fig. 102) clearly differentiate these two species. Most of these mytilid species have a low umbo, round posterior margin, and more pointed anterior margin, although *A. papyria* is distinguished by a high, prominent umbo. The larval shells of *G. demissa* and *I. recurvum* are difficult to differentiate because of the similarity in their shapes and hinge dentition; however, as articulated by Fuller and Lutz (1989), "discriminant analysis using larval shell length, shell height, provinculum length, and number of teeth aided in classification of these and other sympatric species."

By contrast, post-larval stages of these six mytilid species are plainly distinguished by the presence and type of lateral teeth seen in the SEM sequences published by Fuller and Lutz (1989). *Brachidontes exustus* has all three types of mytilid lateral teeth, including (1) primary lateral teeth, which form immediately posterior to provincular teeth; (2) secondary lateral teeth, which are posterior to the primary lateral teeth and are part of the dissoconch; and (3) dysodont teeth, which form on the anterior margin of the dissoconch (Figs. 83 and 84). *Modiolus modiolus* has primary lateral teeth (Figs. 99 and 100), *Ischadium recurvum* has dysodont teeth (Figs. 91 and 92), *Mytilus edulis* has secondary lateral and dysodont teeth (Figs. 103 and 104), and there are no lateral teeth in *Geukensia demissa* (Figs. 87 and 88) or *Arcuatula papyria* (Figs. 79 and 80) during early post-larval development. The provinculum increases in size and complexity during post-larval development in *A. papyria*, *B. exustus*, *G. demissa*, *I. recurvum*, and *M. modiolus*, but not in *M. edulis* (Fuller & Lutz 1989).

Ostreidae

Hu et al. (1993) published scanning electron micrograph sequences to elucidate species-specific shell features in larval and post-larval stages of four Ostreidae species: *Crassostrea gigas*, *Crassostrea virginica*, *Ostrea edulis*, and *Ostrea stentina* (= *Ostrea equestris*) (Figs. 105–123). Useful features for distinguishing larvae of the Ostreidae from those within other families of bivalves include asymmetry of left and right valves associated with a pronounced umbo of the left valve; one or two provincular teeth on each side of the provinculum; and a fasciole with a corresponding notch on the left valve. Qualitative characters, such as hinge dentition and shell shape of the larvae and postlarvae of the four ostreids, distinguish noncongeneric species, whereas species in the same genus generally are differentiated by quantitative features such as the dimensions of the provinculum and shell.

The results of the study by Hu et al. (1993), when combined with those of previous studies on *Crassostrea angulata* (Pascual 1971), *Crassostrea ariakensis* (Tanaka 1980), *Crassostrea glomerata* (Dinamani 1973), *Crassostrea iredalei* (Ver 1986), *Ostrea denselamellosa* (Tanaka 1980), *Ostrea lurida* (Loosanoff et al. 1966), *Ostrea permollis* (Forbes 1967), *Ostrea puelchana* (Castro & Le Pennec 1988), *Ostrea stentina* (Pascual 1972), and *Ostrea* spp. (Chanley & Dinamani 1980), illustrate that the morphological differences between early ontogenetic stages of species within the genus *Crassostrea* and those within the genus *Ostrea* are quite striking. The diagnostic characters for larval and post-larval shells of species within these two genera are summarized as follows.

Morphological larval features of species within the genus *Crassostrea* include (1) a knobby or beak-shaped umbo directed posteriorly; (2) shell height that is generally greater than shell length; (3) provinculum length that ranges from 68 to 88 μm; (4) the presence of two rectangular teeth on each side of the provinculum; (5) a well-defined central apparatus; and (6) posterior obscured teeth. By contrast, morphological features of species within the genus *Ostrea* include (1) a round shell with a large, moderately prominent umbo directed dorsally; (2) shell length that is greater than shell height; (3) provinculum length that ranges from 70 to 100 μm; (4) the presence of one anterior and one posterior tooth on the left valve and two anterior and two posterior teeth on the right valve, with teeth that are square or triangular; (5) a partially developed central apparatus; and (6) anterior obscured teeth.

Post-larval features of species within the genus *Crassostrea* include (1) a left valve umbo that is beak shaped and skews backward; (2) two posterior hinge teeth in shells up to 500 μm in length; and (3) a ligament that is 40 μm from the anterior end of the provinculum. By contrast, post-larval features of species within the genus *Ostrea* include (1) an umbo that is round and prominent dorsally; (2) one or two anterior hinge teeth in shells

Downloaded From: https://bioone.org/journals/Journal-of-Shellfish-Research on 25 Feb 2020
Terms of Use: https://bioone.org/terms-of-use Access provided by IFREMER

up to 500 μm in length; and (3) a ligament that is close to the anterior end of the provinculum (Hu et al. 1993).

The shell morphological features that are most useful for discriminating larval and post-larval specimens of the four ostreids that are included in this monograph are articulated by Hu et al. (1993) and may be summarized as follows:

(1) The species-specific characteristics of the provinculum remain relatively constant throughout the developmental stages. These diagnostic characters include the dimensions of the provinculum, the shape of the hinge teeth, and the modification pattern of the hinge teeth during the late larval stages. For example, the provinculum of larval and post-larval (up to a shell length of 550 μm) specimens of *Crassostrea virginica* is shorter but wider (50 μm long and 14 μm wide) than that of *Crassostrea gigas* (56 μm long and 10 μm wide). The transverse ridges are less defined and fewer in *C. gigas* than in *C. virginica*. The posterior hinge teeth of *C. virginica* are well defined even in late-stage larvae. These observations agree with the pattern of larval hinge modification in the genus *Crassostrea* postulated by Dinamani (1976). The range of provincular lengths of *Ostrea stentina* is 70–79 μm, which is much shorter than the 80–95 μm provincular length range of *Ostrea edulis* (Hu et al. 1993).
(2) The four species have different shell shapes, including prominence of umbos, shapes of anterior and posterior ends, rotation of the longitudinal axis, and shell length–height ratio. The shell shape of larval specimens of *Crassostrea virginica* is relatively compressed dorsoventrally, with a narrow and pointed anterior end, whereas that of *Crassostrea gigas* larvae is more extended in dorsoventral directions and its anterior end appears broad and blunt. A knobby umbo with an elongated anterior end is present in late-stage larval specimens of *Ostrea stentina*, whereas the umbo of *Ostrea edulis* is always flat and the anterior and posterior are nearly equally developed. Shell shape is also useful for identification of post-larval specimens. For example, two shoulders (anterior and posterior dorsal margins) extend at an angle of approximately 90 deg in *C. gigas* and at an angle of 140 deg in *C. virginica*, and were well defined in *O. stentina* but irregular in *O. edulis* (Hu et al. 1993).

In summary, generic and species diagnostic shell characters have been identified for early life-history stages of two species within the genus *Crassostrea* (*C. gigas* and *C. virginica*) and two species within the genus *Ostrea* (*O. edulis* and *O. stentina*). A key has been presented by Hu et al. (1993) summarizing these morphological characteristics that should provide a practical tool for the identification of larval and post-larval specimens of these ostreids isolated from planktonic and benthic samples.

Teredinidae

Scanning electron micrograph sequences published by Fuller et al. (1989a) and Tan et al. (1993) of disarticulated shell valves of *Teredo navalis* and *Bankia gouldi*, respectively, revealed qualitative and quantitative differences in larval and post-larval morphological features (Figs. 69–76). These sequences provide useful aids for the identification of larval and post-larval specimens of these two species isolated from plankton and benthic samples. In particular, the following features are important in distinguishing the larvae of *B. gouldi* from those of *T. navalis*: slope of the shoulders [the dorsal shell margin on the anterior and posterior ends of the hinge (Chanley & Dinamani 1980)]; length of the provinculum/hinge-line; and length of the posterior tooth of the left valve provinculum.

Tan et al. (1993) point out that, in larval shells of similar size, the shoulders of *Teredo navalis* (Fig. 73) are considerably steeper (less rounded) than those of *Bankia gouldi* (Fig. 69). This difference in shell shape is useful in distinguishing the two species. The initial size of the planktonic stage of a *B. gouldi* larva is much smaller than that of the larviparous *T. navalis* because of the difference in their development. Despite the difference in initial larval shell size, both species metamorphose at a shell height of about 230 μm, as indicated by the appearance of the ligament pit.

The larvae of *Bankia gouldi* and *Teredo navalis* can be distinguished on the basis of the length of the provinculum of the left valve. The average length of the provinculum/hinge-line measured by Tan et al. (1993) from micrographs of the left valves of *B. gouldi* (38.1 ± 1.8 μm, $n = 9$) (Fig. 70) is significantly smaller than that of *T. navalis* (46.7 ± 1.3 μm, $n = 9$) (Fig. 74). The provincular length measurements of the left valve are more useful than those of the right valve because the latter varies significantly with growth.

Larvae of *Bankia gouldi* can also be distinguished from those of *Teredo navalis* by the length of the posterior provincular tooth of the left valve (6.4 ± 0.6 μm, $n = 7$) (Fig. 70) which is significantly shorter than that of *T. navalis* (8.2 ± 0.3 μm) (Fig. 74) (Tan et al. 1993).

Practical Use of this Monograph

Although the SEM sequences presented in Figures 1–195 accurately depict the gross morphologies/morphometrics and hinge structures of the disarticulated shell valves of the larvae and/or postlarvae of 56 species of bivalves, it is important to emphasize that a scanning electron microscope is not necessary to observe even fine hinge structures associated with the ontogenetic stages of these species. Such structures are readily visible using a wide range of optical compound microscopes equipped with high-intensity reflected light sources, although the disarticulated shell valves must be viewed in several planes of focus to discern the often subtle details seen clearly in the scanning electron micrographs.

The comparisons of the larval and early post-larval stages of two mytilids (*Mytilus edulis* and *Modiolus modiolus*) published by Lutz and Hidu (1979) and depicted in Figures 97–104 dramatically illustrate this point. In their studies, measurements of larval dimensions (shell length, height, and provinculum length) and dentition counts were made under a standard petrographic microscope equipped with a high-intensity reflected light source. Using this procedure, Lutz and Hidu (1979) were able to obtain quantitative measurements and counts on approximately 20 specimens per hour. Numerous specimens were also examined and measured under a scanning electron microscope to confirm the accuracy of these optical microscopic measurements and counts.

Downloaded From: https://bioone.org/journals/Journal-of-Shellfish-Research on 25 Feb 2020
Terms of Use: https://bioone.org/terms-of-use Access provided by IFREMER

Their results indicated that, for a given number of provincular teeth, there was no overlap between the range extremes in either provinculum length or total shell length of the two species. There were no quantitative differences between left and right valve of individual specimens other than occasional minor discrepancies in dentition counts due to the interlocking nature of the hinge teeth. Lutz and Hidu (1979, p. 115) concluded that "careful examination of the hinge morphology of prodissoconchs and early dissoconchs using routine optical microscopic techniques should facilitate unambiguous differentiation of all early life-history stages of these two species."

In conclusion, scanning electron microscopy provides a powerful tool for photographically depicting the accurate gross shell morphology/morphometry and details of the hinge structure of the disarticulated shell valves of the larvae and early postlarvae of known species of bivalves cultured under controlled laboratory conditions. These morphological characters, in turn, provide researchers with invaluable aids for identifying (using routine optical microscopic techniques) the early life-history stages of these species isolated from plankton and benthic samples.

ACKNOWLEDGMENTS

The authors thank William Arnold, Robert Bisker, Thomas Bright, Bernardita Campos, Judy McDowell Capuzzo, Melbourne Carriker, Paul Chanley, Alison Craig, Greg Debrosse, William Foster, Mary Gibbons, John Grazul, Victor Greenhut, Harold Haskin, Kathleen Huntington, John Kraeuter, Dale Leavitt, Robert Loveland, William Mook, James Moore, Steven Murawski, Elizabeth W. North, Hugh Porter, Robert Prezant, Robert Robertson, John Ropes, William Sacco, Neil Savage, Rudolf Scheltema, Ruth Turner, Rosa Van Dessel, Eric Wagner, Randy Walker, Thomas Waller, Jean Watkinson, and John Whitcomb for their advice, assistance, and helpful comments. This research was supported by the New Jersey and South Carolina Agricultural Experiment Stations; the School of Environmental and Biological Sciences of Rutgers University; the South Carolina Sea Grant Consortium; Steinetz Awards from the Department of Biological Sciences, Rutgers University; a Grant-in-Aid of Research from the Society of Sigma Xi (SCF); the Maryland Power Plant Research Program; the Center for Environmental and Estuarine Studies, University of Maryland; NSF Grants EAR 81-21212 and EAR-84-17011 (RAL); and various NOAA Sea Grants (RAL).

LITERATURE CITED

Ansell, A. D. 1962. The functional morphology of the larva, and the post-larval development of *Venus striatula* (da Costa). *J. Mar. Biol. Assoc. U.K.* 42:419–443.

Baldwin, B. S., A. S. Pooley, Y.-P. Hu, D. B. Conn, V. S. Kennedy & R. A. Lutz. 1994. Identification of larval and post-larval zebra mussels and co-occurring bivalves in freshwater and estuarine habitats using shell morphology. In: Proceedings of the Fourth International Zebra Mussel Conference. Madison, WI: Wisconsin Sea Grant Institute. pp. 479–488.

Bayne, B. L. 1965. Growth and the delay of metamorphosis of the larvae of *Mytilus edulis* (L.). *Ophelia* 2:1–47.

Bayne, B. L. 1971. Some morphological changes that occur at the metamorphosis of the larvae of *Mytilus edulis*. In: Crisp, D. J., editor. Proceedings of the Fourth European Marine Biology Symposium, Bangor, 1969. New York, NY: Cambridge University Press. pp. 259–280.

Bayne, B. L. 1976. The biology of mussel larvae. In: Bayne, B. L., editor. Marine mussels: their ecology and physiology. New York, NY: Cambridge University Press. pp. 81–120.

Bernard, F. 1895. Première note sur le développement et la morphologie de la coquille chez les lamellibranches. *Bull. Soc. Géol. Fr. Ser. 3* 23:104–154.

Bernard, F. 1896a. Deuxième note sur le développement et la morphologie de la coquille chez les lamellibranches (Taxodontes). *Bull. Soc. Géol. Fr. Ser. 3* 24:54–82.

Bernard, F. 1896b. Troisième note sur le développement et la morphologie de la coquille chez les lamellibranches (Anisomyaires). *Bull. Soc. Géol. Fr. Ser. 3* 24:412–449.

Bernard, F. 1897. Quatrième et dernière note sur le développement et la morphologie de la coquille chez les lamellibranches. *Bull. Soc. Géol. Fr. Ser. 3* 25:559–566.

Bernard, F. 1898. Recherches ontogéniques et morphologiques sur la coquille des lamellibranches. Premiere partie: taxodontes et anisomyaires. *Ann. Sci. Nat. Zool.* 8:1–208.

Booth, J. D. 1977. Common bivalve larvae from New Zealand: Mytilacea. *N. Z. J. Mar. Freshw. Res.* 11:407–440.

Booth, J. D. 1979a. Common bivalve larvae from New Zealand: Pteriacea, Anomiacea, Ostreacea. *N. Z. J. Mar. Freshw. Res.* 13:131–139.

Booth, J. D. 1979b. Common bivalve larvae from New Zealand: Leptonacea. *N. Z. J. Mar. Freshw. Res.* 13:241–254.

Boyle, P. J. & R. D. Turner. 1976. The larval development of the wood boring piddock *Martesia striata* (L.) (Mollusca: Bivalvia: Pholadidae). *J. Exp. Mar. Biol. Ecol.* 22:55–68.

Calloway, C. B. & R. D. Turner. 1979. New techniques for preparing shells of bivalve larvae for examination with the scanning electron microscope. *Ann. Rep. Am. Malacol. Union. Inc.* 1978: 17–24.

Carlton, J. T. 1999. Molluscan invasions in marine and estuarine communities. *Malacologia* 41:439–454.

Carriker, M. R. & R. E. Palmer. 1979. Ultrastructural morphogenesis of prodissoconch and early dissoconch valves of the oyster *Crassostrea virginica*. *Proc. Natl. Shellfish. Assoc.* 69:103–128.

Castagna, M. 1975. Culture of the bay scallop, *Argopecten irradians*, in Virginia. *Mar. Fish. Rev.* 37:19–24.

Castagna, M. & J. Kraeuter. 1977. *Mercenaria* culture using stone aggregate for predator protection. *Proc. Natl. Shellfish. Assoc.* 67: 1–6.

Castro, N. F. & M. Le Pennec. 1988. Modalities of brooding and morphogenesis of larvae in *Ostrea puelchana* (D'Orbigny) under experimental rearing. *J. Mar. Biol. Assoc. U.K.* 68:399–407.

Chanley, P. E. 1965. Larval development of a boring clam, *Barnea truncata*. *Chesap. Sci.* 6:162–166.

Chanley, P. E. 1969. Larval development of the coquina clam, *Donax variabilis* Say, with a discussion of the structure of the larval hinge in the Tellinacea. *Bull. Mar. Sci.* 19:214–224.

Chanley, P. E. & J. D. Andrews. 1971. Aids for identification of bivalve larvae of Virginia. *Malacologia* 11:45–119.

Chanley, P. E. & M. Chanley. 1980. Reproductive biology of *Arthritica crassiformis* and *A. bifurca*, two commensal bivalve molluscs (Leptonacea). *N. Z. J. Mar. Freshw. Res.* 14:31–43.

Chanley, P. E. & P. Dinamani. 1980. Comparative descriptions of some oyster larvae from New Zealand and Chile, and a description of a new genus of oyster, Tiostrea. *N. Z. J. Mar. Freshw. Res.* 14:103–120.

Cohen, A. N. & J. T. Carlton. 1998. Accelerating invasion rate in a highly invaded estuary. *Science* 279:555–558.

Downloaded From: https://bioone.org/journals/Journal-of-Shellfish-Research on 25 Feb 2020
Terms of Use: https://bioone.org/terms-of-use Access provided by IFREMER

Culliney, J. L. & R. D. Turner. 1976. Larval development of the deep-water wood boring bivalve, *Xylophaga atlantica* Richards (Mollusca, Bivalvia, Pholadidae). *Ophelia* 15:149–161.

de Schweinitz, E. H. & R. A. Lutz. 1976. Larval development of the northern horse mussel, *Modiolus modiolus* (L.), including a comparison with the larvae of *Mytilus edulis* L. as an aid in planktonic identification. *Biol. Bull.* 150:348–360.

Dinamani, P. 1973. Embryonic and larval development in the New Zealand rock oyster, *Crassostrea glomerata* (Gould). *Veliger* 15:295–299.

Dinamani, P. 1976. The morphology of the larval shell in the genus *Crassostrea* Sacco, 1897 (Ostreidae). *J. Moll. Stud.* 42:95–107.

Forbes, M. L. 1967. Generic differences in prodissoconchs of Gulf of Mexico oysters. *Bull. Mar. Sci.* 17:338–347.

Fuller, S. C., Y.-P. Hu, R. A. Lutz & M. Castagna. 1989a. Shell and pallet morphology in early developmental stages of *Teredo navalis* L. (Bivalvia: Teredinidae). *Nautilus* 103:24–35.

Fuller, S. C. & R. A. Lutz. 1989. Shell morphology of larval and post-larval mytilids from the northwestern Atlantic. *J. Mar. Biol. Assoc. U.K.* 69:181–218.

Fuller, S. C., R. A. Lutz & A. Pooley. 1989b. Procedures for accurate documentation of shapes and dimensions of larval bivalve shells with scanning electron microscopy. *Trans. Am. Microsc. Soc.* 108:58–63.

Garland, E. D. & C. A. Zimmer. 2002. Techniques for the identification of bivalve larvae. *Mar. Ecol. Prog. Ser.* 225:299–310.

Gibbons, M. C. & M. Castagna. 1984. Serotonin as an inducer of spawning in six bivalve species. *Aquaculture* 40:189–191.

Gollasch, S. 2002. The importance of ship hull fouling as a vector of species introductions into the North Sea. *Biofouling* 18:105–121.

Goodsell, J. G., S. C. Fuller, A. G. Eversole & R. A. Lutz. 1992. Larval and early postlarval shell morphology of several venerid clams. *J. Mar. Biol. Assoc. U.K.* 72:231–255.

Goodwin, J. D., R. A. Lutz, S. Gallager, S. Johnson & V. S. Kennedy. 2018. Optical imaging and molecular sequencing of a preserved collection of bivalve larvae. *J. Shellfish. Res.* 37:449–466.

Goodwin, J. D., E. W. North & V. S. Kennedy. 2016b. Identification of *Crassostrea virginica* using polarized light microscopy in a mesohaline region of Chesapeake Bay. *J. Shellfish Res.* 35: 157–168.

Goodwin, J. D., E. W. North, I. D. Mitchell, C. M. Thompson & H. R. McFadden. 2016a. Improving a semi-automated classification technique for bivalve larvae: automated image acquisitions and measures of quality control. *Limnol. Oceanogr. Methods* 14: 683–697.

Goodwin, J. D., E. W. North & C. M. Thompson. 2014. Evaluating and improving a semi-automated image analysis technique for identifying bivalve larvae. *Limnol. Oceanogr. Methods* 12:548–562.

Gustafson, R. G. & R. A. Lutz. 1992. Larval and early post-larval development of the protobranch bivalve *Solemya velum* (Mollusca: Bivalvia). *J. Mar. Biol. Assoc. U.K.* 72:383–402.

Hare, M. P., S. R. Palumbi & C. A. Butman. 2000. Single-step species identification of bivalve larvae using multiplex polymerase chain reaction. *Mar. Biol.* 137:953–961.

Hayes, K. R. & C. L. Hewitt. 1998. A risk assessment framework for ballast water introductions. CRIMP technical report #14. Hobart, Australia: CSIRO Division of Marine Research. 68 pp.

Hendriks, I. E., L. A. van Duren & P. M. J. Herman. 2005. Image analysis techniques: a tool for the identification of bivalve larvae? *J. Sea Res.* 54:151–162.

Henzler, C. M., E. A. Hoaglund & S. D. Gaines. 2010. FISH-CS—a rapid method for counting and sorting species of marine zooplankton. *Mar. Ecol. Prog. Ser.* 410:1–11.

Hu, Y.-P., S. C. Fuller, M. Castagna, R. C. Vrijenhoek & R. A. Lutz. 1993. Shell morphology and identification of early life history stages of congeneric species of *Crassostrea* and *Ostrea*. *J. Mar. Biol. Assoc. U.K.* 73:471–496.

Hu, Y.-P., R. A. Lutz & R. C. Vrijenhoek. 1992. Electrophoretic identification and genetic analysis of bivalve larvae. *Mar. Biol.* 113:227–230.

Jablonski, D. & R. A. Lutz. 1980. Molluscan larval shell morphology: ecological and paleontological applications. In: Rhoads, D. C. & R. A. Lutz, editors. Skeletal growth of aquatic organisms. New York, NY: Plenum Press. pp. 323–377.

Jablonski, D. & R. A. Lutz. 1983. Larval ecology of marine benthic invertebrates: paleobiological implications. *Biol. Rev. Camb. Philos. Soc.* 58:21–89.

Jørgensen, C. B. 1946. Lamellibranchia. *Medd. Dan. Fisk. Havunders.* 4:277–311.

Kennedy, V. S., S. C. Fuller & R. A. Lutz. 1991. Shell and hinge development of young *Corbicula fluminea* (Muller) (Bivalvia: Corbiculoidea). *Am. Malacol. Bull.* 8:107–111.

Kennedy, V. S., R. A. Lutz & C. A. Fuller. 1989. Larval and early postlarval development of *Macoma mitchelli* Dall (Bivalvia: Tellinidae). *Veliger* 32:29–38.

LaBarbera, M. 1975. Larval and post-larval development of the giant clams *Tridacna maxima* and *Tridacna squamosa* (Bivalvia, Tridacnidae). *Malacologia* 15:69–79.

Larsen, J. B., M. E. Frischer, K. W. Ockelmann, L. J. Rasmussen & B. W. Hansen. 2007. Temporal occurrence of planktotrophic bivalve larvae identified morphologically and by single step nested multiplex PCR. *J. Plankton Res.* 29:423–436.

Larsen, J. B., M. E. Frischer, L. J. Rasmussen & B. W. Hansen. 2005. Single-step nested multiplex PCR to differentiate between various bivalve larvae. *Mar. Biol.* 146:1119–1129.

Lebour, M. V. 1938. Notes on the breeding of some lamellibranchs from Plymouth and their larvae. *J. Mar. Biol. Assoc. U.K.* 23:119:144.

Le Pennec, M. 1973. Morphogenèse de la charnière chez cinq espèces de Veneridae. *Malacologia* 12:225–245.

Le Pennec, M. 1978. Génèse de la coquille larvaire et postlarvaire chez divers bivalves marins. Thèse de Doctorat d'Etat, Université de Bretagne Occidentale, Brest, France. 219 pp.

Le Pennec, M. 1980. The larval and post-larval hinge of some families of bivalve molluscs. *J. Mar. Biol. Assoc. U.K.* 60:601–617.

Le Pennec, M. & A. Lucas. 1970. Comparative growth and morphology of some venerid larvae (Bivalvia, Veneridae). *Malacol. Rev.* 3:175–183.

Le Pennec, M. & M. Masson. 1976. Morphogenese de la coquille de *Mytilus galloprovincialis* (Lmk.) eleve au laboratoire. *Cah. Biol. Mar.* 17:113–118.

Loosanoff, V. L. & H. C. Davis. 1963. Rearing of bivalve mollusks. *Adv. Mar. Biol.* 1:1–136.

Loosanoff, V. L., H. C. Davis & P. E. Chanley. 1966. Dimensions and shapes of larvae of some marine bivalve mollusks. *Malacologia* 4:351–435.

Lutz, R. A. 1979. The bivalve "larval ligament pit" as an exclusively post-larval feature. *Proc. Natl. Shellfish. Assoc.* 69:197 (Abstract).

Lutz, R. A. 1988. Dispersal of organisms at deep-sea hydrothermal vents: a review. *Oceanol. Acta* 8:23–29.

Lutz, R. A. 2012. Deep-sea hydrothermal vents. In: Bell, E. M., editor. Life at extremes: environments, organisms and strategies for survival. Oxfordshire, UK: CABI. pp. 242–270.

Lutz, R. A., J. Goodsell, M. Castagna, S. Chapman, C. Newell, H. Hidu, R. Mann, D. Jablonski, V. Kennedy, S. Siddall, R. Goldberg, H. Beattie, C. Falmagnem, A. Chestnut & A. Partridge. 1982a. Preliminary observations on the usefulness of hinge structures for identification of bivalve larvae. *J. Shellfish Res.* 2:65–70.

Lutz, R. A. & H. Hidu. 1979. Hinge morphogenesis in the shells of larval and early post-larval mussels (*Mytilus edulis* L. and *Modiolus modiolus* (L.). *J. Mar. Biol. Assoc. U.K.* 59:111–121.

Lutz, R. A. & D. Jablonski. 1978a. Cretaceous bivalve larvae. *Science* 199:439–440.

Lutz, R. A. & D. Jablonski. 1978b. Classification of bivalve larvae and early post-larvae using scanning electron microscopy. *Am. Zool.* 18:647 (Abstract).

Downloaded From: https://bioone.org/journals/Journal-of-Shellfish-Research on 25 Feb 2020
Terms of Use: https://bioone.org/terms-of-use Access provided by IFREMER

Lutz, R. A. & D. Jablonski. 1979. Micro- and ultramorphology of larval bivalve shells: ecological, paleoecological, and paleoclimatic applications. *Proc. Natl. Shellfish. Assoc.* 69:197–198 (Abstract).

Lutz, R. A. & D. Jablonski. 1981. Identification of living and fossil bivalve larvae. *Science* 212:1419.

Lutz, R. A. & M. J. Kennish. 1992. Ecology and morphology of larval and early postlarval mussels. In: Gosling, E. A., editor. The Mussel *Mytilus*. Amsterdam, The Netherlands: Elsevier. pp. 53–85.

Lutz, R. A., R. Mann, J. G. Goodsell & M. Castagna. 1982b. Larval and early post-larval development of the ocean quahog, *Arctica islandica*. *J. Mar. Biol. Assoc. U.K.* 62:745–769.

Malchus, N. & A. F. Sartori. 2013. The early shell: ontogeny, features and evolution. Treatise on invertebrate paleontology, part N, Bivalvia revised, volume 1, chapter 4. *Treatise Online* 61:1–114.

Miyazaki, I. 1962. On the identification of lamellibranch larvae. *Nippon Suisan Gakkaishi* 28:955–966.

Morse, D. E., H. Duncan, N. Hooker & A. Morse. 1977. Hydrogen peroxide induces spawning in mollusks, with activation of prostaglandin endoperoxide synthetase. *Science* 196:298–300.

Murphy, K. R., D. Ritz & C. L. Hewitt. 2002. Heterogeneous zooplankton distribution in a ship's ballast tanks. *J. Plankton Res.* 24:729–734.

Newell, G. E. & R. C. Newell. 1963. Marine plankton: a practical guide. London, UK: Hutchinson Educational Limited. 207 pp.

North, E. W., Z. Schlag, R. R. Hood, M. Li, L. Zhong, T. Gross & V. S. Kennedy. 2008. Vertical swimming behavior influences the dispersal of simulated oyster larvae in a coupled particle-tracking and hydrodynamic model of Chesapeake Bay. *Mar. Ecol. Prog. Ser.* 359:99–115.

Odhner, N. H. 1914. Notizen über die Fauna der Adria bei Rovingo. Berträge zur Kenntnis der marinen Molluskenfauna von Rovigno in Istrien. *Zool. Anz.* 44:156–170.

Pascual, E. 1971. Morfologiá de la Charnela larvaria de *Crassostrea angulata* (Lmk) en differentes fases de su desarrollo. *Investig. Pesq.* 35:549–563.

Pascual, E. 1972. Estudio de las conchas larvarias de *Ostrea stentina* Payr. y *Ostrea edulis* L. *Investig. Pesq.* 36:297–310.

Paugam, A., C. D'Ollone, J.-C. Cochard, P. Garen & M. Le Pennec. 2006. The limits of morphometric features for the identification of black-lip pearl oyster (*Pinctada margaritifera*) larvae. *J. Shellfish Res.* 25:959–967.

Ramorino, L. & B. Campos. 1983. Larvas y postlarvas de Mytilidae de Chile (Mollusca: Bivalvia). *Rev. Biol. Mar. Valparaíso* 19:143–192.

Redfearn, P. 1982. Larval shell development of the toheroa, *Paphies ventricosa* (Gray, 1843) (Mactracea: Mesodesmatidae). *N. Z. J. Mar. Freshw. Res.* 16:241–252.

Redfearn, P. 1987. Larval shell development of the northern tuatua, *Paphies subtriangulata* (Bivalvia, Mesodesmatidae). *N. Z. J. Mar. Freshw. Res.* 21:65–70.

Redfearn, P., P. Chanley & M. Chanley. 1986. Larval shell development of four species of New Zealand mussels: (Bivalvia, Mytilacea). *N. Z. J. Mar. Freshw. Res.* 20:157–172.

Rees, C. B. 1950. The identification and classification of lamellibranch larvae. *Hull Bull. Mar. Ecol.* 3:73–104.

Ruiz, G. M., P. W. Fofonoff, J. T. Carlton, M. J. Wonham & A. H. Hines. 2000. Invasion of coastal marine communities in North America: apparent patterns, processes, and biases. *Annu. Rev. Ecol. Syst.* 31:481–531.

Scheltema, R. S. 1971. Dispersal of phytoplanktotropic shipworm larvae (Bivalvia: Teredinidae) over long distances by ocean currents. *Mar. Biol.* 11:5–11.

Siddall, S. E. 1977. Temperature and salinity effects on mussels. *UNFAO Aquacult. Bull.* 8:12.

Siddall, S. E. 1978. The development of the hinge line in tropical mussel larvae of the genus Perna. *Proc. Natl. Shellfish. Assoc.* 68:86 (Abstract).

Stafford, J. 1912. On the recognition of bivalve larvae in plankton collections. *Contrib. Can. Biol.* 1906–1910:221–242.

Sullivan, C. M. 1948. Bivalve larvae of Malpeque Bay, P.E.I. *Bull. Fish. Res. Board Can.* 77:1–36.

Tan, A., Y.-P. Hu, M. Castagna, R. A. Lutz, M. J. Kennish & A. S. Pooley. 1993. Shell and pallet morphology of early developmental stages of *Bankia gouldi* (Bartsch, 1908) (Bivalva: Teredinidae). *Nautilus* 107:63–75.

Tanaka, Y. 1980. Identification of bivalve larvae. *Aquabiology* 2:289–291, 369–371.

Thompson, C. M., M. P. Hare & S. M. Gallager. 2012a. Semi-automated image analysis for the identification of bivalve larvae from a Cape Cod estuary. *Limnol. Oceanogr. Methods* 10:538–554.

Thompson, C. M., R. H. York & S. M. Gallager. 2012b. Species-specific abundance of bivalve larvae in relation to biological and physical conditions in a Cape Cod estuary. *Mar. Ecol. Prog. Ser.* 469:53–69.

Tiwari, S. & S. M. Gallager. 2003a. Optimizing multiscale invariants for the identification of bivalve larvae. In: Proceedings of the 2003 IEEE International Conference on Image Processing, Barcelona, Spain, September 14–17, 2003.

Tiwari, S. & S. M. Gallager. 2003b. Machine learning and multiscale methods in the identification of bivalve larvae. In: Proceedings of the 9th IEEE International Conference on Computer Vision, Nice, France, October 14–17, 2003.

Tremblay, M. J., L. D. Meade & G. V. Hurley. 1987. Identification of planktonic sea scallop larvae (*Placopecten magellanicus*) (Gmelin). *Can. J. Fish. Aquat. Sci.* 44:1361–1366.

Trueman, E. R. 1950. Observations on the ligament of *Mytilus edulis*. *Q. J. Microsc. Sci.* 91:225–236.

Turner, R. D. 1966. A survey and illustrated catalogue of the Teredinidae (Mollusca: Bivalvia). Cambridge, MA: The Museum of Comparative Zoology, Harvard University. 265 pp.

Turner, R. D. 1971. Identification of marine wood-boring molluscs. In: Jones, E. B. G. & S. K. Eltringham, editors. Marine borers, fungi and fouling organisms of wood. Paris, France: Organization for Economic Co-operation and Development. pp. 17–64.

Turner, R. D. 1976a. Some factors involved in the settlement and metamorphosis of marine bivalve larvae. In: Sharply, J. M. & A. M. Kaplan, editors. Proceedings of the 3rd International Biodegradation Symposium, Kingston, RI. London, UK: Applied Science Publishers. pp. 409–416.

Turner, R. D. 1976b. Search for a 'weak link'. In: Bultman, J. D., editor. In: Proceedings of a Workshop on the Biodeterioration of Tropical Woods: chemical basis for natural resistance. Washington, DC: Naval Research Laboratory. pp. 31–40.

Turner, R. D. & P. J. Boyle. 1975. Studies of bivalve larvae using the scanning electron microscope and critical point drying. *Bull. Am. Malacol. Union Inc.* 40:59–65.

Turner, R. D. & A. C. Johnson. 1970. Some problems and techniques in rearing bivalve larvae. *Ann. Rep. Am. Malacol. Union. Inc.* 1969: 9–13.

Ver, L. M. M. 1986. Early development of *Crassostrea iredalei* (Faustino, 1932) (Bivalvia: Ostreidae), with notes on the structure of the larval hinge. *Veliger* 29:78–85.

Wang, S., Z. Bao, L. Zhang, N. Li, A. Zhan, W. Guo, X. Wang & J. Hu. 2006. A new strategy for species identification of planktonic larvae: PCR-RFLP analysis of the internal transcribed spacer region of ribosomal DNA detected by agarose gel electrophoresis or DHPLC. *J. Plankton Res.* 28:375–384.

Wassnig, M. & P. C. Southgate. 2012. Embryonic and larval development of *Pteria penguin* (Röding, 1798) (Bivalvia: Pteriidae). *J. Moll. Stud.* 78:134–141.

Werner, B. 1939. Über die Entwicklung Artunterscheidung von Muschellarven des Nordseeplanktons, unter besonderer Berücksichtigung der Schalenentwicklung. *Zool. Jahrb. Abt. Anat. Ontog.* 66: 1–54.

Downloaded From: https://bioone.org/journals/Journal-of-Shellfish-Research on 25 Feb 2020
Terms of Use: https://bioone.org/terms-of-use Access provided by IFREMER

TABLE 1.

The 56 species of bivalves for which larval and/or post-larval SEM sequences are depicted in Figures 1–195.

Figure numbers	Order	Family	Genus	Species	Authority	Source of sexually mature adult bivalves
1–4	Adapedonta	Hiatellidae	*Hiatella*	*arctica*	(Linnaeus, 1767)	Pemaquid, ME
5–8	Adapedonta	Pharidae	*Ensis*	*leei*	M. Huber, 2015	Damariscotta River, ME
9–12	Arcida	Arcidae	*Arca*	*noae*	Linnaeus, 1758	Istrian Peninsula Coast, Rovinj, Croatia
13–16	Arcida	Arcidae	*Lunarca*	*ovalis*	(Bruguière, 1789)	Wachapreague, VA
17–19	Arcida	Noetiidae	*Noetia*	*ponderosa*	(Say, 1822)	Wachapreague, VA
20–23	Cardiida	Cardiidae	*Dinocardium*	*robustum*	(Lightfoot, 1786)	Indian River near Grant, FL
24–27	Cardiida	Cardiidae	*Laevicardium*	*mortoni*	(Conrad, 1831)	Coastal bay near Wachapreague, VA
28–31	Cardiida	Solecurtidae	*Tagelus*	*plebeius*	(Lightfoot, 1786)	Delaware Bay, NJ
32–35	Cardiida	Tellinidae	*Ameritella*	*agilis*	(Stimpson, 1857)	Wachapreague Inlet, Wachapreague, VA
36–39	Cardiida	Tellinidae	*Ameritella*	*mitchelli*	(Dall, 1895)	Choptank River, MD
40–43	Cardiida	Tellinidae	*Limecola*	*balthica*	(Linnaeus, 1758)	Lowe's Cove, Walpole, ME
44	Carditida	Carditidae	*Cyclocardia*	*borealis*	(Conrad, 1832)	Continental Shelf off NJ
45	Carditida	Astartidae	*Astarte*	*castanea*	(Say, 1822)	Continental Shelf off NJ
46–49	Myida	Dreissenidae	*Dreissena*	*bugensis*	(Andrusov, 1897)	Lake Ontario near Rochester, NY
50–53	Myida	Dreissenidae	*Dreissena*	*polymorpha*	(Pallas, 1771)	St. Lawrence River near Cape Vincent, NY
54–57	Myida	Dreissenidae	*Mytilopsis*	*leucophaeata*	(Conrad, 1831)	Hudson River near Piermont, NY
58–61	Myida	Myidae	*Mya*	*arenaria*	Linnaeus, 1758	Damariscotta River, Walpole, ME
62–64	Myida	Myidae	*Mya*	*truncata*	Linnaeus, 1758	Gulf of Maine off Boothbay Harbor, ME
65, 66	Myida	Pholadidae	*Cyrtopleura*	*costata*	(Linnaeus, 1758)	Indian River, FL
67, 68	Myida	Pholadidae	*Diplothyra*	*curta*	(G. B. Sowerby I, 1834)	Mississippi Sound, MS
69–72	Myida	Teredinidae	*Bankia*	*gouldi*	(Bartsch, 1908)	York River, Gloucester Point, VA
73–76	Myida	Teredinidae	*Teredo*	*navalis*	Linnaeus, 1758	Coastal bay near Wachapreague Inlet, VA
77–80	Mytilida	Mytilidae	*Arcuatula*	*papyria*	(Conrad, 1846)	Indian River, FL
81–84	Mytilida	Mytilidae	*Brachidontes*	*exustus*	(Linnaeus, 1758)	Cabbage Island and Wilmington Island, GA
85–88	Mytilida	Mytilidae	*Geukensia*	*demissa*	(Dillwyn, 1817)	Maurice River, NJ
89–92	Mytilida	Mytilidae	*Ischadium*	*recurvum*	(Rafinesque, 1820)	James River, VA
93, 94	Mytilida	Mytilidae	*Leiosolenus*	*bisulcatus*	(d'Orbigny, 1853)	Jamaica, West Indies
95, 96	Mytilida	Mytilidae	*Modiolus*	*americanus*	(Leach, 1815)	West coast of Florida
97–100	Mytilida	Mytilidae	*Modiolus*	*modiolus*	(Linnaeus, 1758)	Cape Newagen, ME
101–104	Mytilida	Mytilidae	*Mytilus*	*edulis*	Linnaeus, 1758	Continental Shelf off NJ
105–109	Ostreida	Ostreidae	*Crassostrea*	*gigas*	(Thunberg, 1793)	Coast Oyster Company, Quilcene, WA
110–114	Ostreida	Ostreidae	*Crassostrea*	*virginica*	(Gmelin, 1791)	Delaware Bay, NJ
115–118	Ostreida	Ostreidae	*Ostrea*	*edulis*	Linnaeus, 1758	Walpole, ME
119–123	Ostreida	Ostreidae	*Ostrea*	*stentina*	Payraudeau, 1826	Newport River Estuary, NC
124–127	Pectinida	Anomiidae	*Anomia*	*simplex*	d'Orbigny, 1853	Wachapreague Inlet, Wachapreague, VA
128–130	Pectinida	Pectinidae	*Argopecten*	*irradians*	(Lamarck, 1819)	Cape Cod Bay, MA
131–134	Pectinida	Pectinidae	*Argopecten*	*irradians concentricus*	(Say, 1822)	Coast of North Carolina near Morehead City
135–138	Pectinida	Pectinidae	*Pecten*	*maximus*	(Linnaeus, 1758)	Coast of Brest, France
139–143	Pectinida	Pectinidae	*Placopecten*	*magellanicus*	Gmelin, 1791	St. John's, Newfoundland (larvae); Damariscotta River, ME (postlarvae)
144, 145	Pholadomyida	Lyonsiidae	*Lyonsia*	*hyalina*	(Conrad, 1831)	Mason's Beach, VA
146	Pholadomyida	Periplomatidae	*Periploma*	*leanum*	(Conrad, 1831)	Continental Shelf off New Jersey
147, 148	Solemyida	Solemyidae	*Solemya*	*velum*	Say, 1822	Upper Buttermilk Bay, MA and Shark River, NJ
149–152	Venerida	Arcticidae	*Arctica*	*islandica*	(Linnaeus, 1767)	Continental Shelf, off New Jersey and Rhode Island
153–156	Venerida	Mactridae	*Mulinia*	*Lateralis*	(Say, 1822)	Wachapreague, VA
157–159	Venerida	Mactridae	*Rangia*	*cuneata*	(G. B. Sowerby I, 1832)	Cohansey River near Bridgeton, NJ
160–163	Venerida	Mactridae	*Spisula*	*solidissima*	(Dillwyn, 1817)	Continental Shelf off Rhode Island
164–167	Venerida	Mesodesmatidae	*Mesodesma*	*arctatum*	(Conrad, 1831)	Sable Island Bank (depth 42 m) off Nova Scotia, Canada
168–170	Venerida	Veneridae	*Chione*	*cancellata*	(Linnaeus, 1767)	Indian River, FL
171, 172	Venerida	Veneridae	*Gemma*	*gemma*	(Totten, 1834)	Delaware Bay, NJ
173–175	Venerida	Veneridae	*Mercenaria*	*mercenaria*	(Linnaeus, 1758)	Milford, CT
176–178	Venerida	Veneridae	*Mercenaria*	*campechiensis*	(Gmelin, 1791)	Gulf of Mexico near Apalachicola, FL

continued on next page

Downloaded From: https://bioone.org/journals/Journal-of-Shellfish-Research on 25 Feb 2020
Terms of Use: https://bioone.org/terms-of-use Access provided by IFREMER

TABLE 1.

continued

Figure numbers	Order	Family	Genus	Species	Authority	Source of sexually mature adult bivalves
179–181	Venerida	Veneridae	*Mercenaria*	*campechiensis texana*	(Dall, 1902)	Gulf of Mexico near Galveston, TX
182–185	Venerida	Veneridae	*Petricolaria*	*pholadiformis*	(Lamarck, 1818)	Continental Shelf off southern New Jersey
186–189	Venerida	Veneridae	*Pitar*	*morrhuanus*	(Dall, 1902)	Continental Shelf off Wachapreague, VA
190–193	Venerida	Veneridae	*Ruditapes*	*philippinarum*	(Adams & Reeve, 1850)	Obtained from the Carna Research Station, Galway, Ireland
194, 195	Venerida	Cyrenidae	*Corbicula*	*fluminea*	(O. F. Müller, 1774)	Nassawango Creek, MD

Taxonomic nomenclature was assigned according to the latest ''accepted name'' (or acceptable ''alternate representation'') and associated classification hierarchy in the World Register of Marine Species (www.marinespecies.org). Sexually mature adult bivalves were obtained from the indicated sources and used as broodstock to obtain the larvae and postlarvae depicted in this monograph.

Downloaded From: https://bioone.org/journals/Journal-of-Shellfish-Research on 25 Feb 2020
Terms of Use: https://bioone.org/terms-of-use Access provided by IFREMER

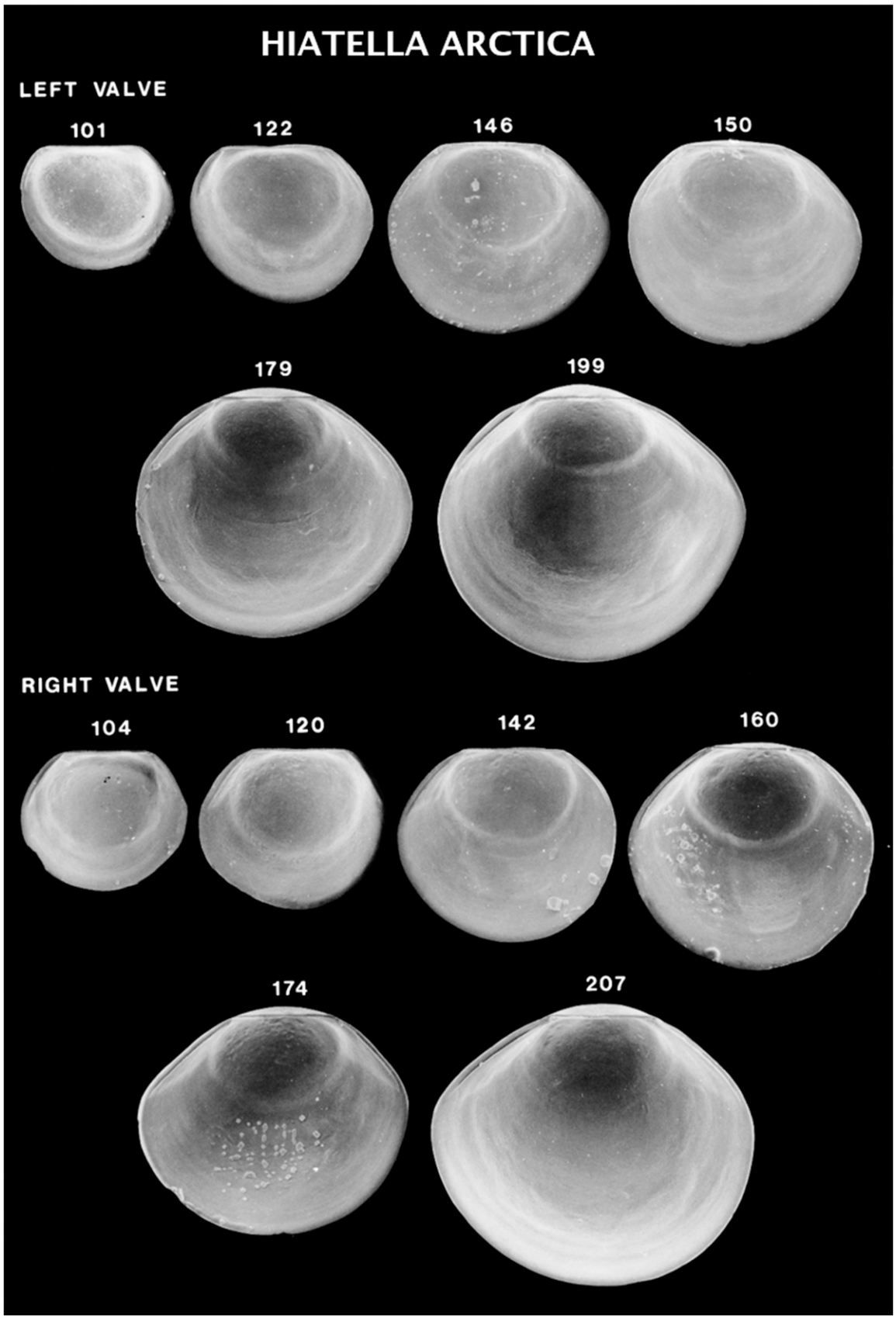

Figure 1. Scanning electron micrographs of disarticulated shell valves of *Hiatella arctica* larvae. Numbers indicate the maximum linear shell dimension in micrometers.

Downloaded From: https://bioone.org/journals/Journal-of-Shellfish-Research on 25 Feb 2020
Terms of Use: https://bioone.org/terms-of-use Access provided by IFREMER

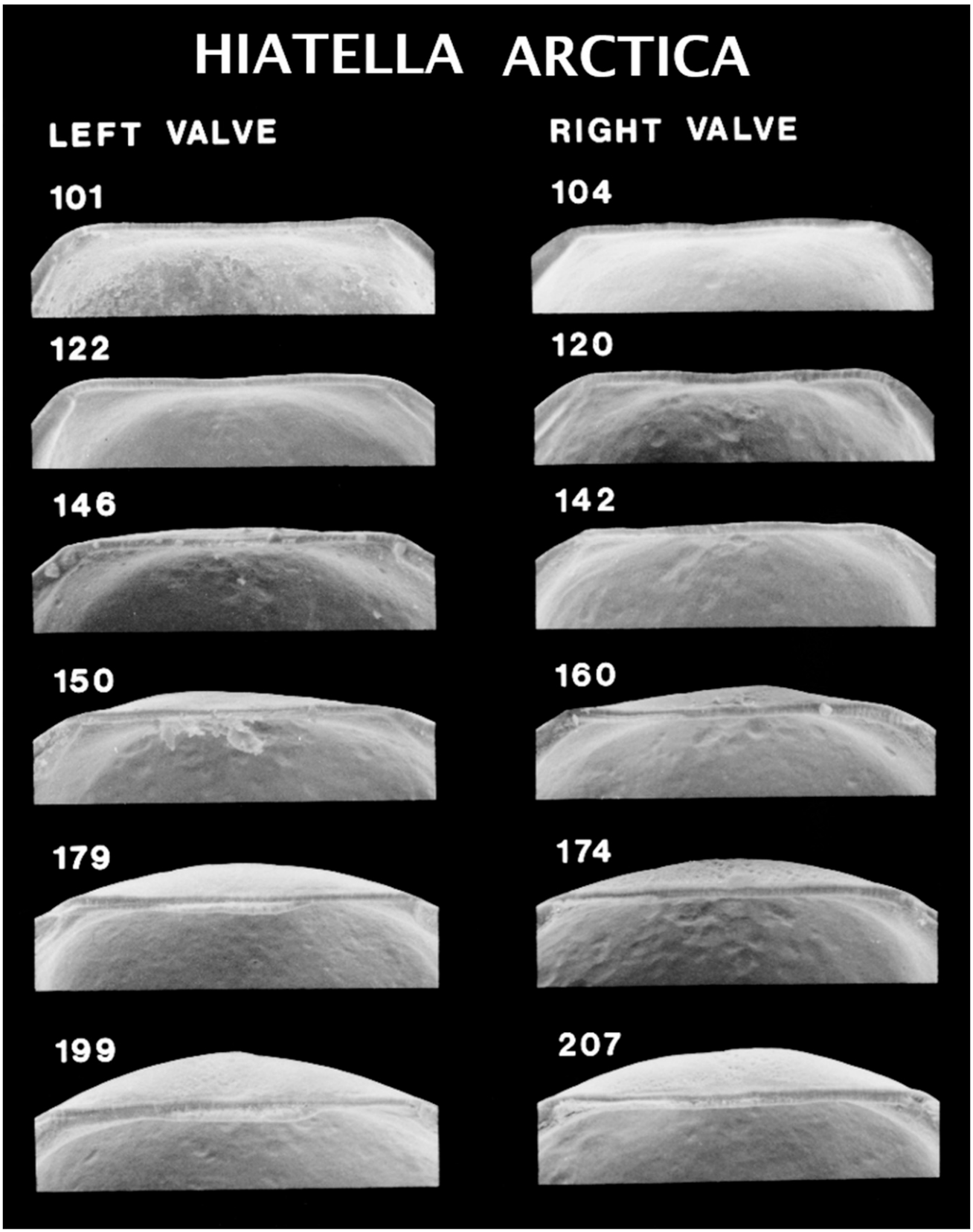

Figure 2. Scanning electron micrographs of the hinge of disarticulated shell valves of *Hiatella arctica* larvae seen in Figure 1. Numbers indicate the maximum linear shell dimension in micrometers.

Downloaded From: https://bioone.org/journals/Journal-of-Shellfish-Research on 25 Feb 2020
Terms of Use: https://bioone.org/terms-of-use Access provided by IFREMER

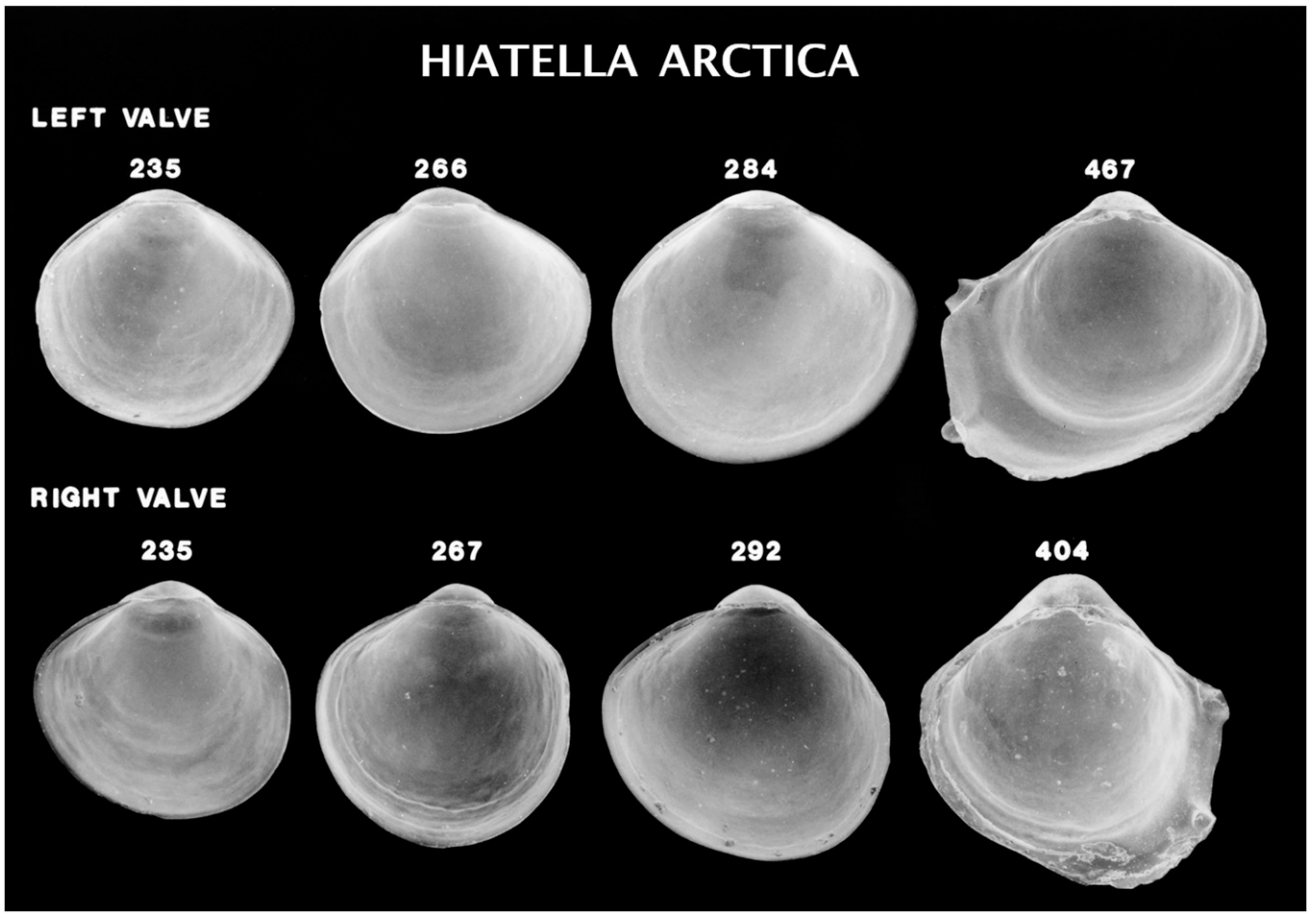

Figure 3. Scanning electron micrographs of disarticulated shell valves of *Hiatella arctica* postlarvae. Numbers indicate the maximum linear shell dimension in micrometers.

Downloaded From: https://bioone.org/journals/Journal-of-Shellfish-Research on 25 Feb 2020
Terms of Use: https://bioone.org/terms-of-use Access provided by IFREMER

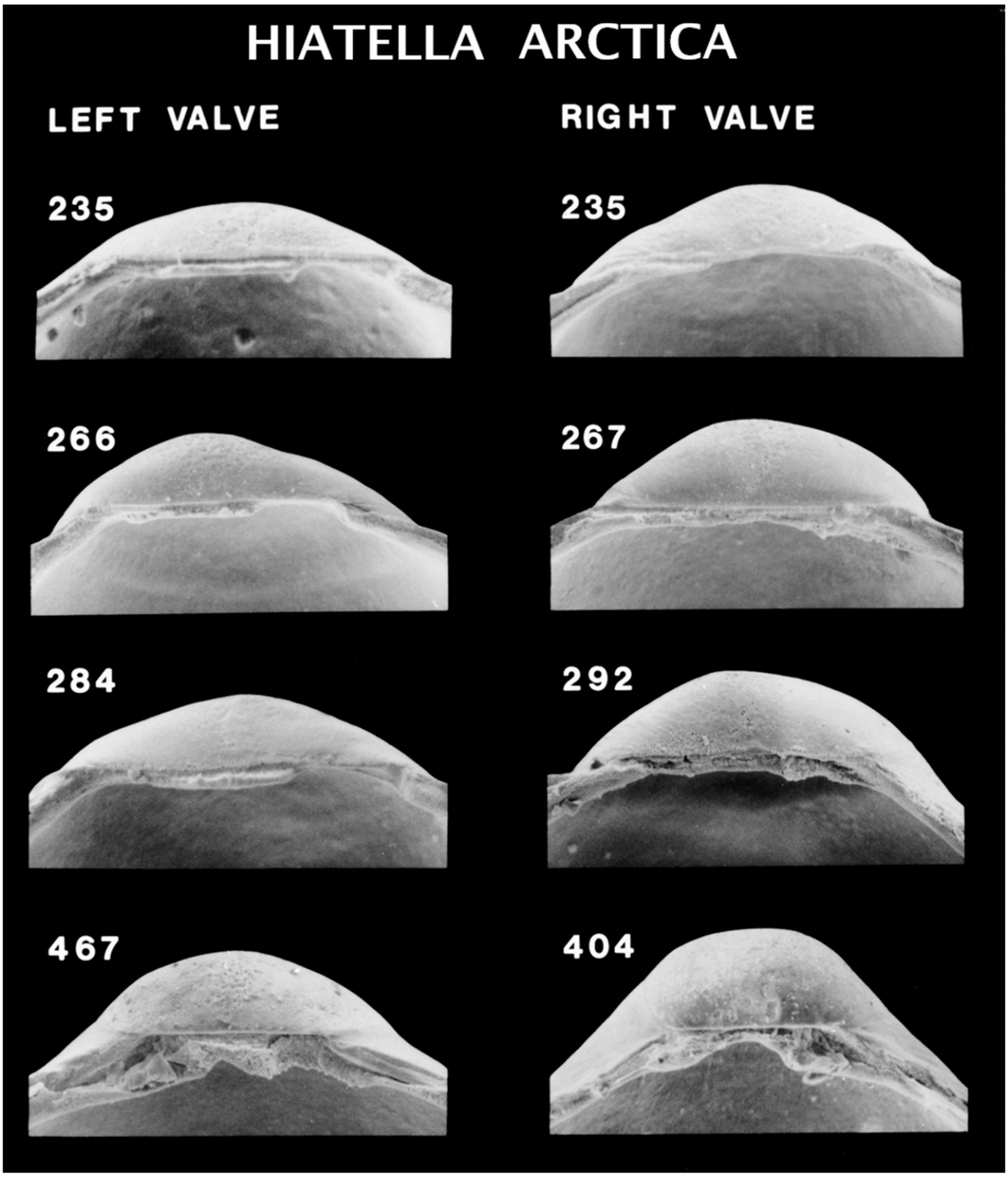

Figure 4. Scanning electron micrographs of the hinge of disarticulated shell valves of *Hiatella arctica* postlarvae seen in Figure 3. Numbers indicate the maximum linear shell dimension in micrometers.

Downloaded From: https://bioone.org/journals/Journal-of-Shellfish-Research on 25 Feb 2020
Terms of Use: https://bioone.org/terms-of-use Access provided by IFREMER

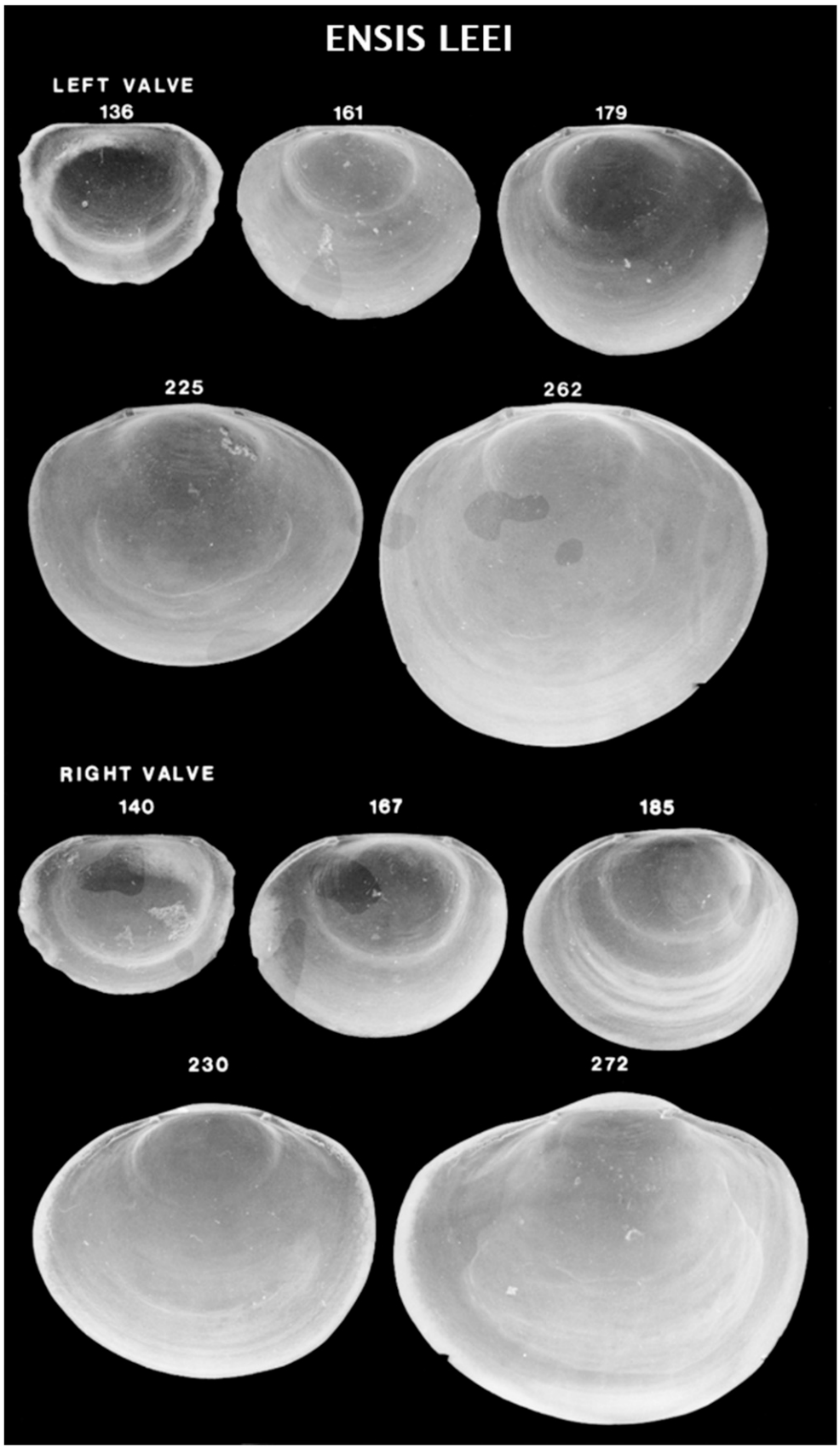

Figure 5. Scanning electron micrographs of disarticulated shell valves of *Ensis leei* larvae. Numbers indicate the maximum linear shell dimension in micrometers.

Downloaded From: https://bioone.org/journals/Journal-of-Shellfish-Research on 25 Feb 2020
Terms of Use: https://bioone.org/terms-of-use Access provided by IFREMER

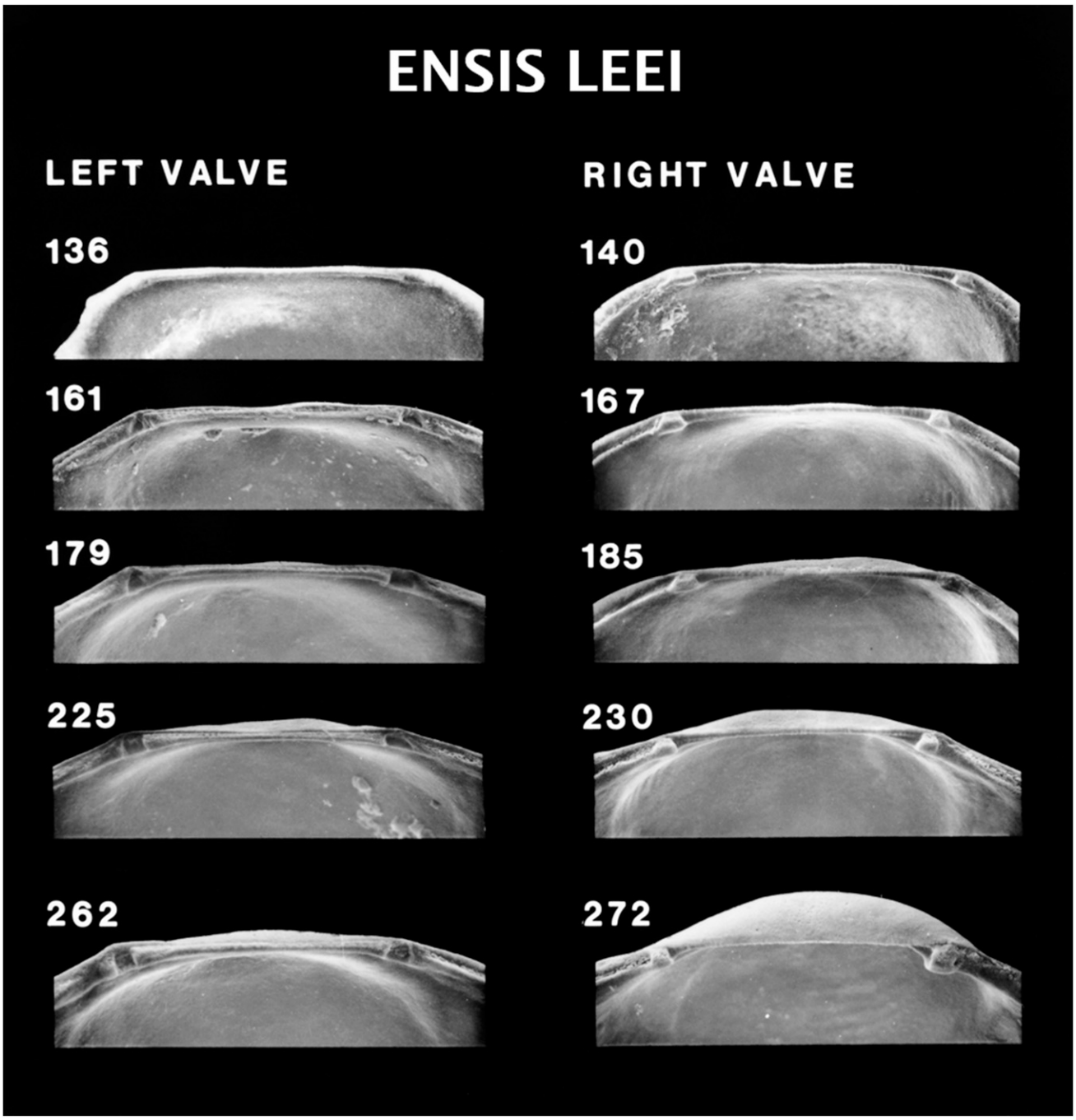

Figure 6. Scanning electron micrographs of the hinge of disarticulated shell valves of *Ensis leei* larvae seen in Figure 5. Numbers indicate the maximum linear shell dimension in micrometers.

Downloaded From: https://bioone.org/journals/Journal-of-Shellfish-Research on 25 Feb 2020
Terms of Use: https://bioone.org/terms-of-use Access provided by IFREMER

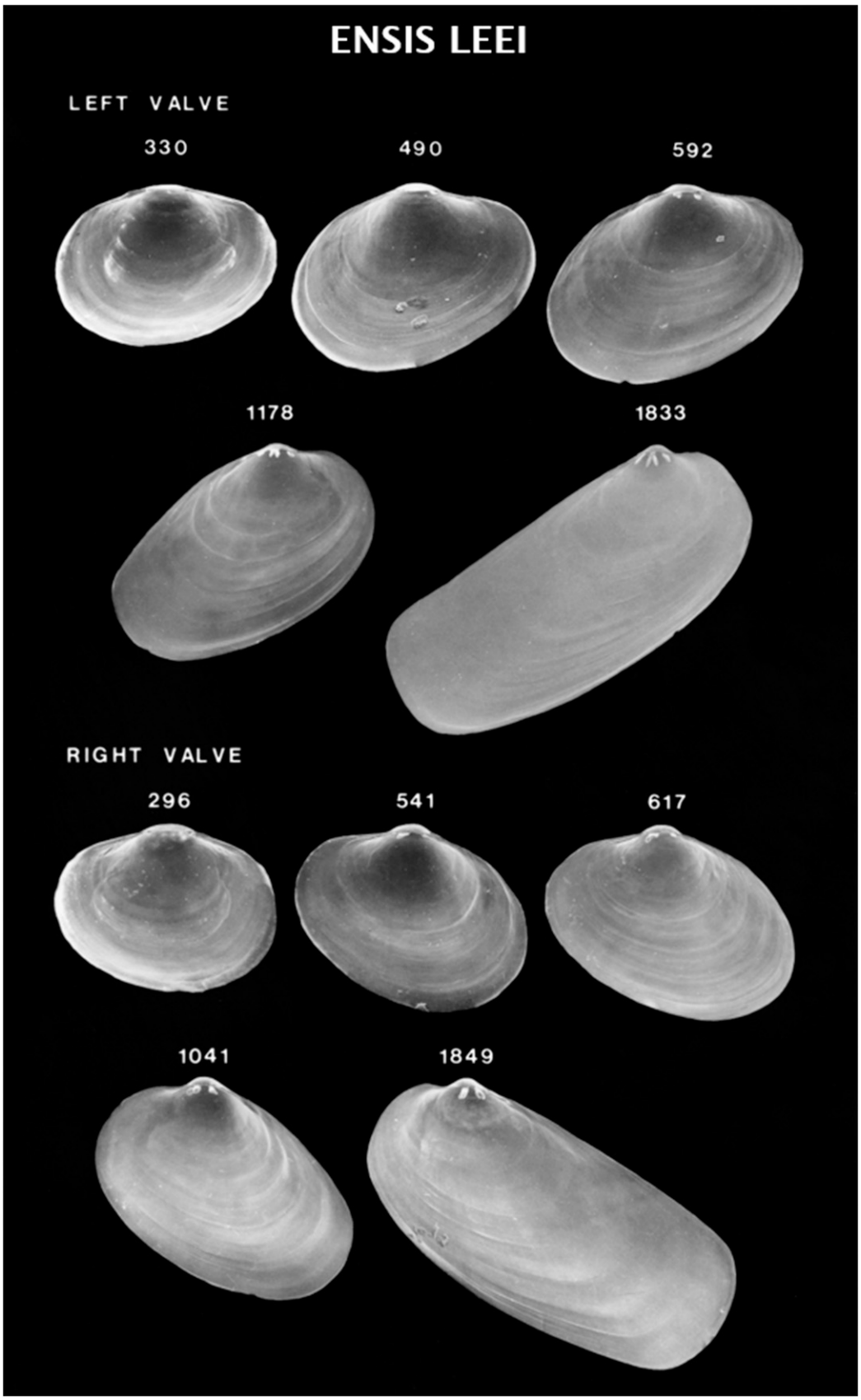

Figure 7. Scanning electron micrographs of disarticulated shell valves of *Ensis leei* postlarvae. Numbers indicate the maximum linear shell dimension in micrometers.

Downloaded From: https://bioone.org/journals/Journal-of-Shellfish-Research on 25 Feb 2020
Terms of Use: https://bioone.org/terms-of-use Access provided by IFREMER

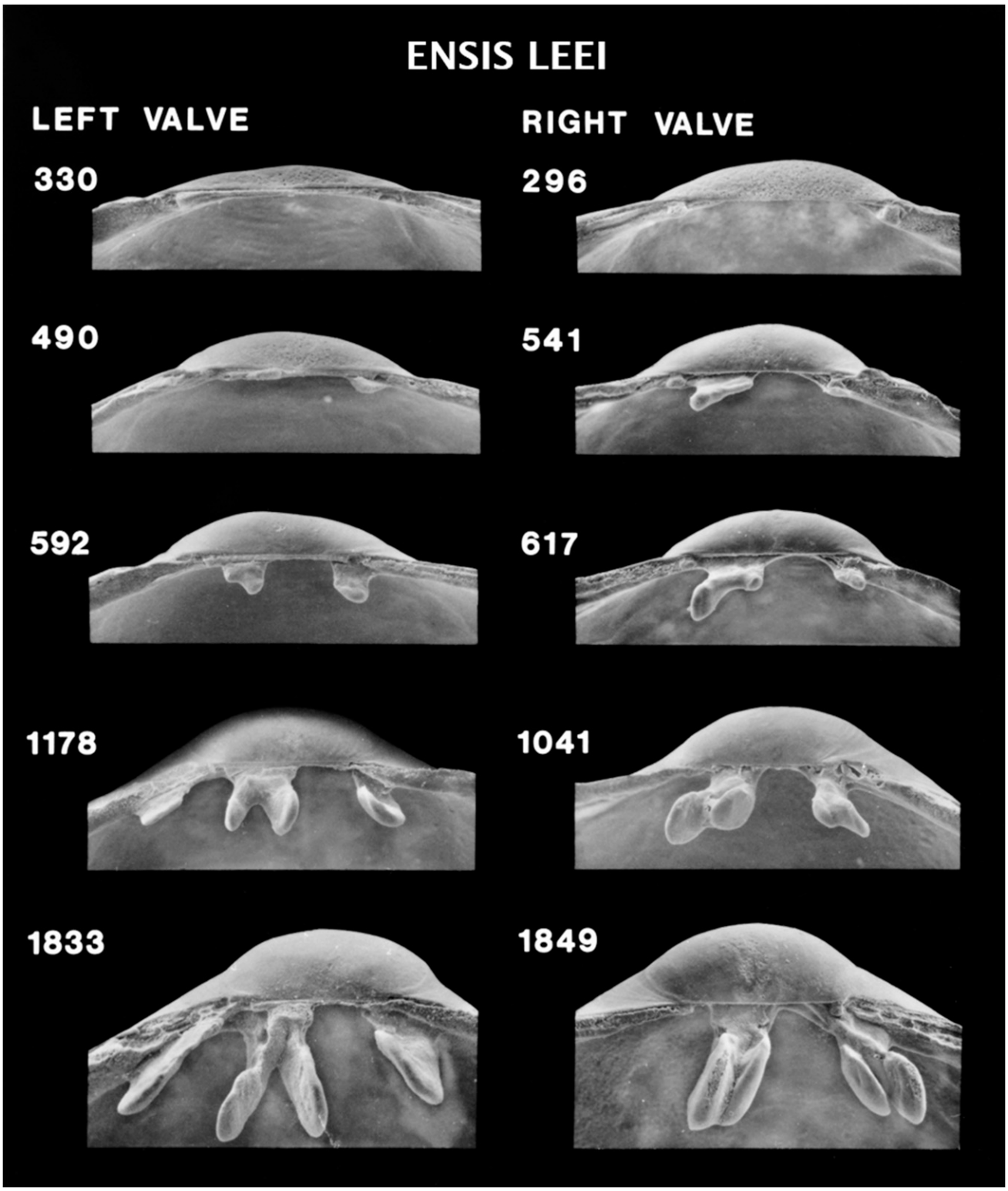

Figure 8. Scanning electron micrographs of the hinge of disarticulated shell valves of *Ensis leei* postlarvae seen in Figure 7. Numbers indicate the maximum linear shell dimension in micrometers.

Downloaded From: https://bioone.org/journals/Journal-of-Shellfish-Research on 25 Feb 2020
Terms of Use: https://bioone.org/terms-of-use Access provided by IFREMER

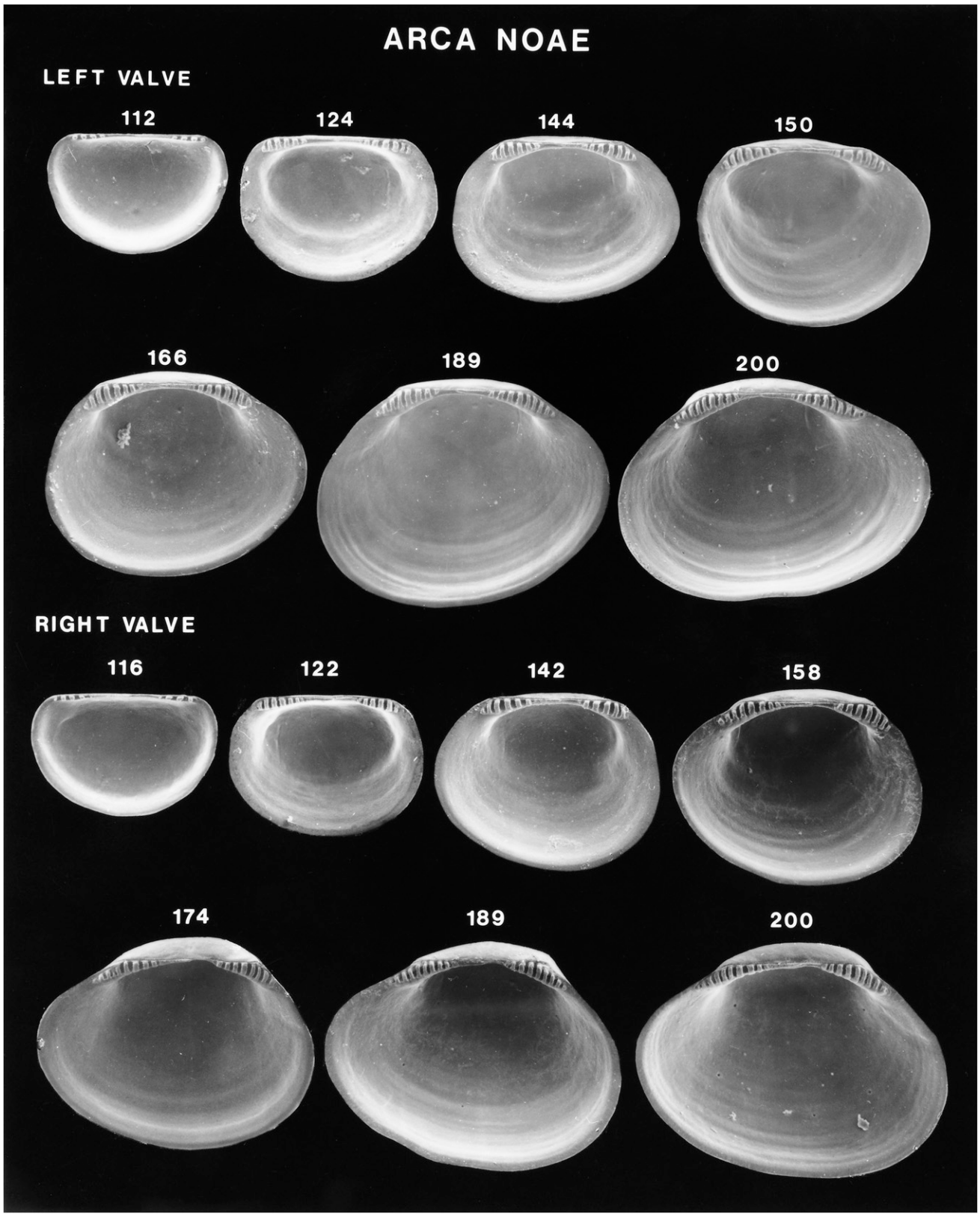

Figure 9. Scanning electron micrographs of disarticulated shell valves of *Arca noae* larvae. Numbers indicate the maximum linear shell dimension in micrometers.

Downloaded From: https://bioone.org/journals/Journal-of-Shellfish-Research on 25 Feb 2020
Terms of Use: https://bioone.org/terms-of-use Access provided by IFREMER

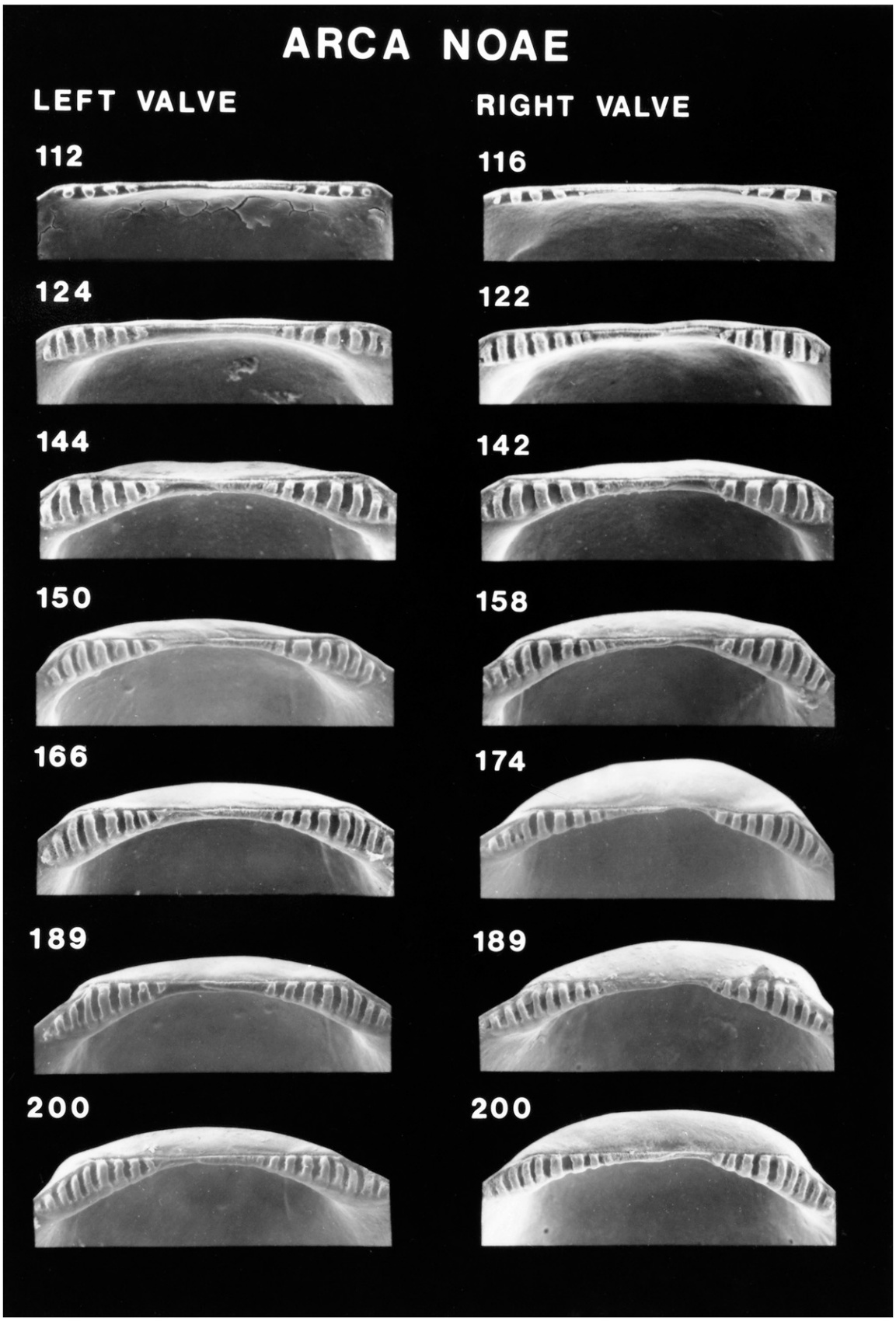

Figure 10. Scanning electron micrographs of the hinge of disarticulated shell valves of *Arca noae* larvae seen in Figure 9. Numbers indicate the maximum linear shell dimension in micrometers.

Downloaded From: https://bioone.org/journals/Journal-of-Shellfish-Research on 25 Feb 2020
Terms of Use: https://bioone.org/terms-of-use Access provided by IFREMER

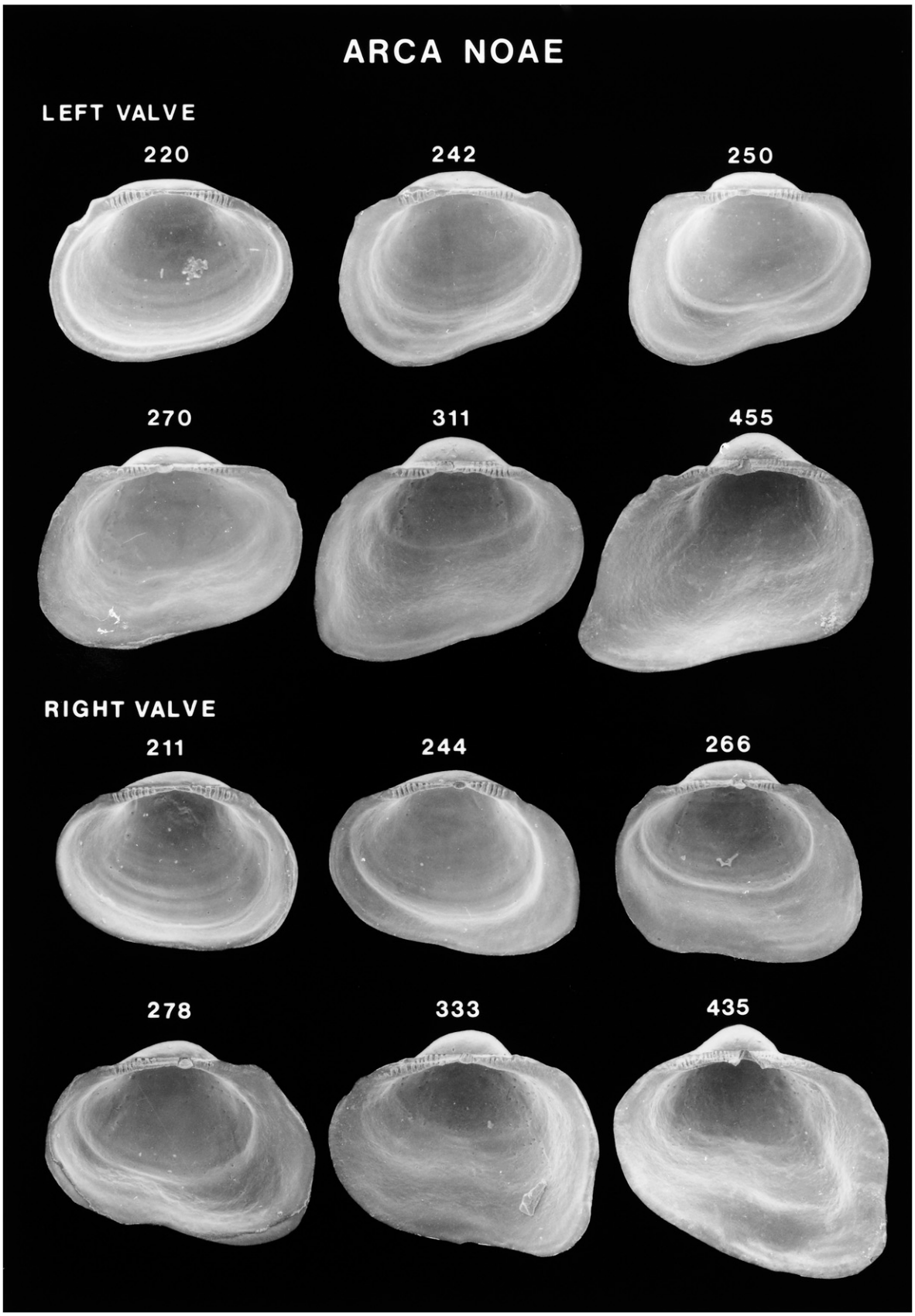

Figure 11. Scanning electron micrographs of disarticulated shell valves of *Arca noae* postlarvae. Numbers indicate the maximum linear shell dimension in micrometers.

Downloaded From: https://bioone.org/journals/Journal-of-Shellfish-Research on 25 Feb 2020
Terms of Use: https://bioone.org/terms-of-use Access provided by IFREMER

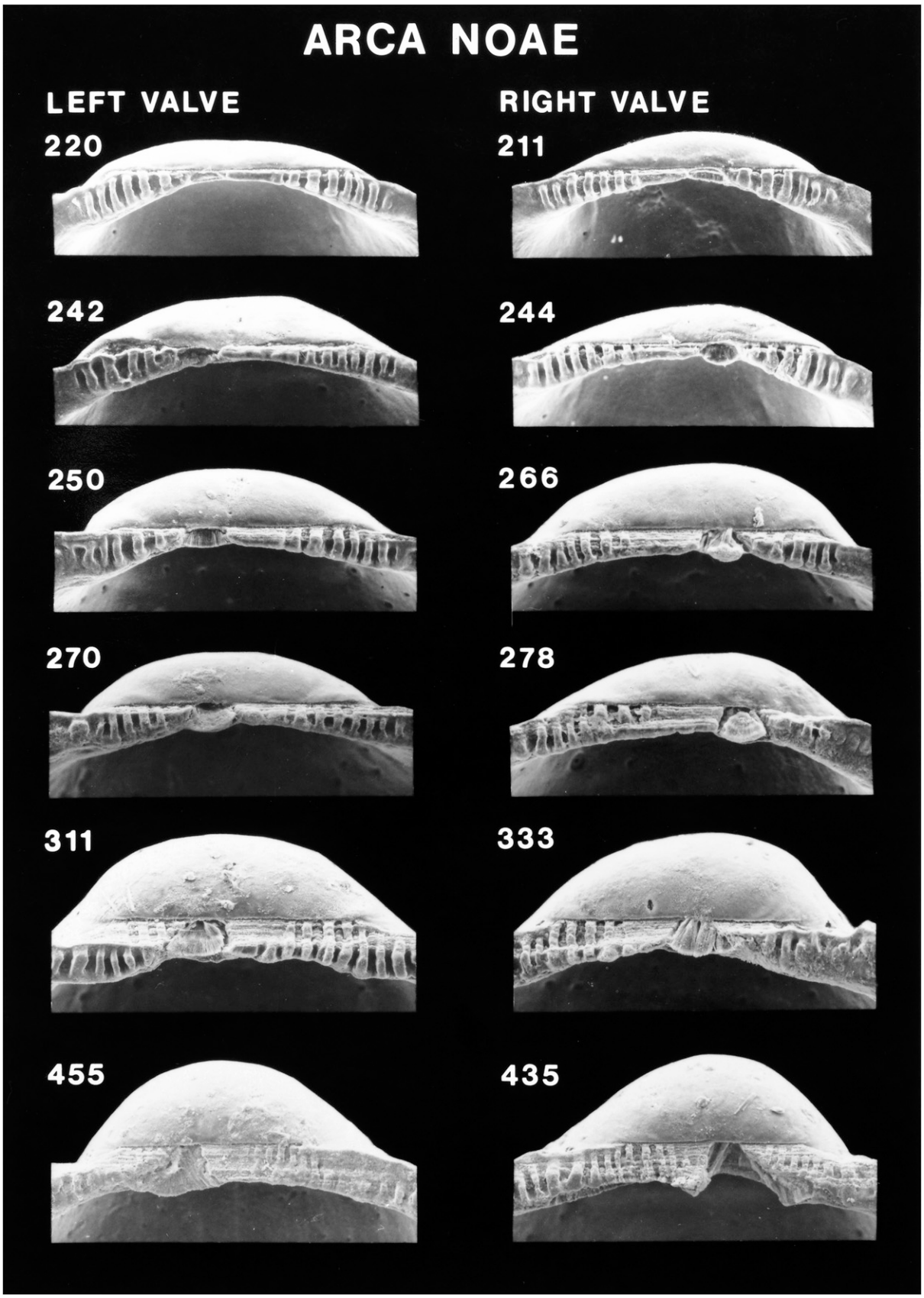

Figure 12. Scanning electron micrographs of the hinge of disarticulated shell valves of *Arca noae* postlarvae seen in Figure 11. Numbers indicate the maximum linear shell dimension in micrometers.

Downloaded From: https://bioone.org/journals/Journal-of-Shellfish-Research on 25 Feb 2020
Terms of Use: https://bioone.org/terms-of-use Access provided by IFREMER

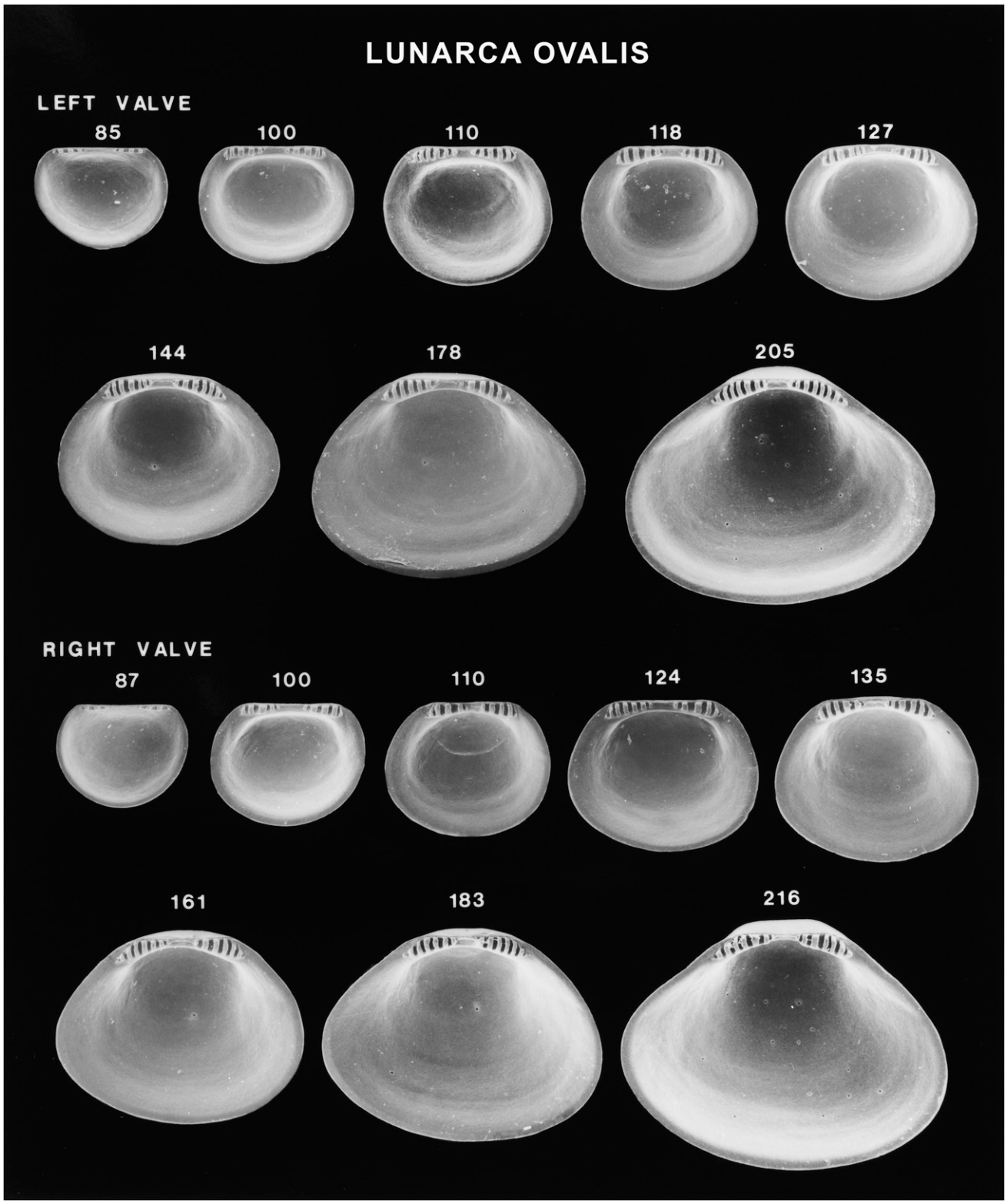

Figure 13. Scanning electron micrographs of disarticulated shell valves of *Lunarca ovalis* larvae. Numbers indicate the maximum linear shell dimension in micrometers.

Downloaded From: https://bioone.org/journals/Journal-of-Shellfish-Research on 25 Feb 2020
Terms of Use: https://bioone.org/terms-of-use Access provided by IFREMER

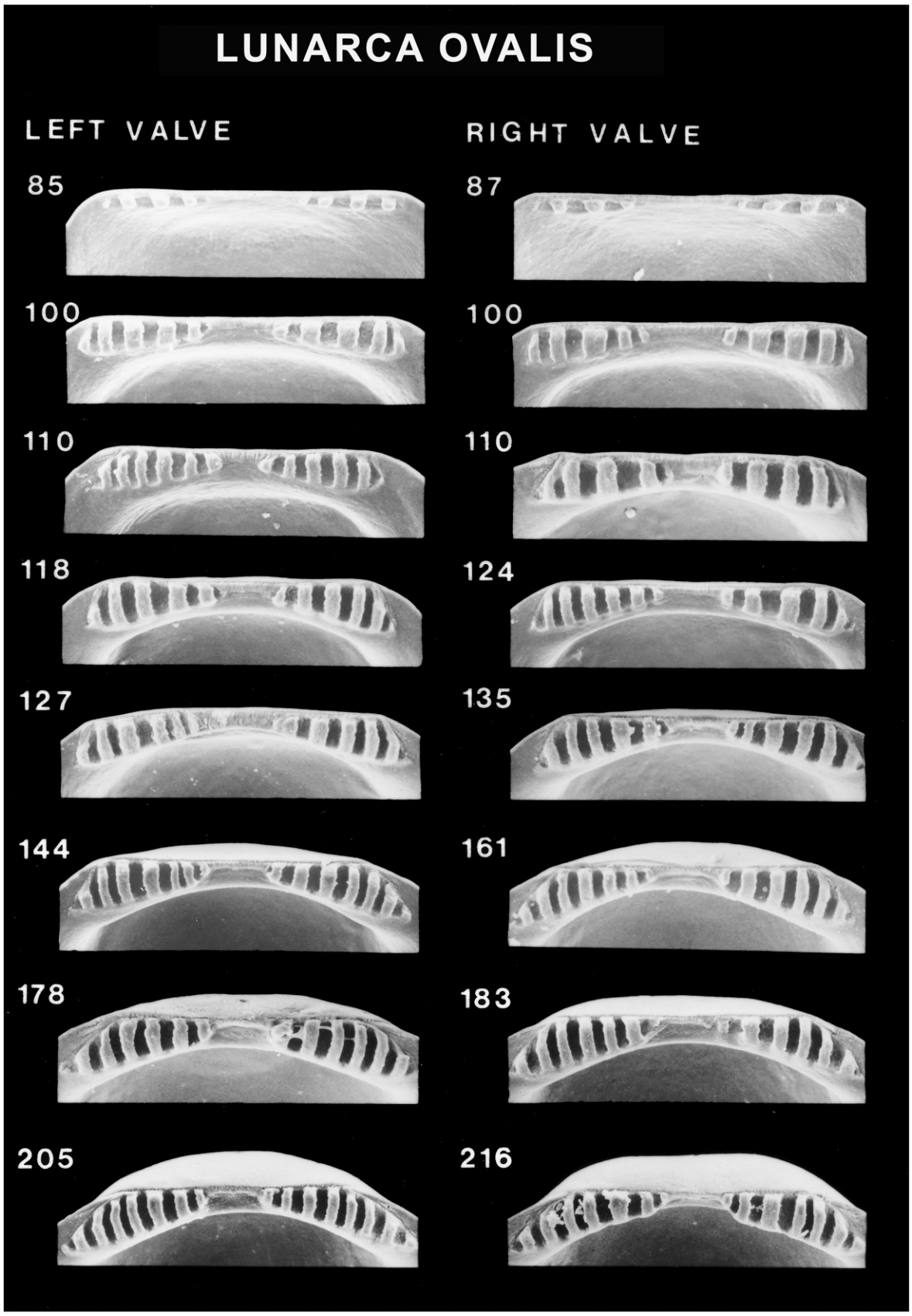

Figure 14. Scanning electron micrographs of the hinge of disarticulated shell valves of *Lunarca ovalis* larvae seen in Figure 13. Numbers indicate the maximum linear shell dimension in micrometers.

Downloaded From: https://bioone.org/journals/Journal-of-Shellfish-Research on 25 Feb 2020
Terms of Use: https://bioone.org/terms-of-use Access provided by IFREMER

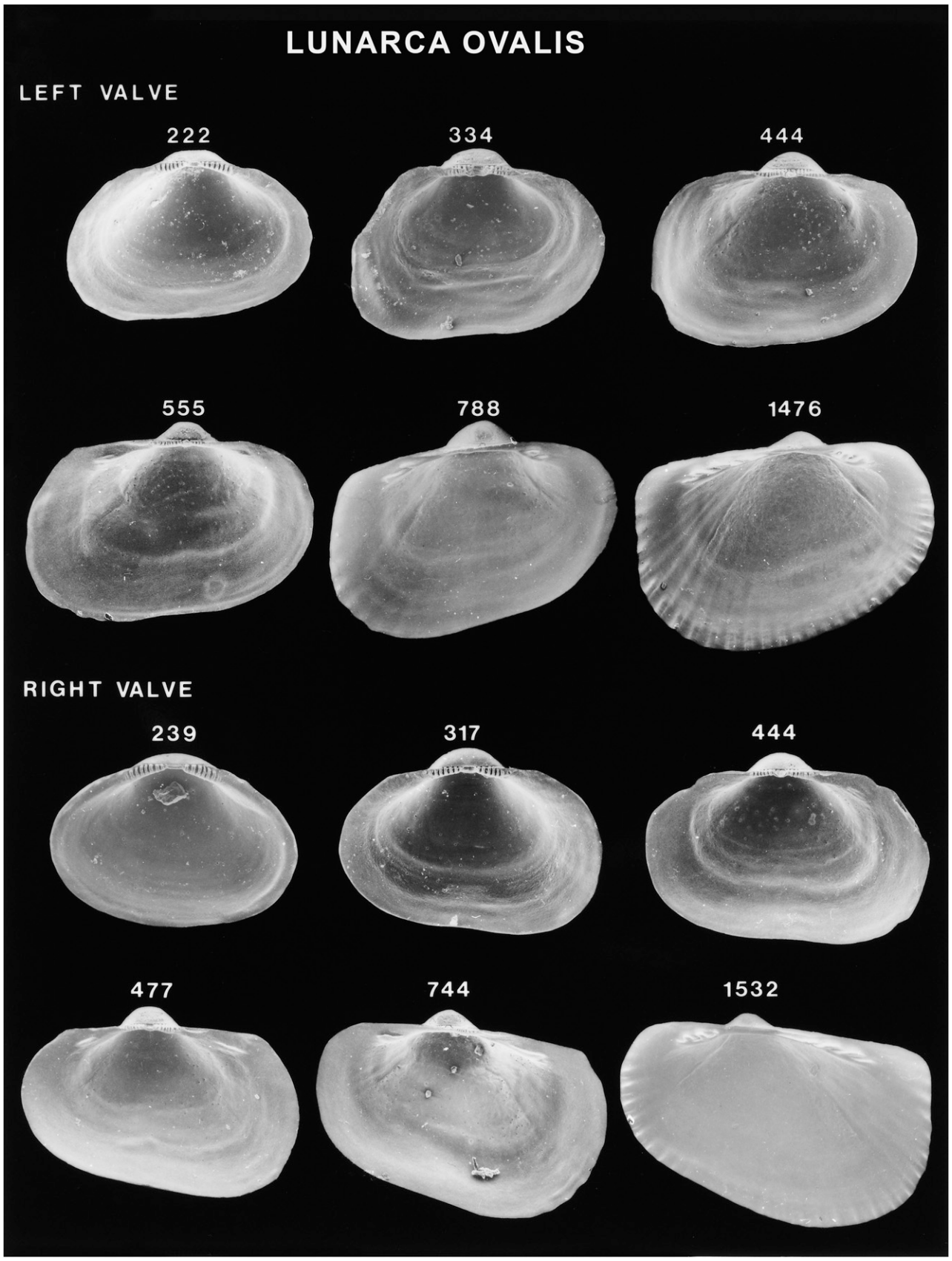

Figure 15. Scanning electron micrographs of disarticulated shell valves of *Lunarca ovalis* postlarvae. Numbers indicate the maximum linear shell dimension in micrometers.

Downloaded From: https://bioone.org/journals/Journal-of-Shellfish-Research on 25 Feb 2020
Terms of Use: https://bioone.org/terms-of-use Access provided by IFREMER

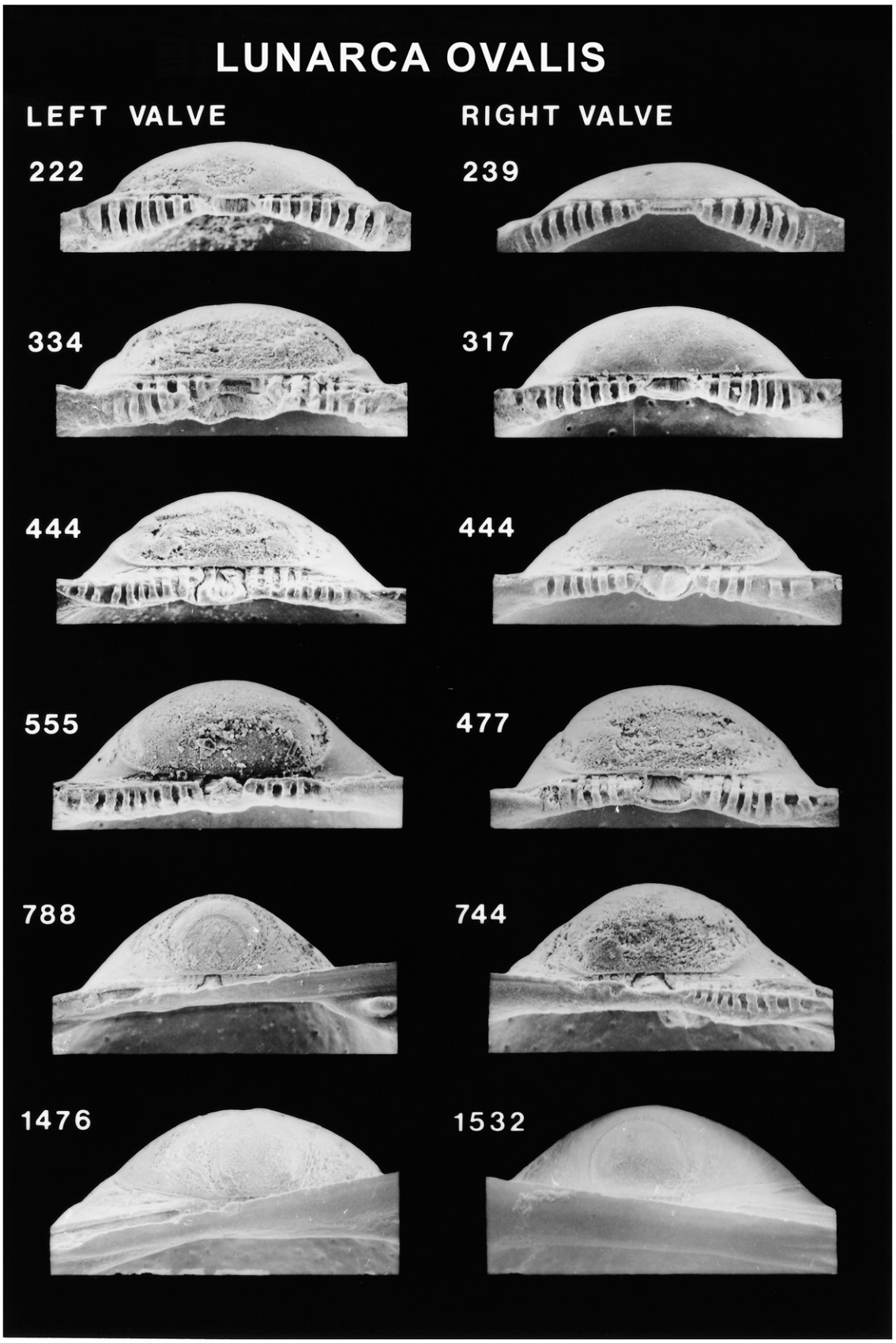

Figure 16. Scanning electron micrographs of the hinge of disarticulated shell valves of *Lunarca ovalis* postlarvae seen in Figure 15. Numbers indicate the maximum linear shell dimension in micrometers.

Downloaded From: https://bioone.org/journals/Journal-of-Shellfish-Research on 25 Feb 2020
Terms of Use: https://bioone.org/terms-of-use Access provided by IFREMER

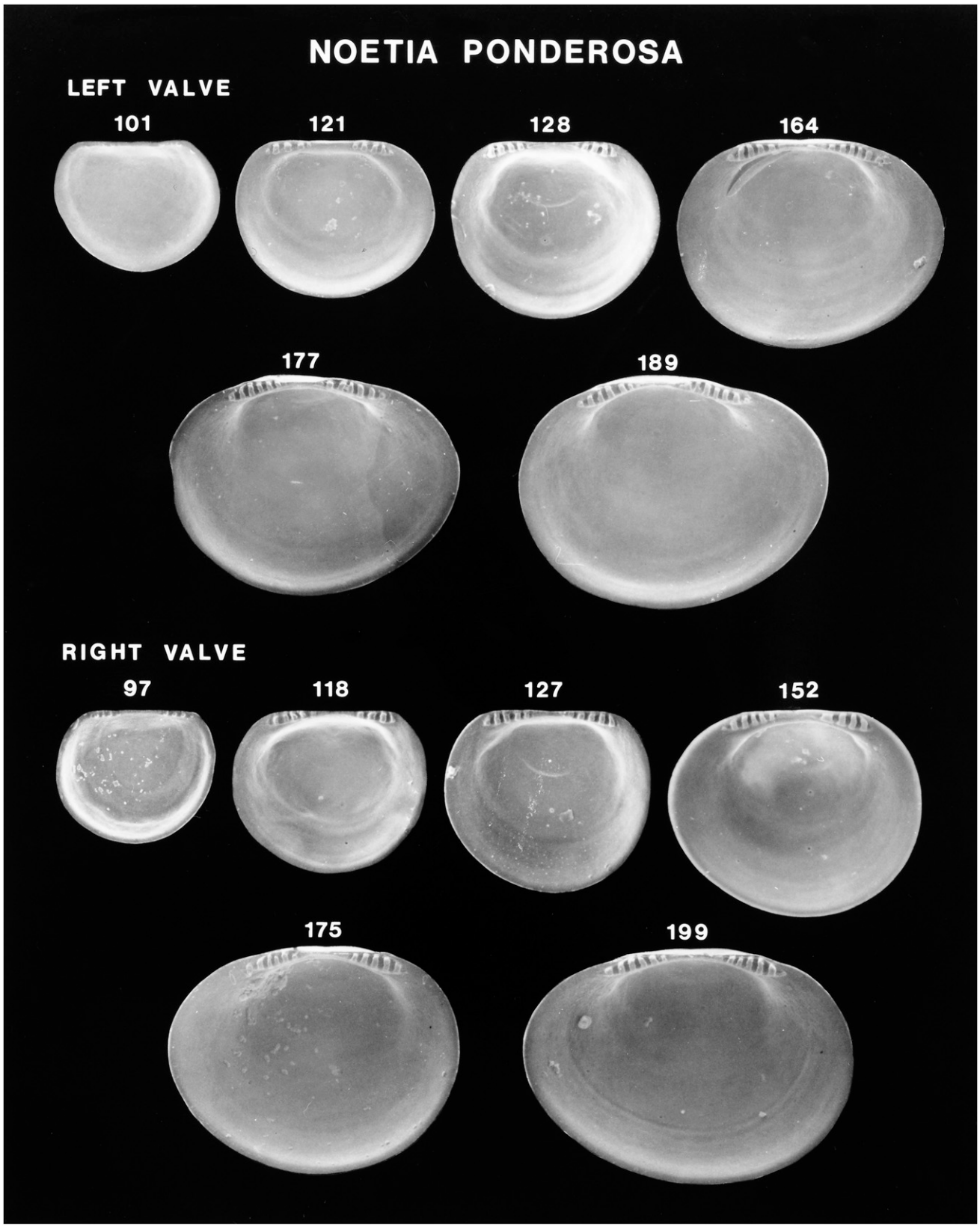

Figure 17. Scanning electron micrographs of disarticulated shell valves of *Noetia ponderosa* larvae. Numbers indicate the maximum linear shell dimension in micrometers.

Downloaded From: https://bioone.org/journals/Journal-of-Shellfish-Research on 25 Feb 2020
Terms of Use: https://bioone.org/terms-of-use Access provided by IFREMER

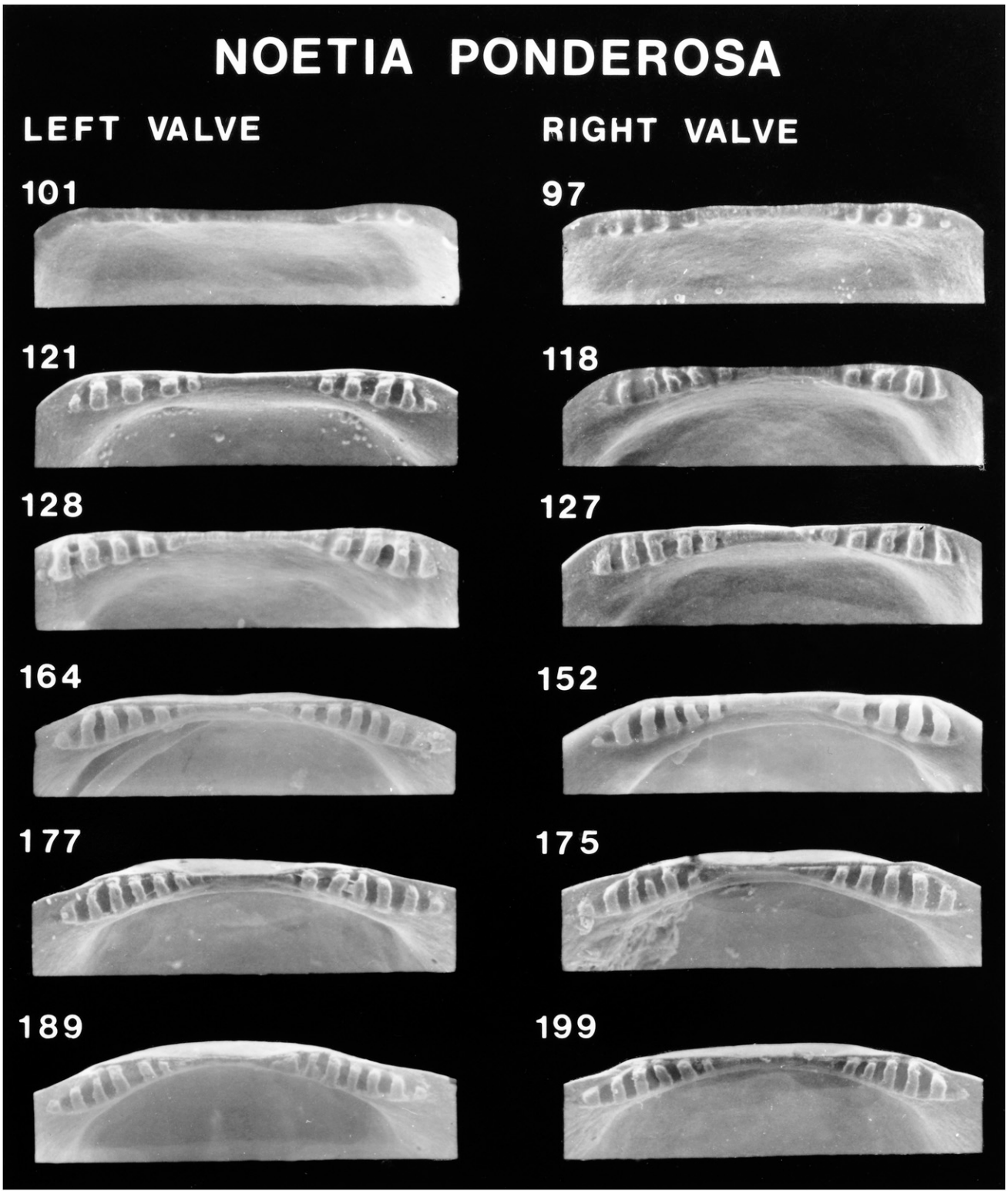

Figure 18. Scanning electron micrographs of the hinge of disarticulated shell valves of *Noetia ponderosa* larvae seen in Figure 17. Numbers indicate the maximum linear shell dimension in micrometers.

Downloaded From: https://bioone.org/journals/Journal-of-Shellfish-Research on 25 Feb 2020
Terms of Use: https://bioone.org/terms-of-use Access provided by IFREMER

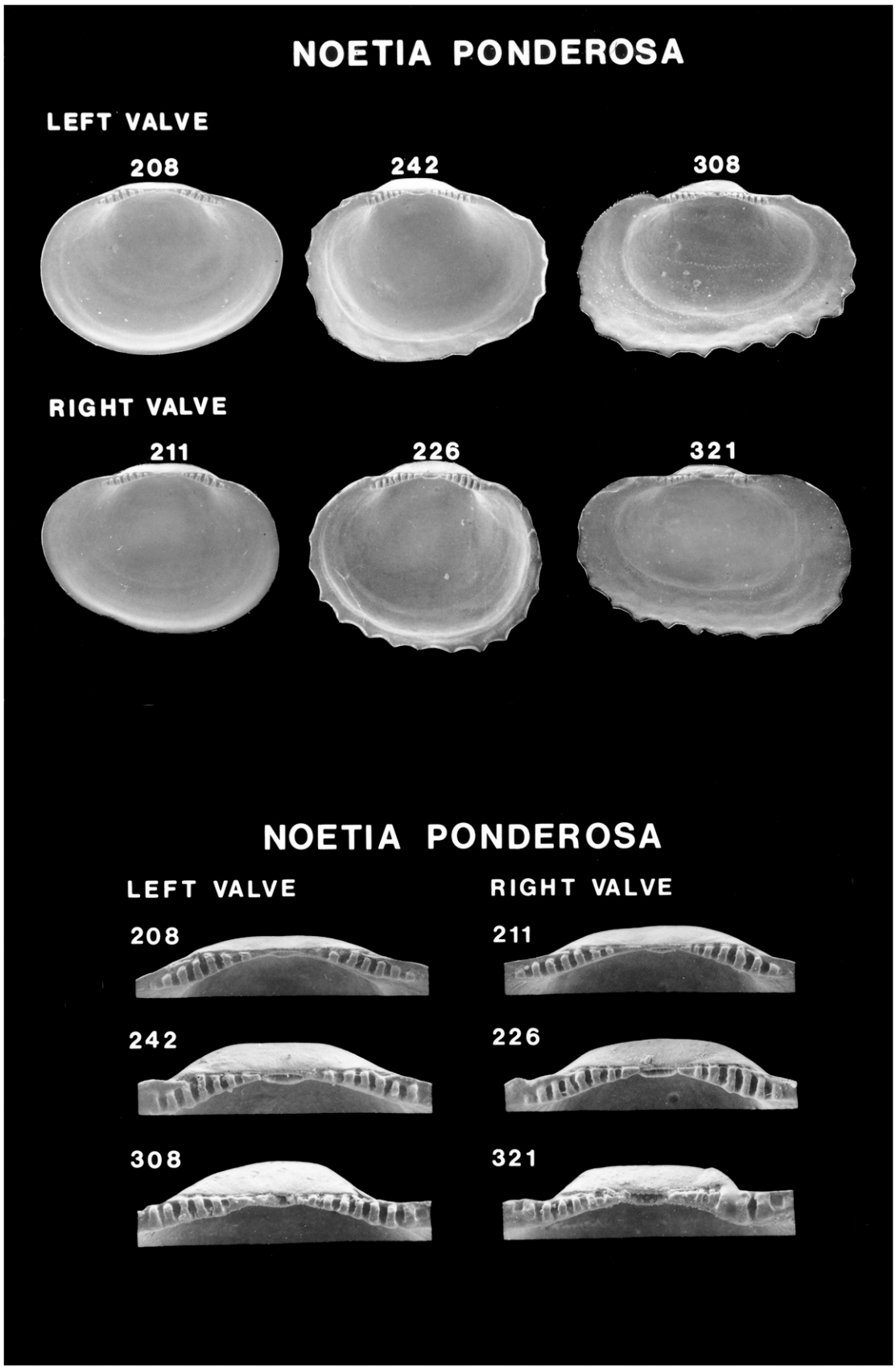

Figure 19. Scanning electron micrographs of disarticulated shell valves of *Noetia ponderosa* postlarvae (top) and higher magnification scanning electron micrographs of the hinge of these shell valves (bottom). Numbers indicate the maximum linear shell dimension in micrometers.

Downloaded From: https://bioone.org/journals/Journal-of-Shellfish-Research on 25 Feb 2020
Terms of Use: https://bioone.org/terms-of-use Access provided by IFREMER

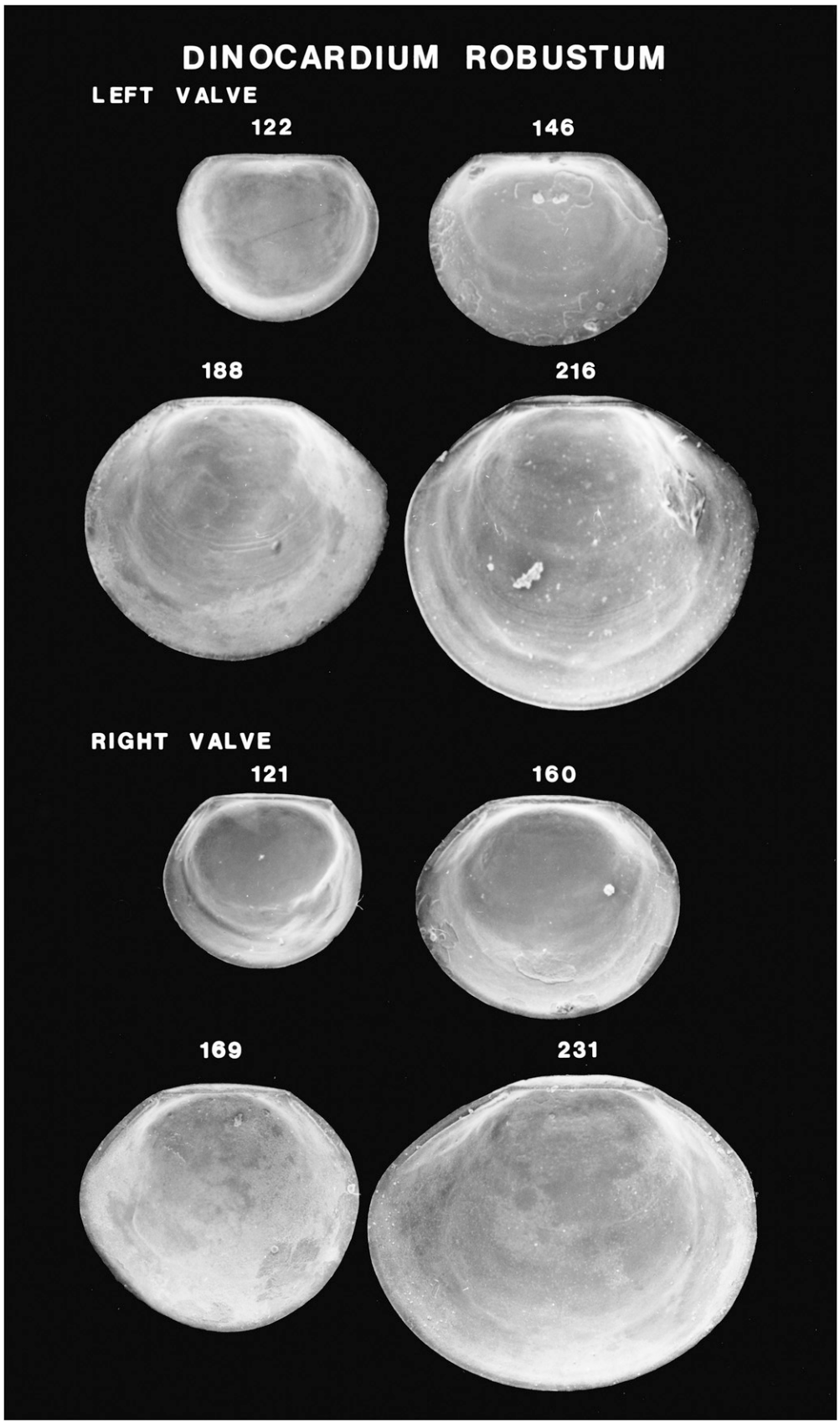

Figure 20. Scanning electron micrographs of disarticulated shell valves of *Dinocardium robustum* larvae. Numbers indicate the maximum linear shell dimension in micrometers.

Downloaded From: https://bioone.org/journals/Journal-of-Shellfish-Research on 25 Feb 2020
Terms of Use: https://bioone.org/terms-of-use Access provided by IFREMER

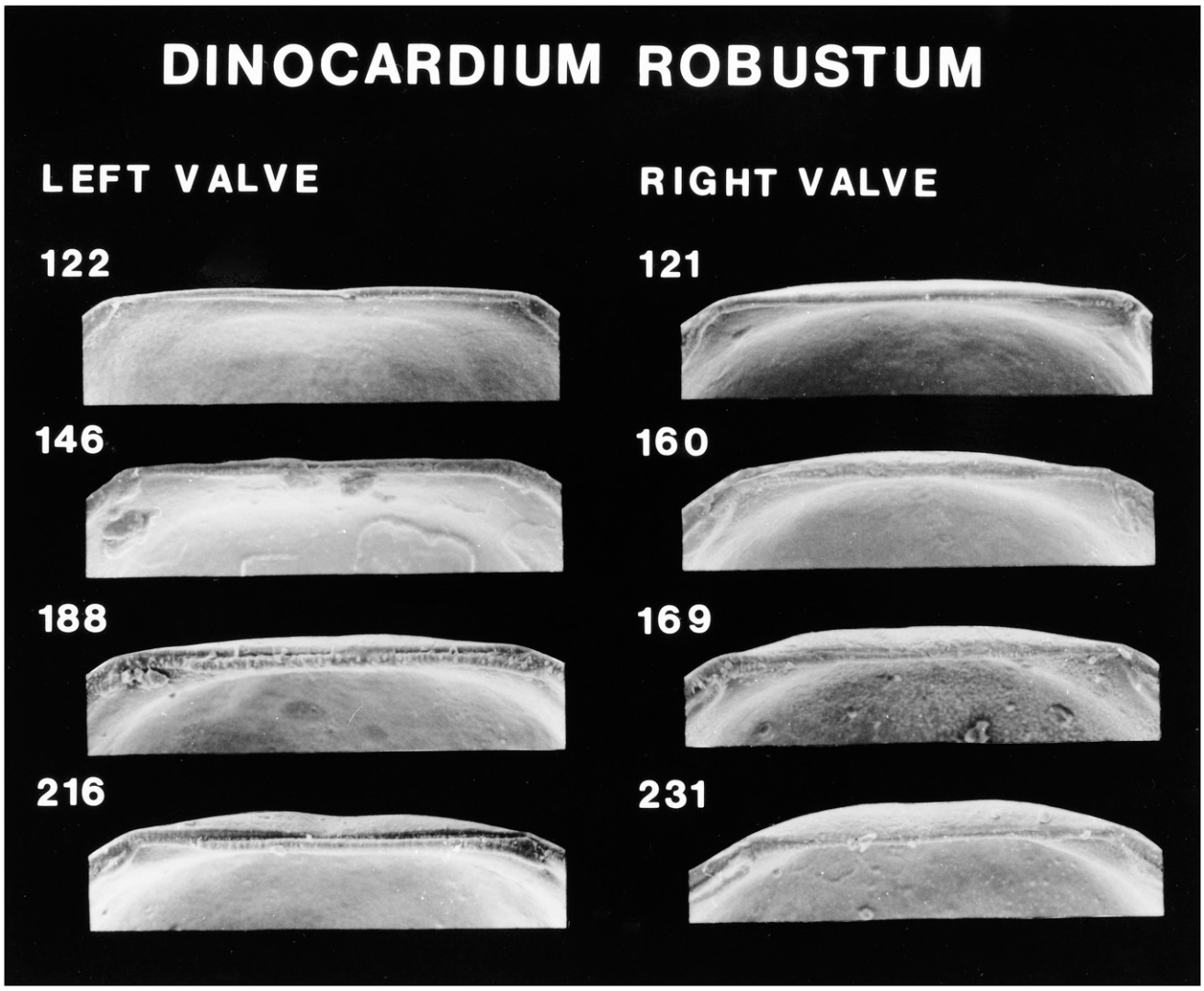

Figure 21. Scanning electron micrographs of the hinge of disarticulated shell valves of *Dinocardium robustum* larvae seen in Figure 20. Numbers indicate the maximum linear shell dimension in micrometers.

Downloaded From: https://bioone.org/journals/Journal-of-Shellfish-Research on 25 Feb 2020
Terms of Use: https://bioone.org/terms-of-use Access provided by IFREMER

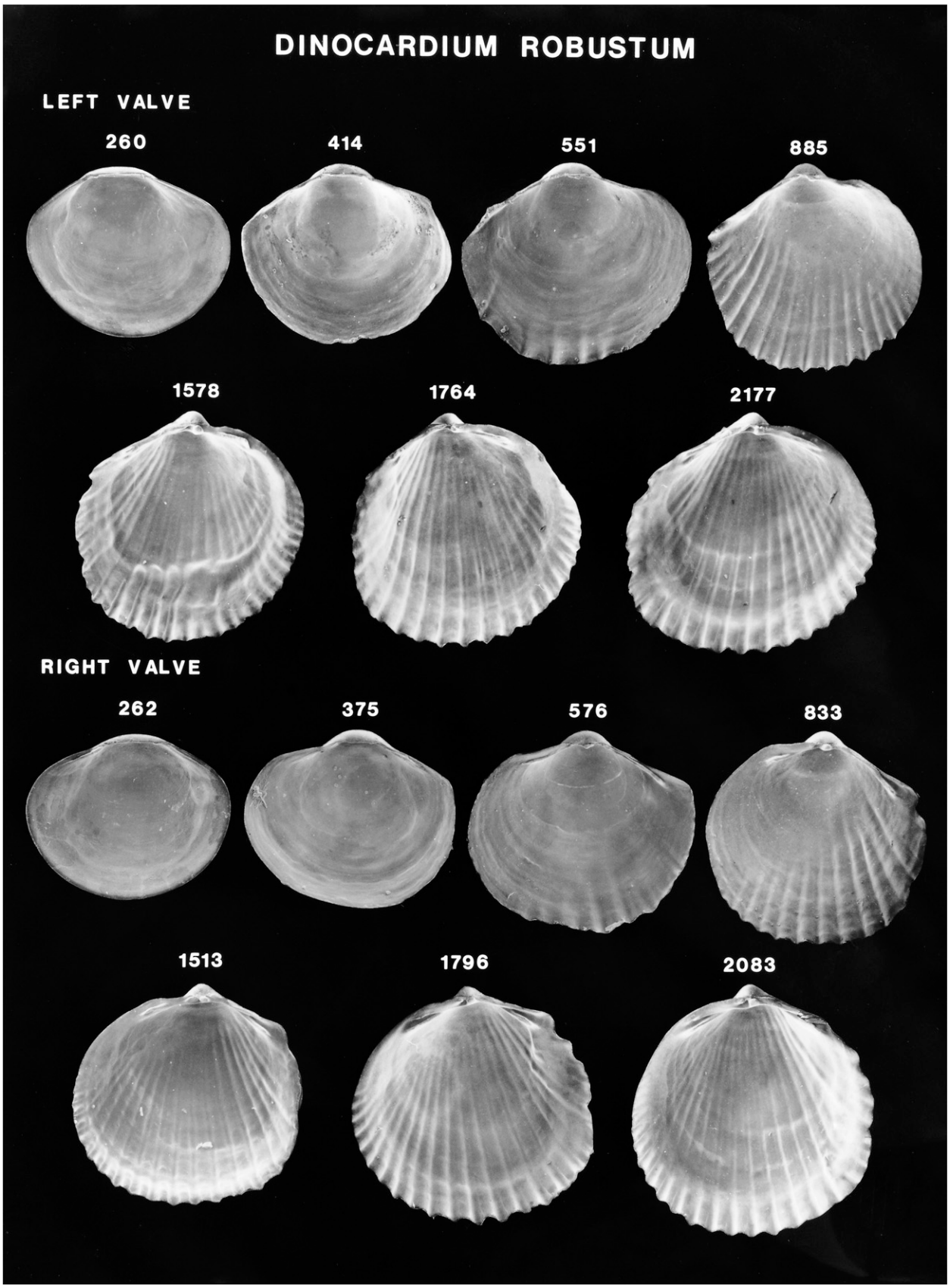

Figure 22. Scanning electron micrographs of disarticulated shell valves of *Dinocardium robustum* postlarvae. Numbers indicate the maximum linear shell dimension in micrometers.

Downloaded From: https://bioone.org/journals/Journal-of-Shellfish-Research on 25 Feb 2020
Terms of Use: https://bioone.org/terms-of-use Access provided by IFREMER

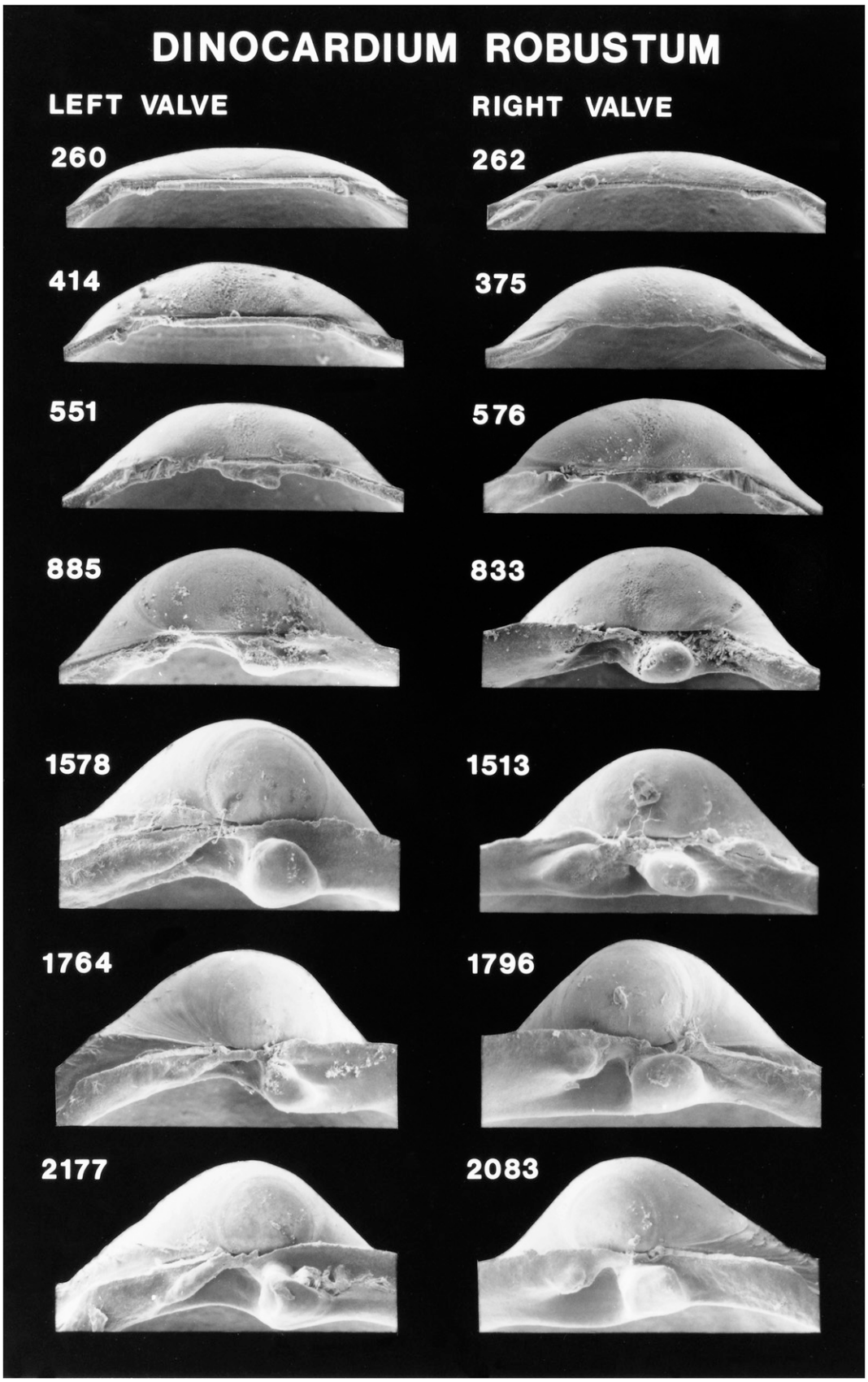

Figure 23. Scanning electron micrographs of the hinge of disarticulated shell valves of *Dinocardium robustum* postlarvae seen in Figure 22. Numbers indicate the maximum linear shell dimension in micrometers.

Downloaded From: https://bioone.org/journals/Journal-of-Shellfish-Research on 25 Feb 2020
Terms of Use: https://bioone.org/terms-of-use Access provided by IFREMER

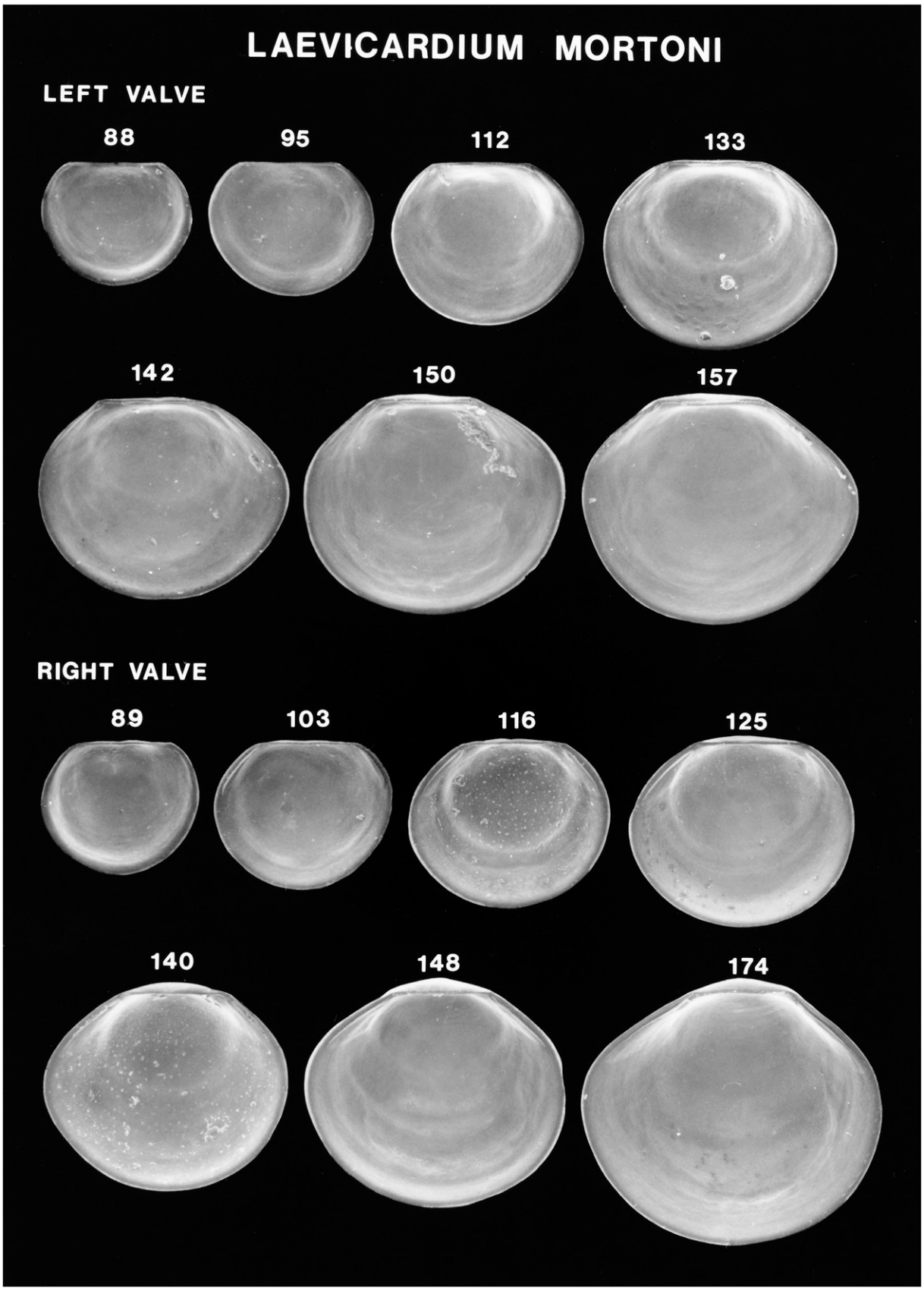

Figure 24. Scanning electron micrographs of disarticulated shell valves of *Laevicardium mortoni* larvae. Numbers indicate the maximum linear shell dimension in micrometers.

Downloaded From: https://bioone.org/journals/Journal-of-Shellfish-Research on 25 Feb 2020
Terms of Use: https://bioone.org/terms-of-use Access provided by IFREMER

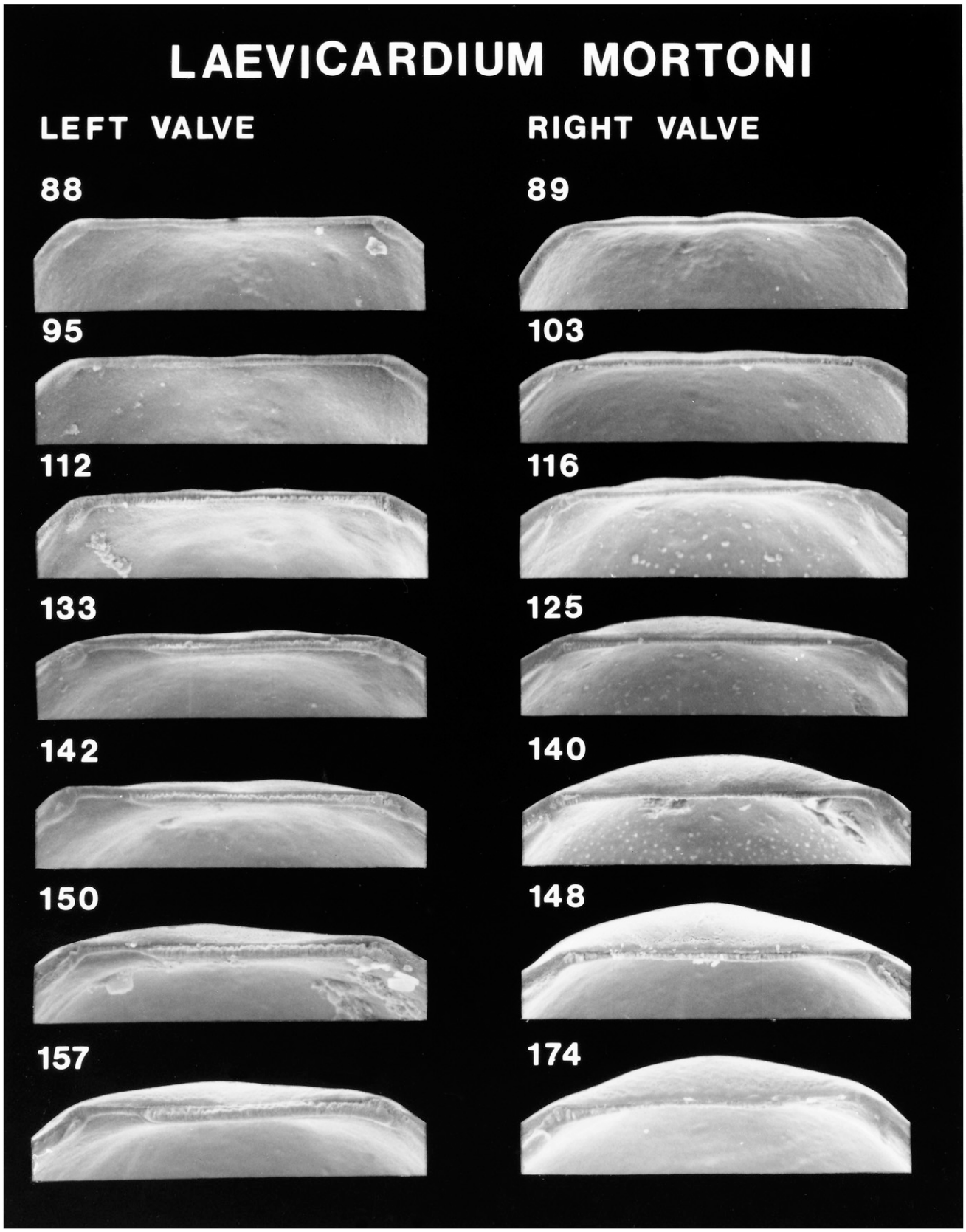

Figure 25. Scanning electron micrographs of the hinge of disarticulated shell valves of *Laevicardium mortoni* larvae seen in Figure 24. Numbers indicate the maximum linear shell dimension in micrometers.

Downloaded From: https://bioone.org/journals/Journal-of-Shellfish-Research on 25 Feb 2020
Terms of Use: https://bioone.org/terms-of-use Access provided by IFREMER

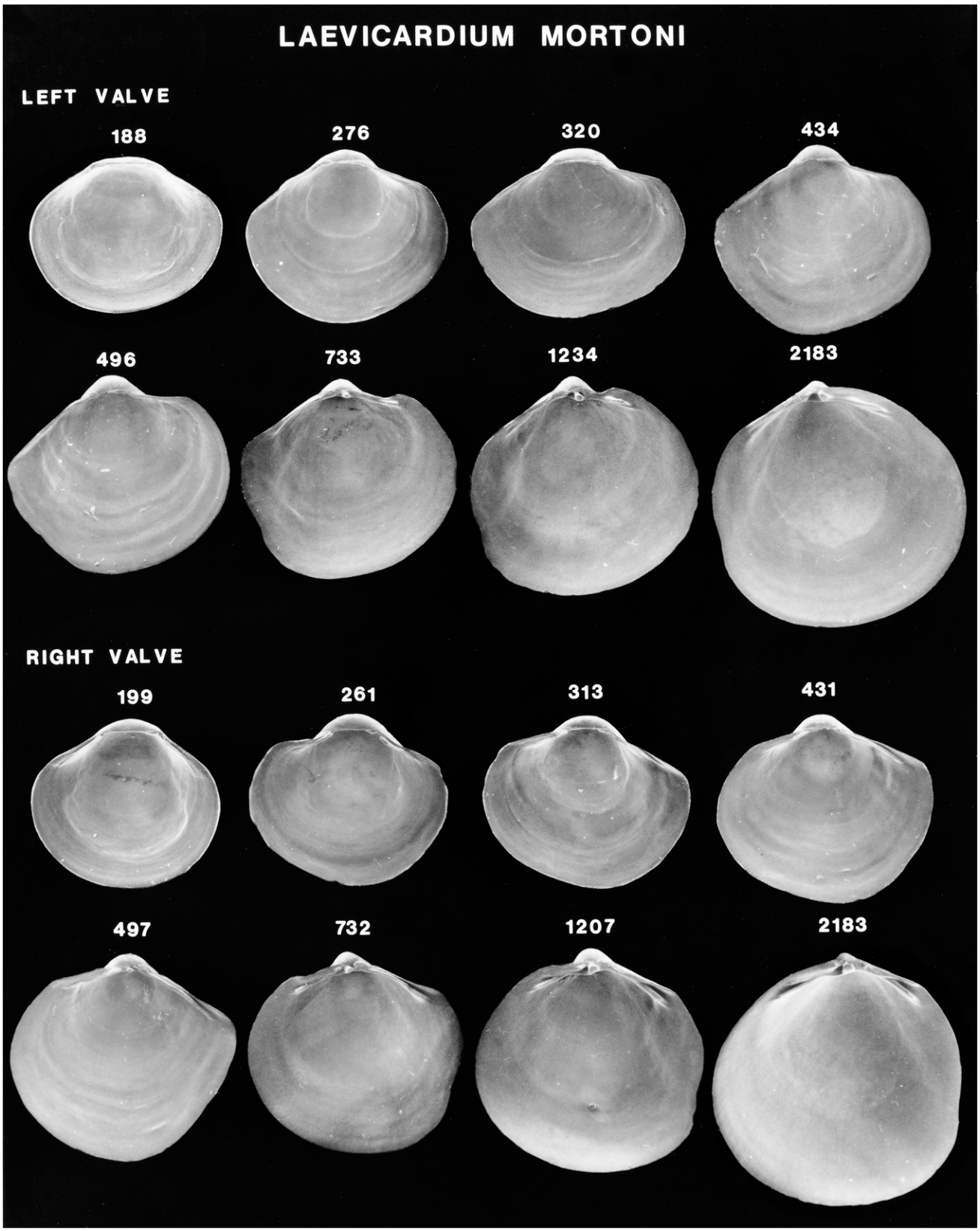

Figure 26. Scanning electron micrographs of disarticulated shell valves of *Laevicardium mortoni* postlarvae. Numbers indicate the maximum linear shell dimension in micrometers.

Downloaded From: https://bioone.org/journals/Journal-of-Shellfish-Research on 25 Feb 2020
Terms of Use: https://bioone.org/terms-of-use Access provided by IFREMER

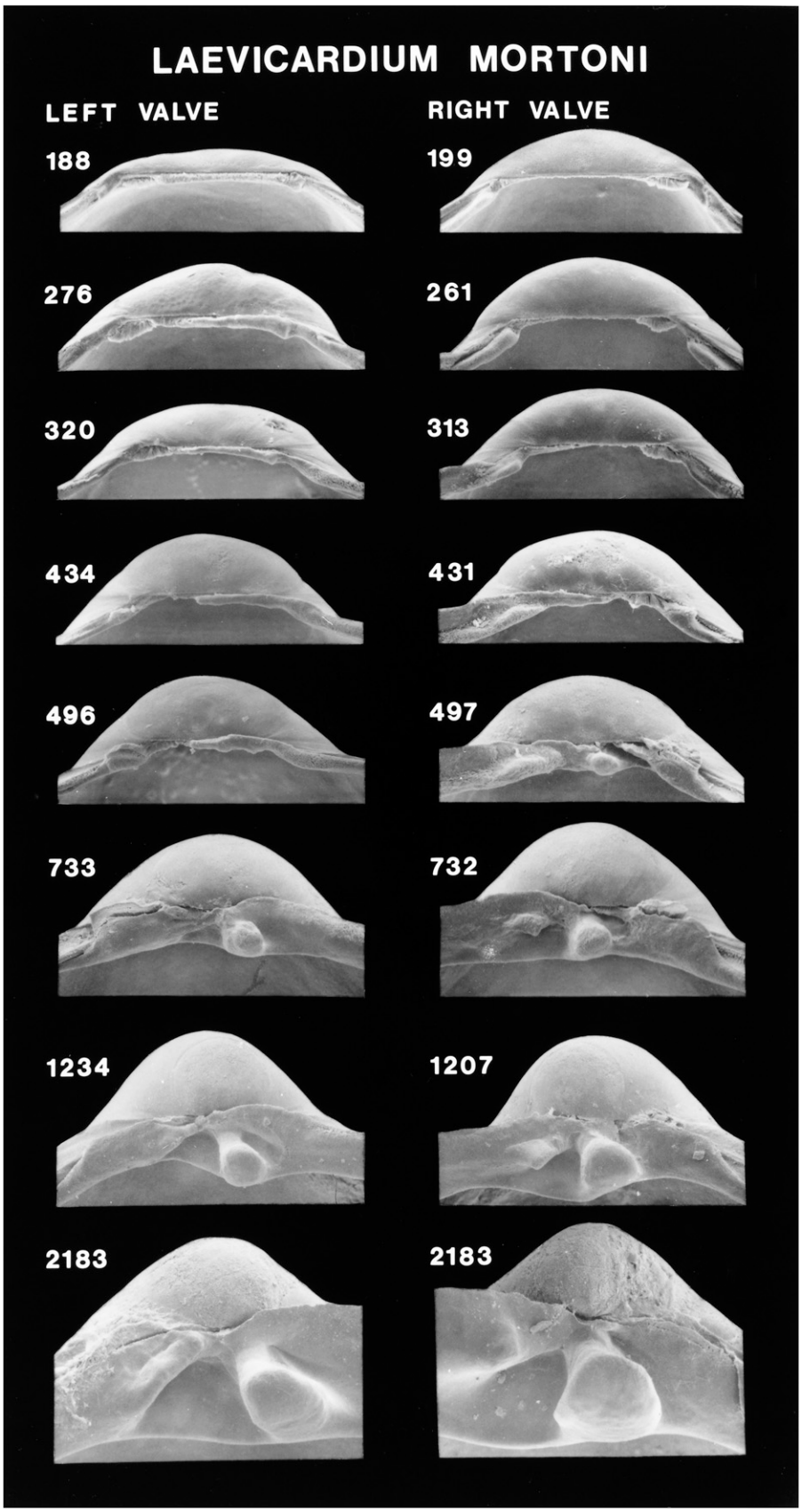

Figure 27. Scanning electron micrographs of the hinge of disarticulated shell valves of *Laevicardium mortoni* postlarvae seen in Figure 26. Numbers indicate the maximum linear shell dimension in micrometers.

Downloaded From: https://bioone.org/journals/Journal-of-Shellfish-Research on 25 Feb 2020
Terms of Use: https://bioone.org/terms-of-use Access provided by IFREMER

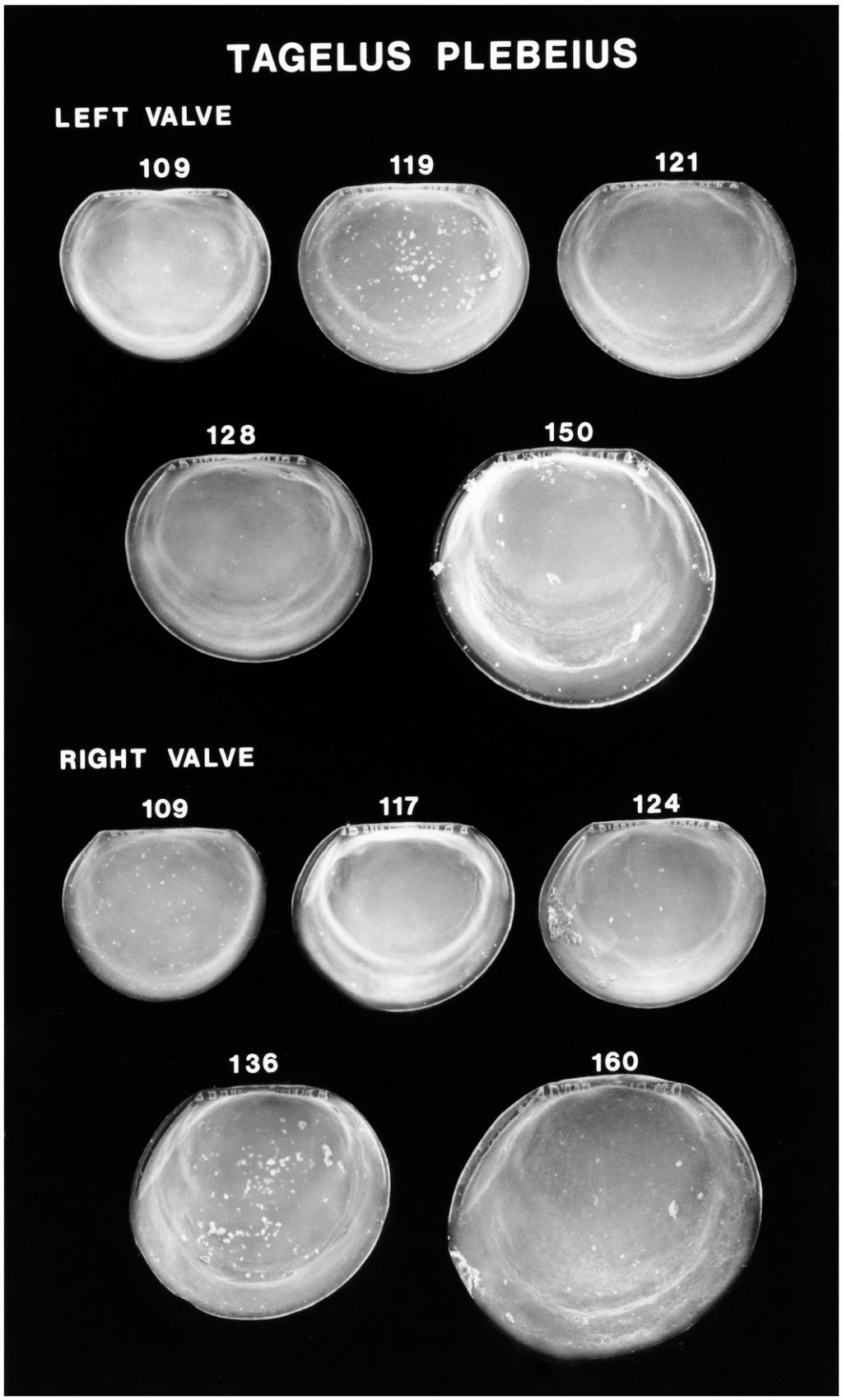

Figure 28. Scanning electron micrographs of disarticulated shell valves of *Tagelus plebeius* larvae. Numbers indicate the maximum linear shell dimension in micrometers.

Downloaded From: https://bioone.org/journals/Journal-of-Shellfish-Research on 25 Feb 2020
Terms of Use: https://bioone.org/terms-of-use Access provided by IFREMER

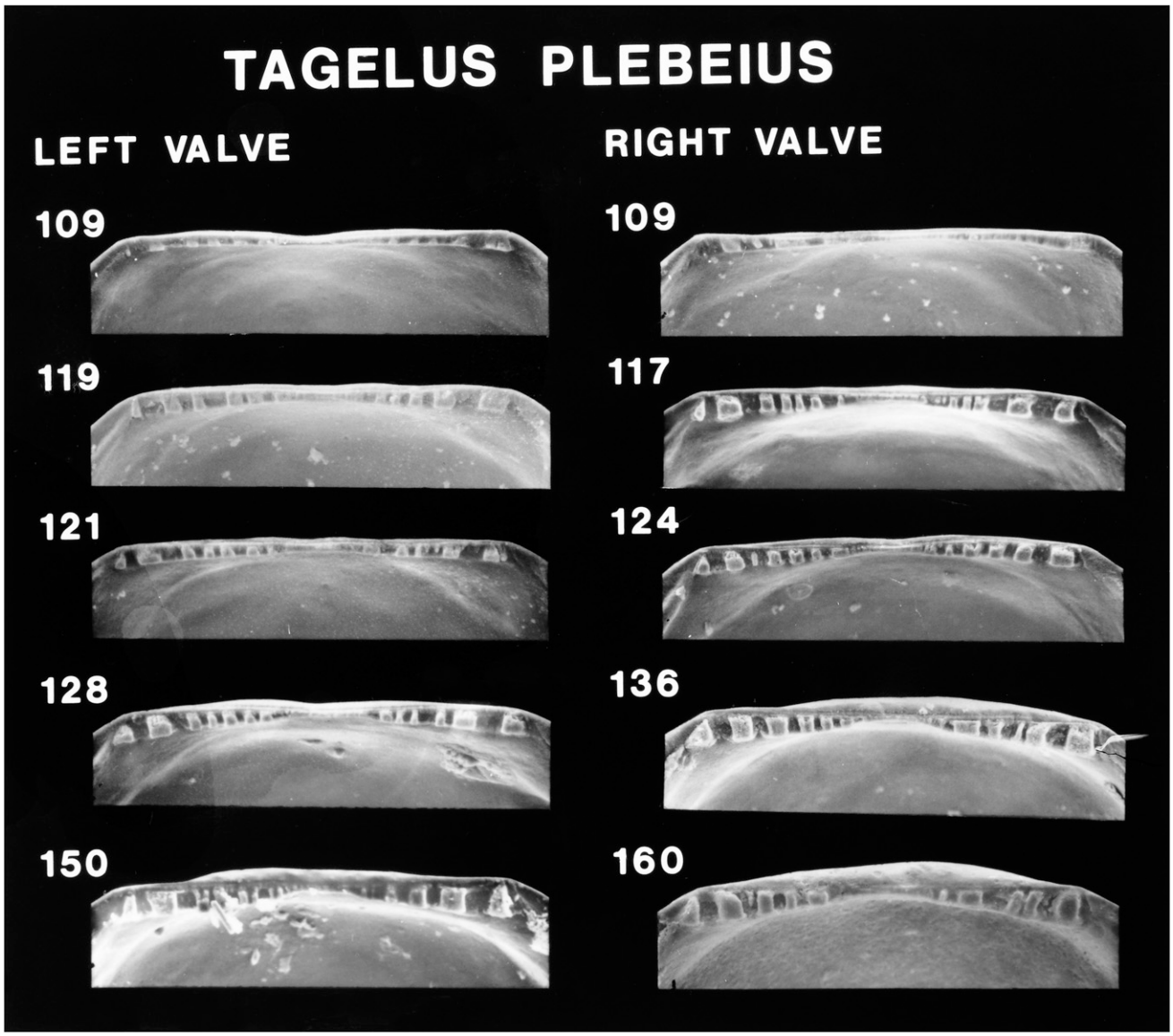

Figure 29. Scanning electron micrographs of the hinge of disarticulated shell valves of *Tagelus plebeius* larvae seen in Figure 28. Numbers indicate the maximum linear shell dimension in micrometers.

Downloaded From: https://bioone.org/journals/Journal-of-Shellfish-Research on 25 Feb 2020
Terms of Use: https://bioone.org/terms-of-use Access provided by IFREMER

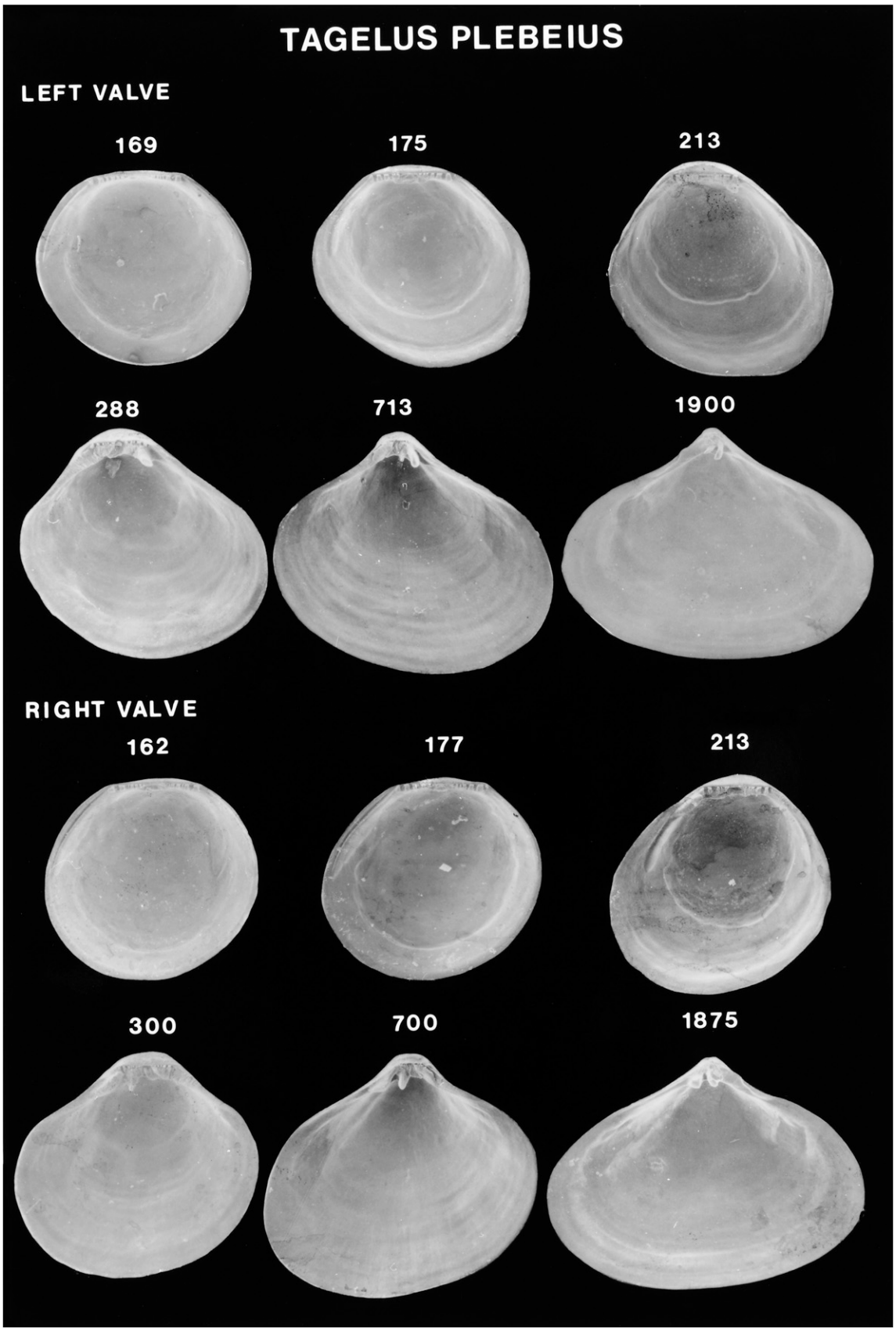

Figure 30. Scanning electron micrographs of disarticulated shell valves of *Tagelus plebeius* postlarvae. Numbers indicate the maximum linear shell dimension in micrometers.

Downloaded From: https://bioone.org/journals/Journal-of-Shellfish-Research on 25 Feb 2020
Terms of Use: https://bioone.org/terms-of-use Access provided by IFREMER

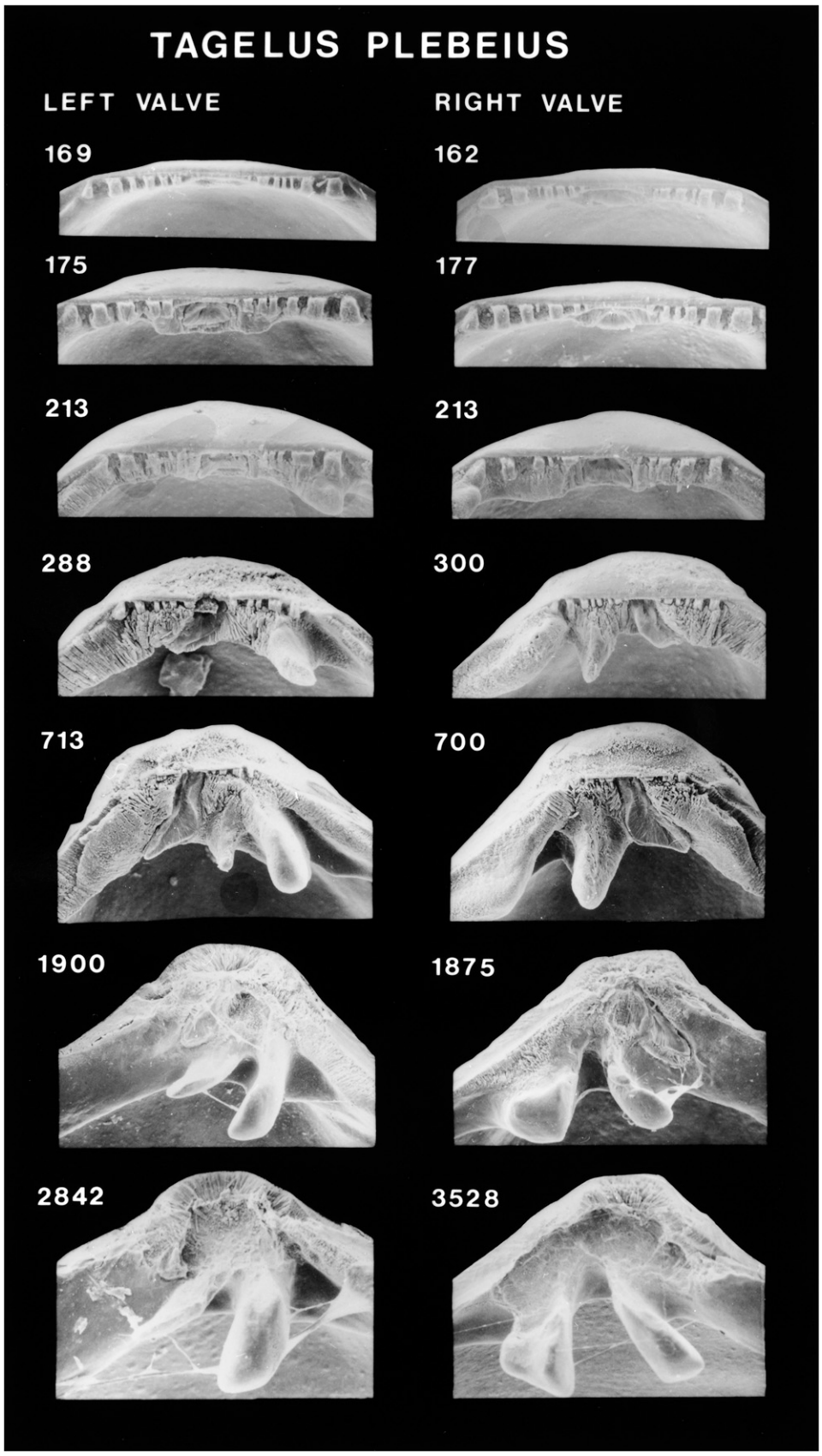

Figure 31. Scanning electron micrographs of the hinge of disarticulated shell valves of *Tagelus plebeius* postlarvae seen in Figure 30. Numbers indicate the maximum linear shell dimension in micrometers.

Downloaded From: https://bioone.org/journals/Journal-of-Shellfish-Research on 25 Feb 2020
Terms of Use: https://bioone.org/terms-of-use Access provided by IFREMER

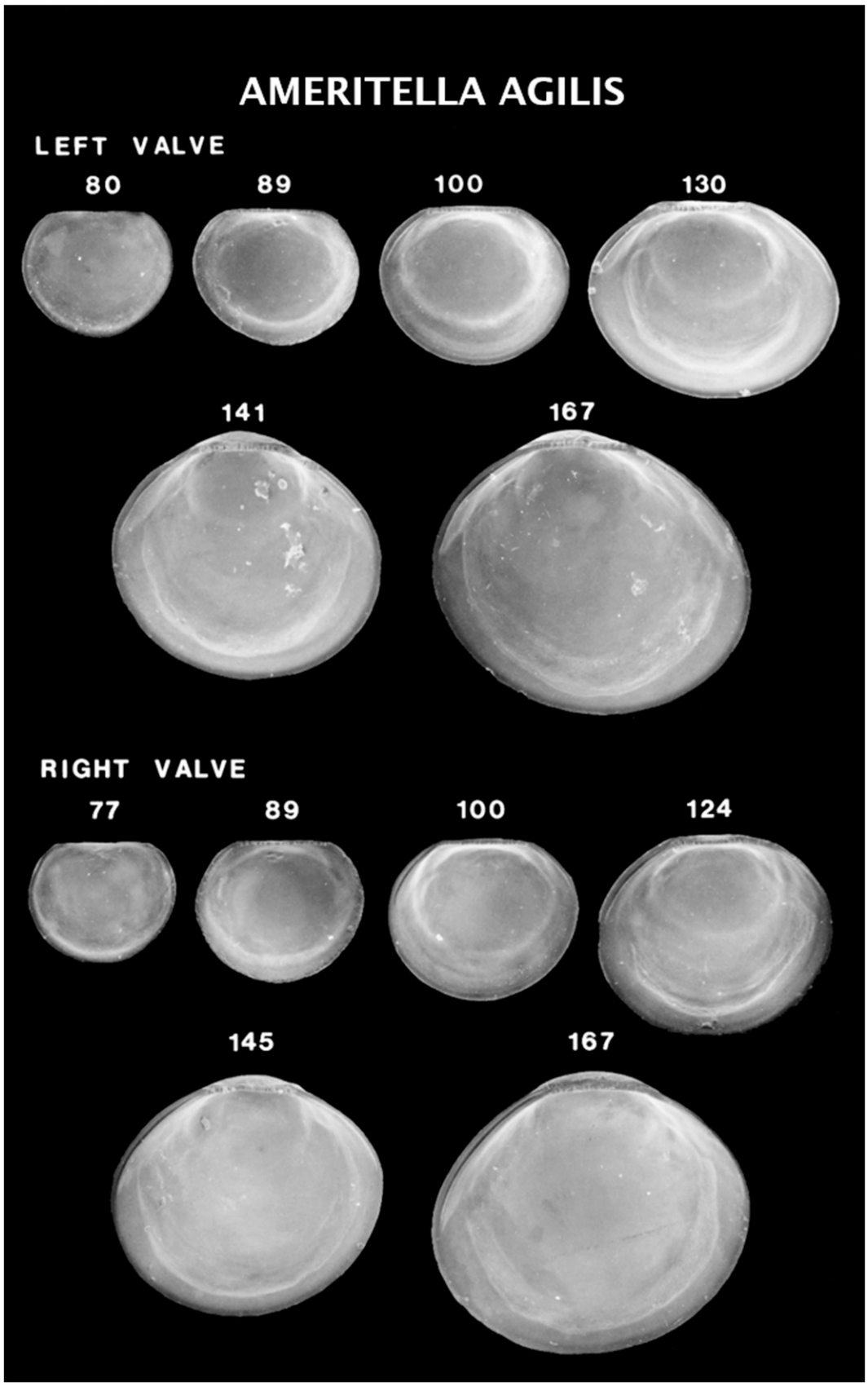

Figure 32. Scanning electron micrographs of disarticulated shell valves of *Ameritella agilis* larvae. Numbers indicate the maximum linear shell dimension in micrometers.

Downloaded From: https://bioone.org/journals/Journal-of-Shellfish-Research on 25 Feb 2020
Terms of Use: https://bioone.org/terms-of-use Access provided by IFREMER

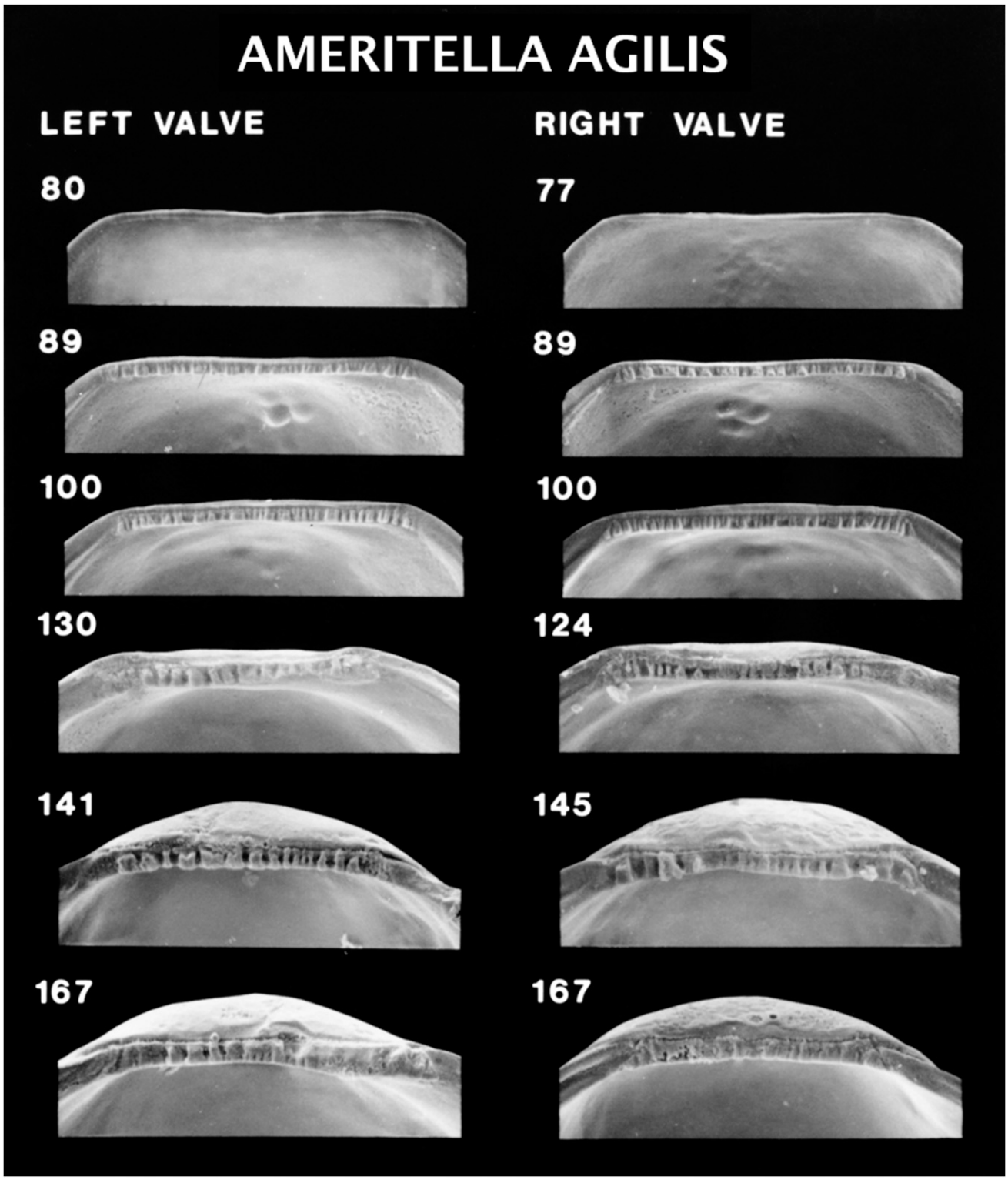

Figure 33. Scanning electron micrographs of the hinge of disarticulated shell valves of *Ameritella agilis* larvae seen in Figure 32. Numbers indicate the maximum linear shell dimension in micrometers.

Downloaded From: https://bioone.org/journals/Journal-of-Shellfish-Research on 25 Feb 2020
Terms of Use: https://bioone.org/terms-of-use Access provided by IFREMER

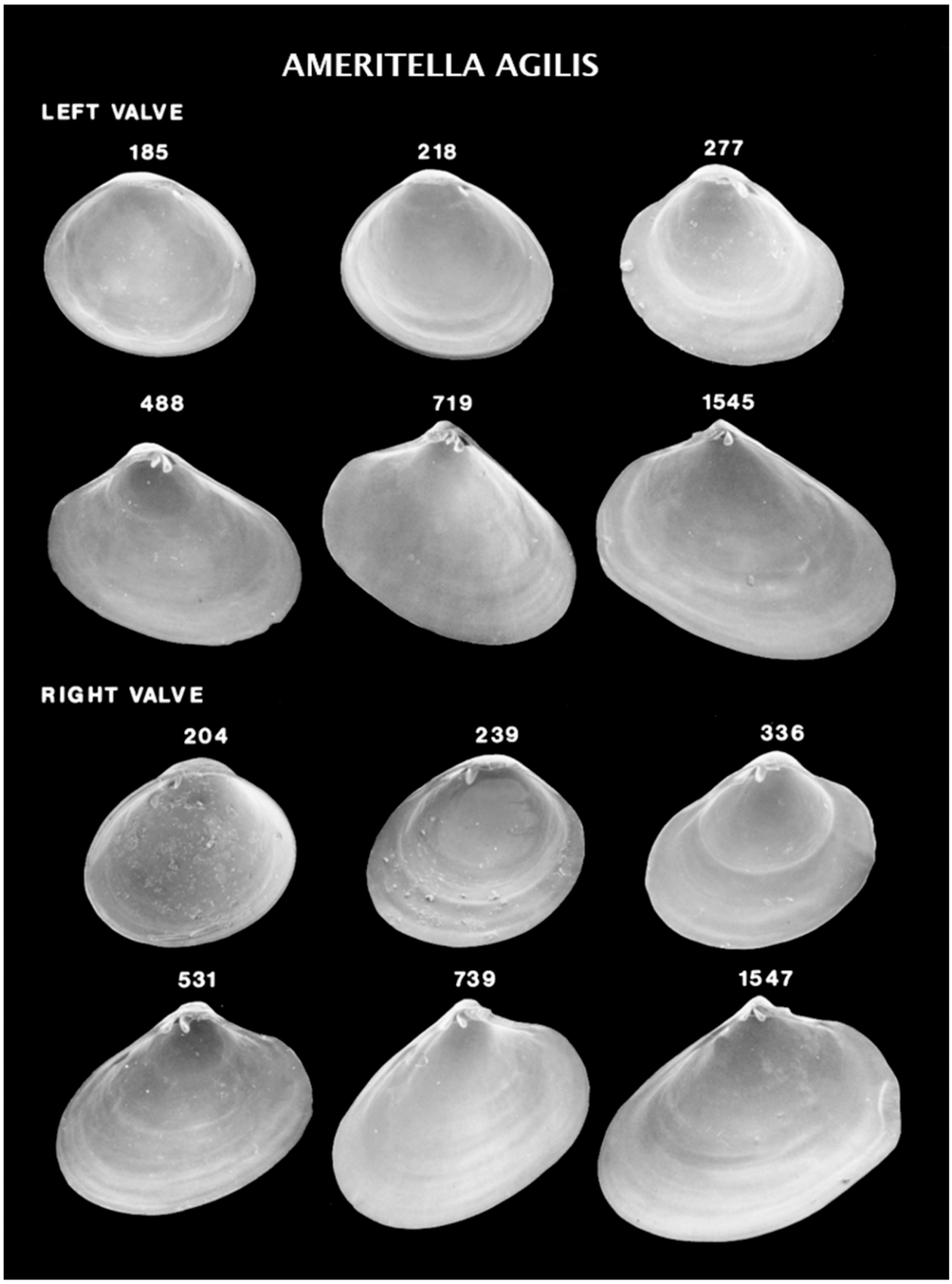

Figure 34. Scanning electron micrographs of disarticulated shell valves of *Ameritella agilis* postlarvae. Numbers indicate the maximum linear shell dimension in micrometers.

Downloaded From: https://bioone.org/journals/Journal-of-Shellfish-Research on 25 Feb 2020
Terms of Use: https://bioone.org/terms-of-use Access provided by IFREMER

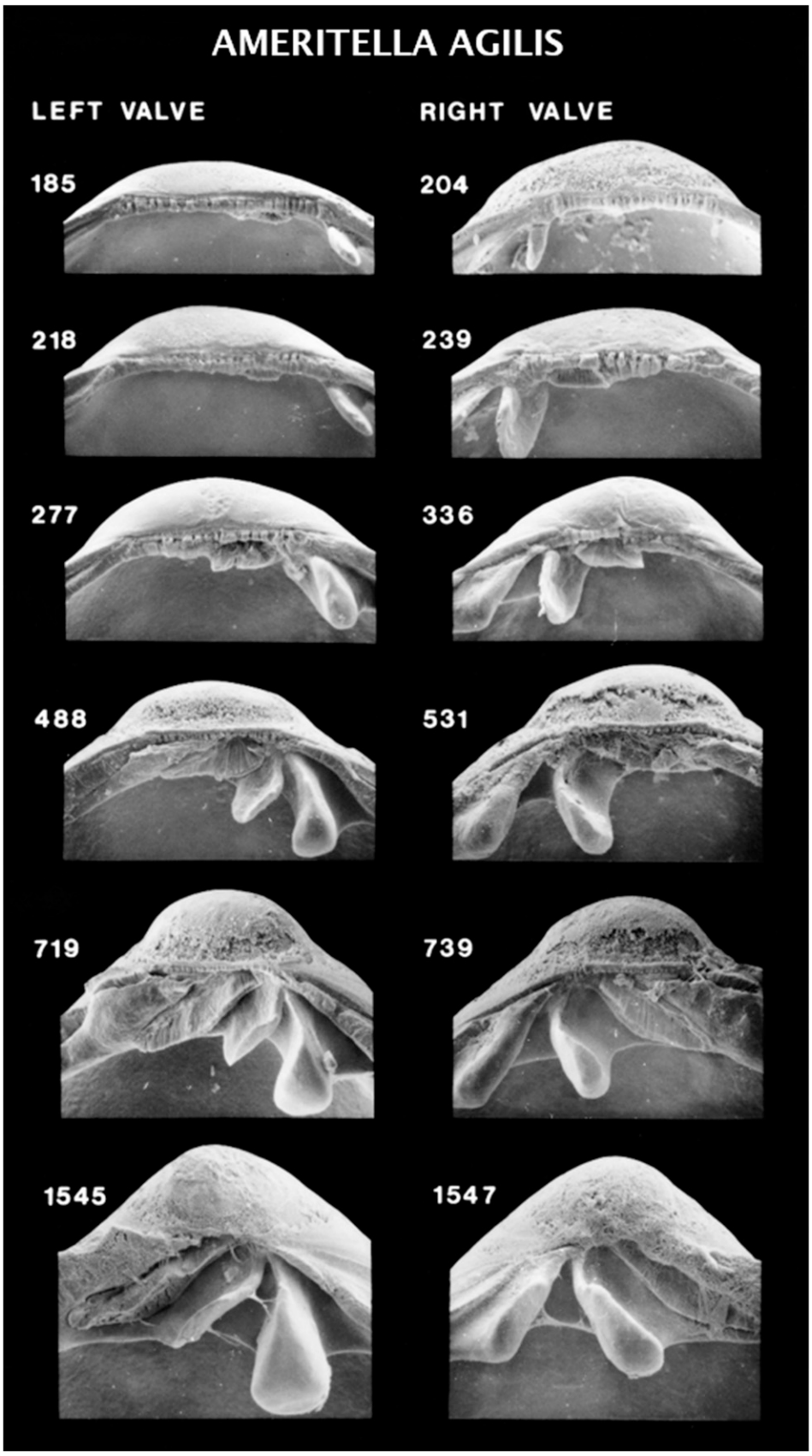

Figure 35. Scanning electron micrographs of the hinge of disarticulated shell valves of *Ameritella agilis* postlarvae seen in Figure 34. Numbers indicate the maximum linear shell dimension in micrometers.

Downloaded From: https://bioone.org/journals/Journal-of-Shellfish-Research on 25 Feb 2020
Terms of Use: https://bioone.org/terms-of-use Access provided by IFREMER

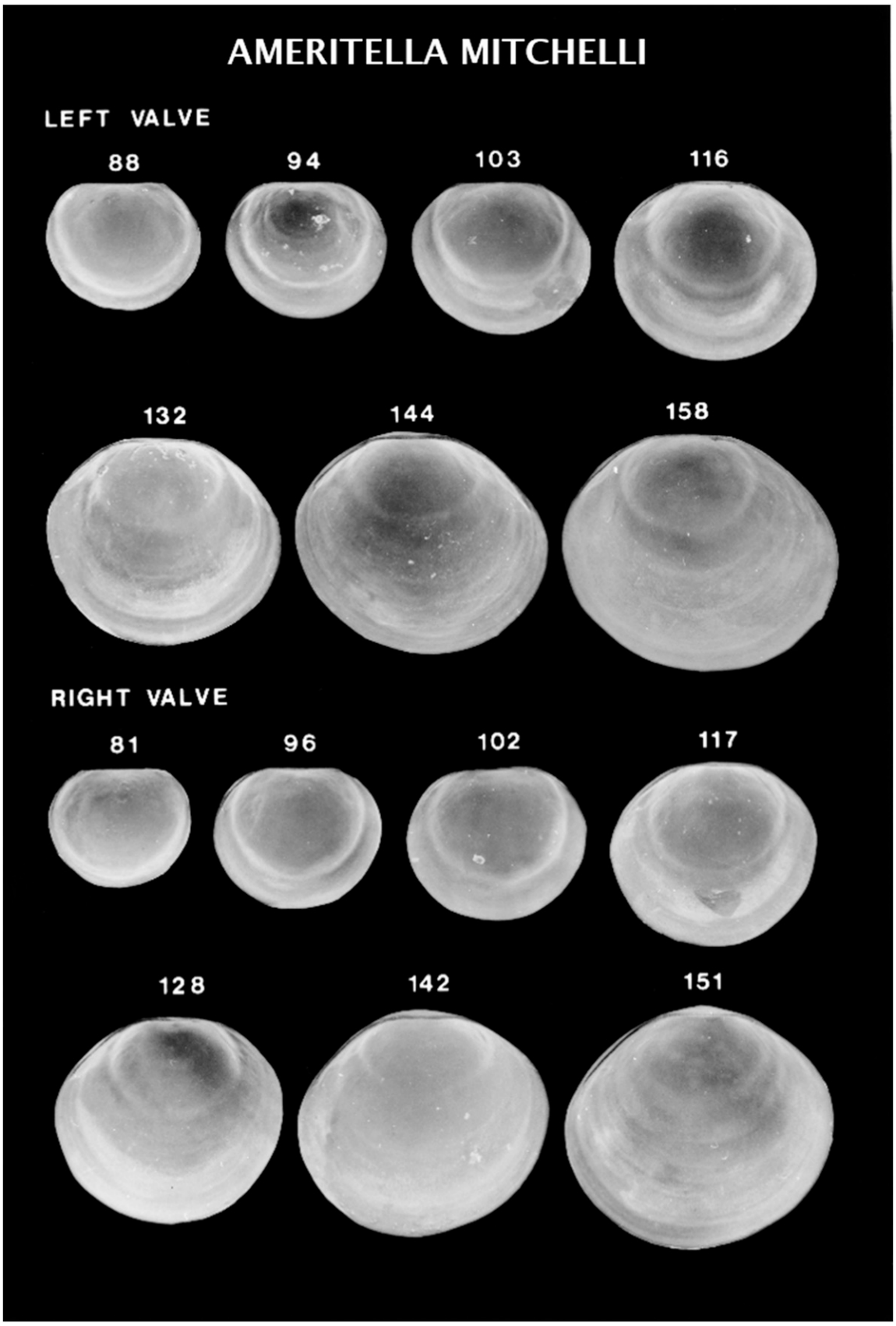

Figure 36. Scanning electron micrographs of disarticulated shell valves of *Ameritella mitchelli* larvae. Numbers indicate the maximum linear shell dimension in micrometers. Modified from Kennedy et al. (1989).

Downloaded From: https://bioone.org/journals/Journal-of-Shellfish-Research on 25 Feb 2020
Terms of Use: https://bioone.org/terms-of-use Access provided by IFREMER

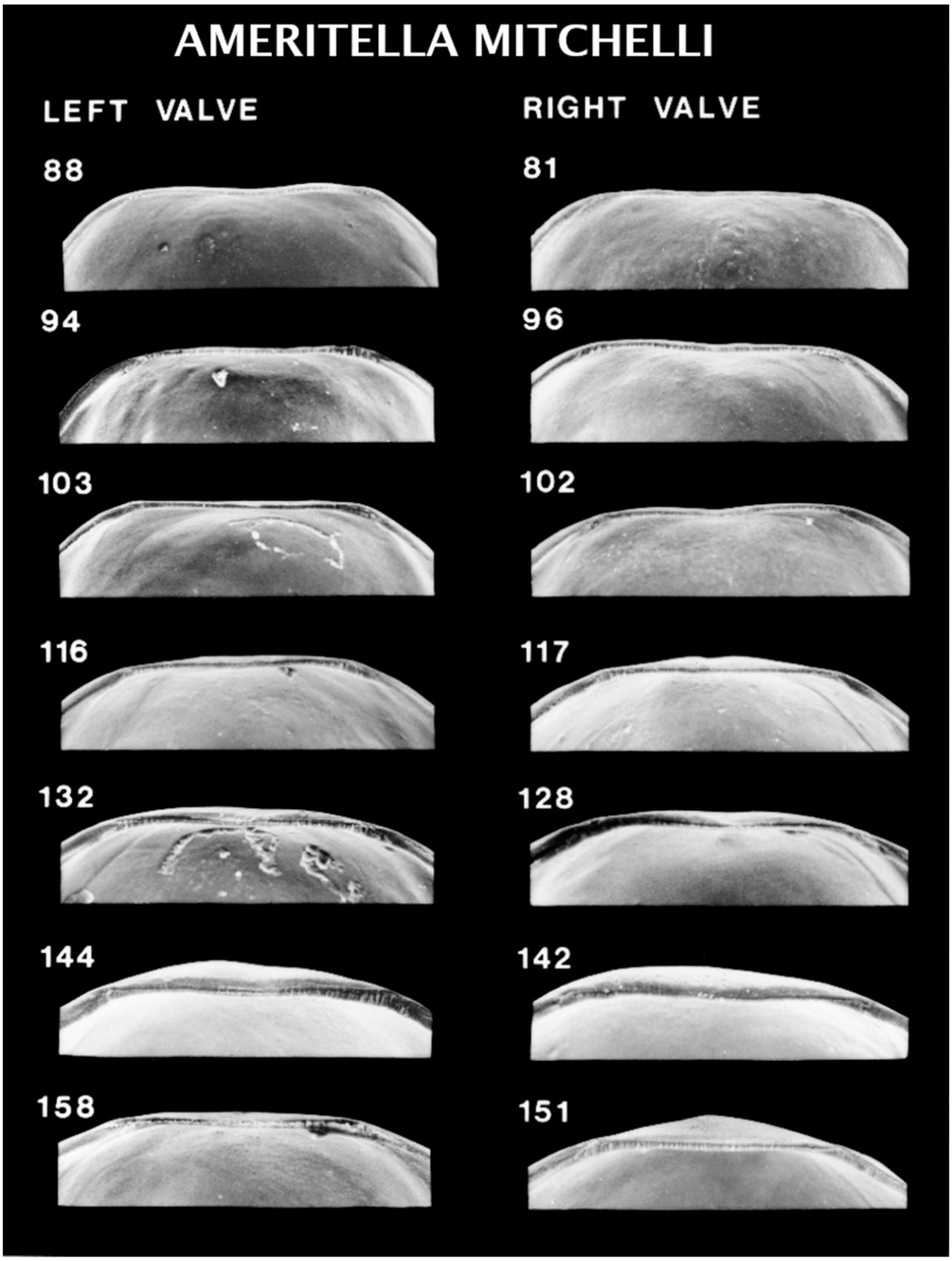

Figure 37. Scanning electron micrographs of the hinge of disarticulated shell valves of *Ameritella mitchelli* larvae seen in Figure 36. Numbers indicate the maximum linear shell dimension in micrometers. Modified from Kennedy et al. (1989).

Downloaded From: https://bioone.org/journals/Journal-of-Shellfish-Research on 25 Feb 2020
Terms of Use: https://bioone.org/terms-of-use Access provided by IFREMER

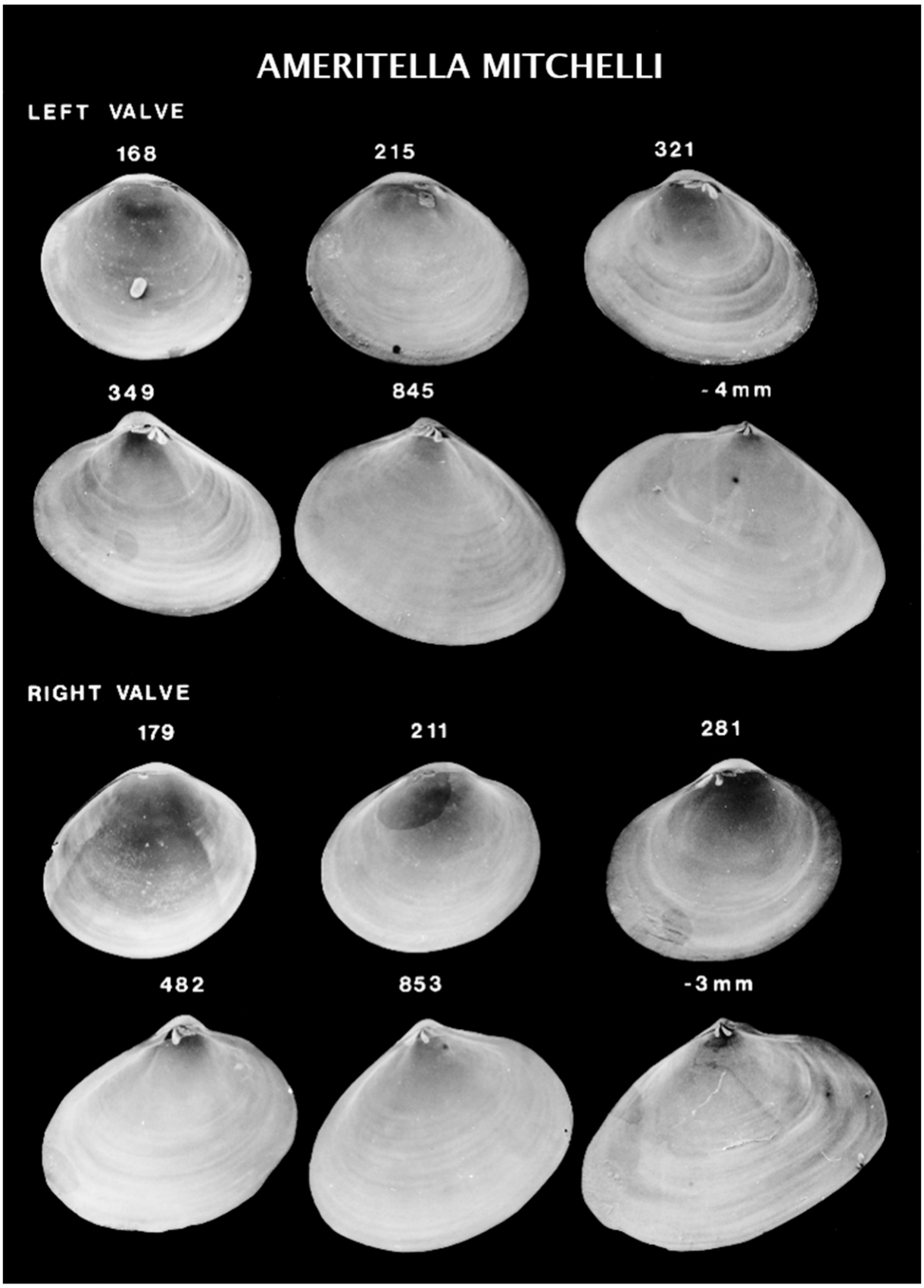

Figure 38. Scanning electron micrographs of disarticulated shell valves of *Ameritella mitchelli* postlarvae. Numbers indicate the maximum linear shell dimension in micrometers. Modified from Kennedy et al. (1989).

Downloaded From: https://bioone.org/journals/Journal-of-Shellfish-Research on 25 Feb 2020
Terms of Use: https://bioone.org/terms-of-use Access provided by IFREMER

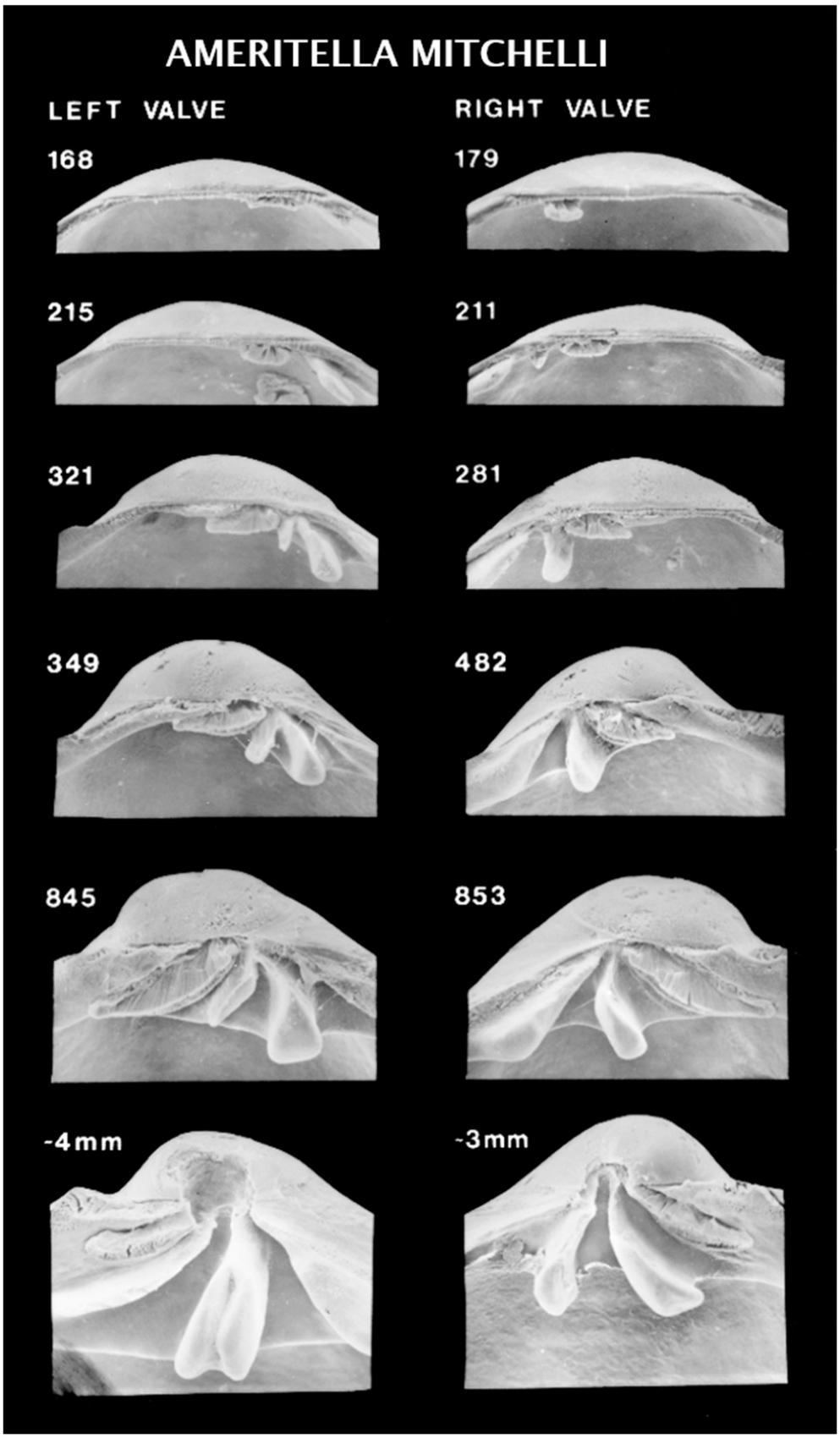

Figure 39. Scanning electron micrographs of the hinge of disarticulated shell valves of *Ameritella mitchelli* postlarvae seen in Figure 38. Numbers indicate the maximum linear shell dimension in micrometers. Modified from Kennedy et al. (1989).

Downloaded From: https://bioone.org/journals/Journal-of-Shellfish-Research on 25 Feb 2020
Terms of Use: https://bioone.org/terms-of-use Access provided by IFREMER

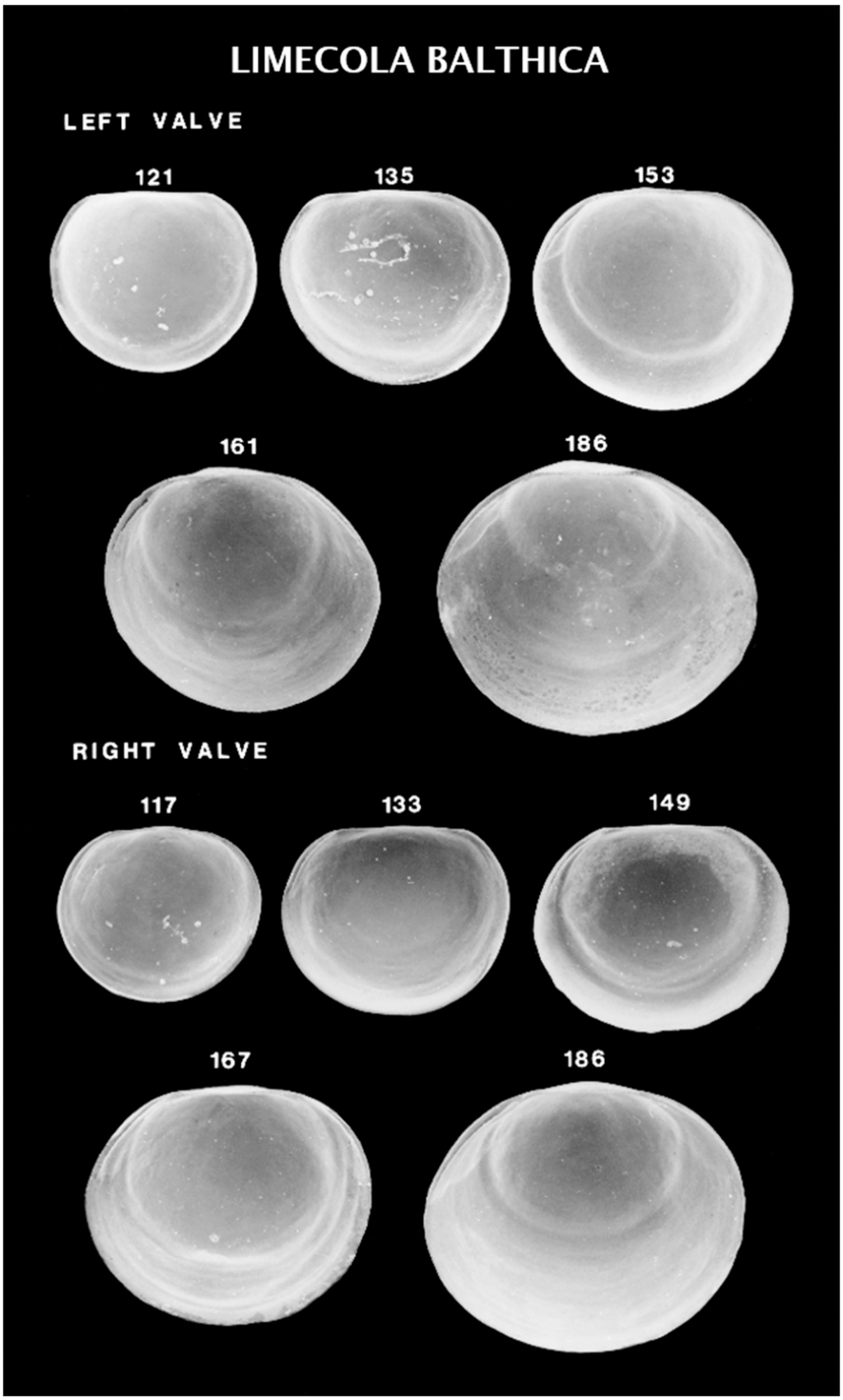

Figure 40. Scanning electron micrographs of disarticulated shell valves of *Limecola balthica* larvae. Numbers indicate the maximum linear shell dimension in micrometers.

Downloaded From: https://bioone.org/journals/Journal-of-Shellfish-Research on 25 Feb 2020
Terms of Use: https://bioone.org/terms-of-use Access provided by IFREMER

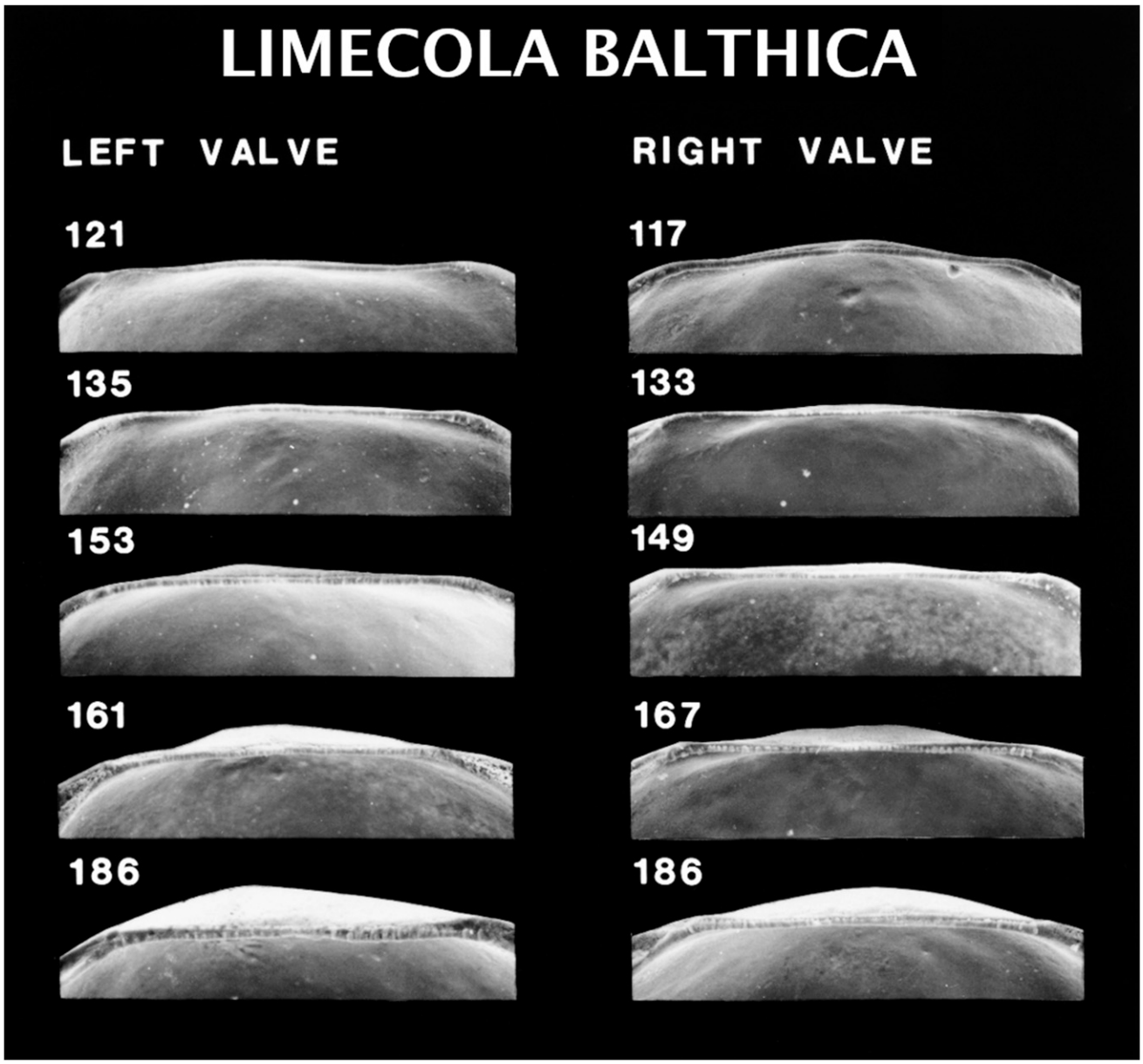

Figure 41. Scanning electron micrographs of the hinge of disarticulated shell valves of *Limecola balthica* larvae seen in Figure 40. Numbers indicate the maximum linear shell dimension in micrometers.

Downloaded From: https://bioone.org/journals/Journal-of-Shellfish-Research on 25 Feb 2020
Terms of Use: https://bioone.org/terms-of-use Access provided by IFREMER

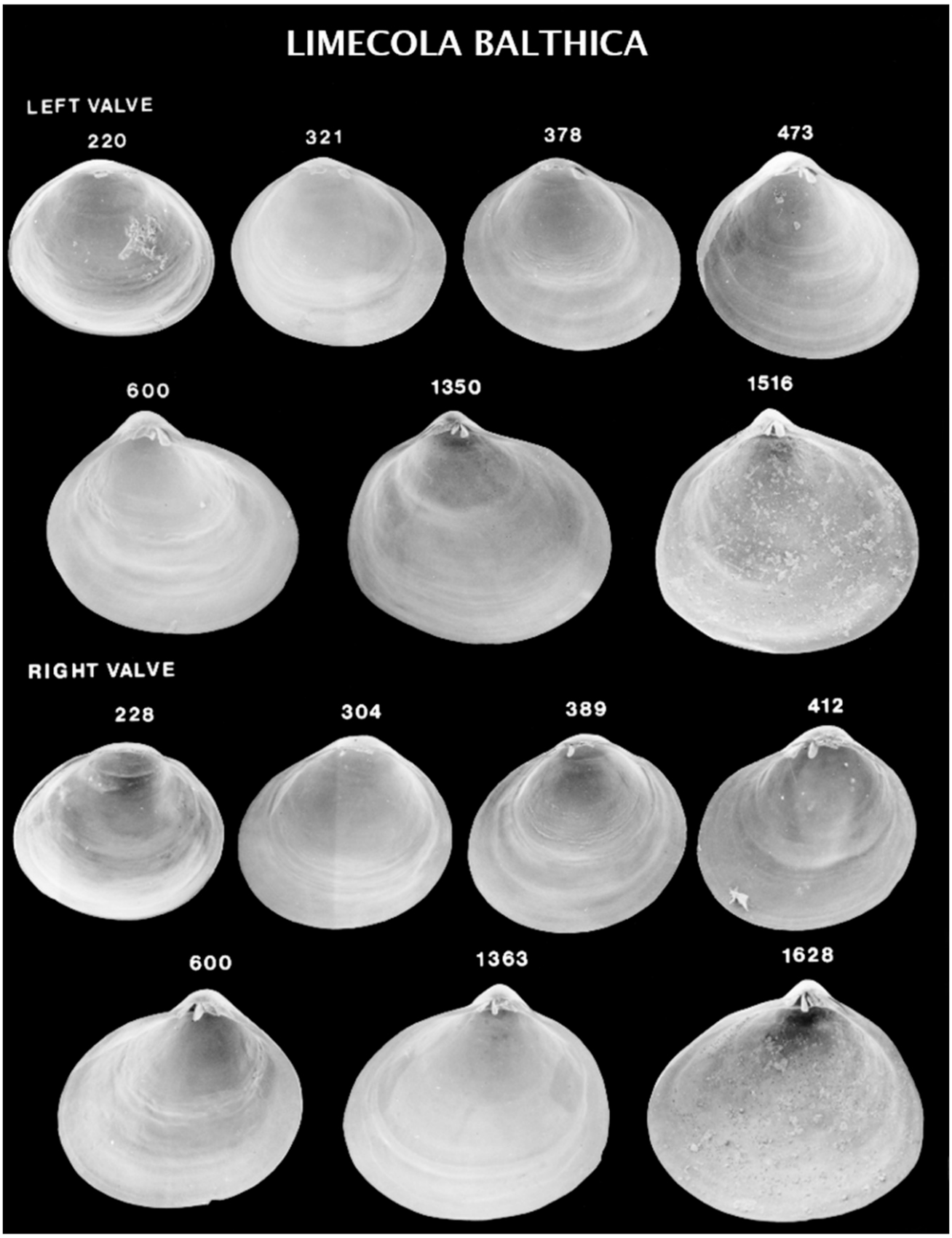

Figure 42. Scanning electron micrographs of disarticulated shell valves of *Limecola balthica* postlarvae. Numbers indicate the maximum linear shell dimension in micrometers.

Downloaded From: https://bioone.org/journals/Journal-of-Shellfish-Research on 25 Feb 2020
Terms of Use: https://bioone.org/terms-of-use Access provided by IFREMER

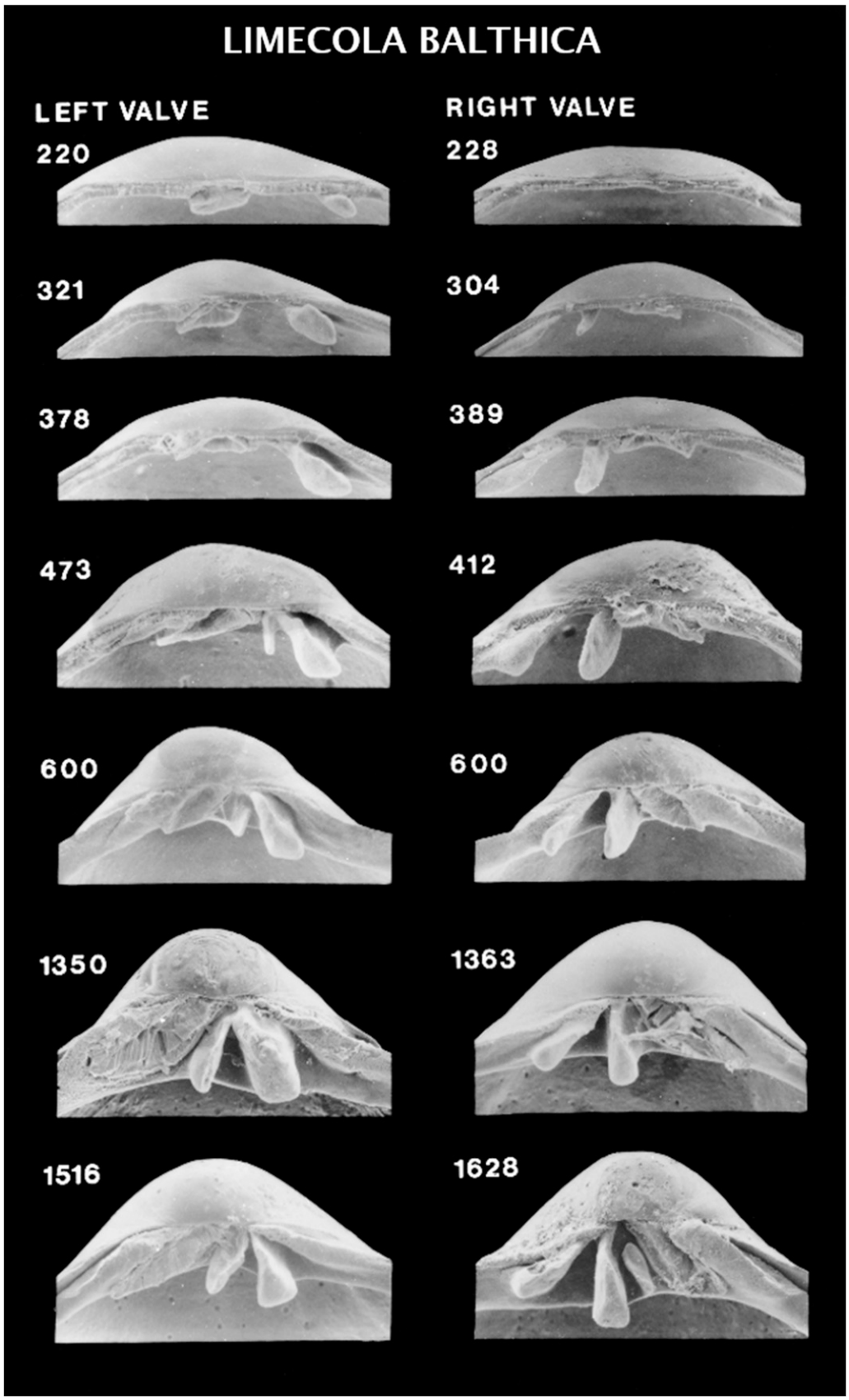

Figure 43. Scanning electron micrographs of the hinge of disarticulated shell valves of *Limecola balthica* postlarvae seen in Figure 42. Numbers indicate the maximum linear shell dimension in micrometers.

Downloaded From: https://bioone.org/journals/Journal-of-Shellfish-Research on 25 Feb 2020
Terms of Use: https://bioone.org/terms-of-use Access provided by IFREMER

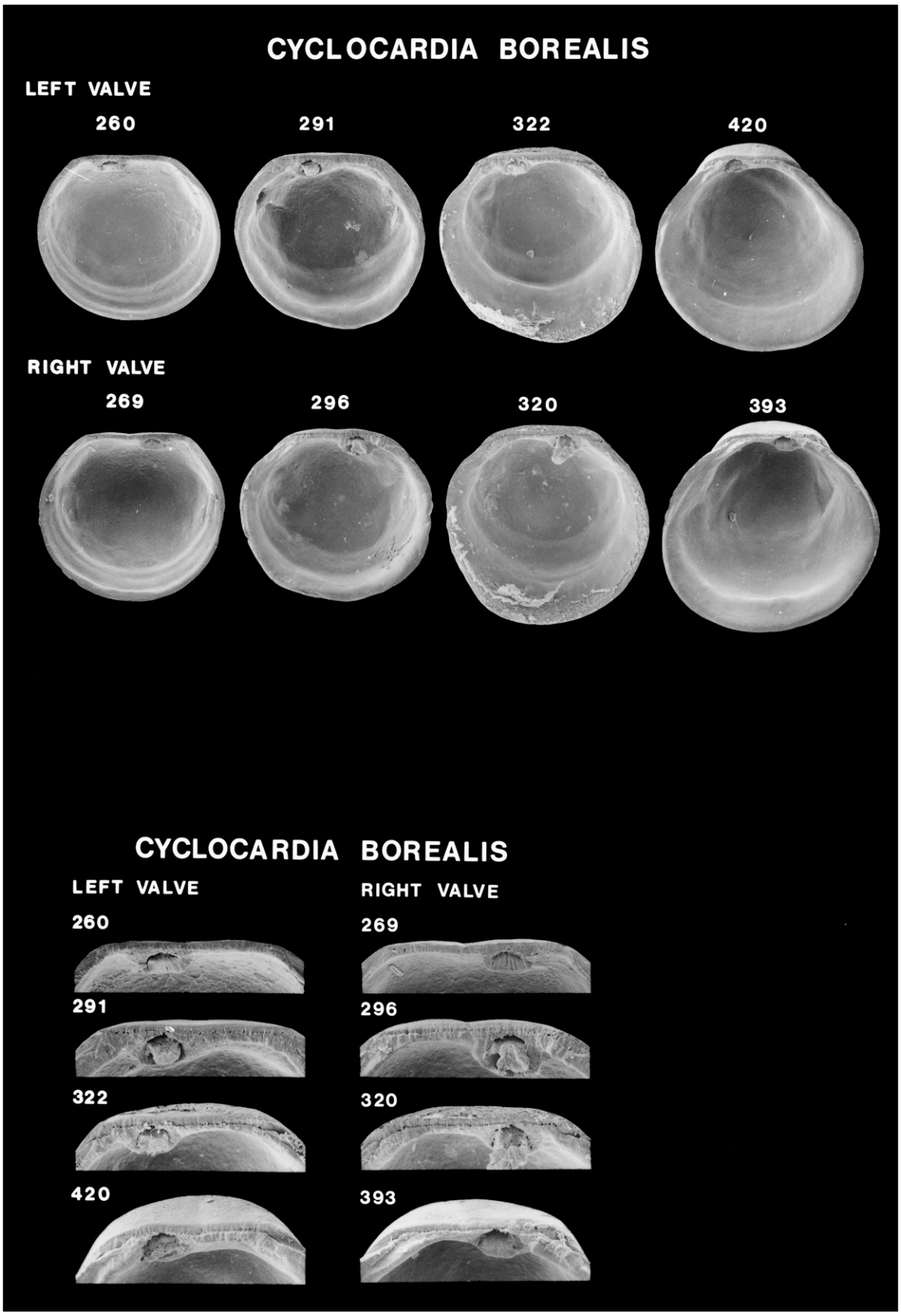

Figure 44. Scanning electron micrographs of disarticulated shell valves of *Cyclocardia borealis* postlarvae (top) and higher magnification scanning electron micrographs of the hinge of these shell valves (bottom). Numbers indicate the maximum linear shell dimension in micrometers.

Downloaded From: https://bioone.org/journals/Journal-of-Shellfish-Research on 25 Feb 2020
Terms of Use: https://bioone.org/terms-of-use Access provided by IFREMER

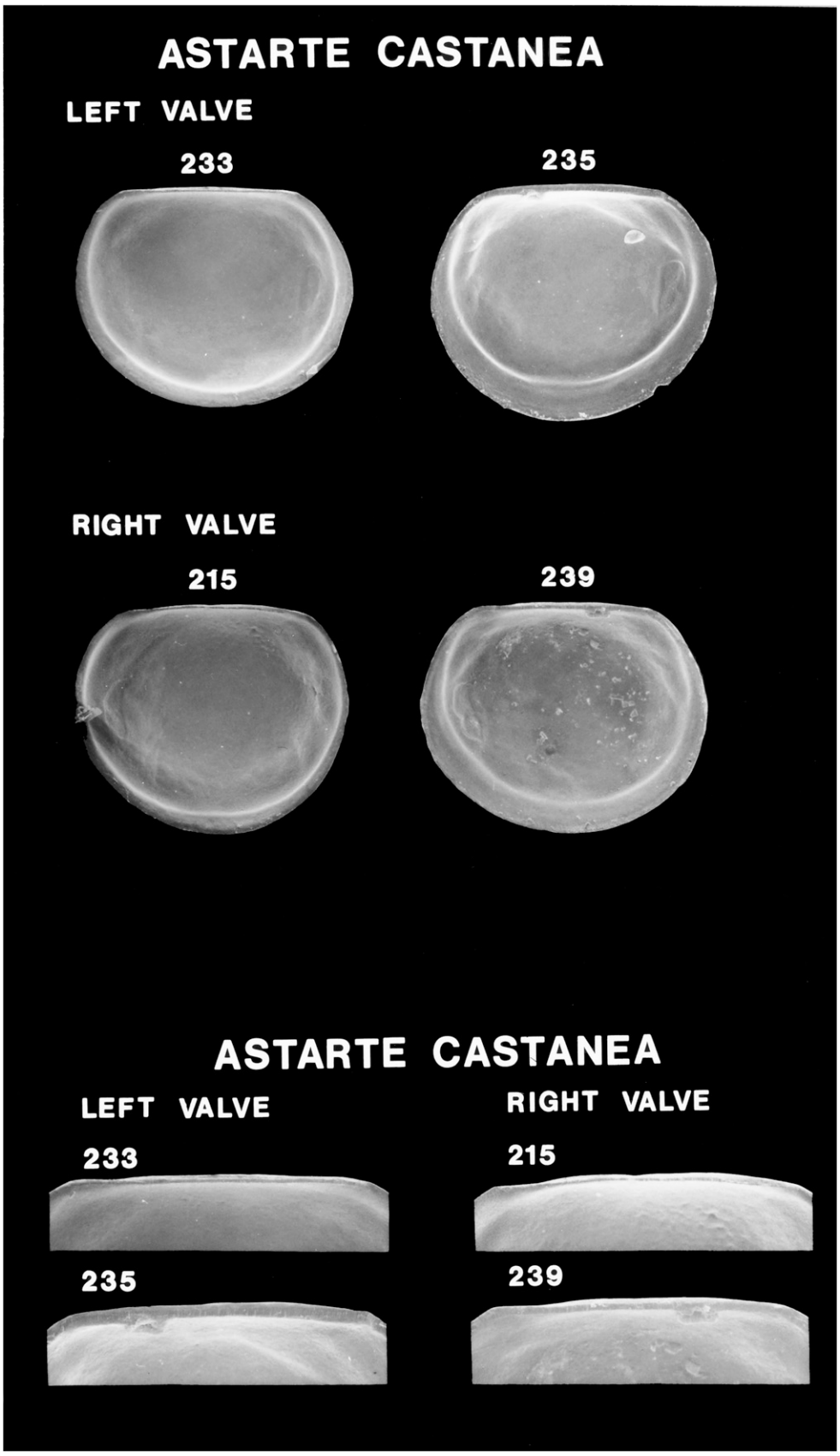

Figure 45. Scanning electron micrographs of disarticulated shell valves of *Astarte castanea* postlarvae (top) and higher magnification scanning electron micrographs of the hinge of these shell valves (bottom). Numbers indicate the maximum linear shell dimension in micrometers.

Downloaded From: https://bioone.org/journals/Journal-of-Shellfish-Research on 25 Feb 2020
Terms of Use: https://bioone.org/terms-of-use Access provided by IFREMER

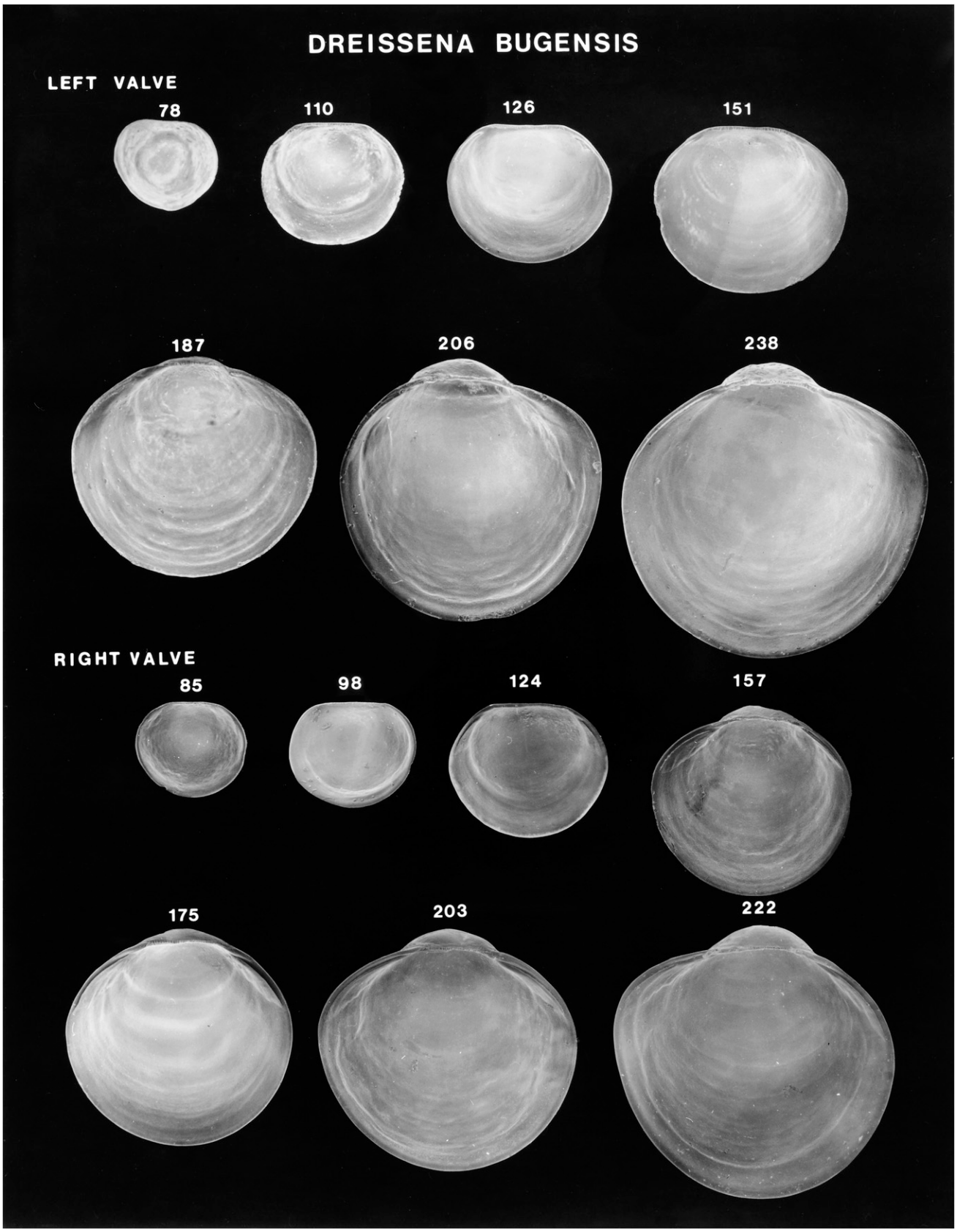

Figure 46. Scanning electron micrographs of disarticulated shell valves of *Dreissena bugensis* larvae. Numbers indicate the maximum linear shell dimension in micrometers.

Downloaded From: https://bioone.org/journals/Journal-of-Shellfish-Research on 25 Feb 2020
Terms of Use: https://bioone.org/terms-of-use Access provided by IFREMER

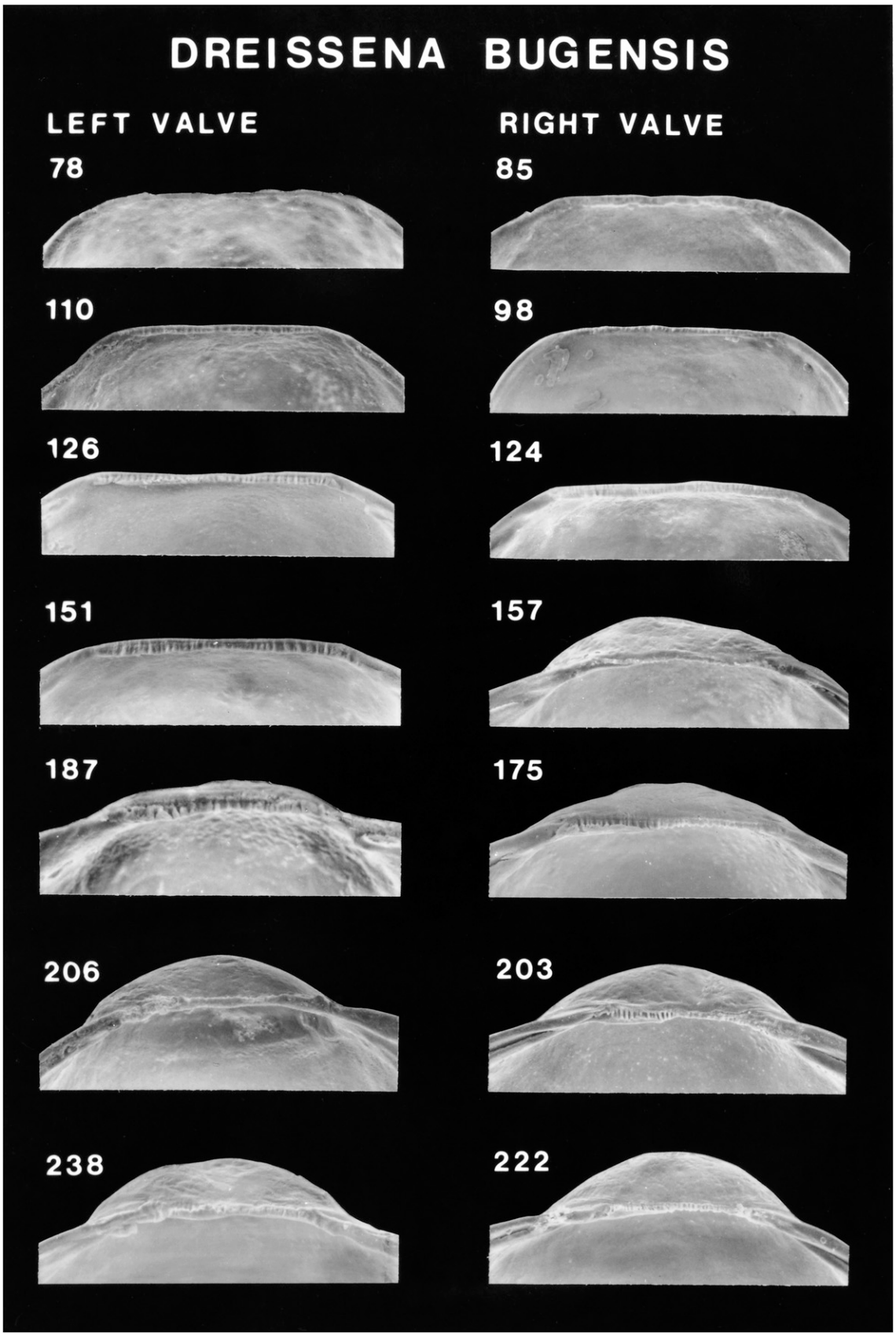

Figure 47. Scanning electron micrographs of the hinge of disarticulated shell valves of *Dreissena bugensis* larvae seen in Figure 46. Numbers indicate the maximum linear shell dimension in micrometers.

Downloaded From: https://bioone.org/journals/Journal-of-Shellfish-Research on 25 Feb 2020
Terms of Use: https://bioone.org/terms-of-use Access provided by IFREMER

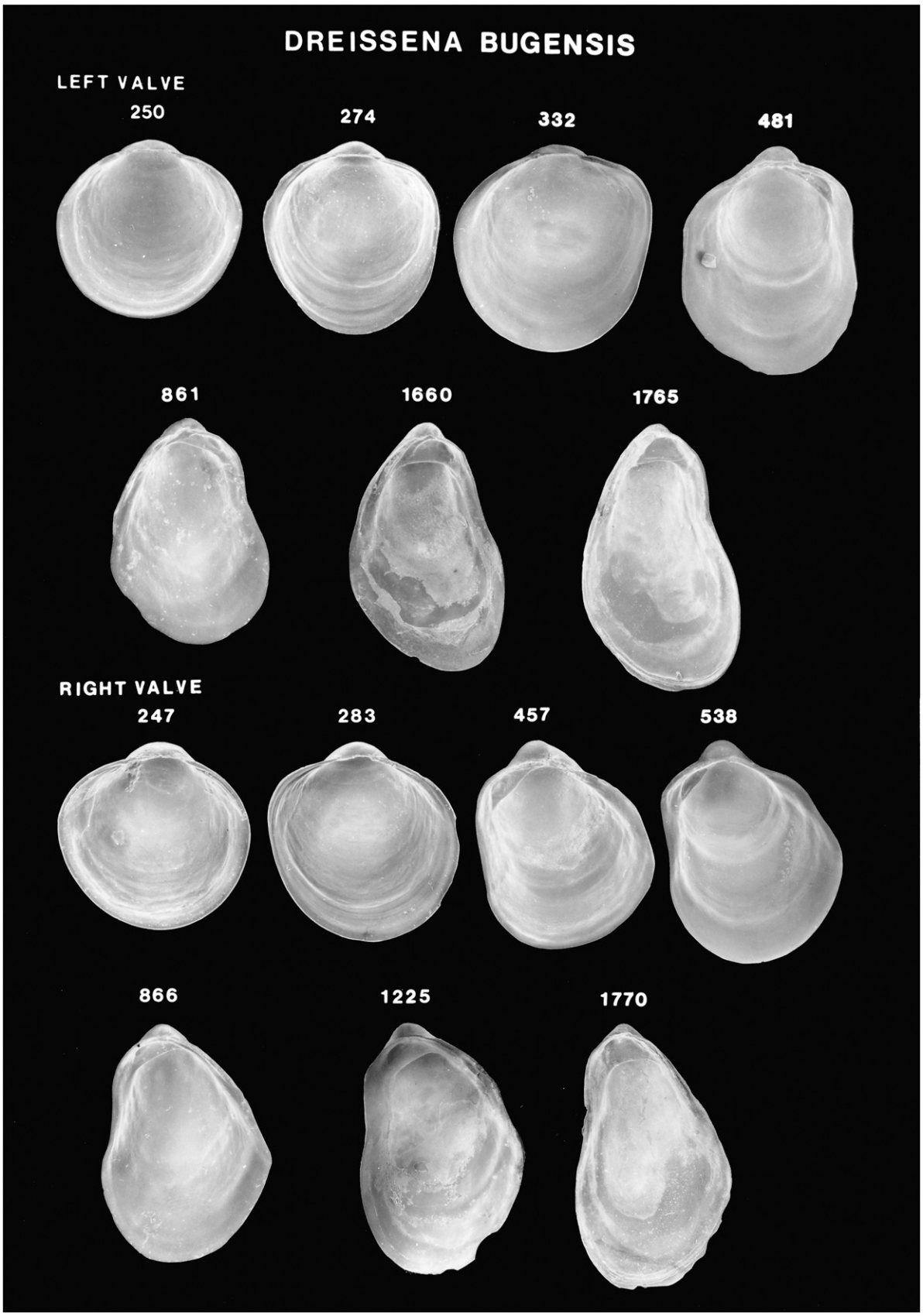

Figure 48. Scanning electron micrographs of disarticulated shell valves of *Dreissena bugensis* postlarvae. Numbers indicate the maximum linear shell dimension in micrometers.

Downloaded From: https://bioone.org/journals/Journal-of-Shellfish-Research on 25 Feb 2020
Terms of Use: https://bioone.org/terms-of-use Access provided by IFREMER

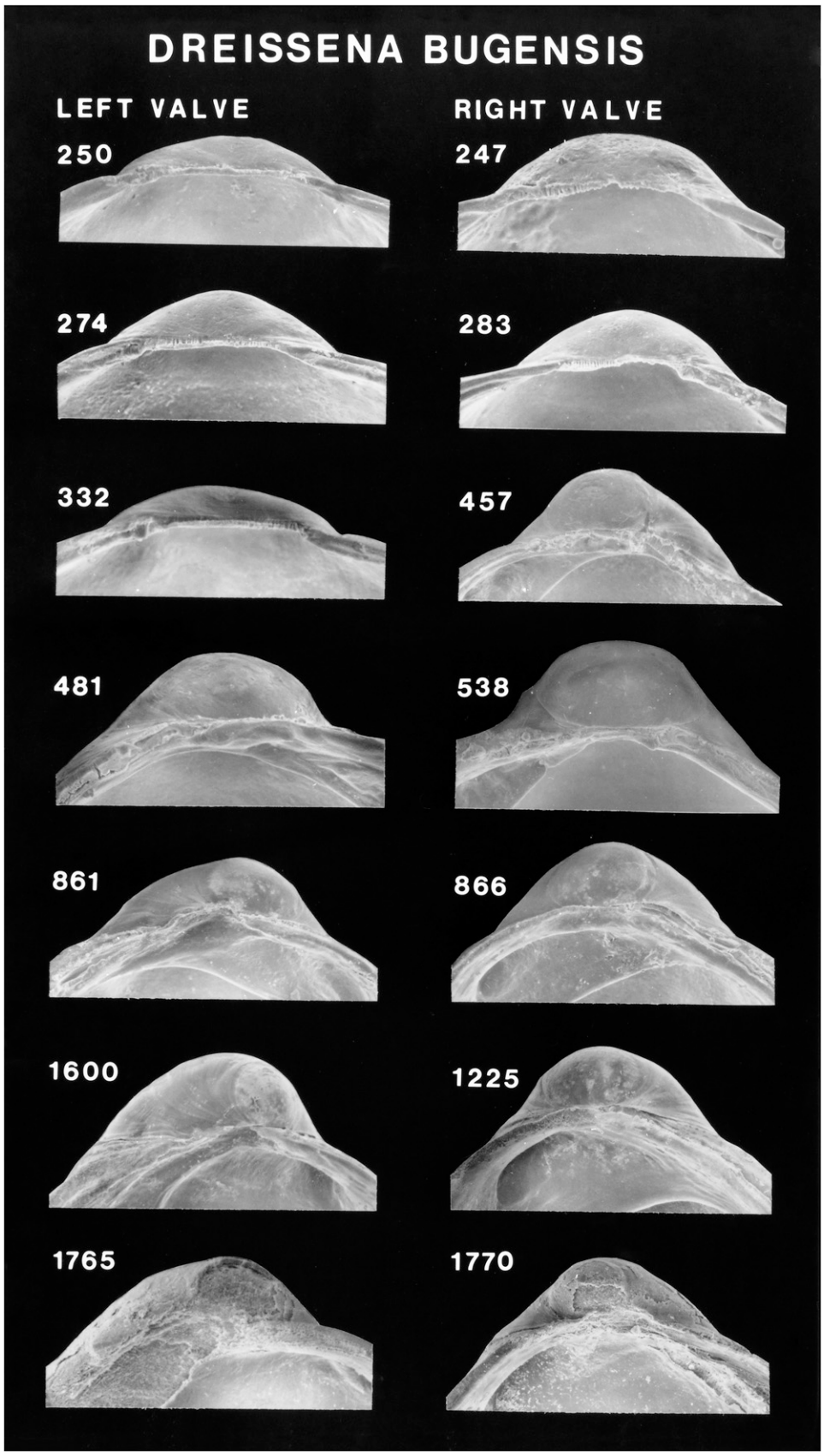

Figure 49. Scanning electron micrographs of the hinge of disarticulated shell valves of *Dreissena bugensis* postlarvae seen in Figure 48. Numbers indicate the maximum linear shell dimension in micrometers.

Downloaded From: https://bioone.org/journals/Journal-of-Shellfish-Research on 25 Feb 2020
Terms of Use: https://bioone.org/terms-of-use Access provided by IFREMER

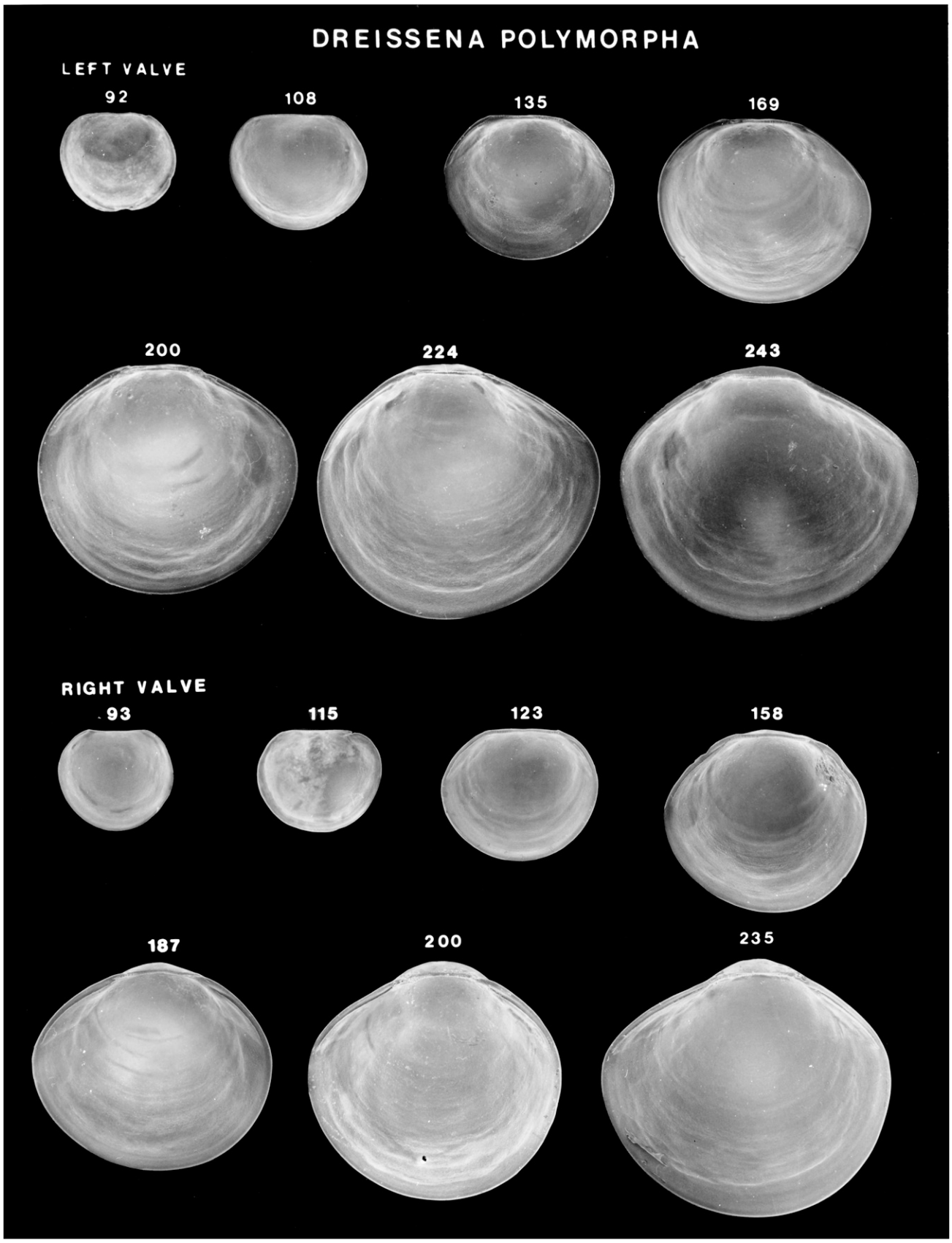

Figure 50. Scanning electron micrographs of disarticulated shell valves of *Dreissena polymorpha* larvae. Numbers indicate the maximum linear shell dimension in micrometers.

Downloaded From: https://bioone.org/journals/Journal-of-Shellfish-Research on 25 Feb 2020
Terms of Use: https://bioone.org/terms-of-use Access provided by IFREMER

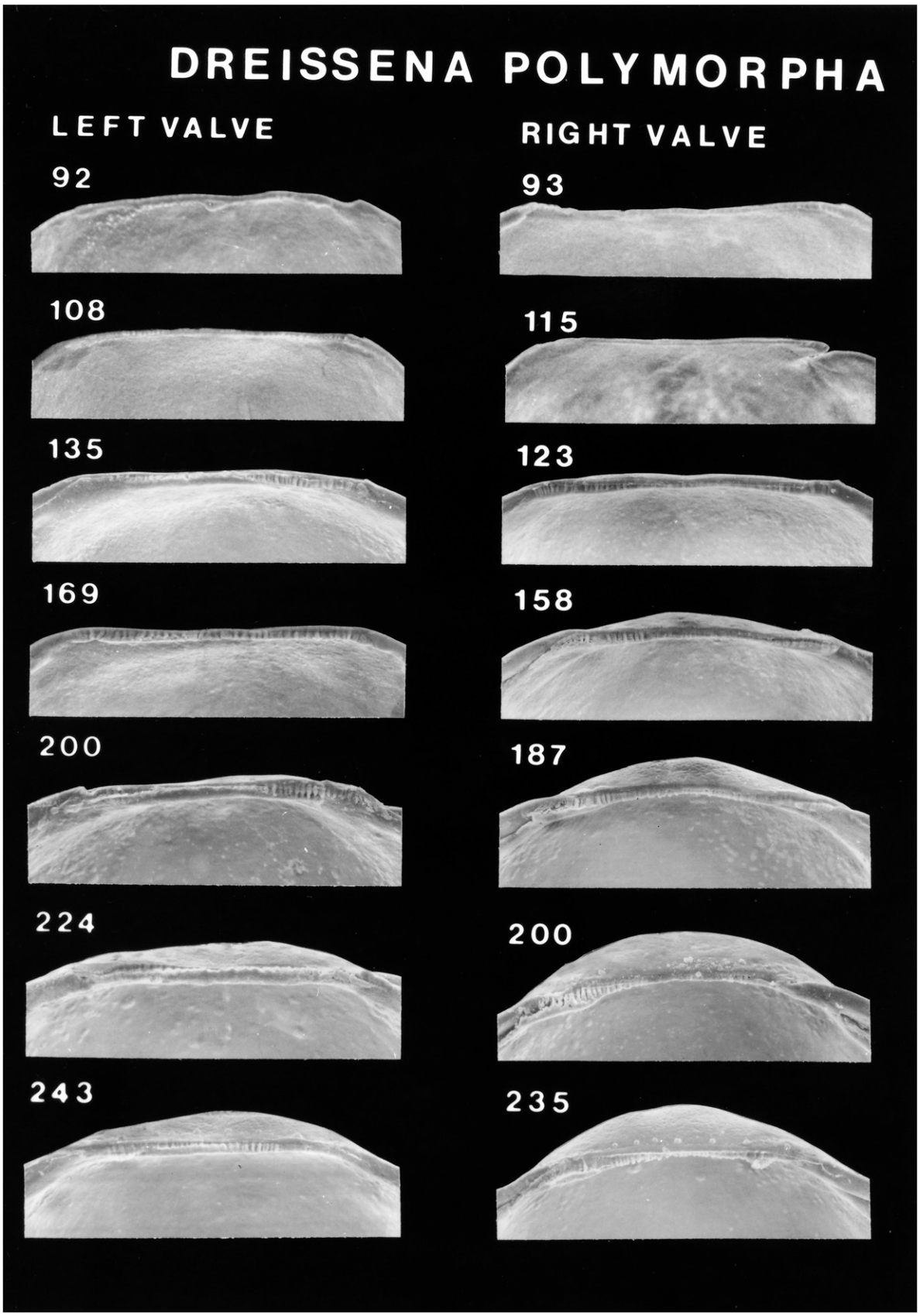

Figure 51. Scanning electron micrographs of the hinge of disarticulated shell valves of *Dreissena polymorpha* larvae seen in Figure 50. Numbers indicate the maximum linear shell dimension in micrometers.

Downloaded From: https://bioone.org/journals/Journal-of-Shellfish-Research on 25 Feb 2020
Terms of Use: https://bioone.org/terms-of-use Access provided by IFREMER

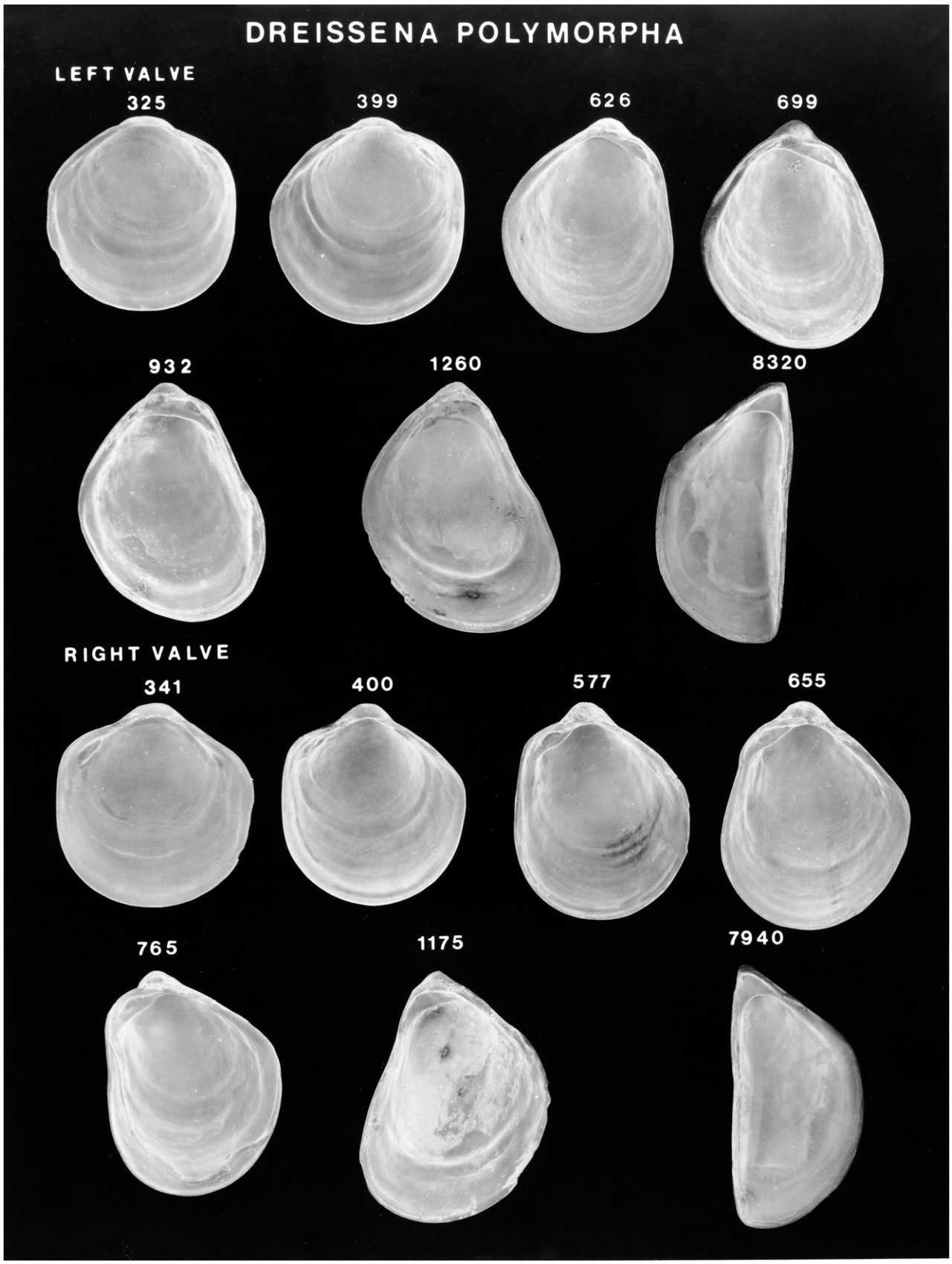

Figure 52. Scanning electron micrographs of disarticulated shell valves of *Dreissena polymorpha* postlarvae. Numbers indicate the maximum linear shell dimension in micrometers.

Downloaded From: https://bioone.org/journals/Journal-of-Shellfish-Research on 25 Feb 2020
Terms of Use: https://bioone.org/terms-of-use Access provided by IFREMER

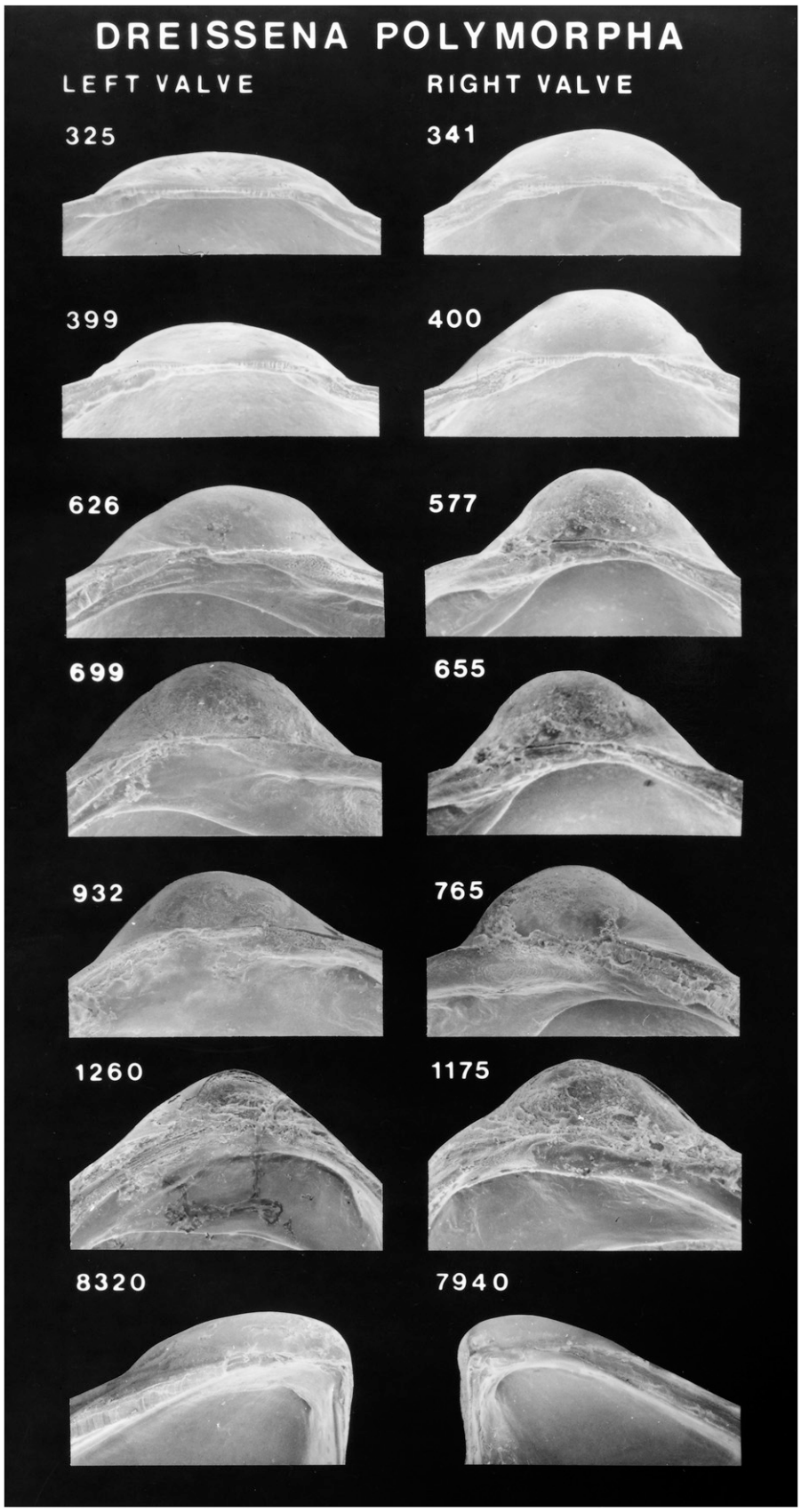

Figure 53. Scanning electron micrographs of the hinge of disarticulated shell valves of *Dreissena polymorpha* postlarvae seen in Figure 52. Numbers indicate the maximum linear shell dimension in micrometers.

Downloaded From: https://bioone.org/journals/Journal-of-Shellfish-Research on 25 Feb 2020
Terms of Use: https://bioone.org/terms-of-use Access provided by IFREMER

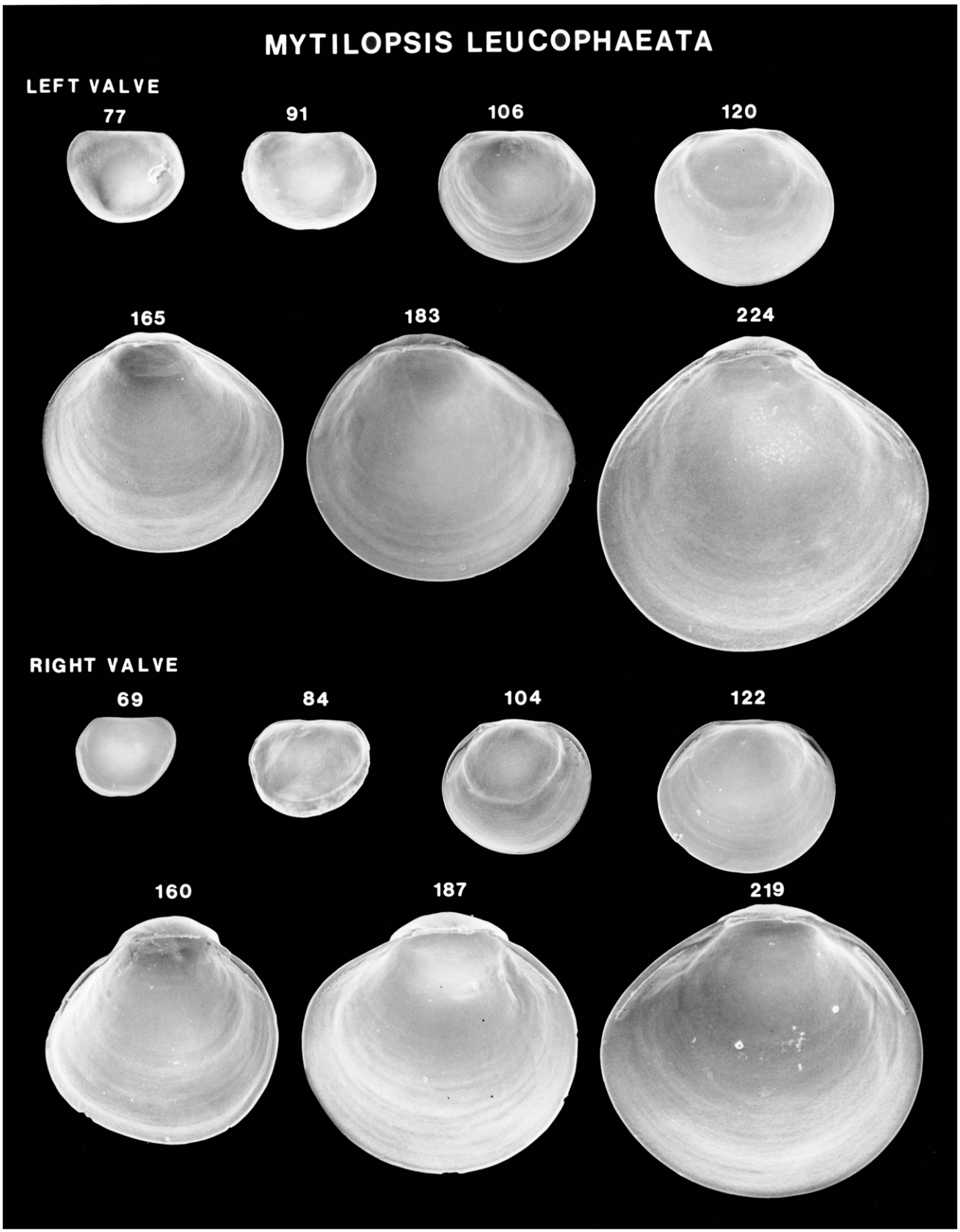

Figure 54. Scanning electron micrographs of disarticulated shell valves of *Mytilopsis leucophaeata* larvae. Numbers indicate the maximum linear shell dimension in micrometers.

Downloaded From: https://bioone.org/journals/Journal-of-Shellfish-Research on 25 Feb 2020
Terms of Use: https://bioone.org/terms-of-use Access provided by IFREMER

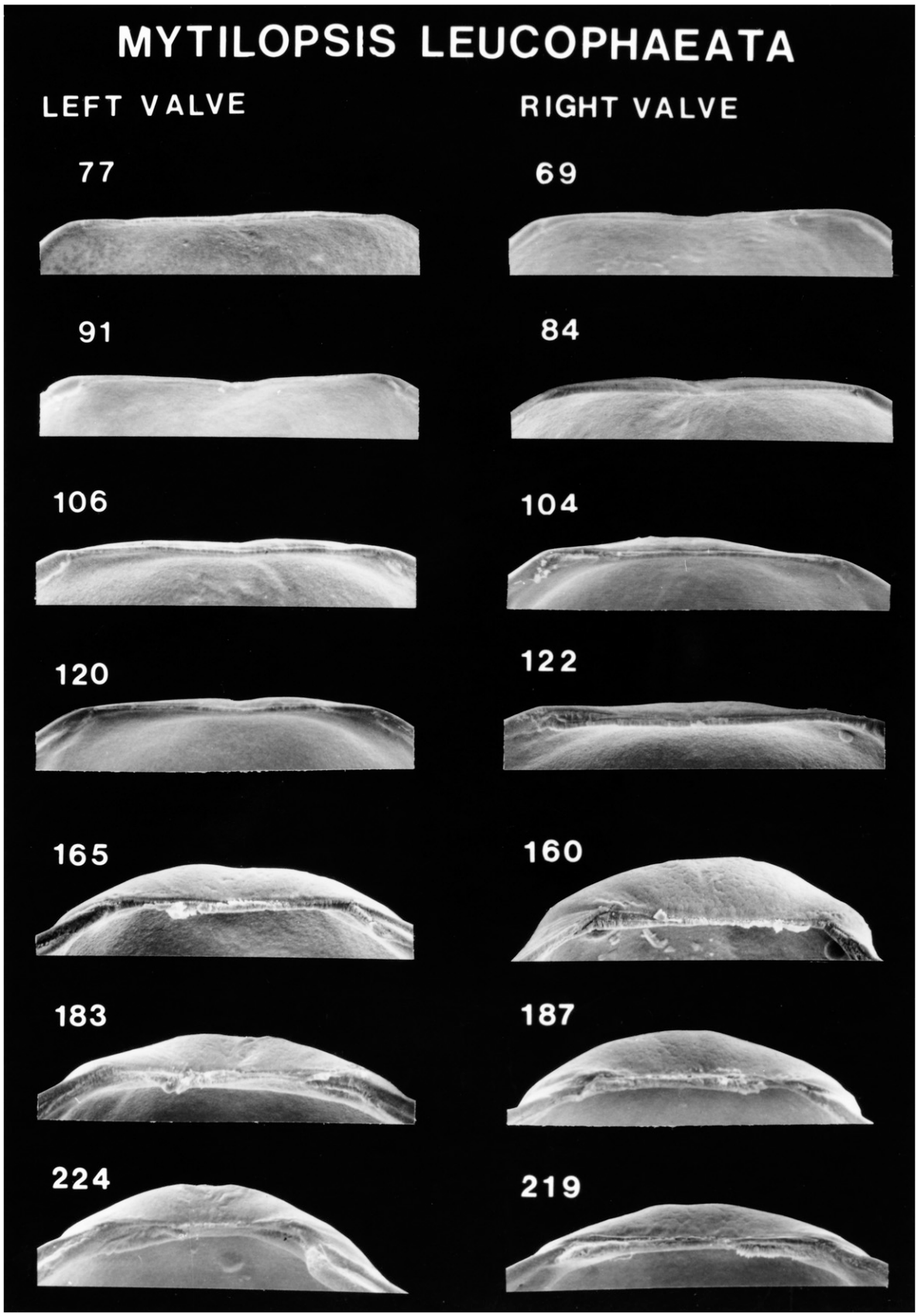

Figure 55. Scanning electron micrographs of the hinge of disarticulated shell valves of *Mytilopsis leucophaeata* larvae seen in Figure 54. Numbers indicate the maximum linear shell dimension in micrometers.

Downloaded From: https://bioone.org/journals/Journal-of-Shellfish-Research on 25 Feb 2020
Terms of Use: https://bioone.org/terms-of-use Access provided by IFREMER

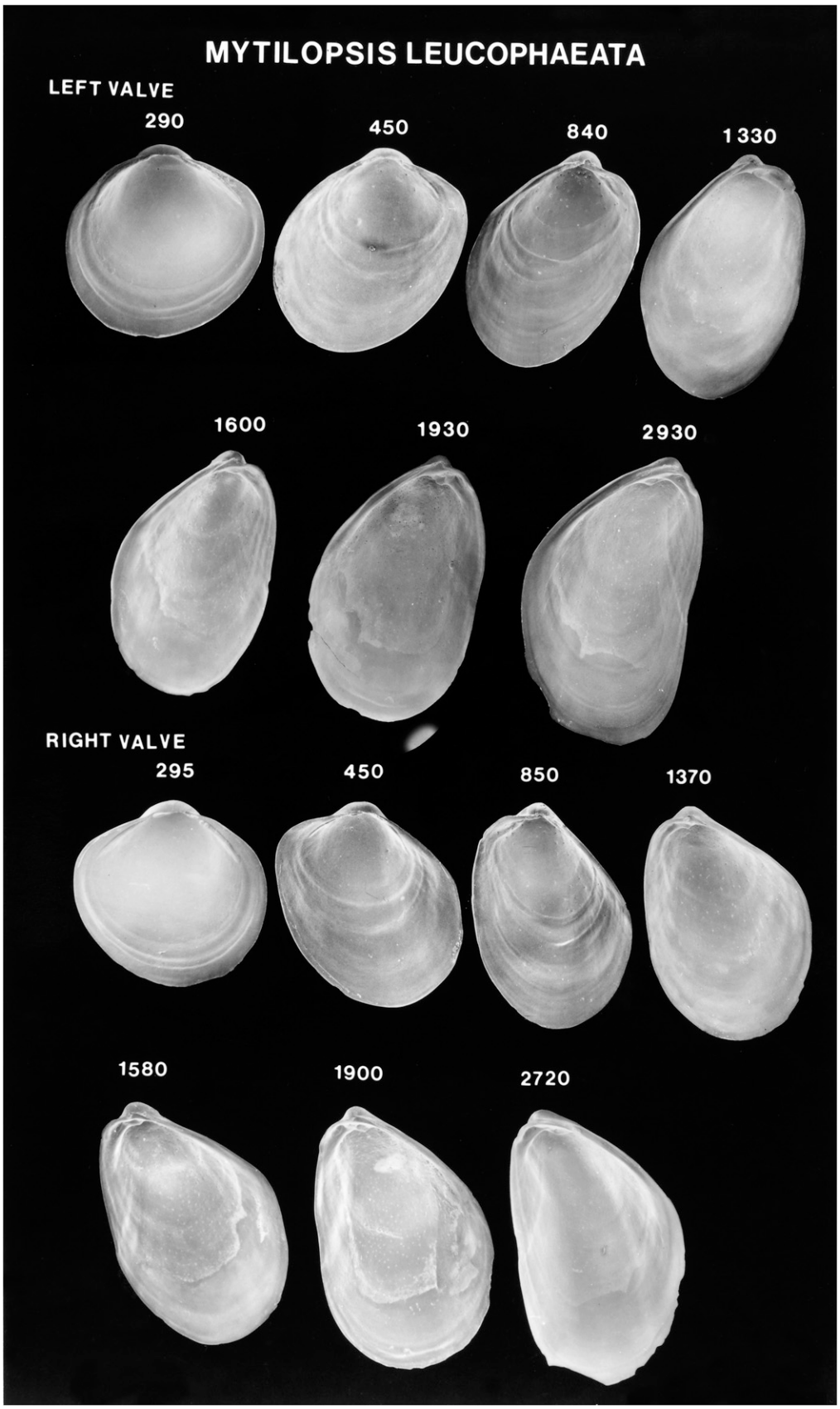

Figure 56. Scanning electron micrographs of disarticulated shell valves of *Mytilopsis leucophaeata* postlarvae. Numbers indicate the maximum linear shell dimension in micrometers.

Downloaded From: https://bioone.org/journals/Journal-of-Shellfish-Research on 25 Feb 2020
Terms of Use: https://bioone.org/terms-of-use Access provided by IFREMER

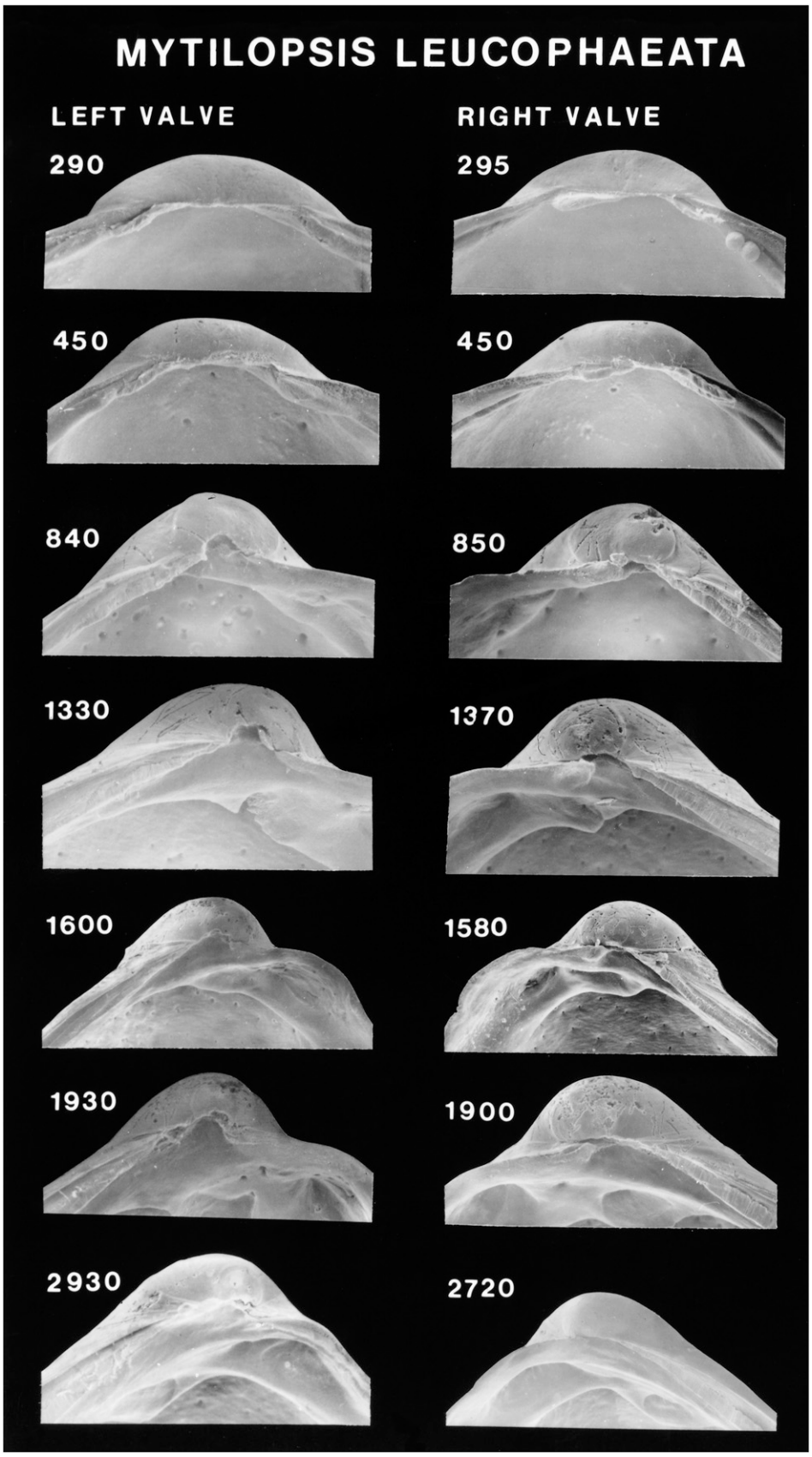

Figure 57. Scanning electron micrographs of the hinge of disarticulated shell valves of *Mytilopsis leucophaeata* postlarvae seen in Figure 56. Numbers indicate the maximum linear shell dimension in micrometers.

Downloaded From: https://bioone.org/journals/Journal-of-Shellfish-Research on 25 Feb 2020
Terms of Use: https://bioone.org/terms-of-use Access provided by IFREMER

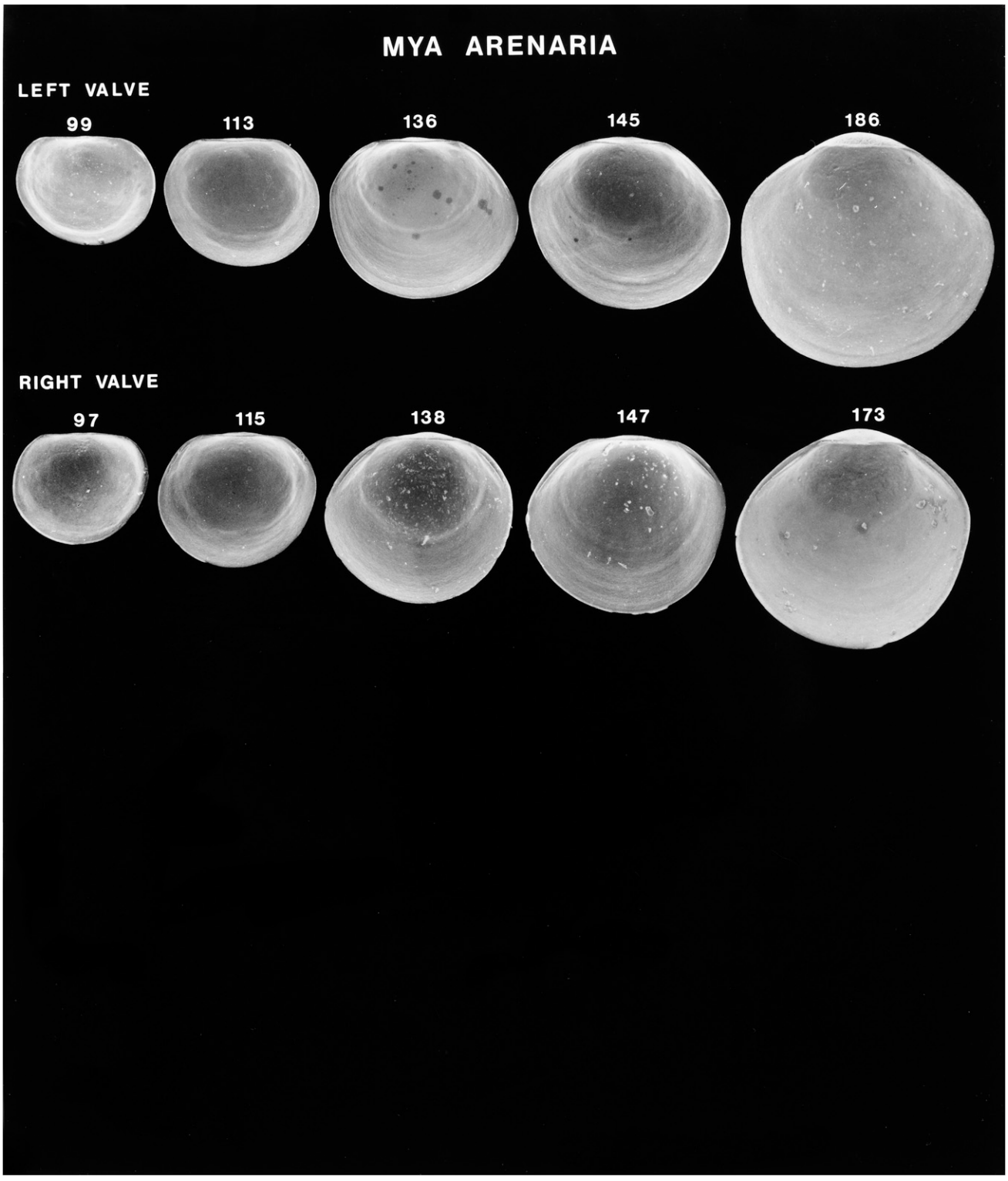

Figure 58. Scanning electron micrographs of disarticulated shell valves of *Mya arenaria* larvae. Numbers indicate the maximum linear shell dimension in micrometers.

Downloaded From: https://bioone.org/journals/Journal-of-Shellfish-Research on 25 Feb 2020
Terms of Use: https://bioone.org/terms-of-use Access provided by IFREMER

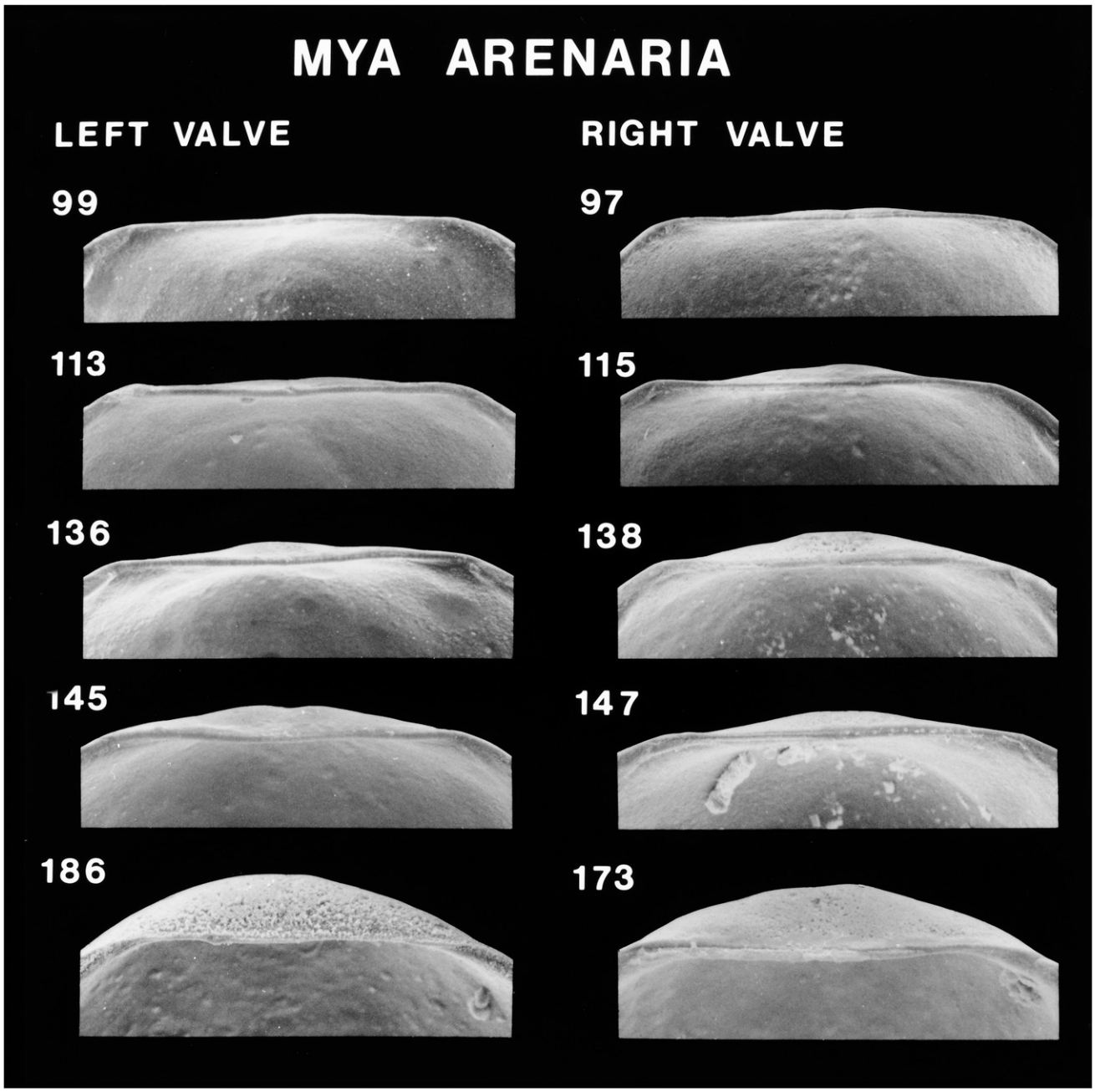

Figure 59. Scanning electron micrographs of the hinge of disarticulated shell valves of *Mya arenaria* larvae seen in Figure 58. Numbers indicate the maximum linear shell dimension in micrometers.

Downloaded From: https://bioone.org/journals/Journal-of-Shellfish-Research on 25 Feb 2020
Terms of Use: https://bioone.org/terms-of-use Access provided by IFREMER

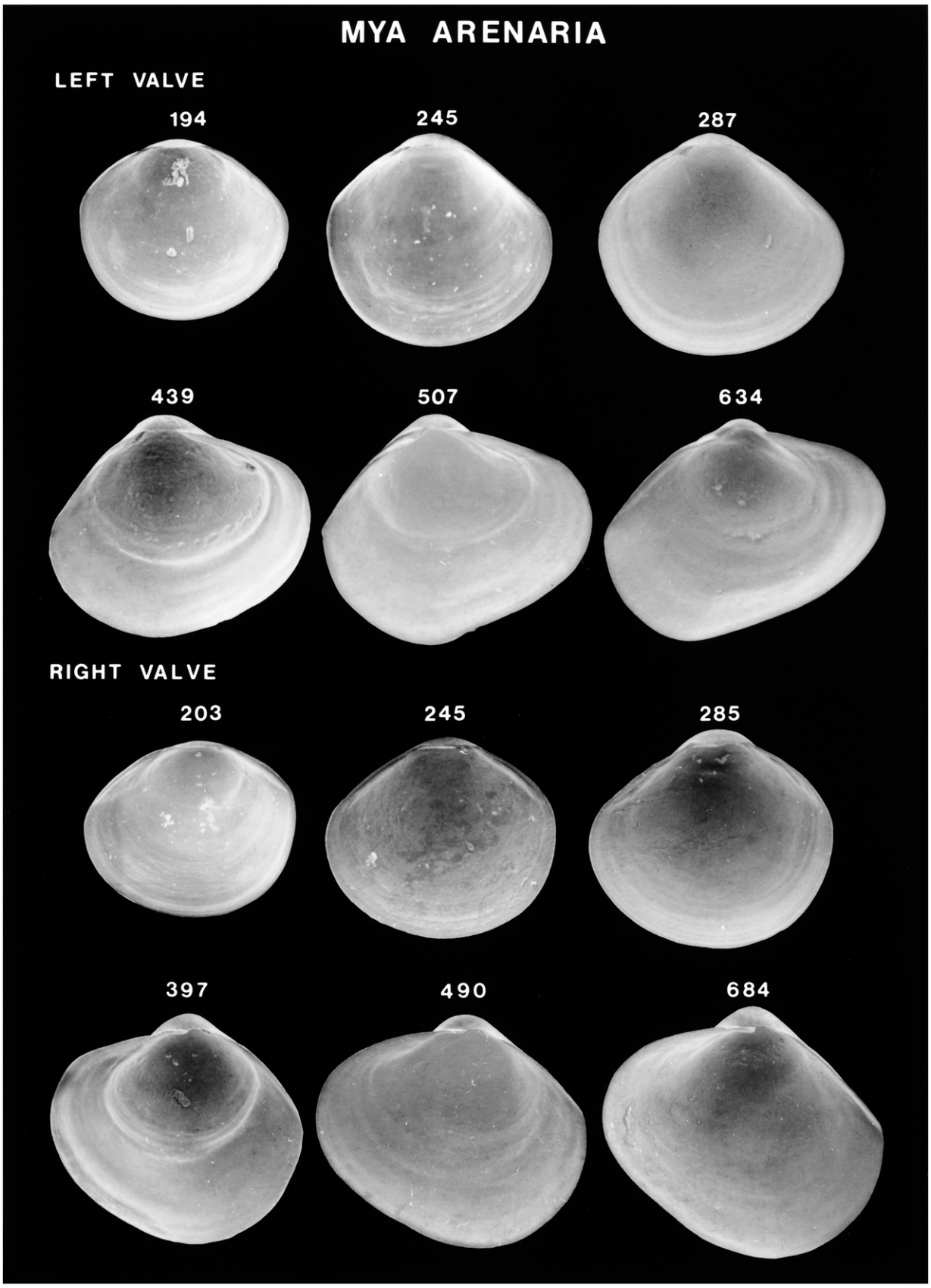

Figure 60. Scanning electron micrographs of disarticulated shell valves of *Mya arenaria* postlarvae. Numbers indicate the maximum linear shell dimension in micrometers.

Downloaded From: https://bioone.org/journals/Journal-of-Shellfish-Research on 25 Feb 2020
Terms of Use: https://bioone.org/terms-of-use Access provided by IFREMER

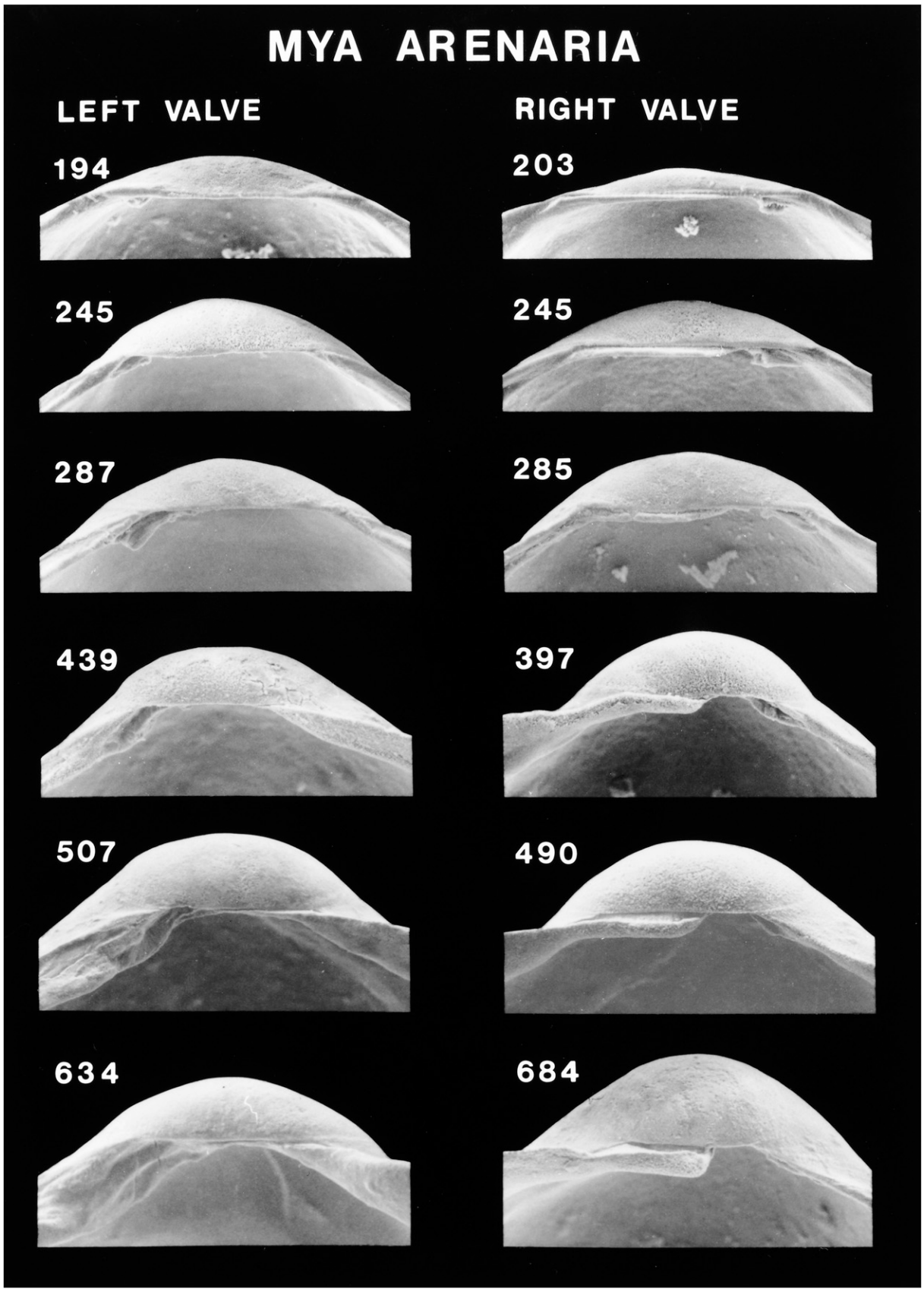

Figure 61. Scanning electron micrographs of the hinge of disarticulated shell valves of *Mya arenaria* postlarvae seen in Figure 60. Numbers indicate the maximum linear shell dimension in micrometers.

Downloaded From: https://bioone.org/journals/Journal-of-Shellfish-Research on 25 Feb 2020
Terms of Use: https://bioone.org/terms-of-use Access provided by IFREMER

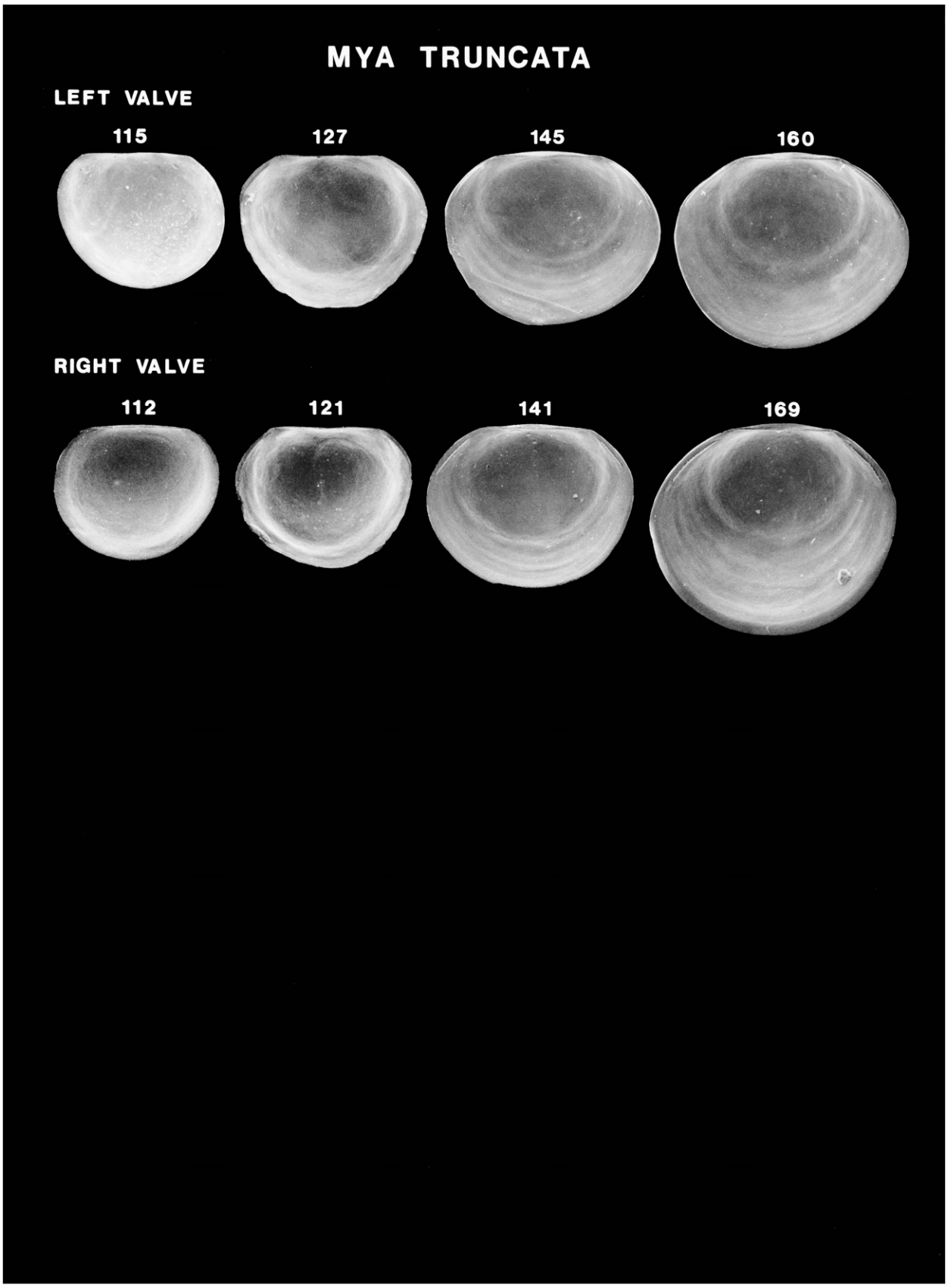

Figure 62. Scanning electron micrographs of disarticulated shell valves of *Mya truncata* larvae. Numbers indicate the maximum linear shell dimension in micrometers.

Downloaded From: https://bioone.org/journals/Journal-of-Shellfish-Research on 25 Feb 2020
Terms of Use: https://bioone.org/terms-of-use Access provided by IFREMER

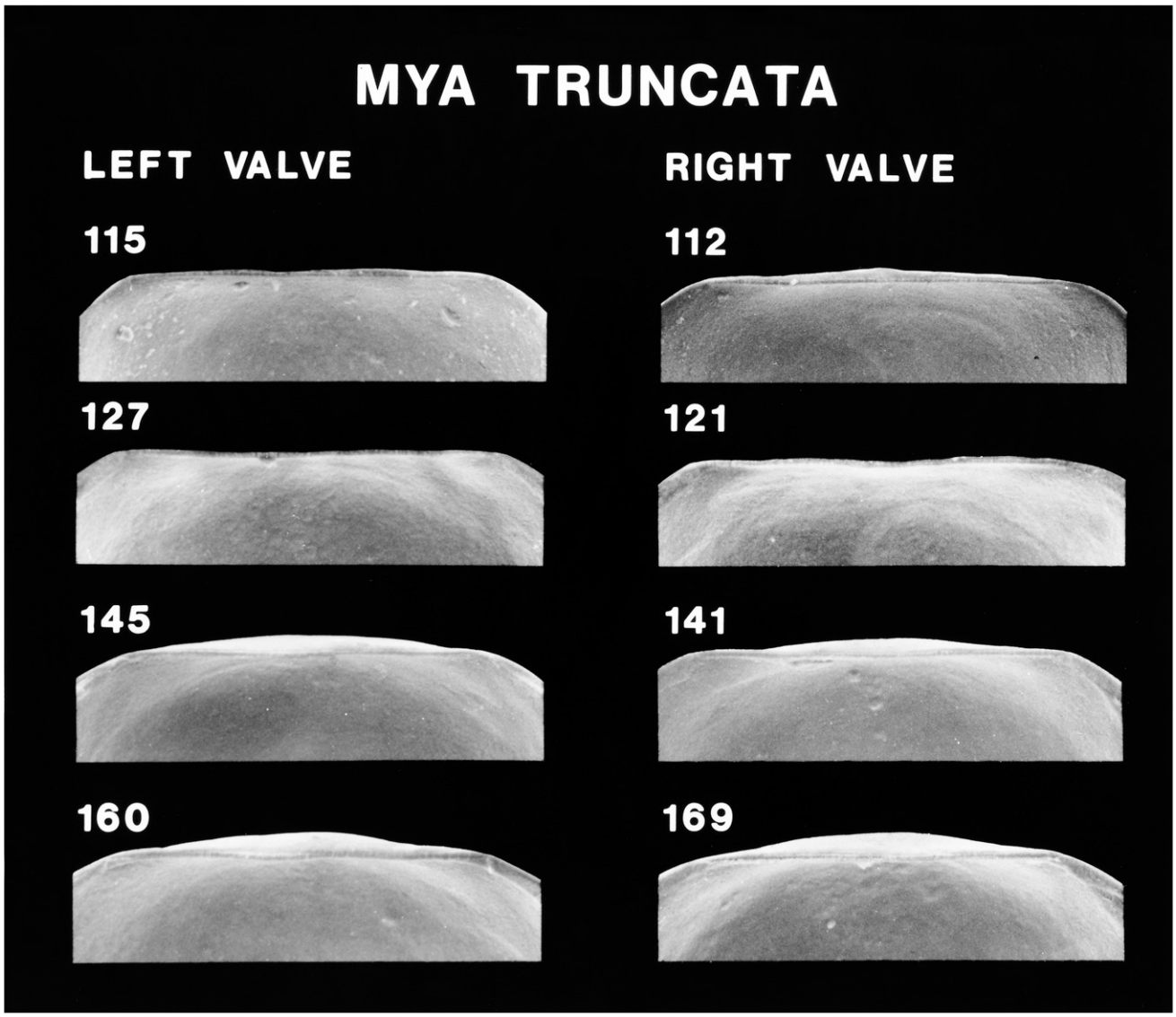

Figure 63. Scanning electron micrographs of the hinge of disarticulated shell valves of *Mya truncata* larvae seen in Figure 62. Numbers indicate the maximum linear shell dimension in micrometers.

Downloaded From: https://bioone.org/journals/Journal-of-Shellfish-Research on 25 Feb 2020
Terms of Use: https://bioone.org/terms-of-use Access provided by IFREMER

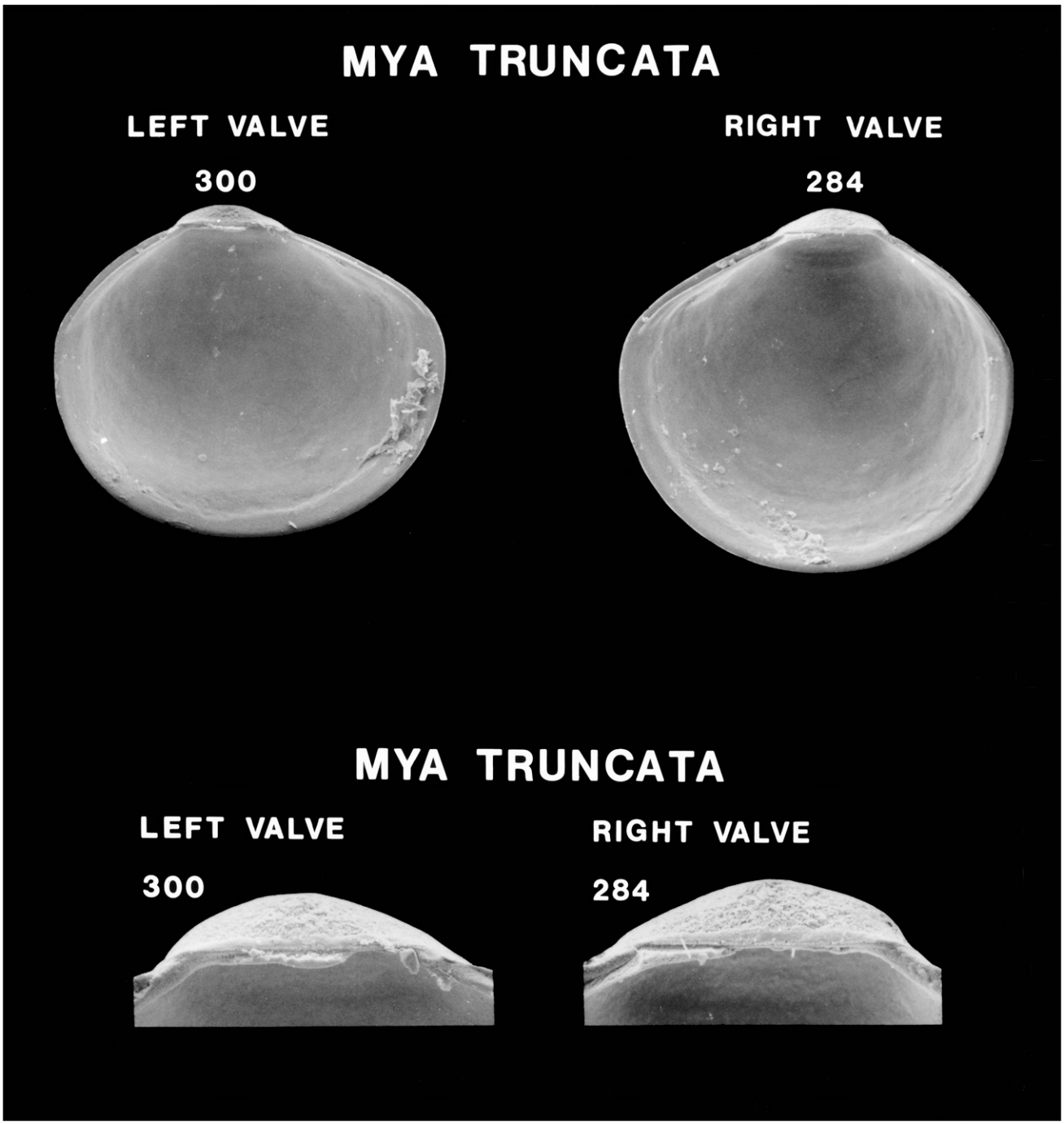

Figure 64. Scanning electron micrographs of disarticulated shell valves of *Mya truncata* postlarvae (top) and higher magnification scanning electron micrographs of the hinge of these shell valves (bottom). Numbers indicate the maximum linear shell dimension in micrometers.

Downloaded From: https://bioone.org/journals/Journal-of-Shellfish-Research on 25 Feb 2020
Terms of Use: https://bioone.org/terms-of-use Access provided by IFREMER

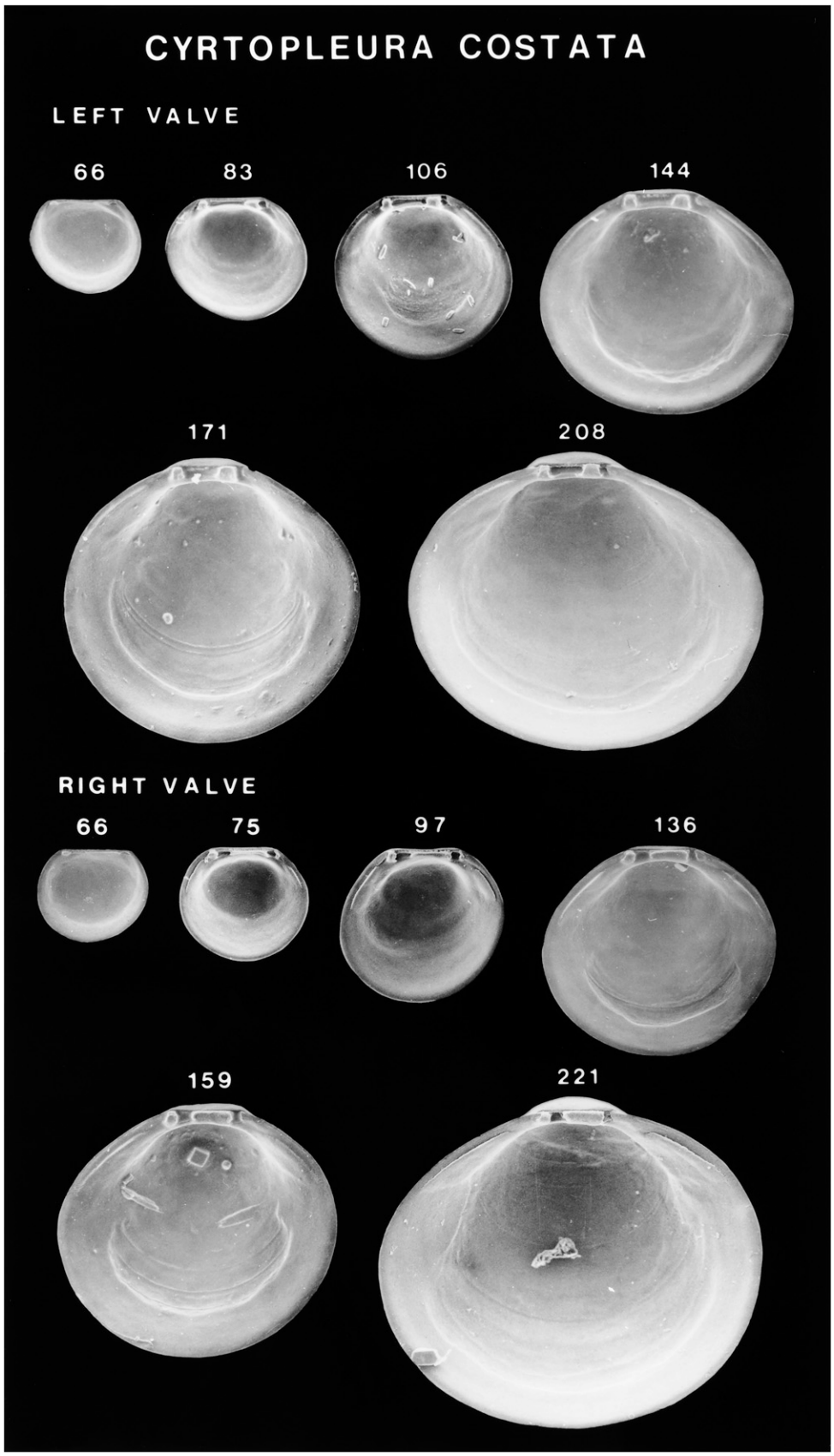

Figure 65. Scanning electron micrographs of disarticulated shell valves of *Cyrtopleura costata* larvae. Numbers indicate the maximum linear shell dimension in micrometers.

Downloaded From: https://bioone.org/journals/Journal-of-Shellfish-Research on 25 Feb 2020
Terms of Use: https://bioone.org/terms-of-use Access provided by IFREMER

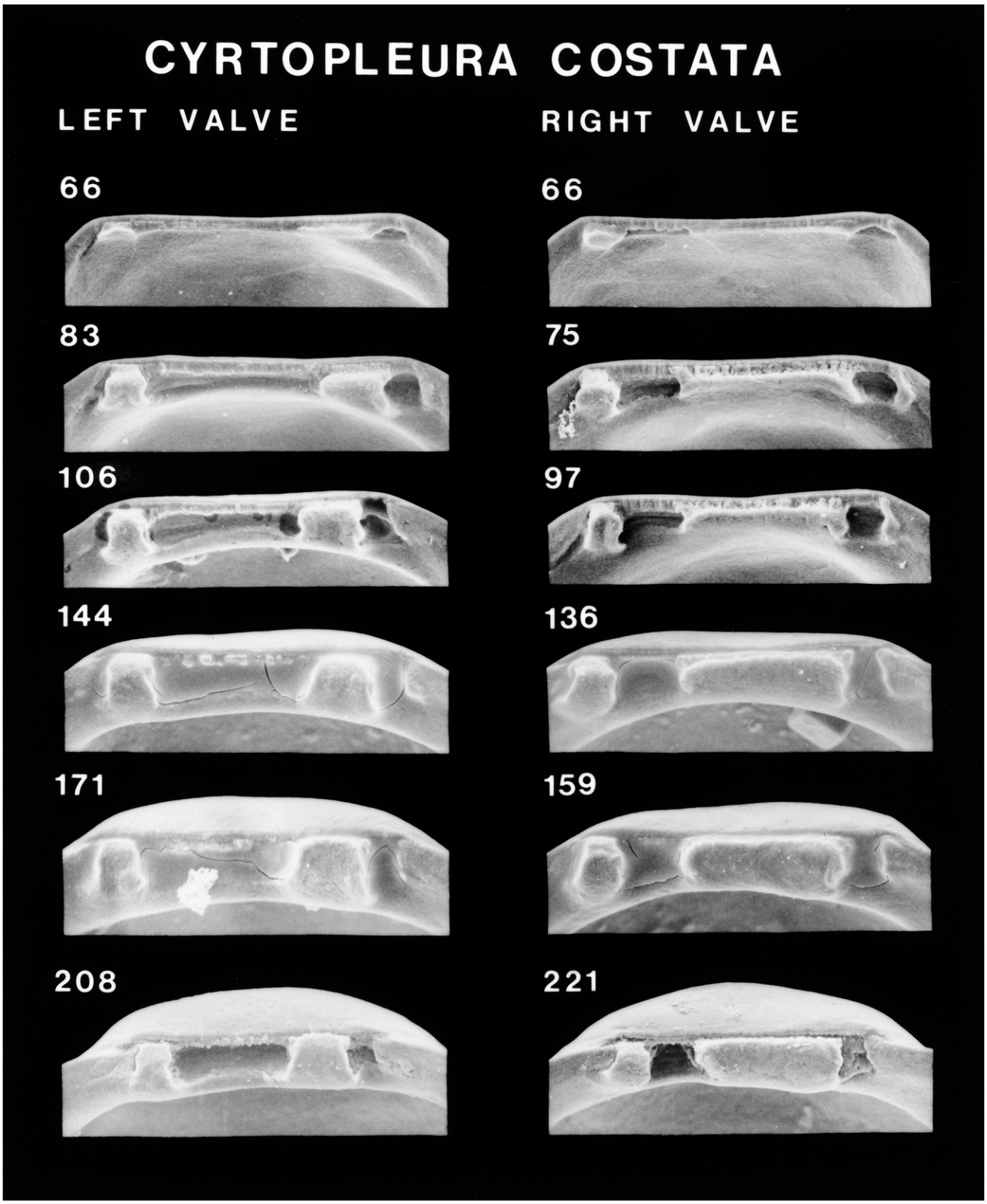

Figure 66. Scanning electron micrographs of the hinge of disarticulated shell valves of *Cyrtopleura costata* larvae seen in Figure 65. Numbers indicate the maximum linear shell dimension in micrometers.

Downloaded From: https://bioone.org/journals/Journal-of-Shellfish-Research on 25 Feb 2020
Terms of Use: https://bioone.org/terms-of-use Access provided by IFREMER

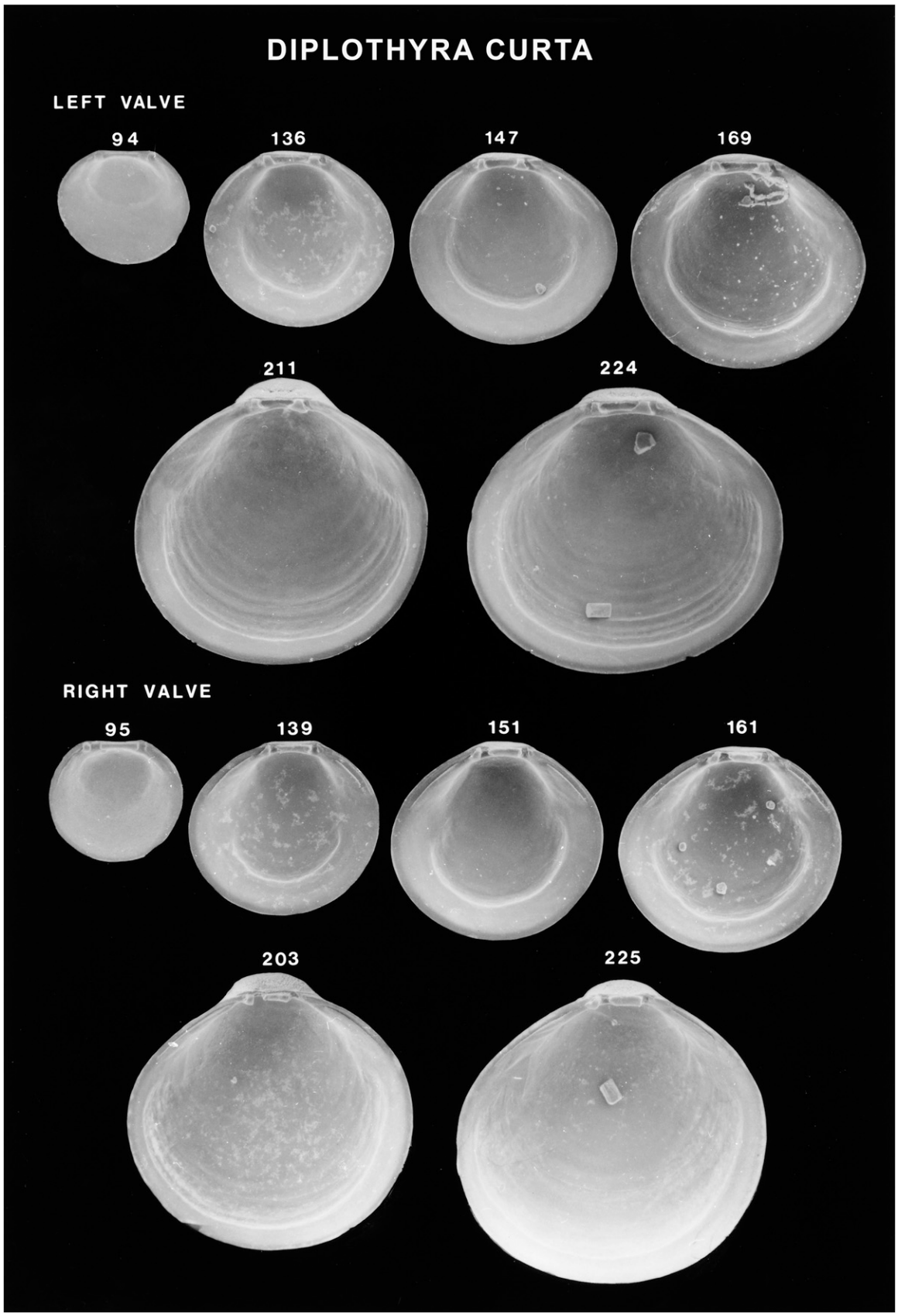

Figure 67. Scanning electron micrographs of disarticulated shell valves of *Diplothyra curta* larvae. Numbers indicate the maximum linear shell dimension in micrometers.

Downloaded From: https://bioone.org/journals/Journal-of-Shellfish-Research on 25 Feb 2020
Terms of Use: https://bioone.org/terms-of-use Access provided by IFREMER

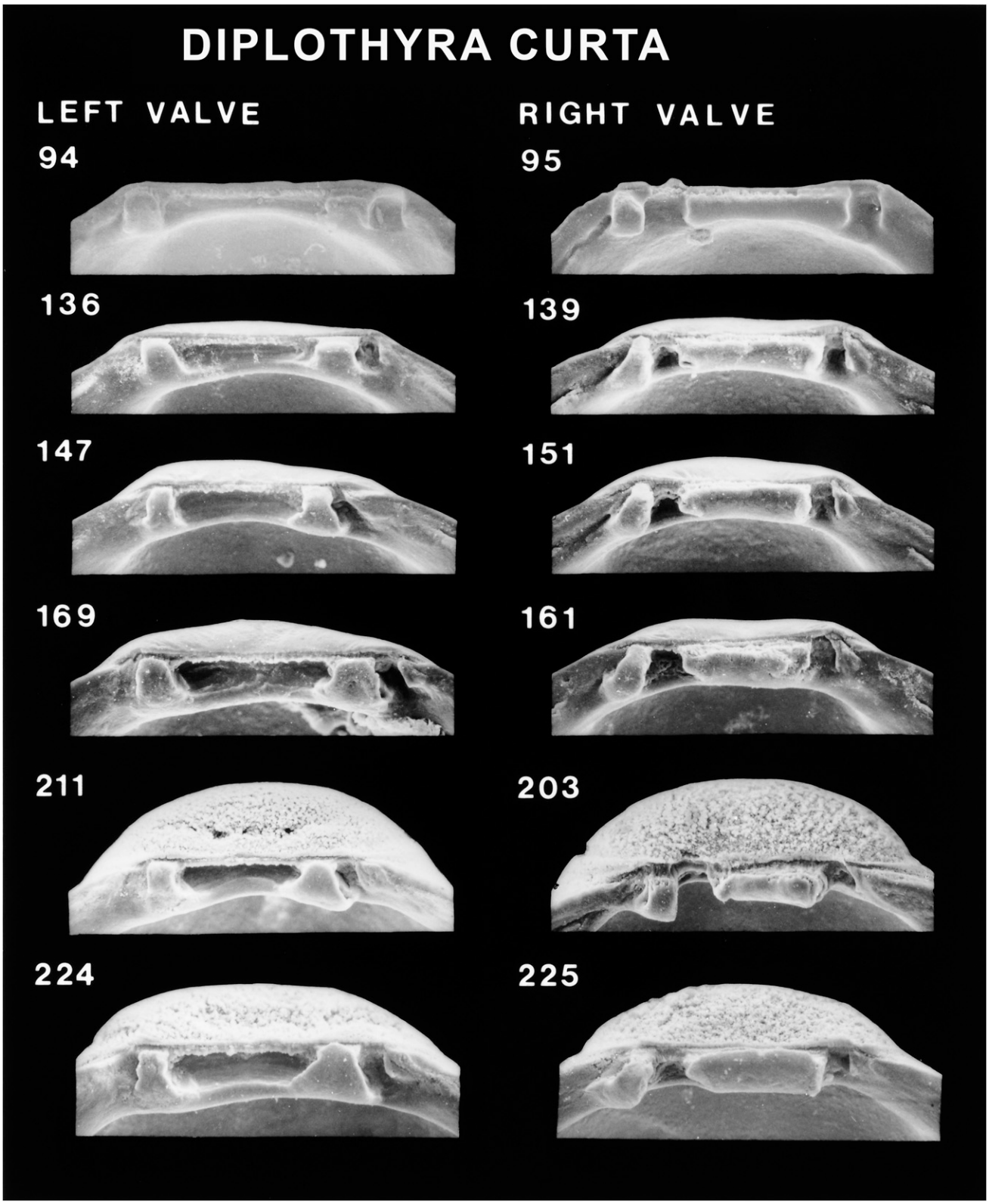

Figure 68. Scanning electron micrographs of the hinge of disarticulated shell valves of *Diplothyra curta* larvae seen in Figure 67. Numbers indicate the maximum linear shell dimension in micrometers.

Downloaded From: https://bioone.org/journals/Journal-of-Shellfish-Research on 25 Feb 2020
Terms of Use: https://bioone.org/terms-of-use Access provided by IFREMER

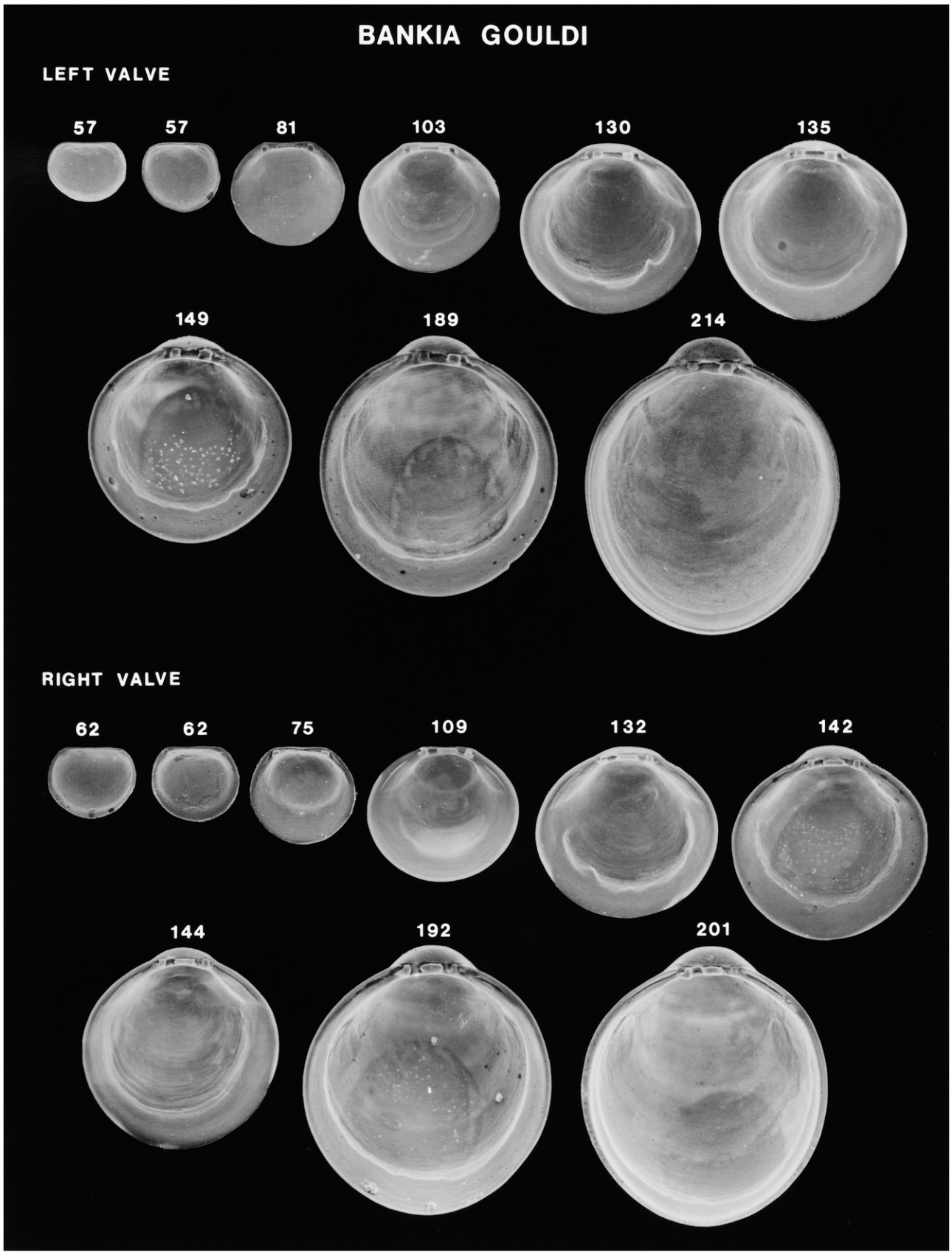

Figure 69. Scanning electron micrographs of disarticulated shell valves of *Bankia gouldi* larvae. Numbers indicate the maximum linear shell dimension in micrometers. Modified from Tan et al. (1993).

Downloaded From: https://bioone.org/journals/Journal-of-Shellfish-Research on 25 Feb 2020
Terms of Use: https://bioone.org/terms-of-use Access provided by IFREMER

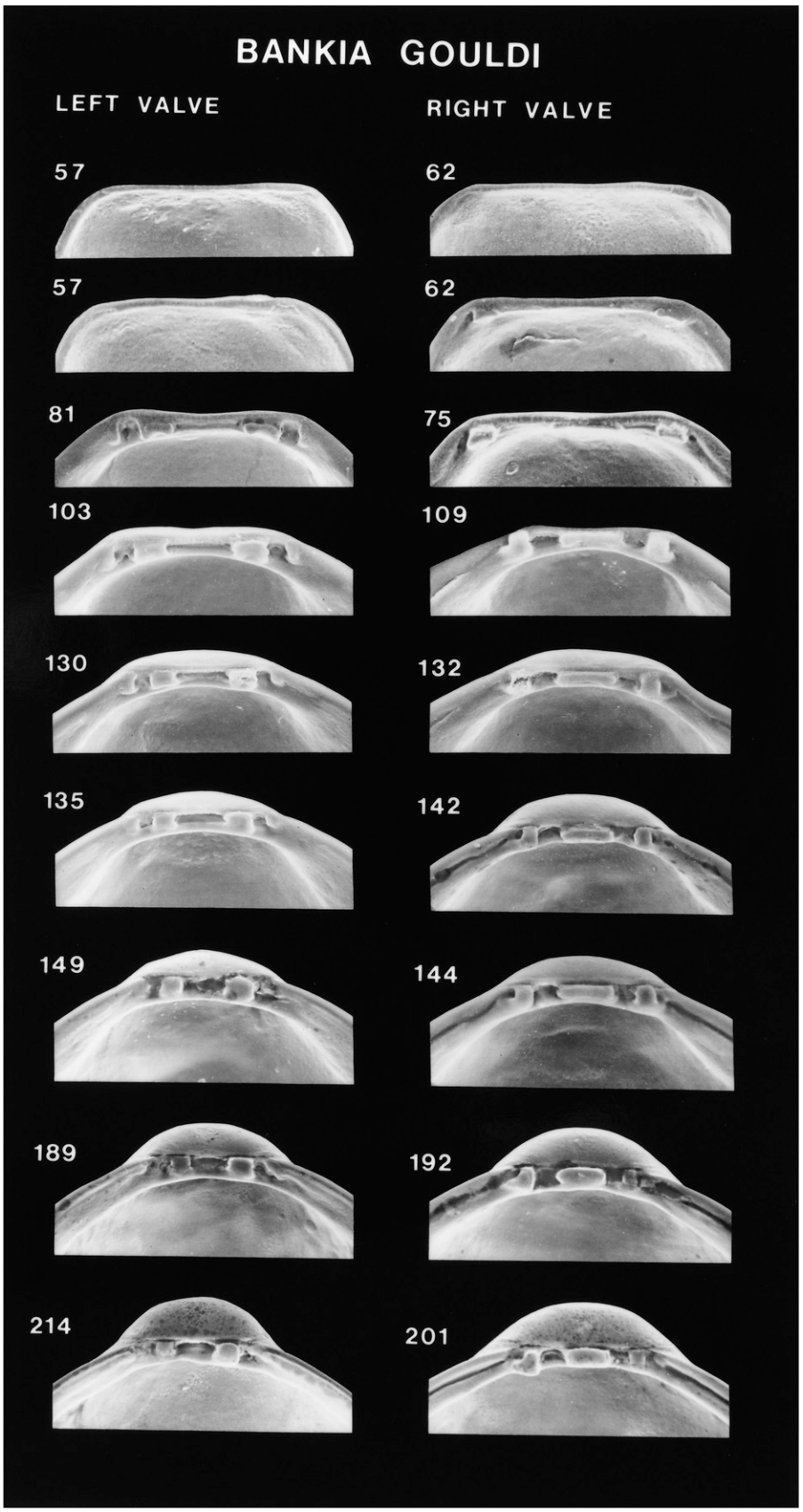

Figure 70. Scanning electron micrographs of the hinge of disarticulated shell valves of *Bankia gouldi* larvae seen in Figure 69. Numbers indicate the maximum linear shell dimension in micrometers. Modified from Tan et al. (1993).

Downloaded From: https://bioone.org/journals/Journal-of-Shellfish-Research on 25 Feb 2020
Terms of Use: https://bioone.org/terms-of-use Access provided by IFREMER

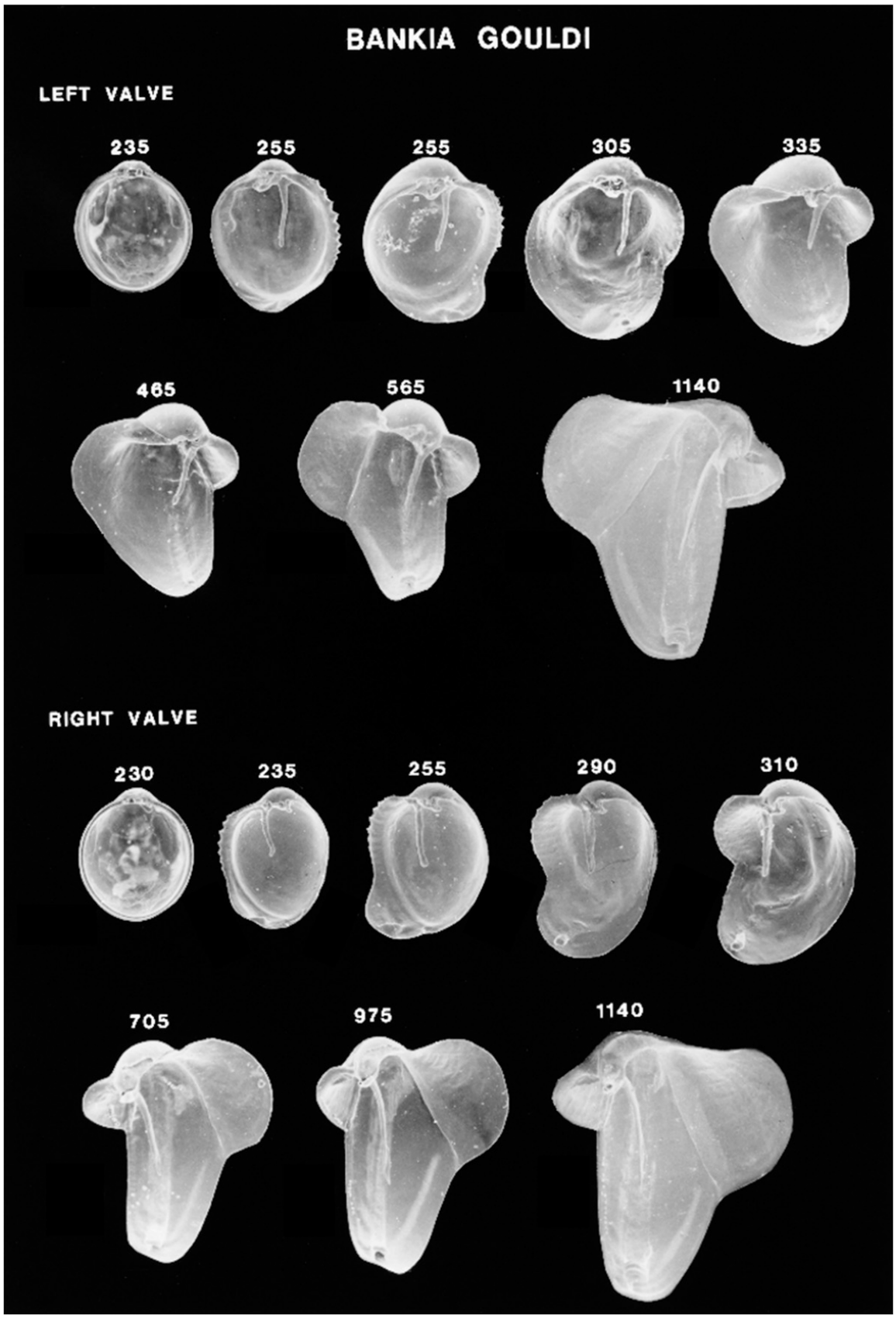

Figure 71. Scanning electron micrographs of disarticulated shell valves of *Bankia gouldi* postlarvae. Numbers indicate shell height (the greatest dorsoventral dimension) in micrometers. Modified from Tan et al. (1993).

Downloaded From: https://bioone.org/journals/Journal-of-Shellfish-Research on 25 Feb 2020
Terms of Use: https://bioone.org/terms-of-use Access provided by IFREMER

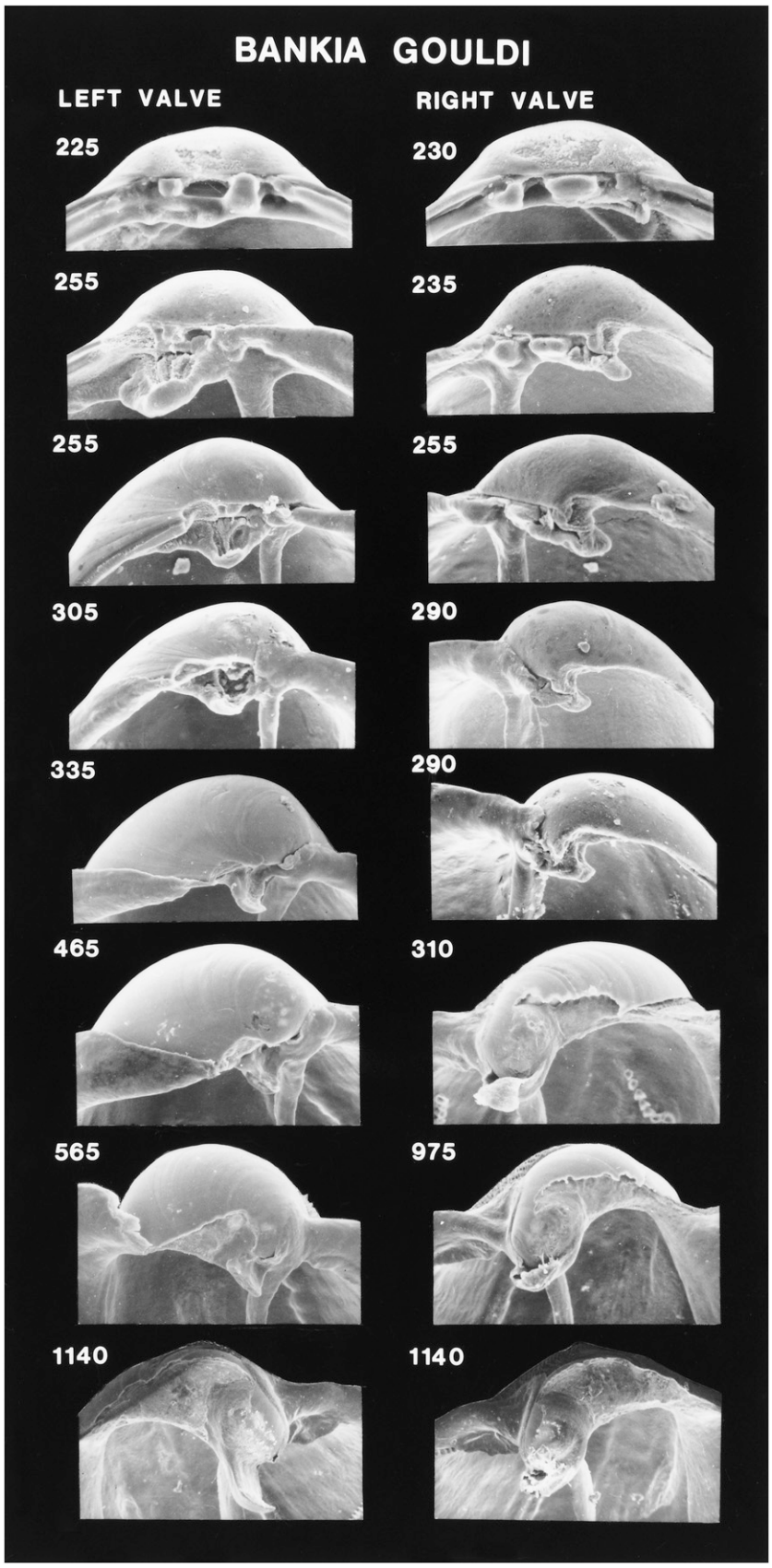

Figure 72. Scanning electron micrographs of the hinge of disarticulated shell valves of *Bankia gouldi* postlarvae seen in Figure 71. Numbers indicate shell height (the greatest dorsoventral dimension) in micrometers. Modified from Tan et al. (1993).

Downloaded From: https://bioone.org/journals/Journal-of-Shellfish-Research on 25 Feb 2020
Terms of Use: https://bioone.org/terms-of-use Access provided by IFREMER

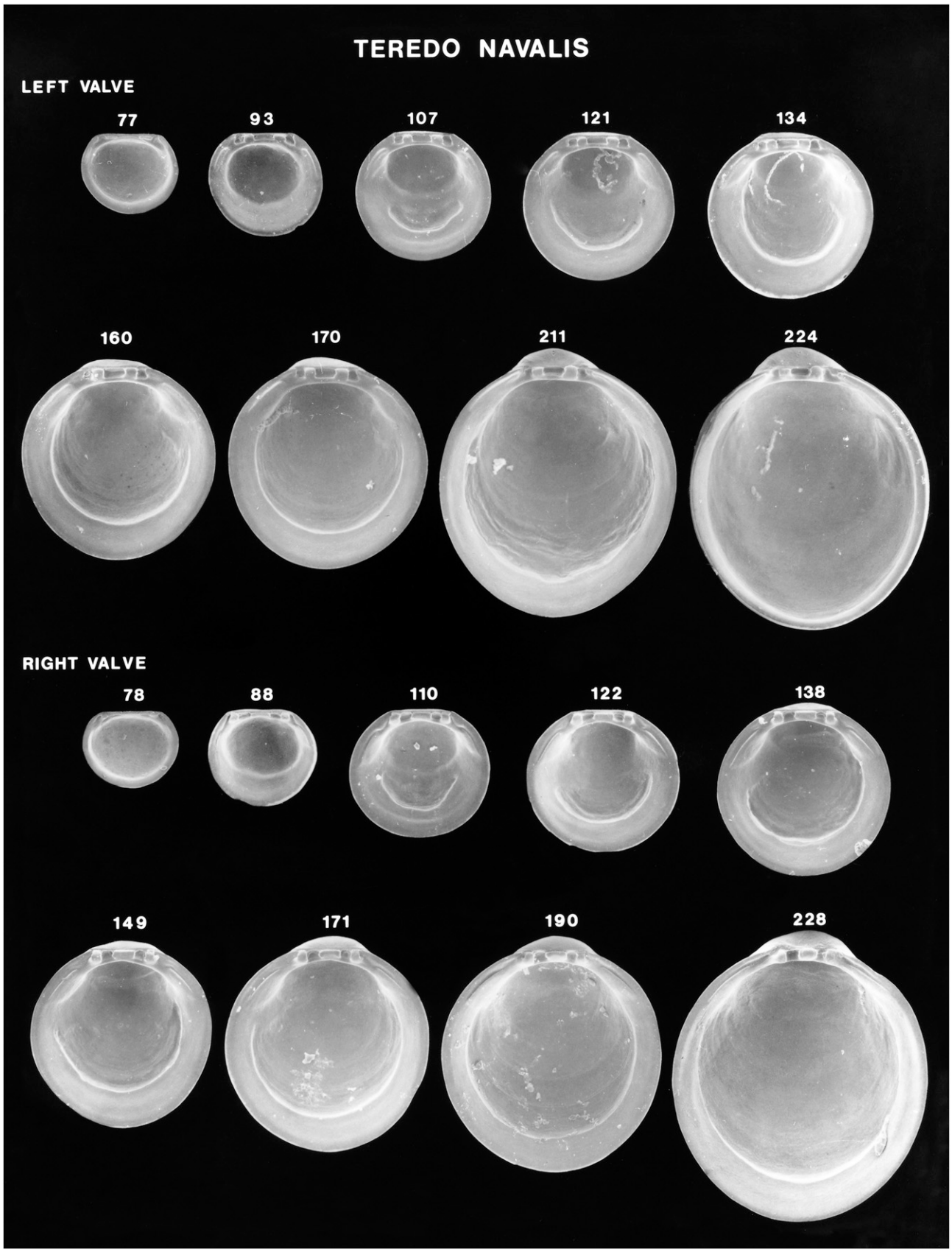

Figure 73. Scanning electron micrographs of disarticulated shell valves of *Teredo navalis* larvae. Numbers indicate the maximum linear shell dimension in micrometers. Modified from Fuller et al. (1989a).

Downloaded From: https://bioone.org/journals/Journal-of-Shellfish-Research on 25 Feb 2020
Terms of Use: https://bioone.org/terms-of-use Access provided by IFREMER

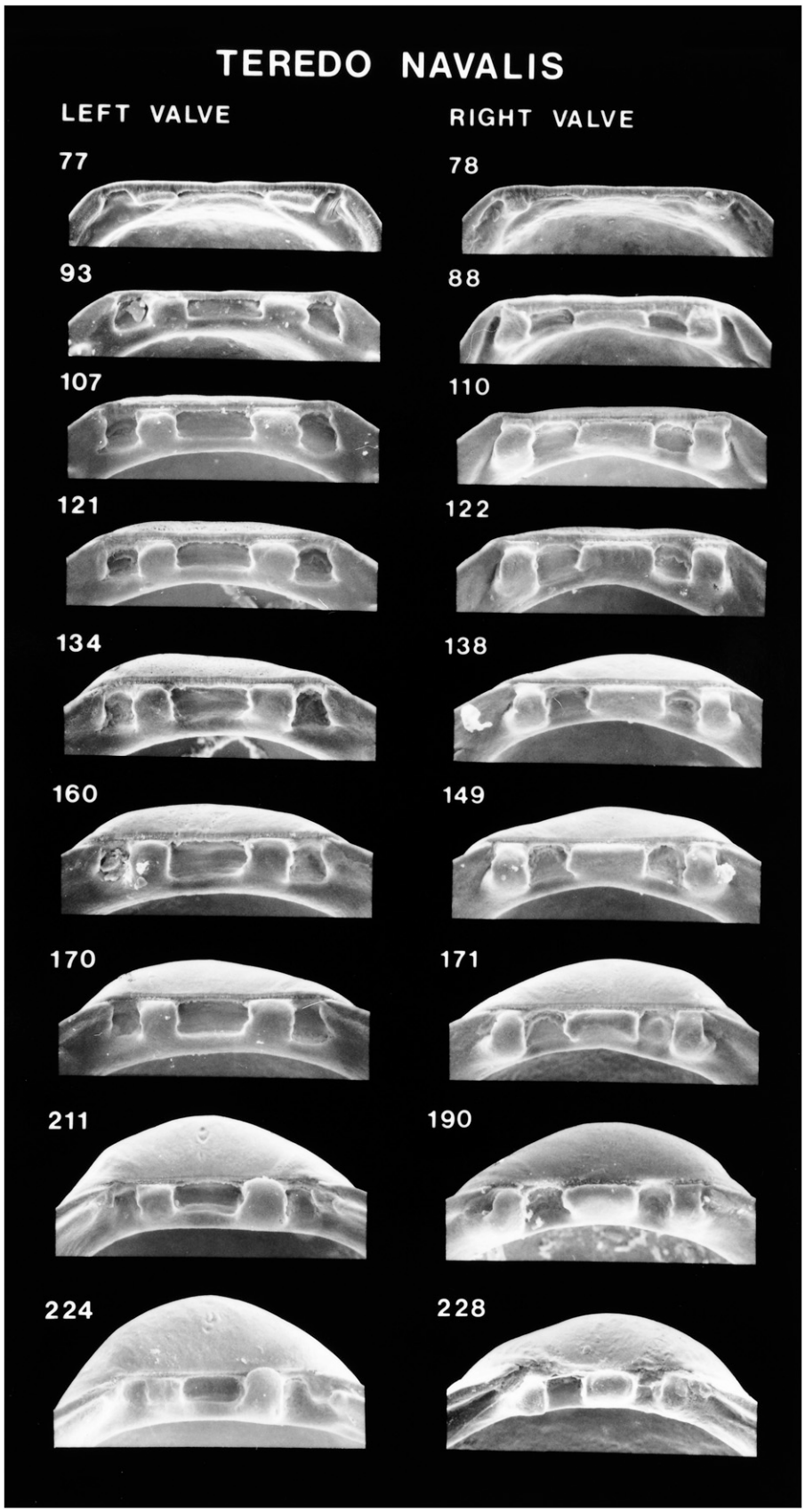

Figure 74. Scanning electron micrographs of the hinge of disarticulated shell valves of *Teredo navalis* larvae seen in Figure 73. Numbers indicate the maximum linear shell dimension in micrometers. Modified from Fuller et al. (1989a).

Downloaded From: https://bioone.org/journals/Journal-of-Shellfish-Research on 25 Feb 2020
Terms of Use: https://bioone.org/terms-of-use Access provided by IFREMER

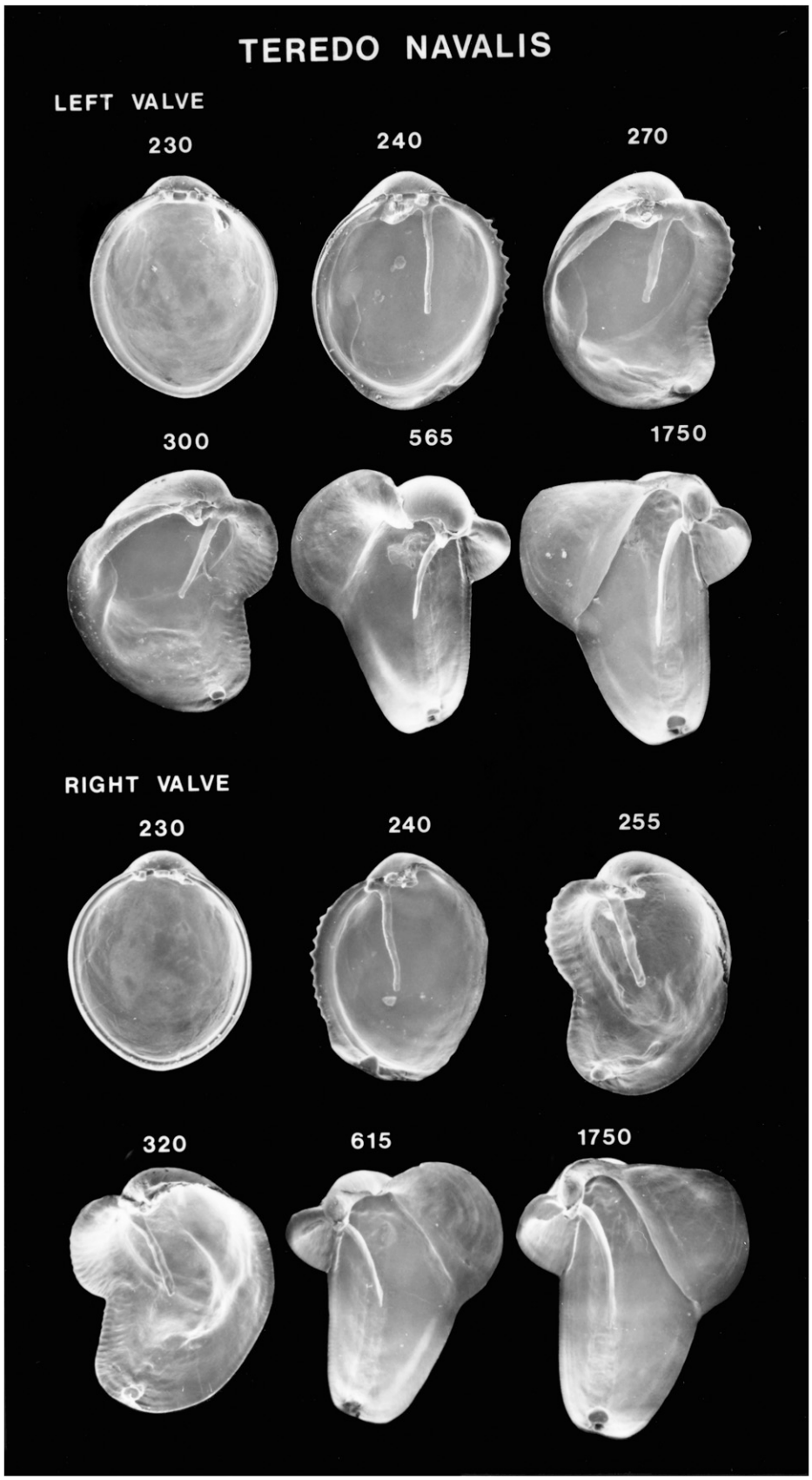

Figure 75. Scanning electron micrographs of disarticulated shell valves of *Teredo navalis* postlarvae. Numbers indicate shell height (the greatest dorsoventral dimension) in micrometers. Modified from Fuller et al. (1989a).

Downloaded From: https://bioone.org/journals/Journal-of-Shellfish-Research on 25 Feb 2020
Terms of Use: https://bioone.org/terms-of-use Access provided by IFREMER

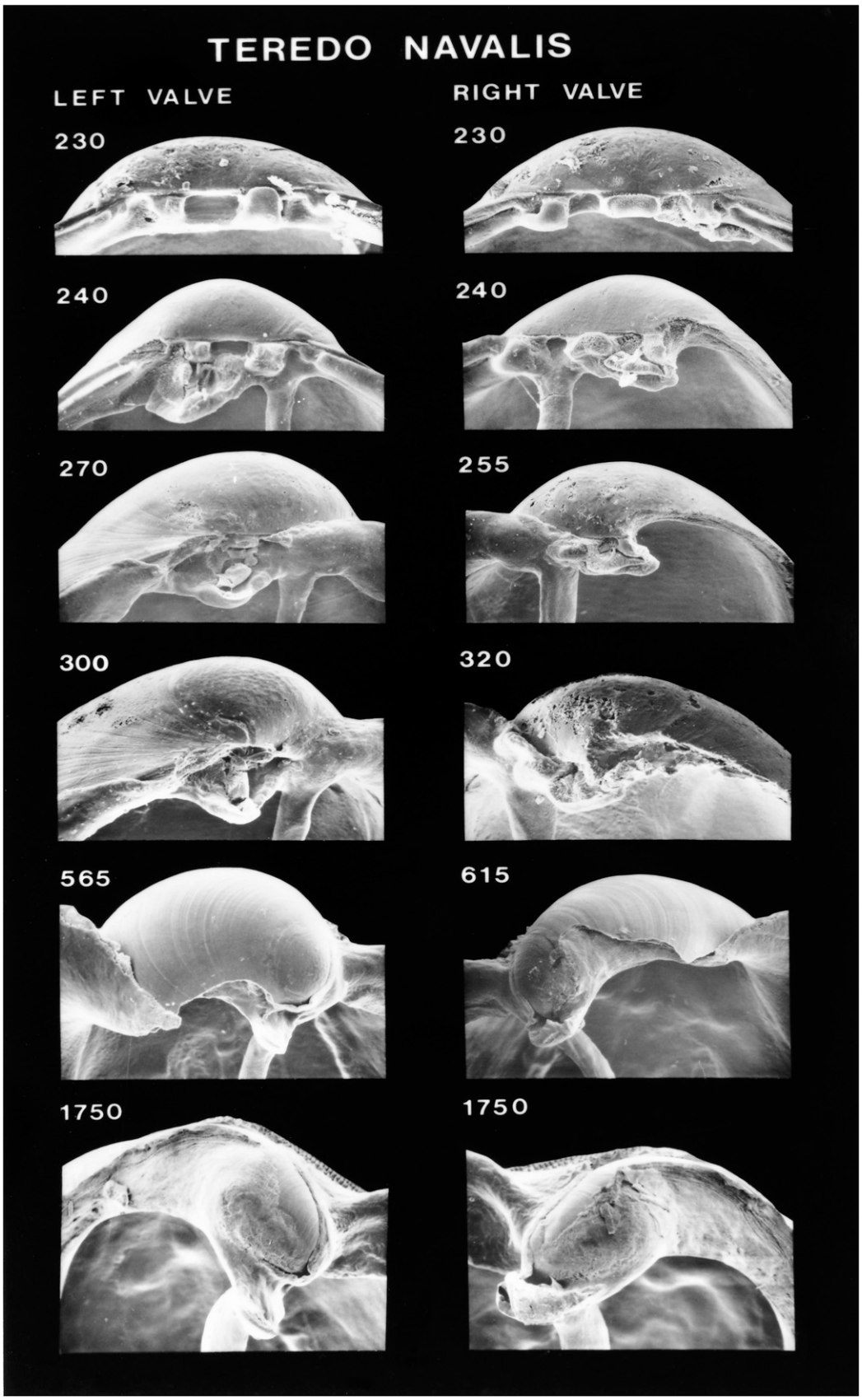

Figure 76. Scanning electron micrographs of the hinge of disarticulated shell valves of *Teredo navalis* postlarvae seen in Figure 75. Numbers indicate shell height (the greatest dorsoventral dimension) in micrometers. Modified from Fuller et al. (1989a).

Downloaded From: https://bioone.org/journals/Journal-of-Shellfish-Research on 25 Feb 2020
Terms of Use: https://bioone.org/terms-of-use Access provided by IFREMER

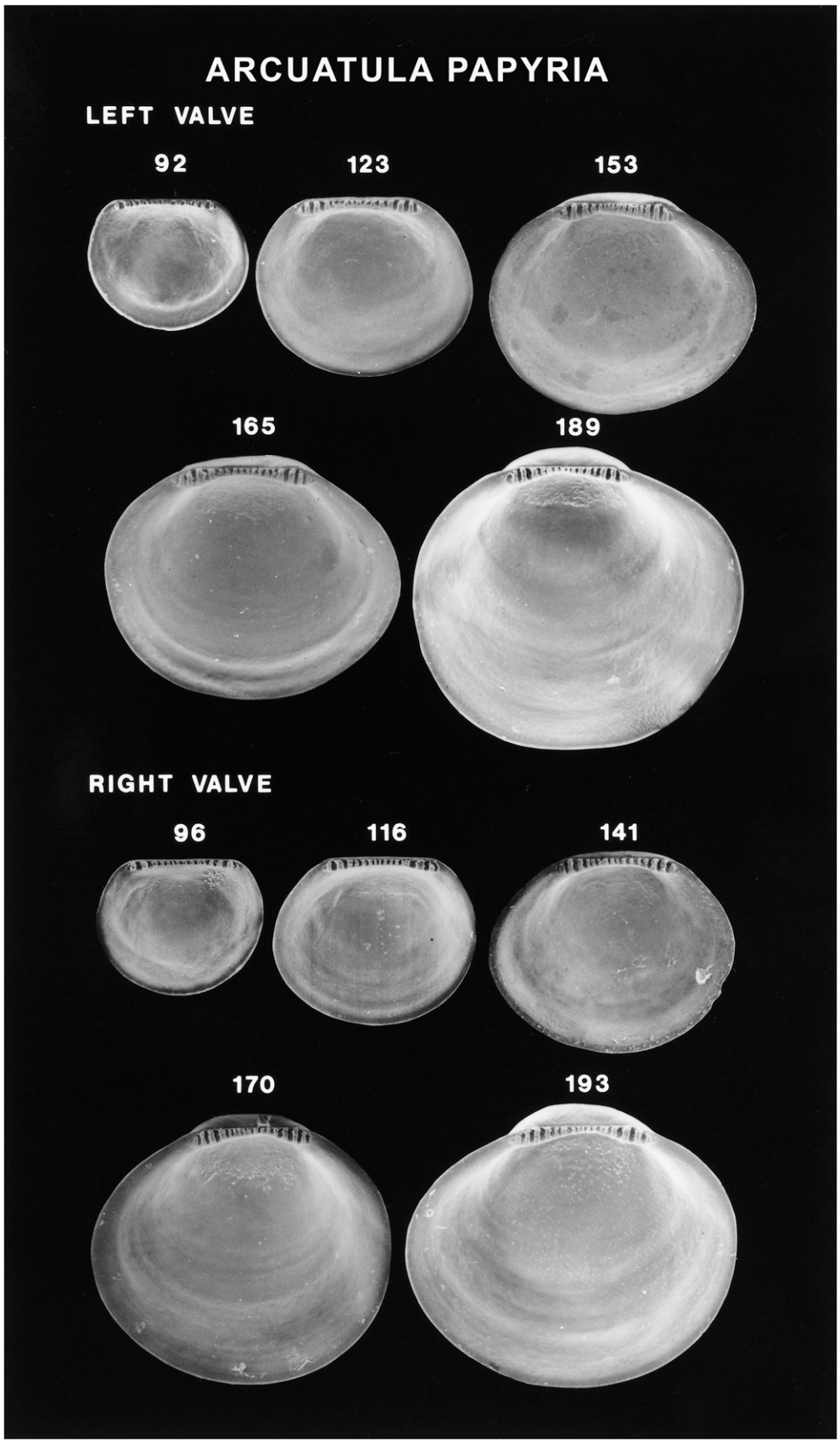

Figure 77. Scanning electron micrographs of disarticulated shell valves of *Arcuatula papyria* larvae. Numbers indicate the maximum linear shell dimension in micrometers.

Downloaded From: https://bioone.org/journals/Journal-of-Shellfish-Research on 25 Feb 2020
Terms of Use: https://bioone.org/terms-of-use Access provided by IFREMER

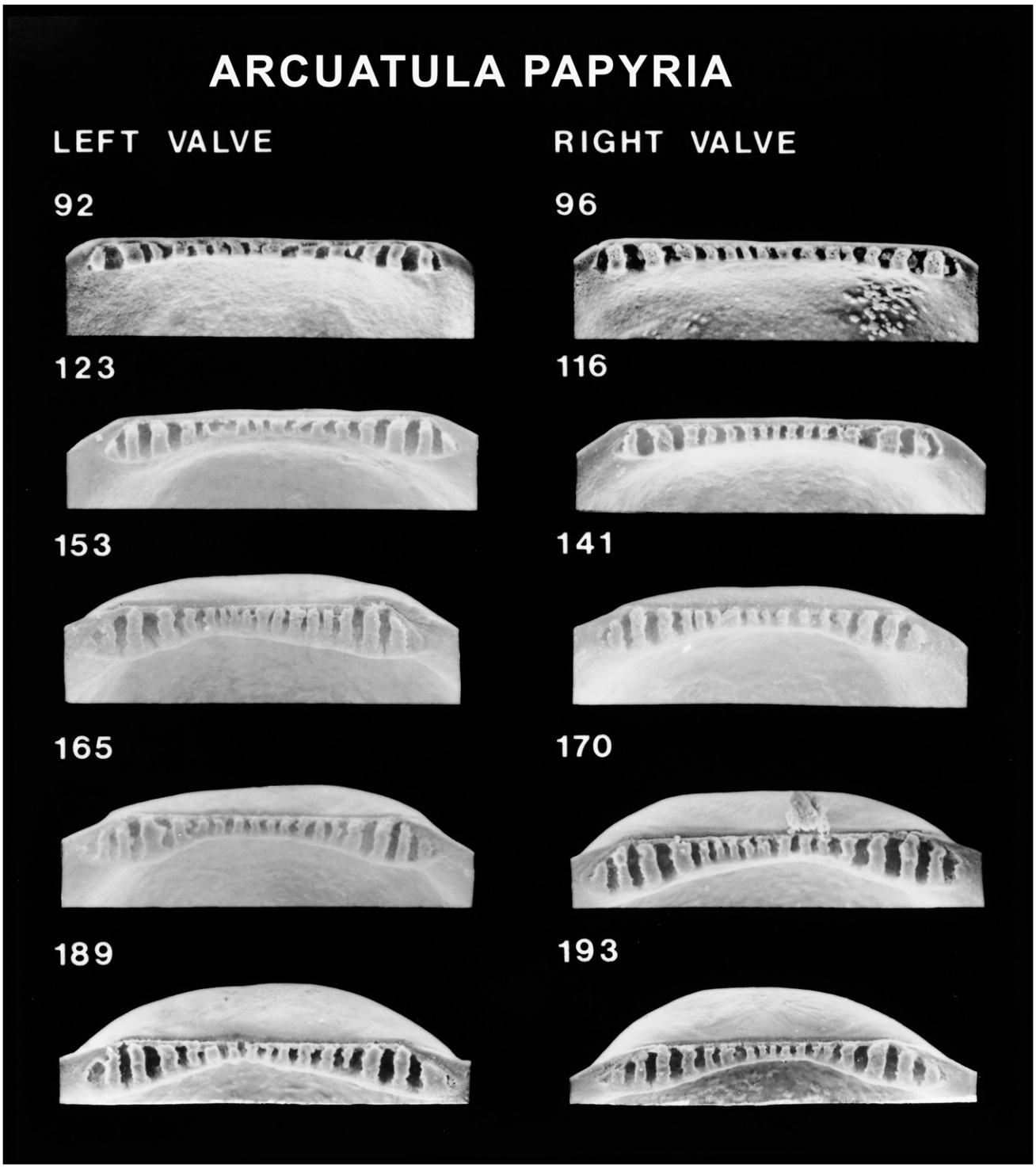

Figure 78. Scanning electron micrographs of the hinge of disarticulated shell valves of *Arcuatula papyri* larvae seen in Figure 77. Numbers indicate the maximum linear shell dimension in micrometers.

Downloaded From: https://bioone.org/journals/Journal-of-Shellfish-Research on 25 Feb 2020
Terms of Use: https://bioone.org/terms-of-use Access provided by IFREMER

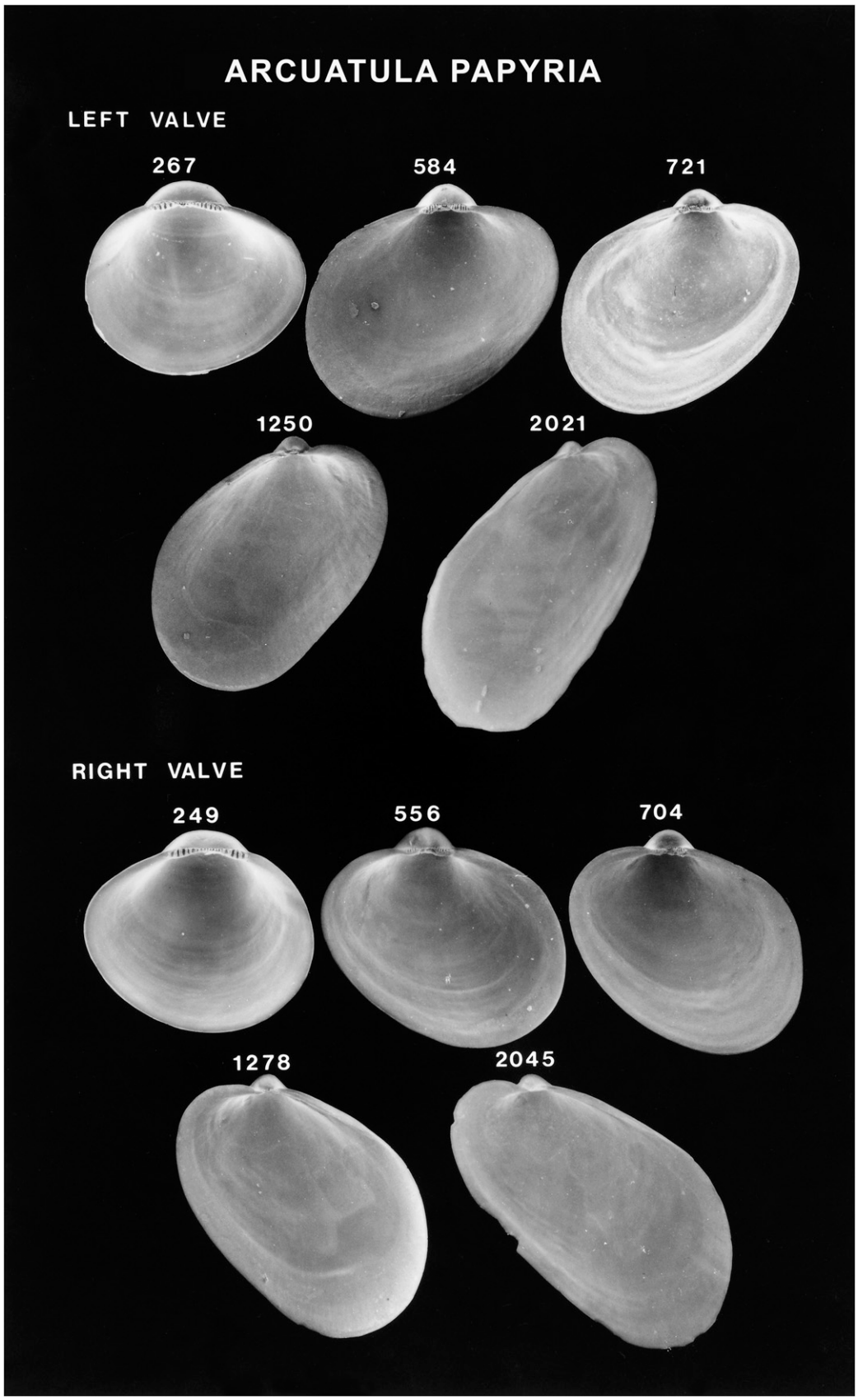

Figure 79. Scanning electron micrographs of disarticulated shell valves of *Arcuatula papyri* postlarvae. Numbers indicate the maximum linear shell dimension in micrometers.

Downloaded From: https://bioone.org/journals/Journal-of-Shellfish-Research on 25 Feb 2020
Terms of Use: https://bioone.org/terms-of-use Access provided by IFREMER

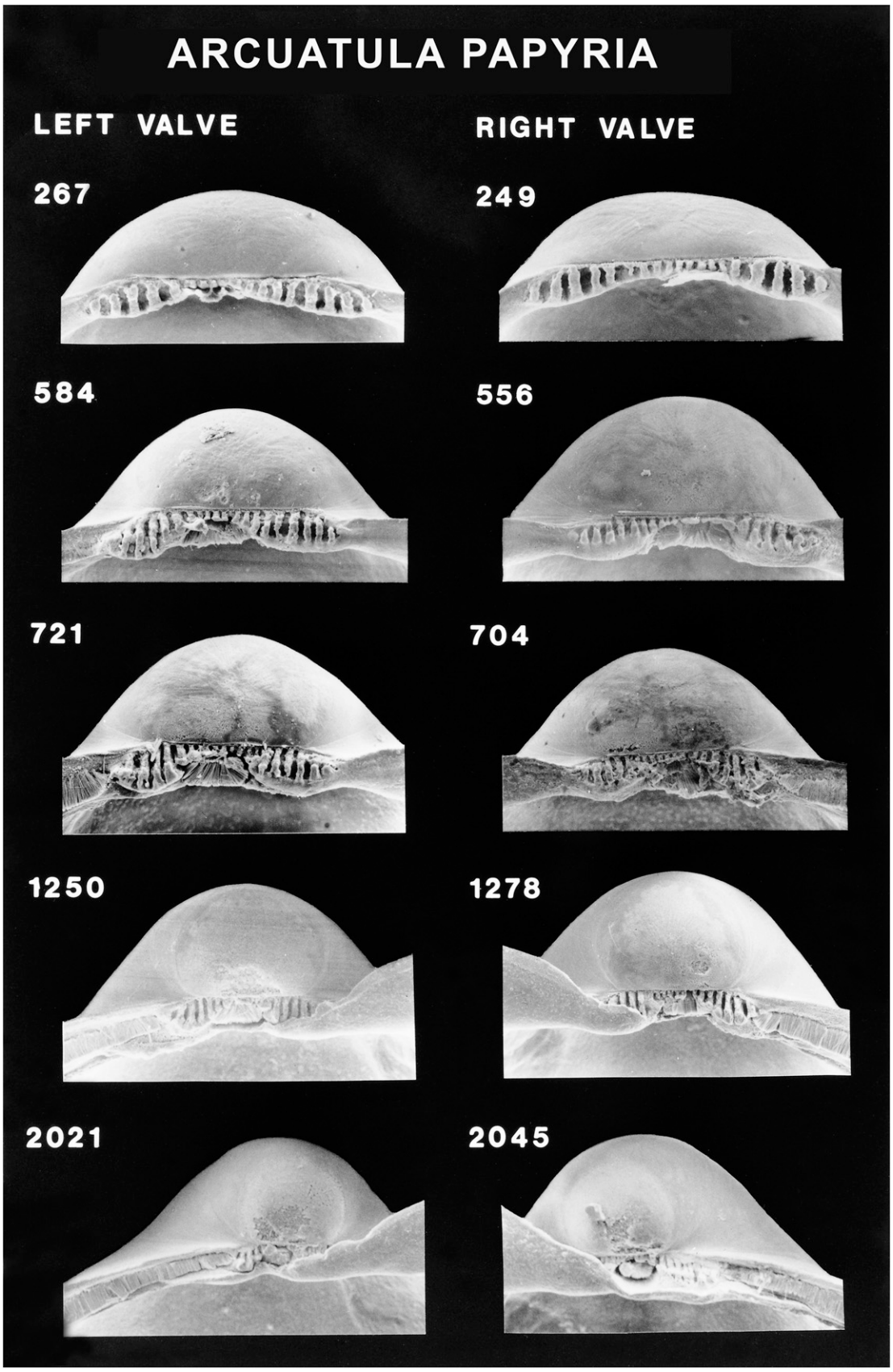

Figure 80. Scanning electron micrographs of the hinge of disarticulated shell valves of *Arcuatula papyri* postlarvae seen in Figure 79. Numbers indicate the maximum linear shell dimension in micrometers.

Downloaded From: https://bioone.org/journals/Journal-of-Shellfish-Research on 25 Feb 2020
Terms of Use: https://bioone.org/terms-of-use Access provided by IFREMER

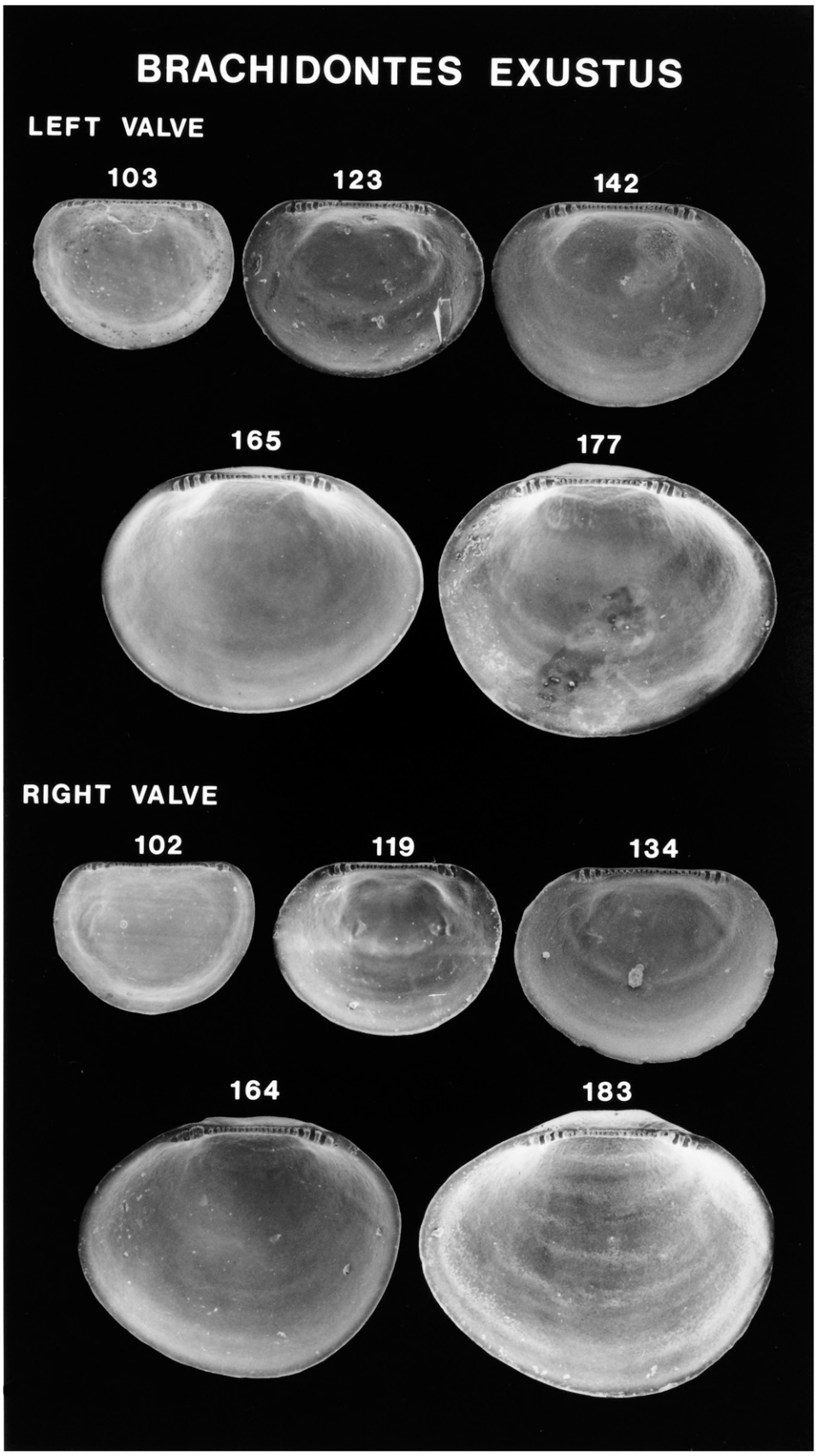

Figure 81. Scanning electron micrographs of disarticulated shell valves of *Brachidontes exustus* larvae. Numbers indicate the maximum linear shell dimension in micrometers. Modified from Fuller and Lutz (1989).

Downloaded From: https://bioone.org/journals/Journal-of-Shellfish-Research on 25 Feb 2020
Terms of Use: https://bioone.org/terms-of-use Access provided by IFREMER

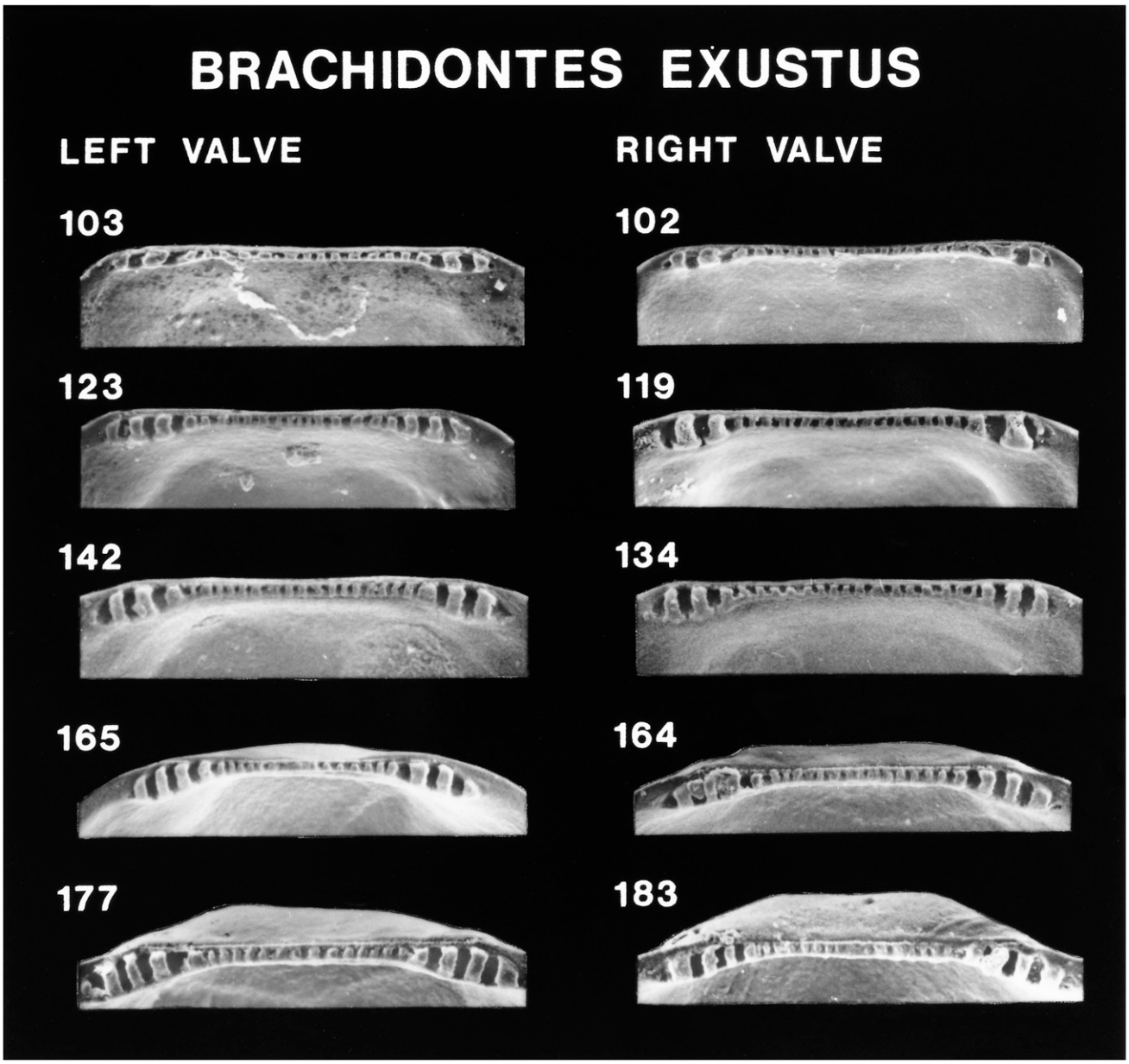

Figure 82. Scanning electron micrographs of the hinge of disarticulated shell valves of *Brachidontes exustus* larvae seen in Figure 81. Numbers indicate the maximum linear shell dimension in micrometers. Modified from Fuller and Lutz (1989).

Downloaded From: https://bioone.org/journals/Journal-of-Shellfish-Research on 25 Feb 2020
Terms of Use: https://bioone.org/terms-of-use Access provided by IFREMER

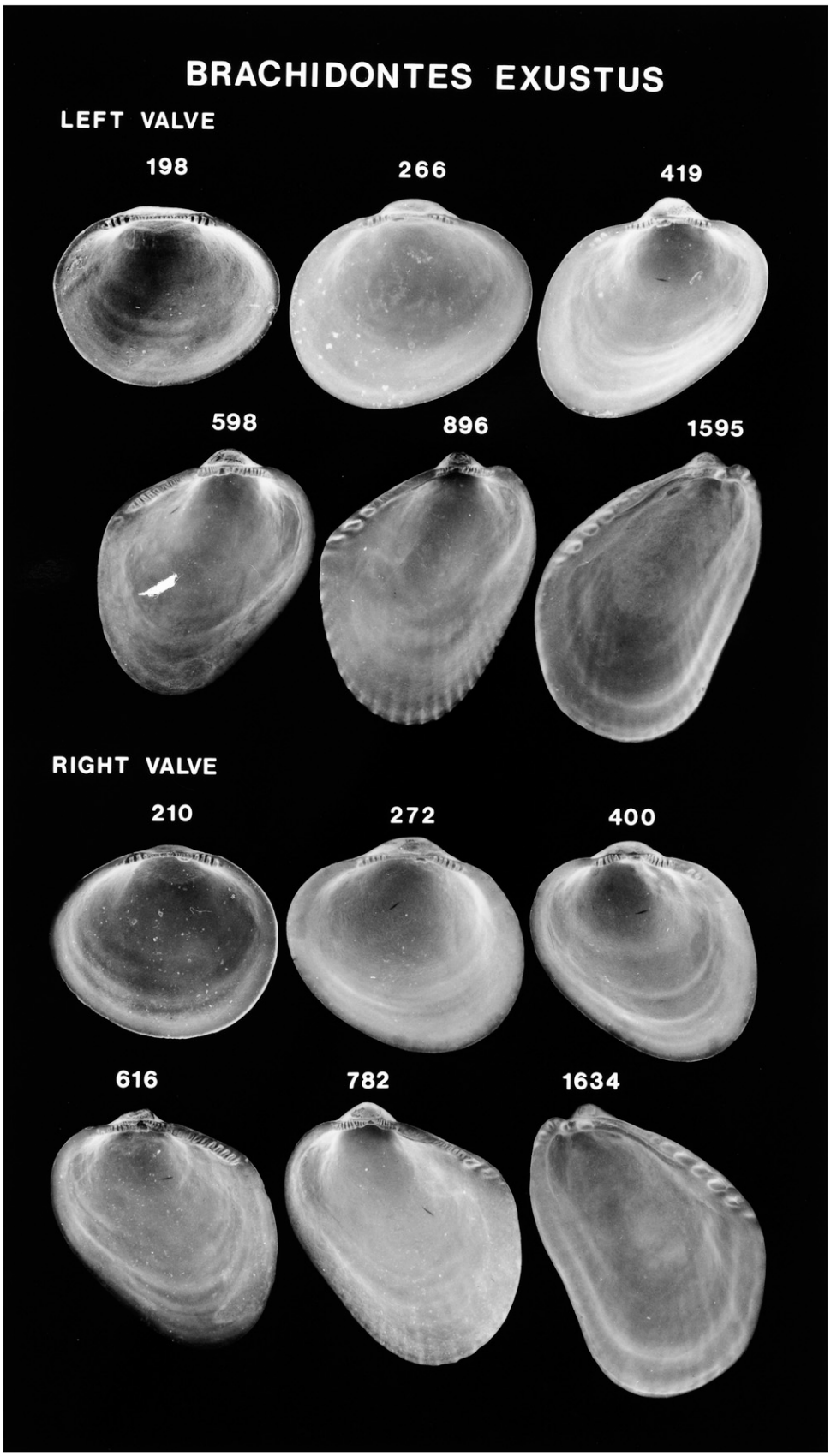

Figure 83. Scanning electron micrographs of disarticulated shell valves of *Brachidontes exustus* postlarvae. Numbers indicate the maximum linear shell dimension in micrometers. Modified from Fuller and Lutz (1989).

Downloaded From: https://bioone.org/journals/Journal-of-Shellfish-Research on 25 Feb 2020
Terms of Use: https://bioone.org/terms-of-use Access provided by IFREMER

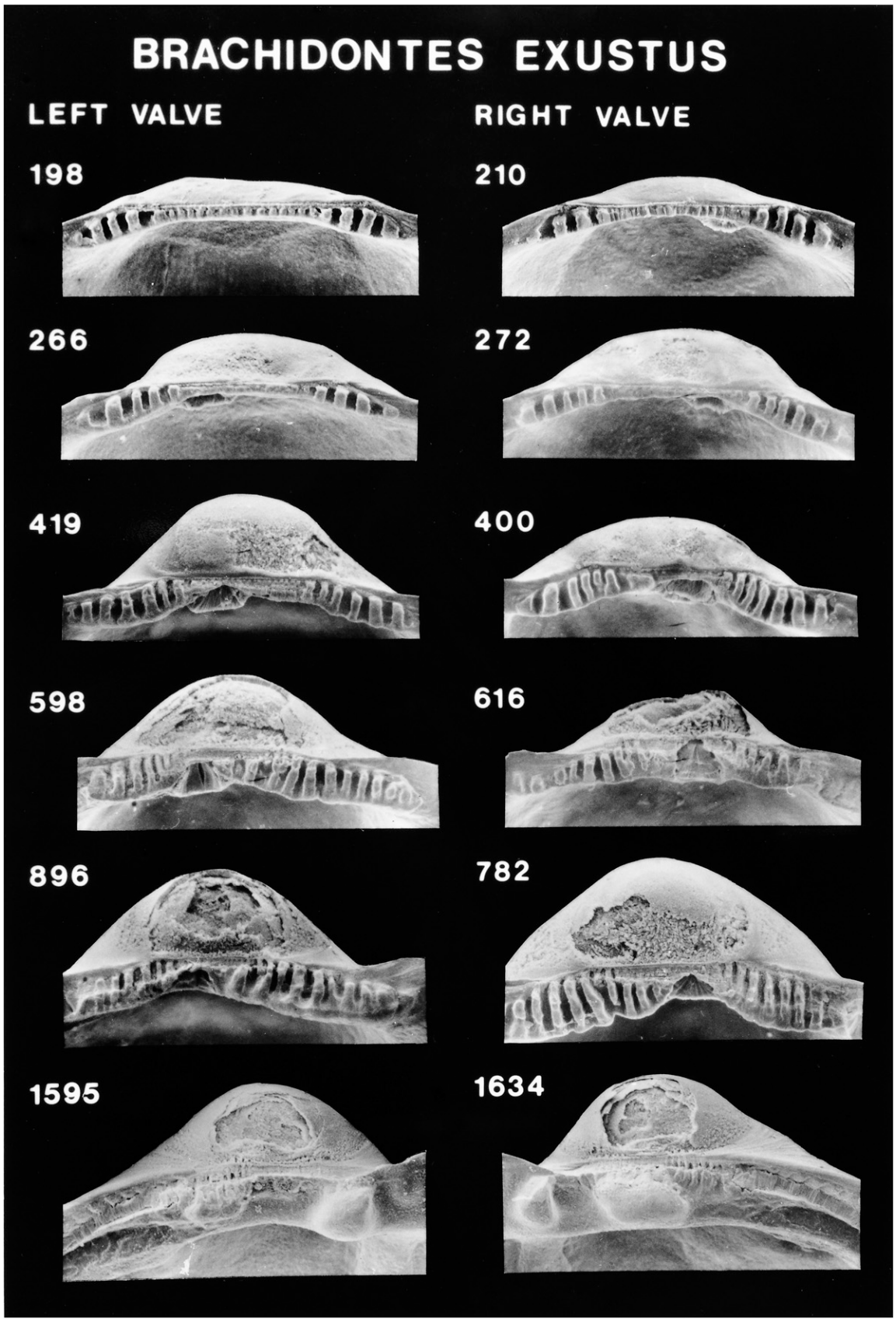

Figure 84. Scanning electron micrographs of the hinge of disarticulated shell valves of *Brachidontes exustus* postlarvae seen in Figure 83. Numbers indicate the maximum linear shell dimension in micrometers. Modified from Fuller and Lutz (1989).

Downloaded From: https://bioone.org/journals/Journal-of-Shellfish-Research on 25 Feb 2020
Terms of Use: https://bioone.org/terms-of-use Access provided by IFREMER

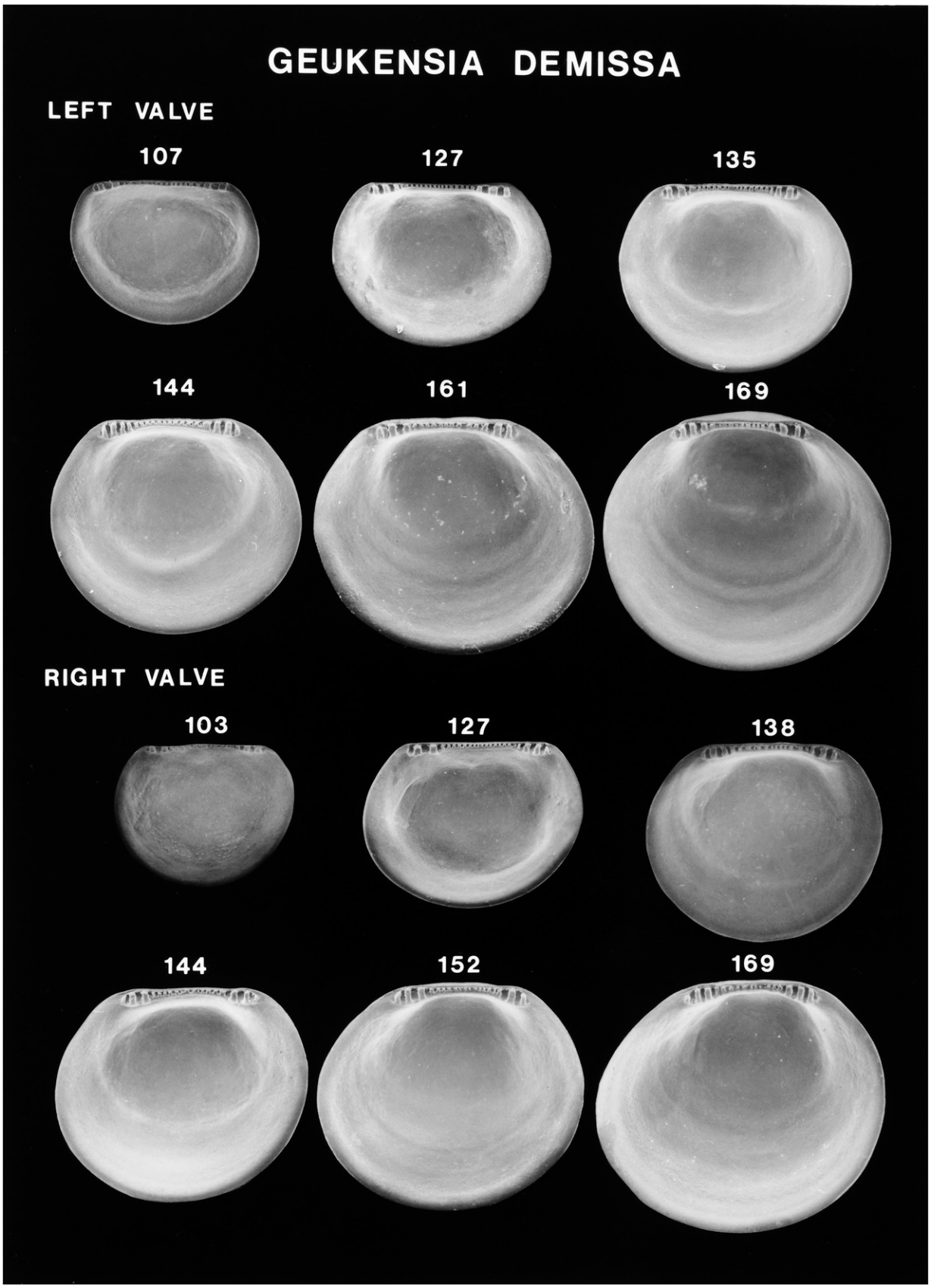

Figure 85. Scanning electron micrographs of disarticulated shell valves of *Geukensia demissa* larvae. Numbers indicate the maximum linear shell dimension in micrometers. Modified from Fuller and Lutz (1989).

Downloaded From: https://bioone.org/journals/Journal-of-Shellfish-Research on 25 Feb 2020
Terms of Use: https://bioone.org/terms-of-use Access provided by IFREMER

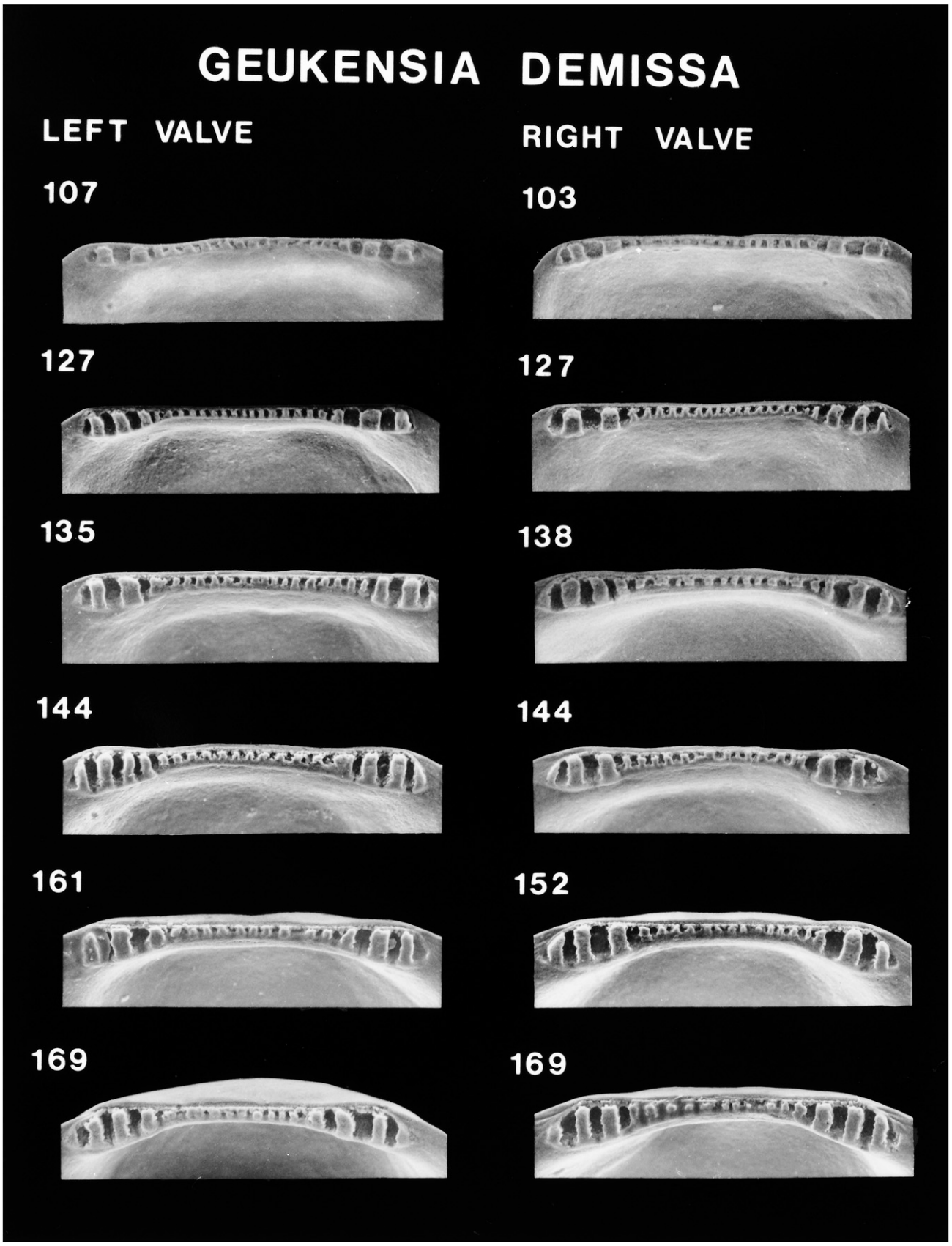

Figure 86. Scanning electron micrographs of the hinge of disarticulated shell valves of *Geukensia demissa* larvae seen in Figure 85. Numbers indicate the maximum linear shell dimension in micrometers. Modified from Fuller and Lutz (1989).

Downloaded From: https://bioone.org/journals/Journal-of-Shellfish-Research on 25 Feb 2020
Terms of Use: https://bioone.org/terms-of-use Access provided by IFREMER

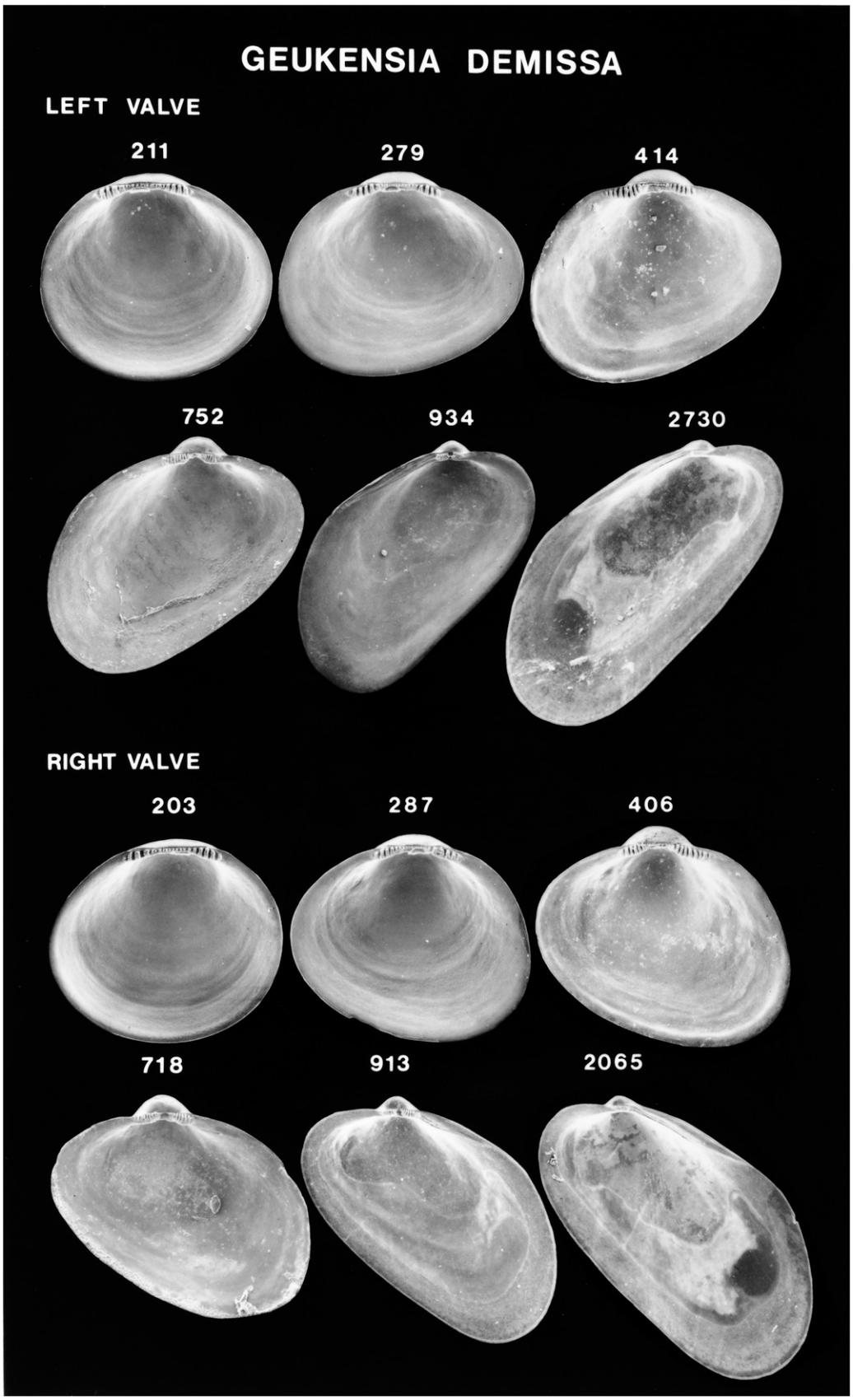

Figure 87. Scanning electron micrographs of disarticulated shell valves of *Geukensia demissa* postlarvae. Numbers indicate the maximum linear shell dimension in micrometers. Modified from Fuller and Lutz (1989).

Downloaded From: https://bioone.org/journals/Journal-of-Shellfish-Research on 25 Feb 2020
Terms of Use: https://bioone.org/terms-of-use Access provided by IFREMER

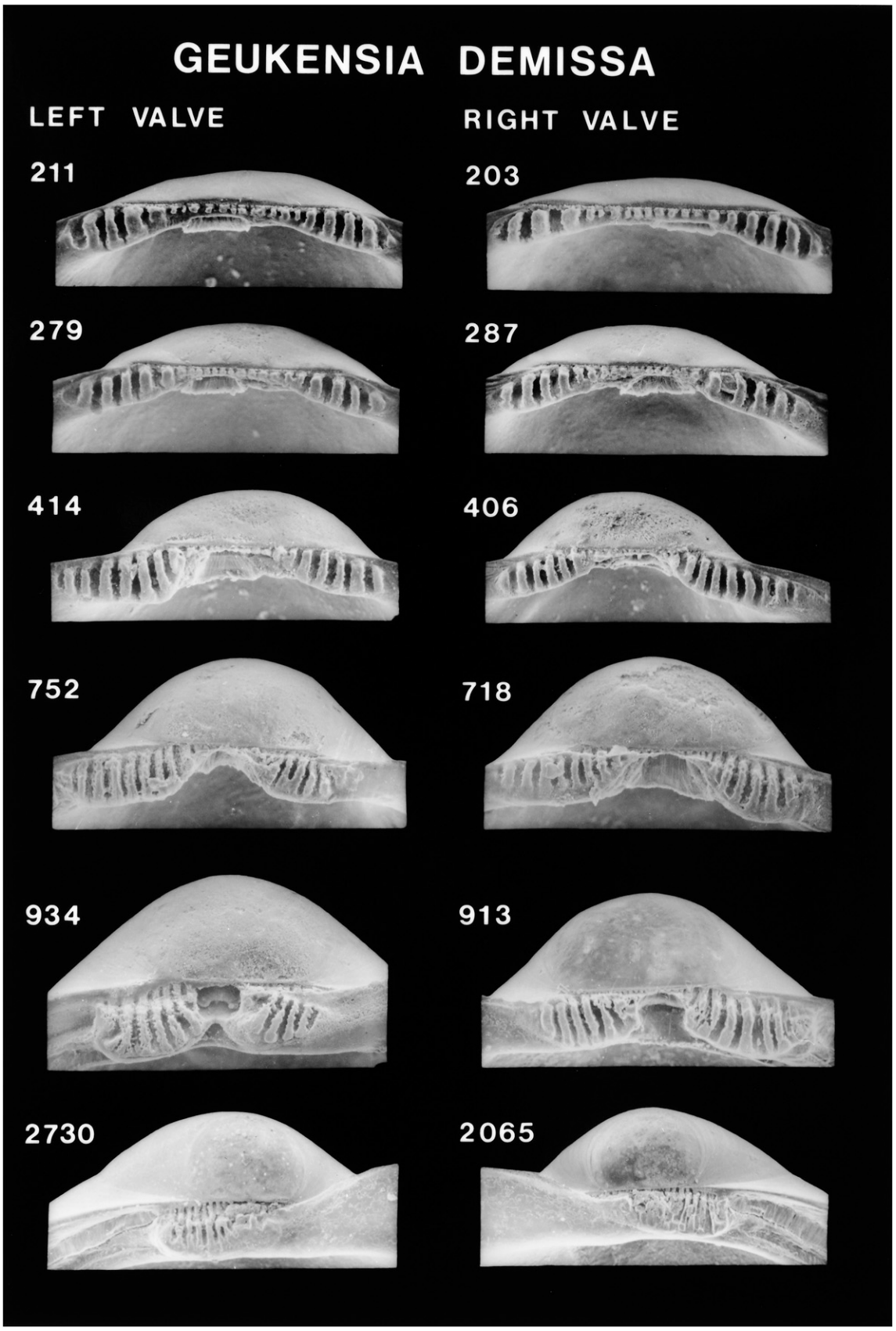

Figure 88. Scanning electron micrographs of the hinge of disarticulated shell valves of *Geukensia demissa* postlarvae seen in Figure 87. Numbers indicate the maximum linear shell dimension in micrometers. Modified from Fuller and Lutz (1989).

Downloaded From: https://bioone.org/journals/Journal-of-Shellfish-Research on 25 Feb 2020
Terms of Use: https://bioone.org/terms-of-use Access provided by IFREMER

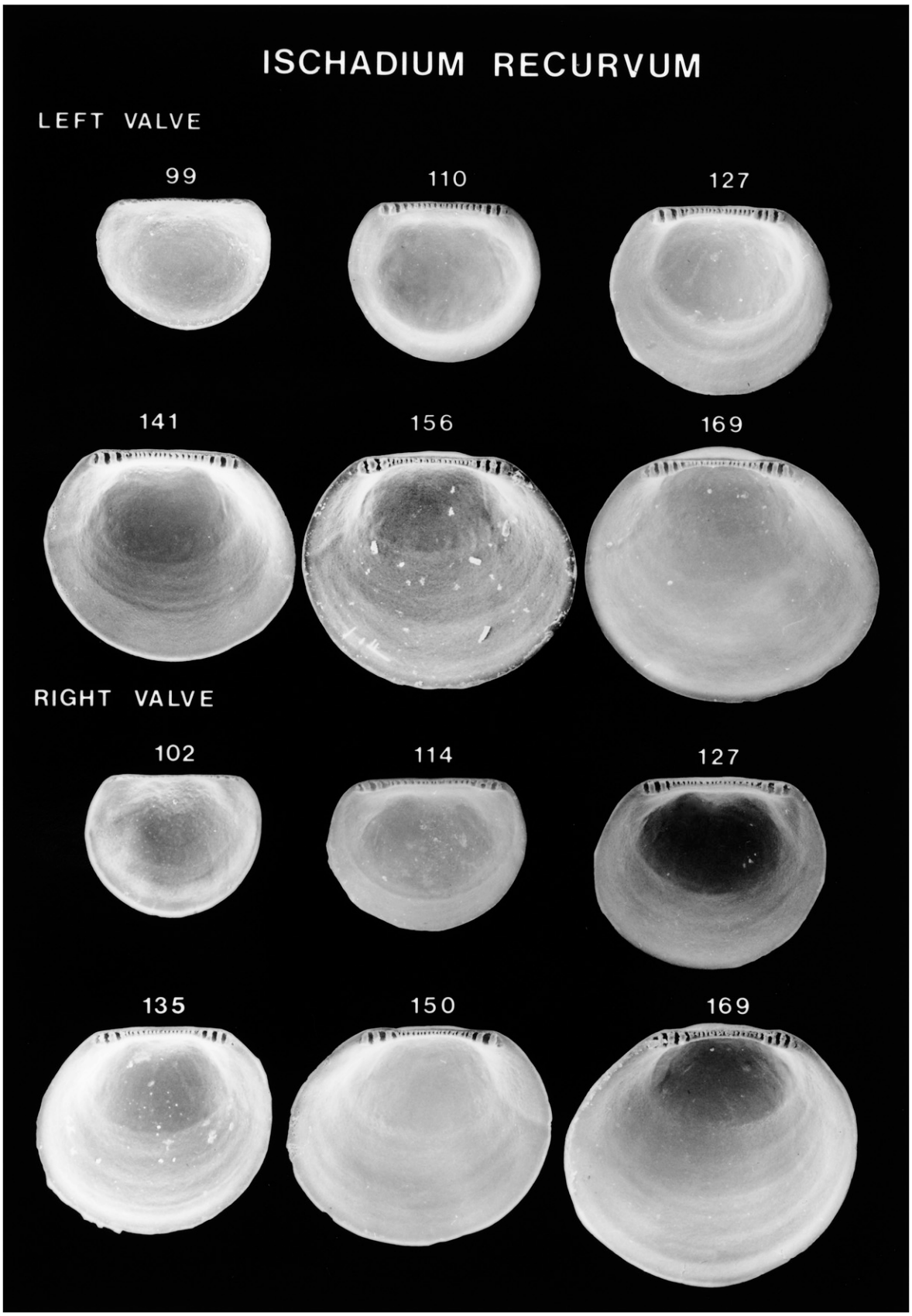

Figure 89. Scanning electron micrographs of disarticulated shell valves of *Ischadium recurvum* larvae. Numbers indicate the maximum linear shell dimension in micrometers. Modified from Fuller and Lutz (1989).

Downloaded From: https://bioone.org/journals/Journal-of-Shellfish-Research on 25 Feb 2020
Terms of Use: https://bioone.org/terms-of-use Access provided by IFREMER

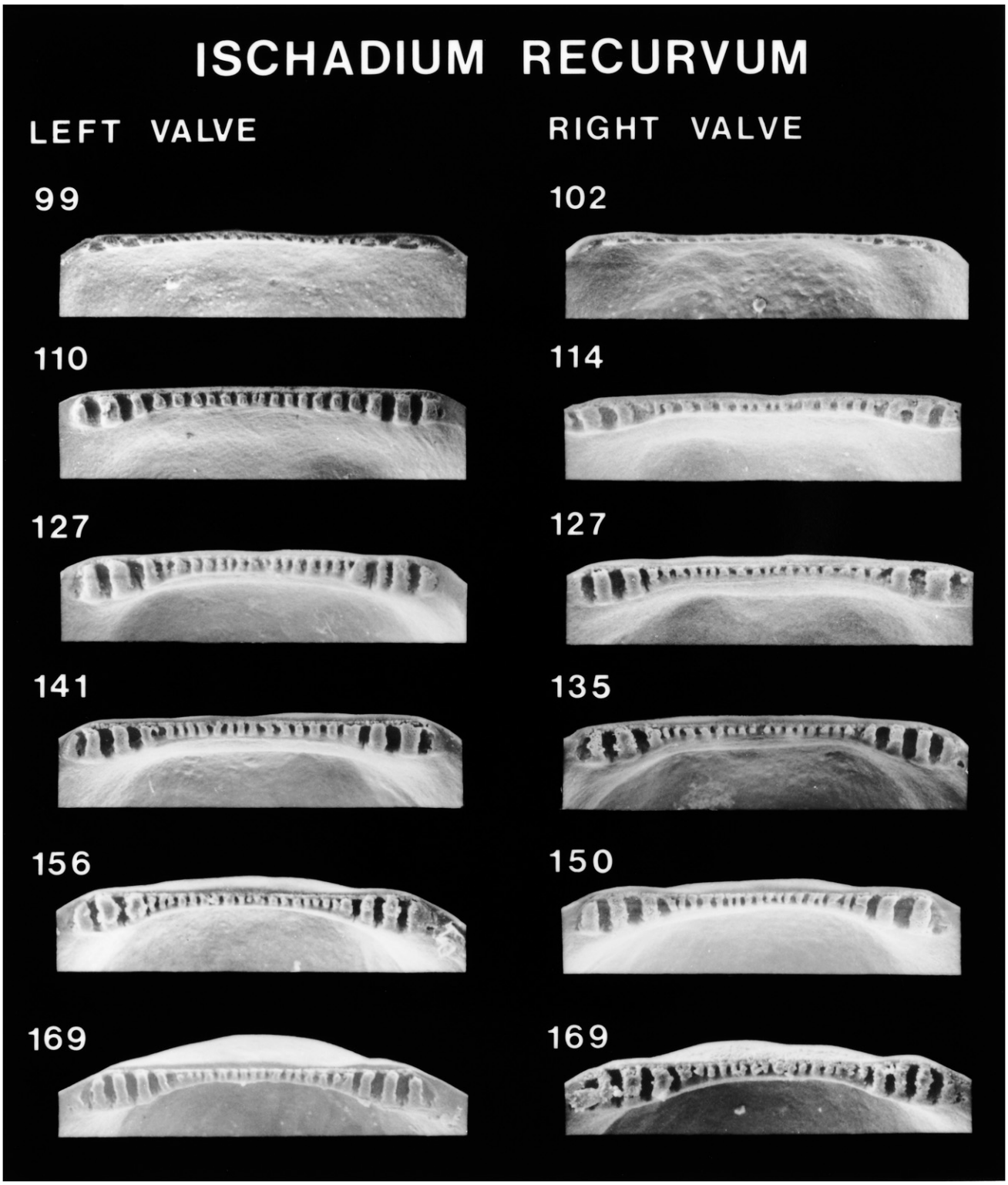

Figure 90. Scanning electron micrographs of the hinge of disarticulated shell valves of *Ischadium recurvum* larvae seen in Figure 89. Numbers indicate the maximum linear shell dimension in micrometers. Modified from Fuller and Lutz (1989).

Downloaded From: https://bioone.org/journals/Journal-of-Shellfish-Research on 25 Feb 2020
Terms of Use: https://bioone.org/terms-of-use Access provided by IFREMER

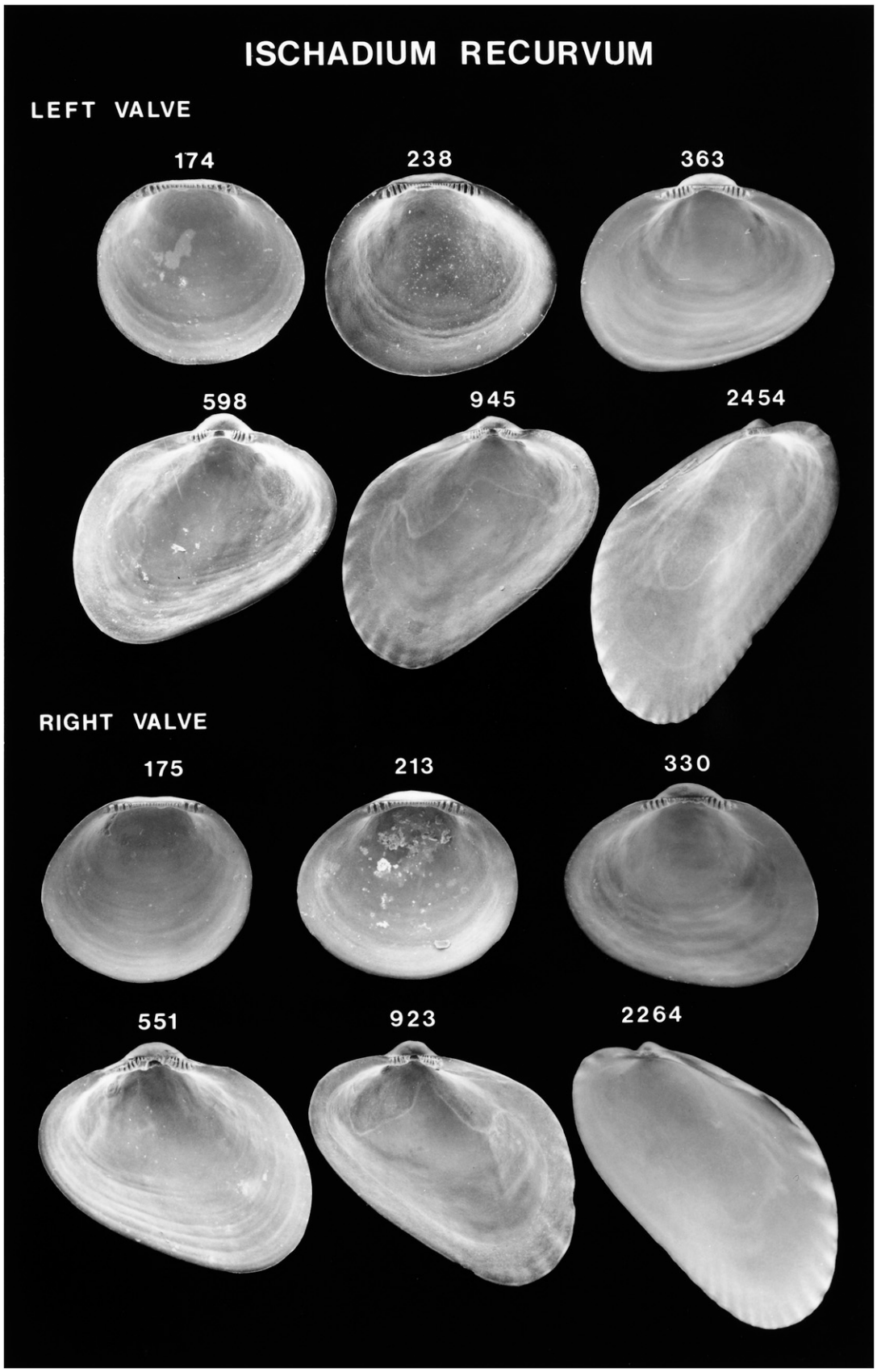

Figure 91. Scanning electron micrographs of disarticulated shell valves of *Ischadium recurvum* postlarvae. Numbers indicate the maximum linear shell dimension in micrometers. Modified from Fuller and Lutz (1989).

Downloaded From: https://bioone.org/journals/Journal-of-Shellfish-Research on 25 Feb 2020
Terms of Use: https://bioone.org/terms-of-use Access provided by IFREMER

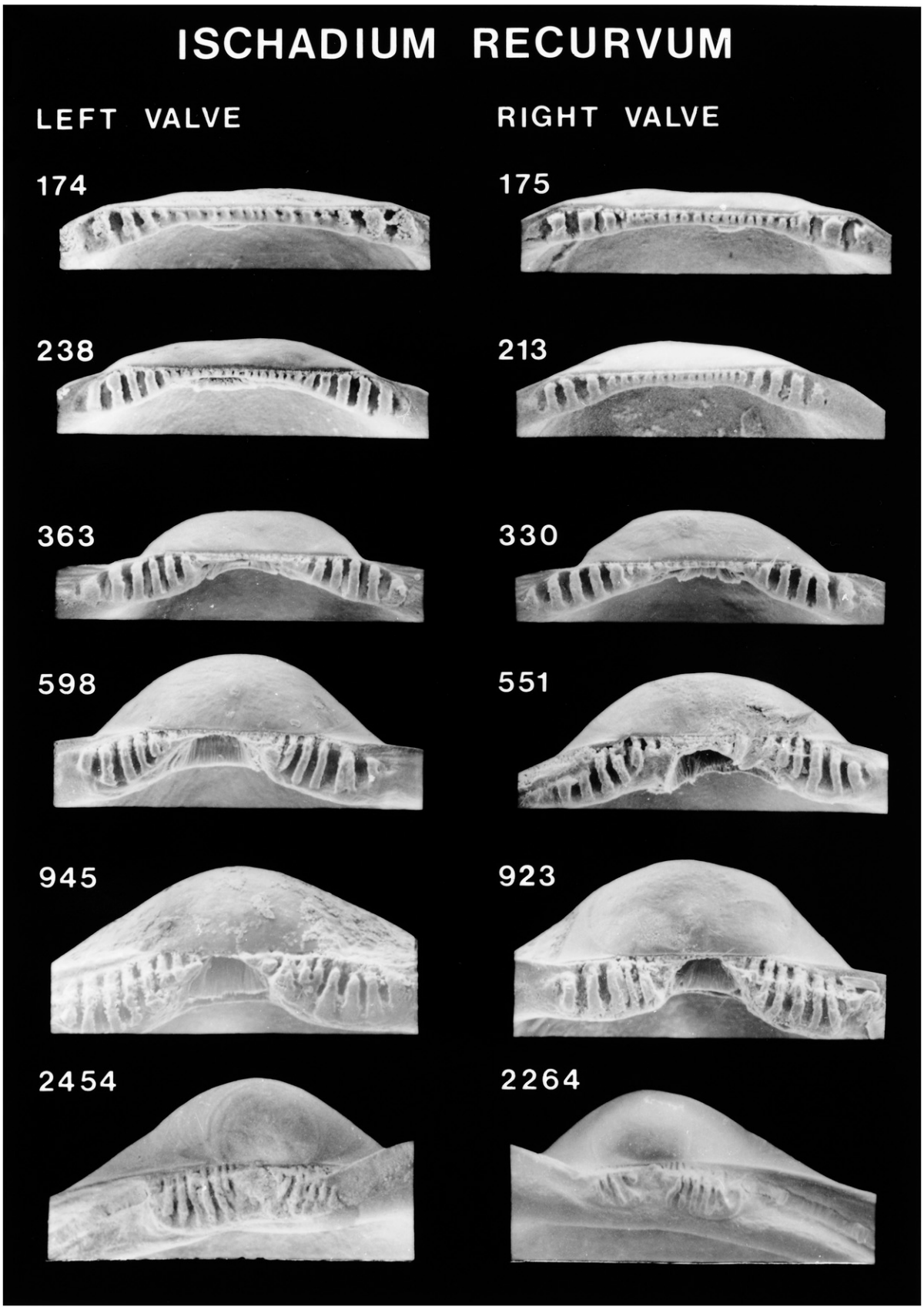

Figure 92. Scanning electron micrographs of the hinge of disarticulated shell valves of *Ischadium recurvum* postlarvae seen in Figure 91. Numbers indicate the maximum linear shell dimension in micrometers. Modified from Fuller and Lutz (1989).

Downloaded From: https://bioone.org/journals/Journal-of-Shellfish-Research on 25 Feb 2020
Terms of Use: https://bioone.org/terms-of-use Access provided by IFREMER

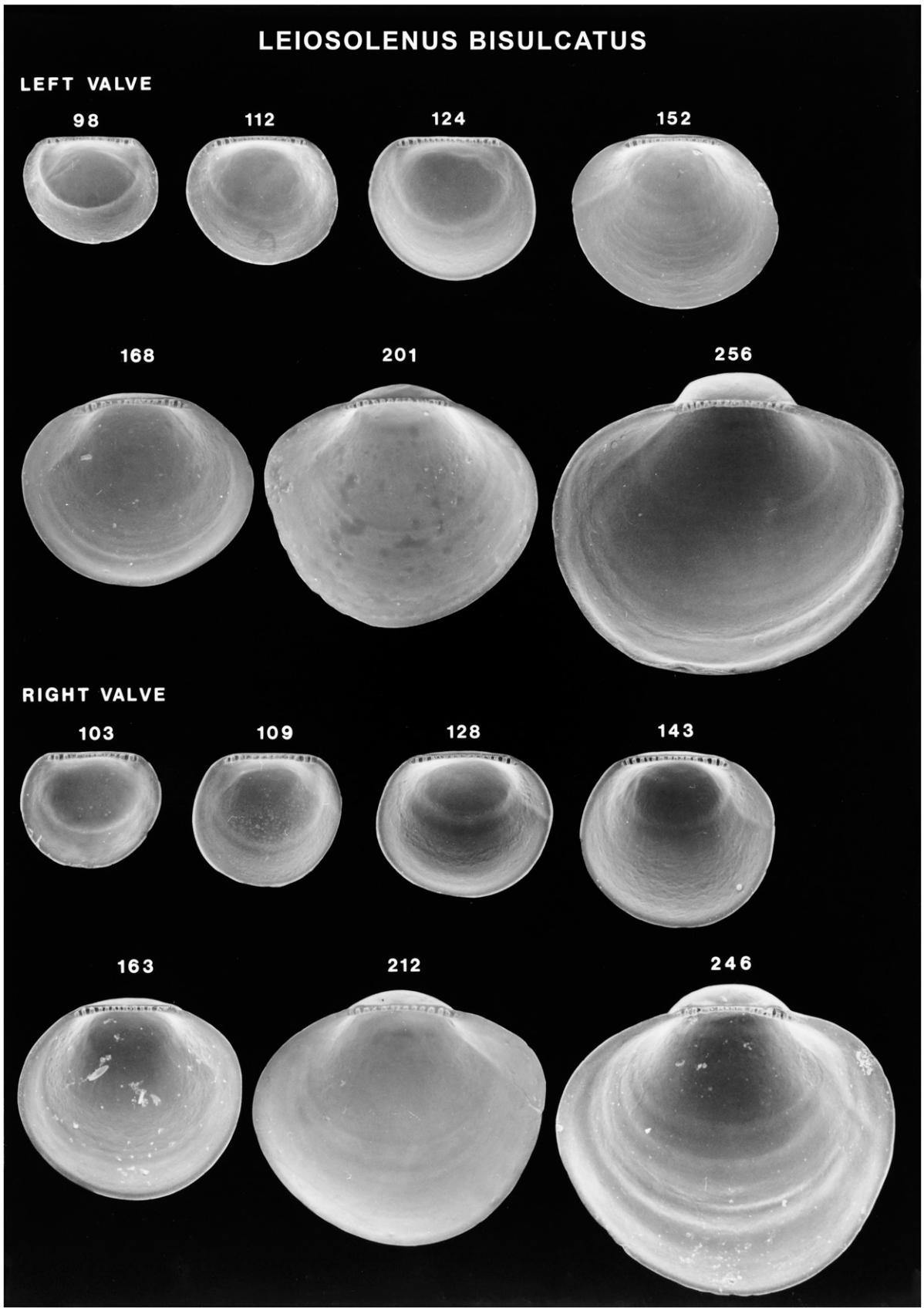

Figure 93. Scanning electron micrographs of disarticulated shell valves of *Leiosolenus bisulcatus* larvae. Numbers indicate the maximum linear shell dimension in micrometers.

Downloaded From: https://bioone.org/journals/Journal-of-Shellfish-Research on 25 Feb 2020
Terms of Use: https://bioone.org/terms-of-use Access provided by IFREMER

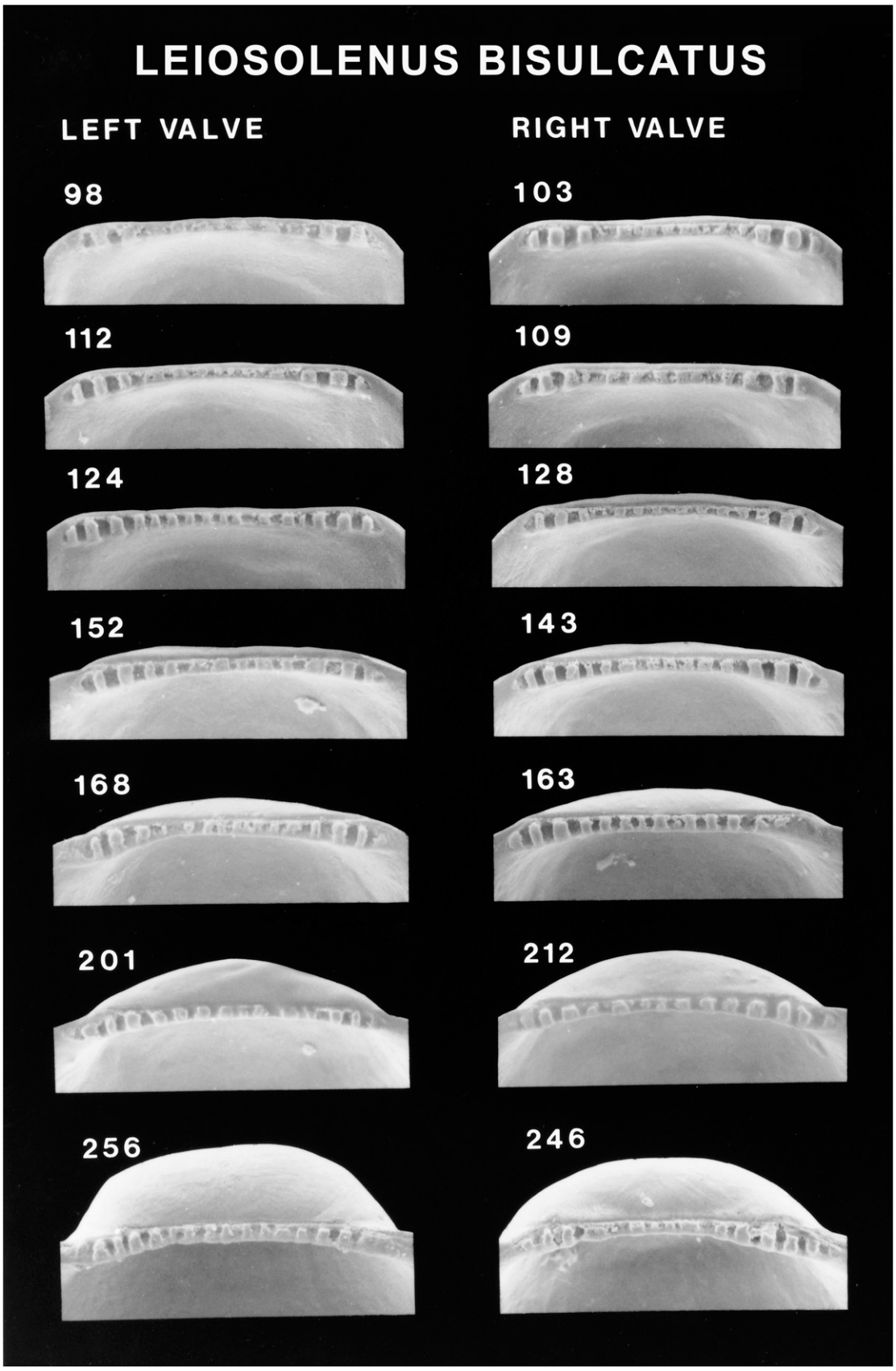

Figure 94. Scanning electron micrographs of the hinge of disarticulated shell valves of *Leiosolenus bisulcatus* larvae seen in Figure 93. Numbers indicate the maximum linear shell dimension in micrometers.

Downloaded From: https://bioone.org/journals/Journal-of-Shellfish-Research on 25 Feb 2020
Terms of Use: https://bioone.org/terms-of-use Access provided by IFREMER

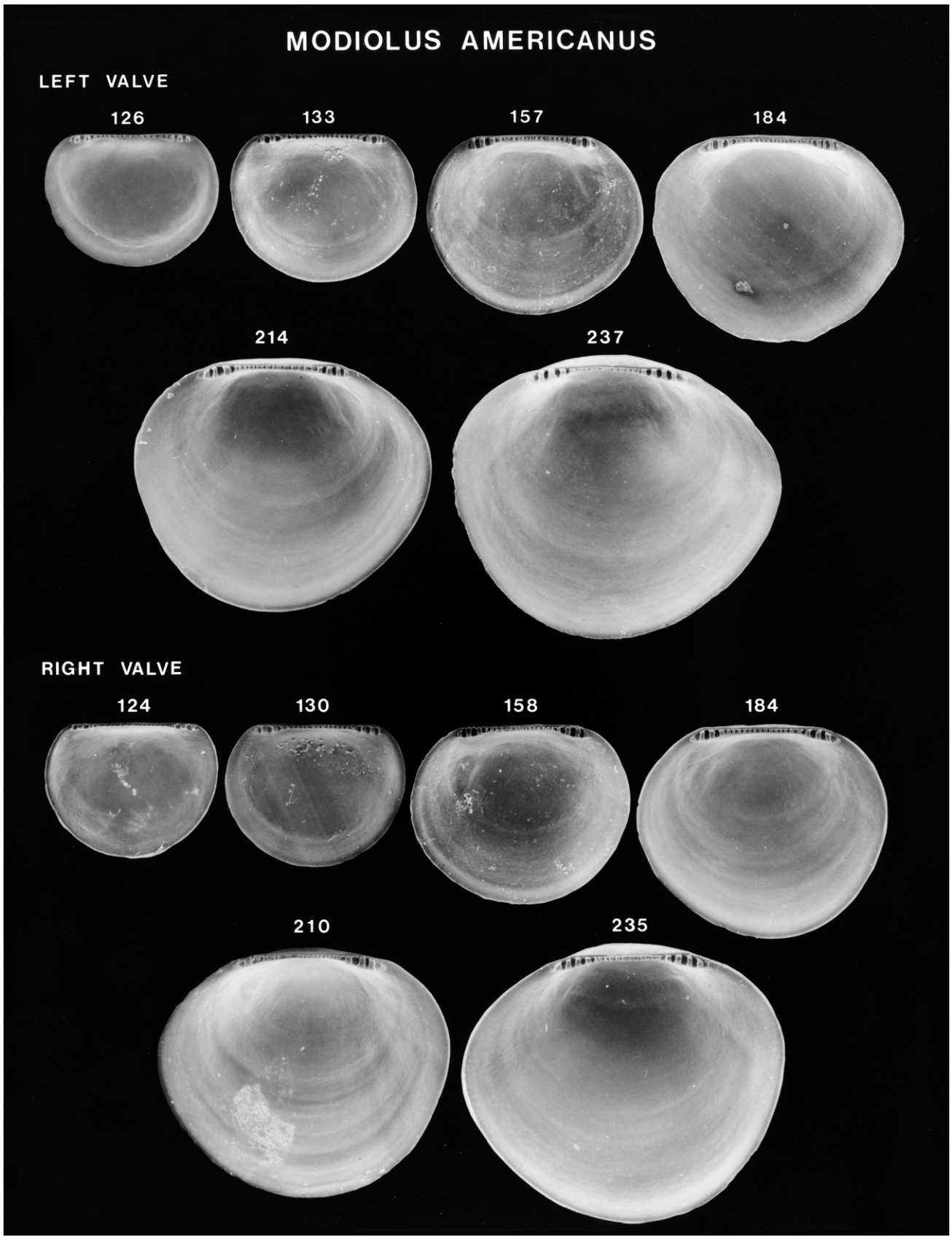

Figure 95. Scanning electron micrographs of disarticulated shell valves of *Modiolus americanus* larvae. Numbers indicate the maximum linear shell dimension in micrometers. Modified from Fuller and Lutz (1989).

Downloaded From: https://bioone.org/journals/Journal-of-Shellfish-Research on 25 Feb 2020
Terms of Use: https://bioone.org/terms-of-use Access provided by IFREMER

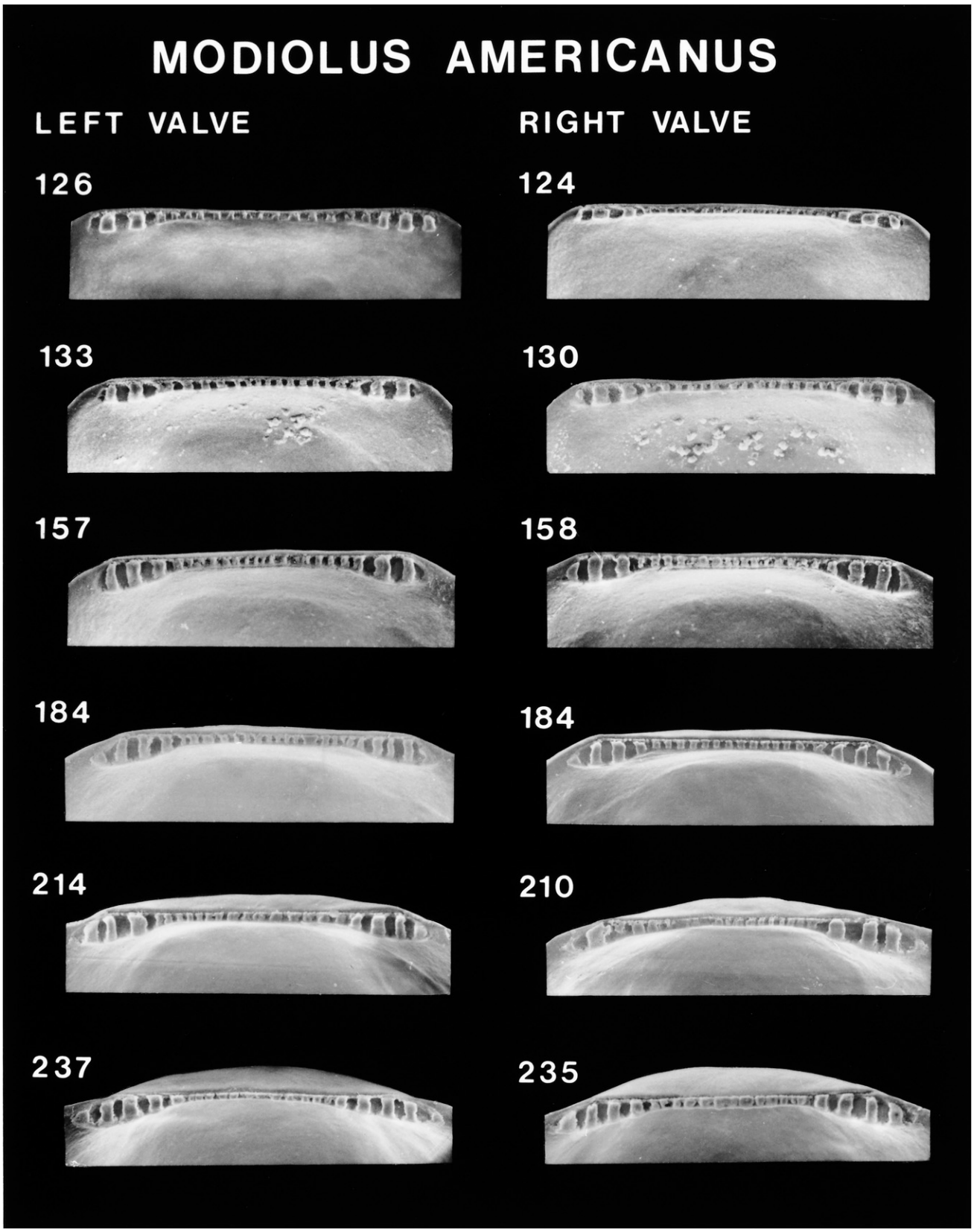

Figure 96. Scanning electron micrographs of the hinge of disarticulated shell valves of *Modiolus americanus* larvae seen in Figure 95. Numbers indicate the maximum linear shell dimension in micrometers. Modified from Fuller and Lutz (1989).

Downloaded From: https://bioone.org/journals/Journal-of-Shellfish-Research on 25 Feb 2020
Terms of Use: https://bioone.org/terms-of-use Access provided by IFREMER

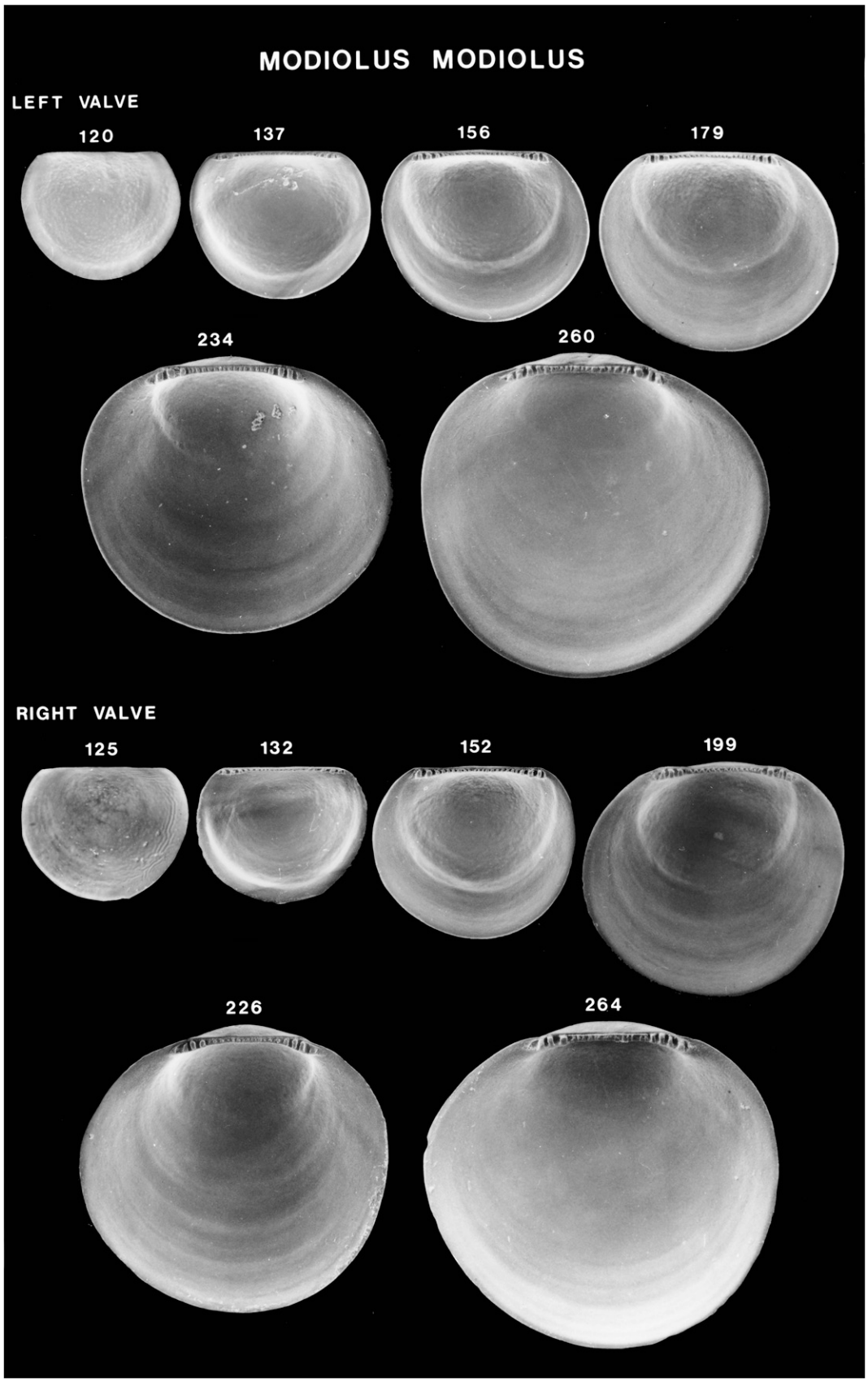

Figure 97. Scanning electron micrographs of disarticulated shell valves of *Modiolus modiolus* larvae. Numbers indicate the maximum linear shell dimension in micrometers. Modified from Fuller and Lutz (1989).

Downloaded From: https://bioone.org/journals/Journal-of-Shellfish-Research on 25 Feb 2020
Terms of Use: https://bioone.org/terms-of-use Access provided by IFREMER

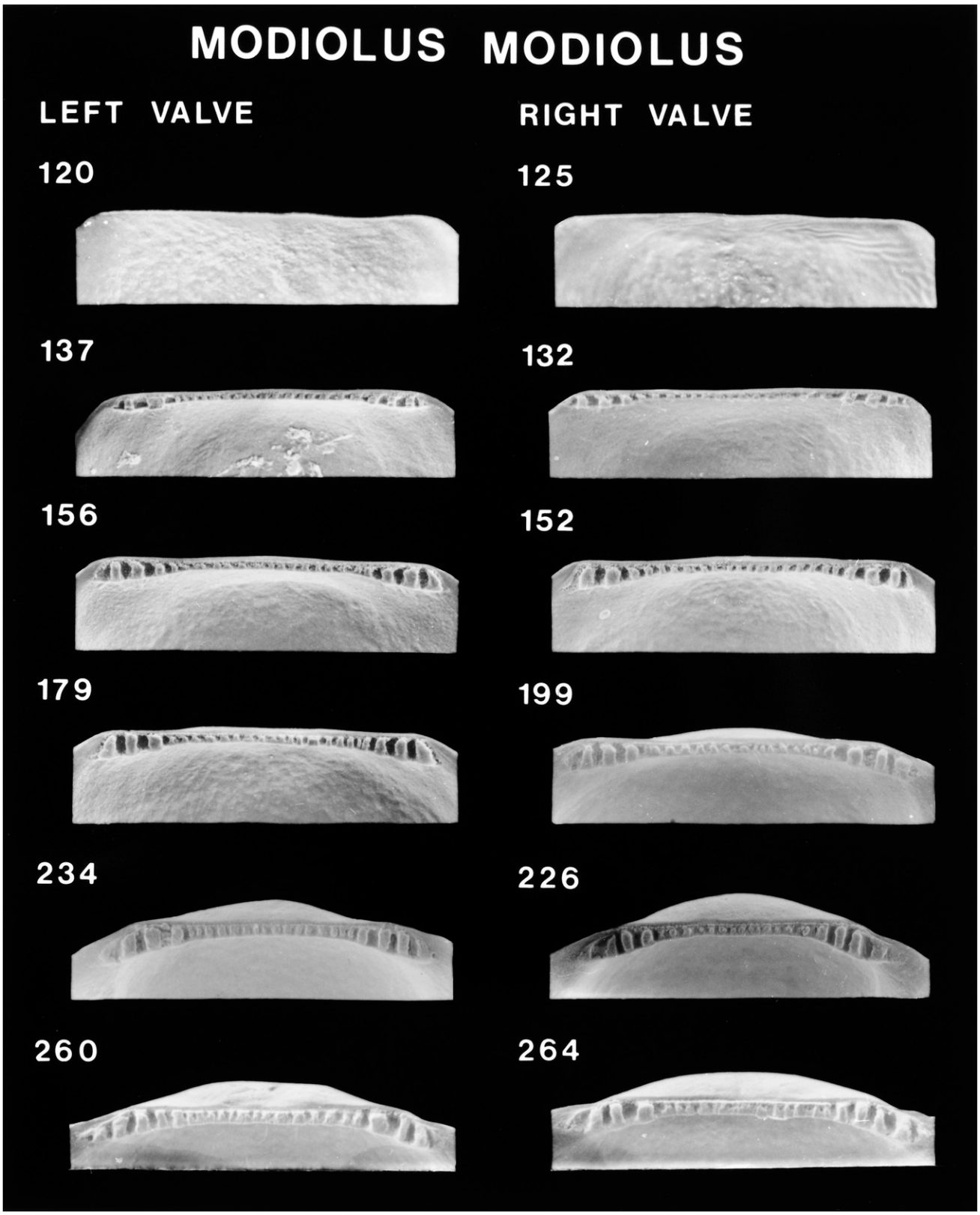

Figure 98. Scanning electron micrographs of the hinge of disarticulated shell valves of *Modiolus modiolus* larvae seen in Figure 97. Numbers indicate the maximum linear shell dimension in micrometers. Modified from Fuller and Lutz (1989).

Downloaded From: https://bioone.org/journals/Journal-of-Shellfish-Research on 25 Feb 2020
Terms of Use: https://bioone.org/terms-of-use Access provided by IFREMER

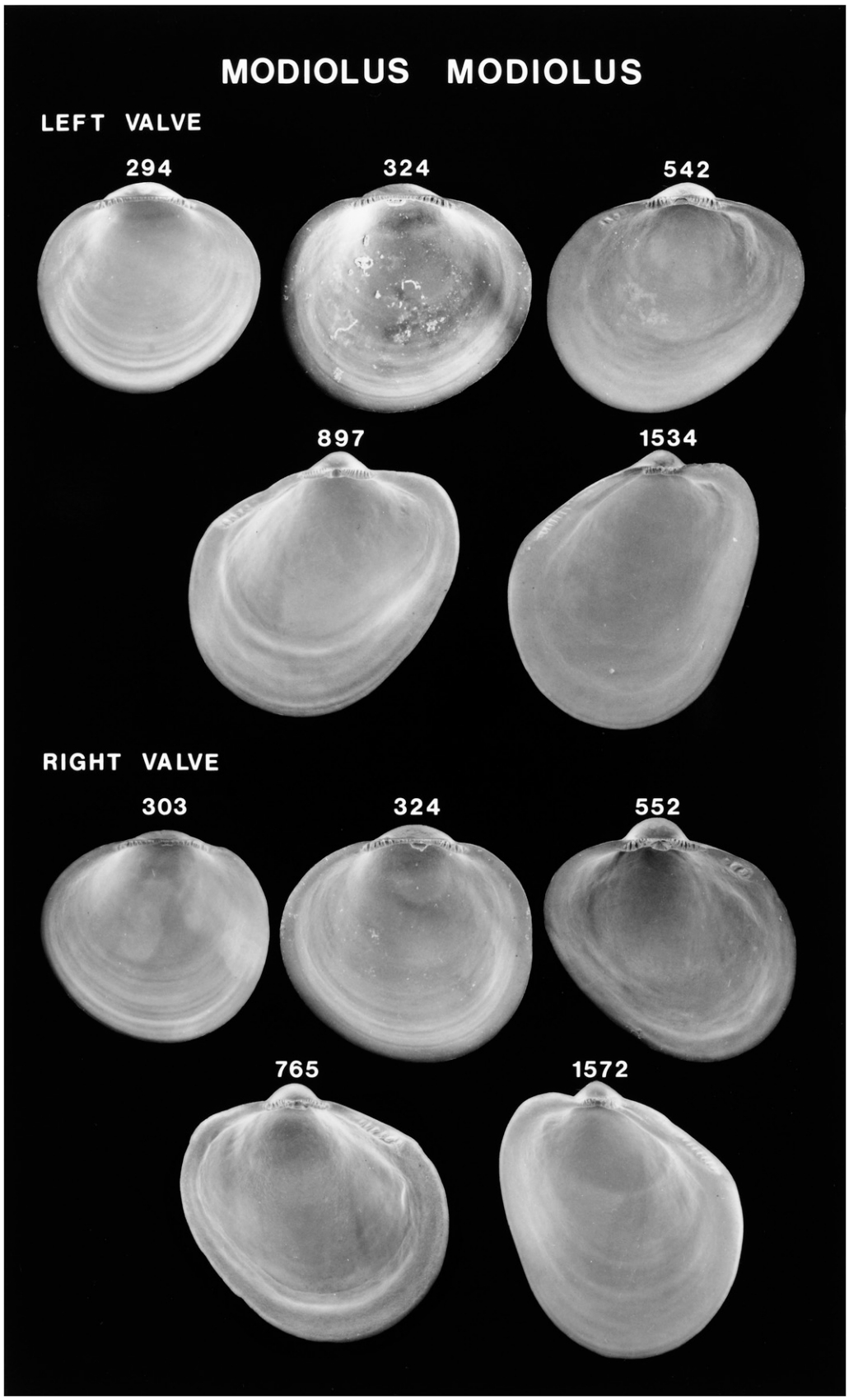

Figure 99. Scanning electron micrographs of disarticulated shell valves of *Modiolus modiolus* postlarvae. Numbers indicate the maximum linear shell dimension in micrometers. Modified from Fuller and Lutz (1989).

Downloaded From: https://bioone.org/journals/Journal-of-Shellfish-Research on 25 Feb 2020
Terms of Use: https://bioone.org/terms-of-use Access provided by IFREMER

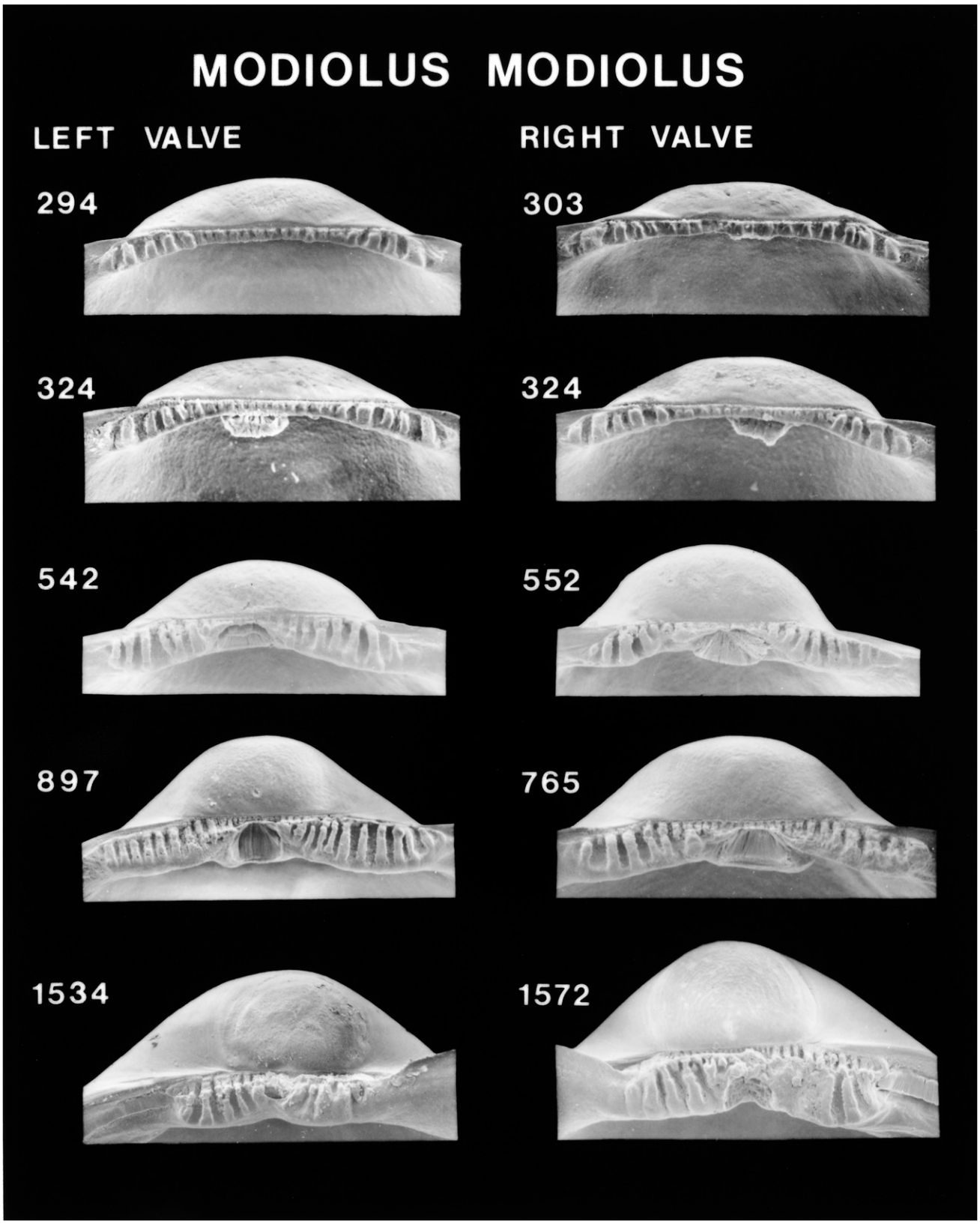

Figure 100. Scanning electron micrographs of the hinge of disarticulated shell valves of *Modiolus modiolus* postlarvae seen in Figure 99. Numbers indicate the maximum linear shell dimension in micrometers. Modified from Fuller and Lutz (1989).

Downloaded From: https://bioone.org/journals/Journal-of-Shellfish-Research on 25 Feb 2020
Terms of Use: https://bioone.org/terms-of-use Access provided by IFREMER

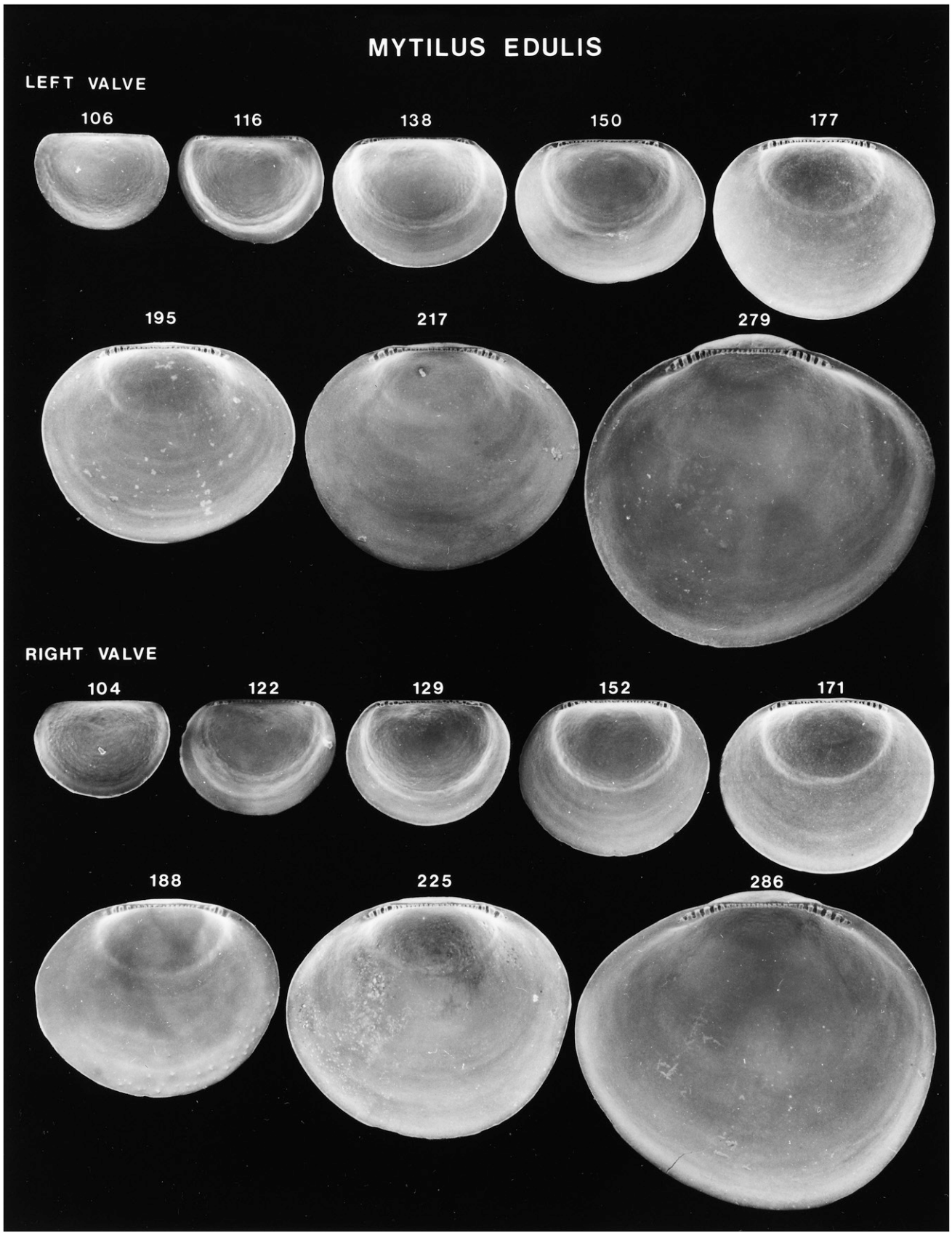

Figure 101. Scanning electron micrographs of disarticulated shell valves of *Mytilus edulis* larvae. Numbers indicate the maximum linear shell dimension in micrometers. Modified from Fuller and Lutz (1989).

Downloaded From: https://bioone.org/journals/Journal-of-Shellfish-Research on 25 Feb 2020
Terms of Use: https://bioone.org/terms-of-use Access provided by IFREMER

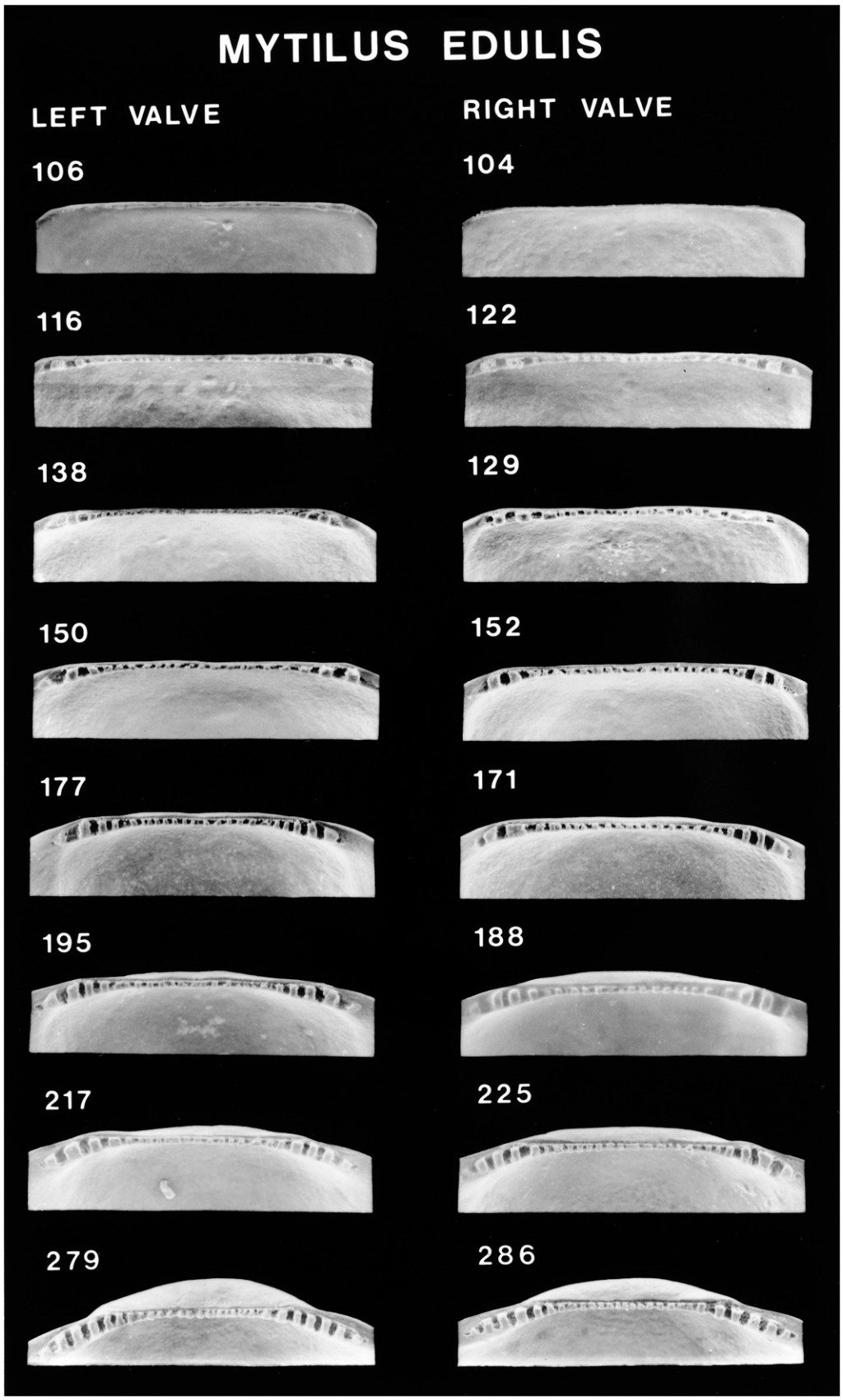

Figure 102. Scanning electron micrographs of the hinge of disarticulated shell valves of *Mytilus edulis* larvae seen in Figure 101. Numbers indicate the maximum linear shell dimension in micrometers. Modified from Fuller and Lutz (1989).

Downloaded From: https://bioone.org/journals/Journal-of-Shellfish-Research on 25 Feb 2020
Terms of Use: https://bioone.org/terms-of-use Access provided by IFREMER

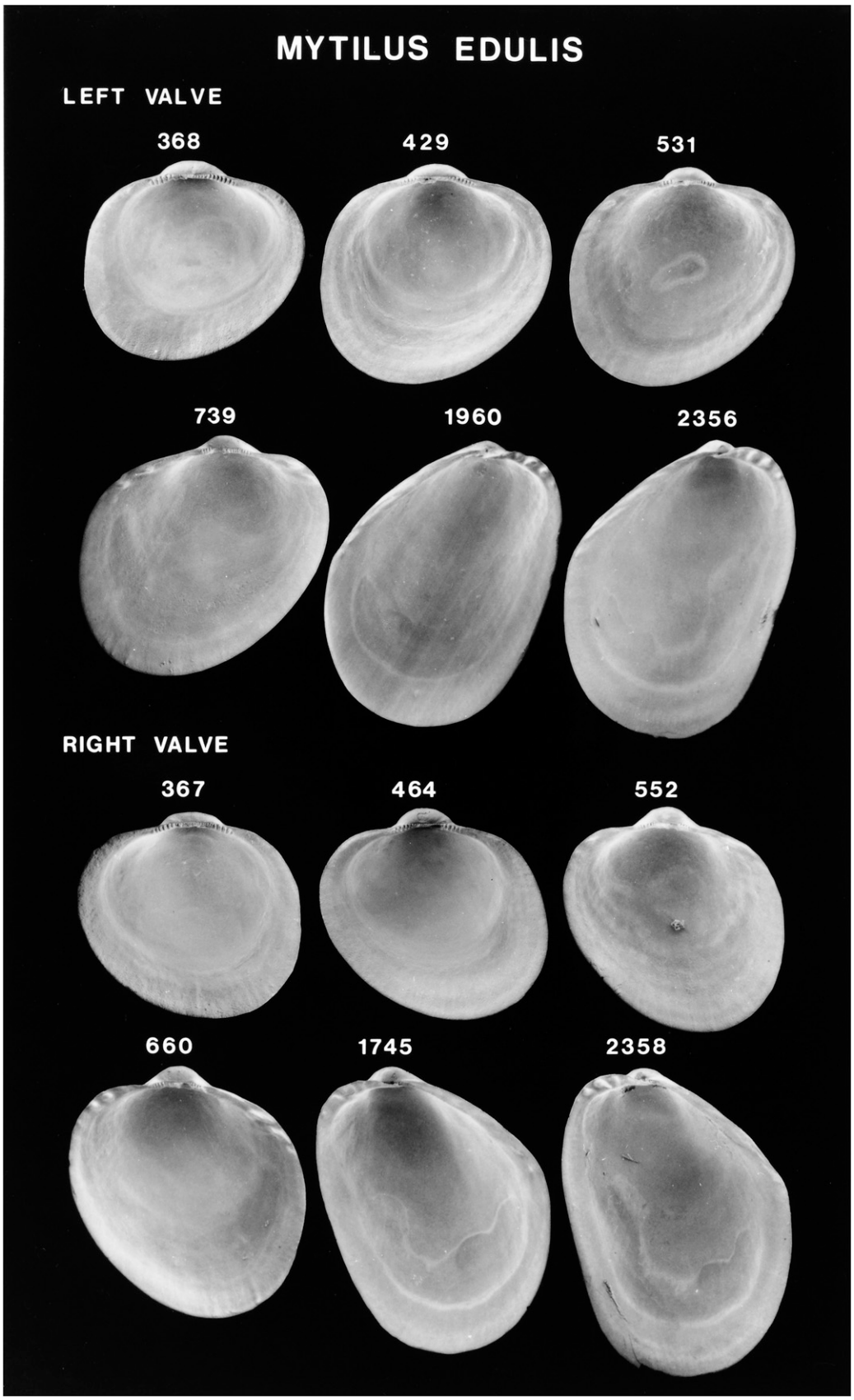

Figure 103. Scanning electron micrographs of disarticulated shell valves of *Mytilus edulis* postlarvae. Numbers indicate the maximum linear shell dimension in micrometers. Modified from Fuller and Lutz (1989).

Downloaded From: https://bioone.org/journals/Journal-of-Shellfish-Research on 25 Feb 2020
Terms of Use: https://bioone.org/terms-of-use Access provided by IFREMER

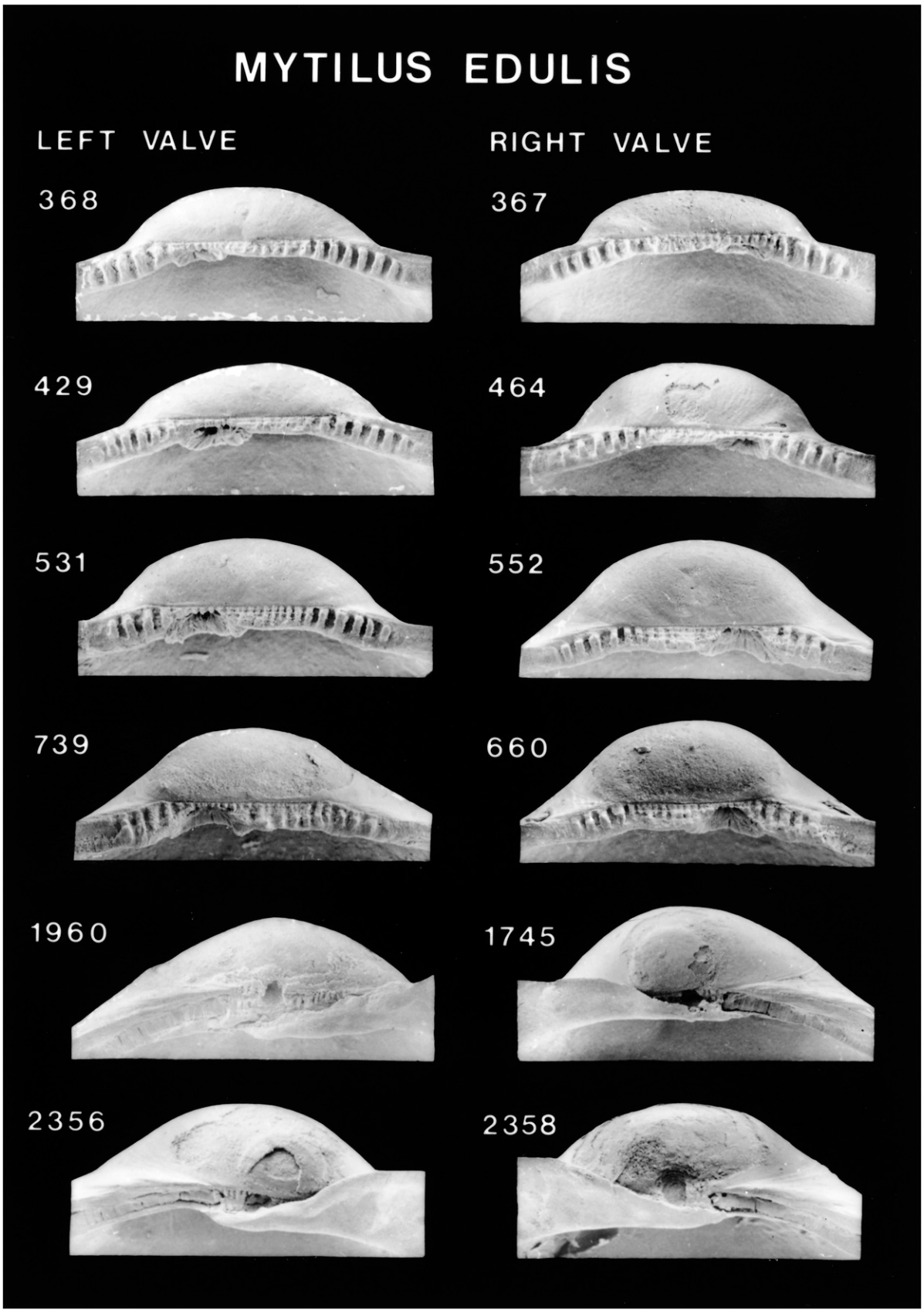

Figure 104. Scanning electron micrographs of the hinge of disarticulated shell valves of *Mytilus edulis* postlarvae seen in Figure 103. Numbers indicate the maximum linear shell dimension in micrometers. Modified from Fuller and Lutz (1989).

Downloaded From: https://bioone.org/journals/Journal-of-Shellfish-Research on 25 Feb 2020
Terms of Use: https://bioone.org/terms-of-use Access provided by IFREMER

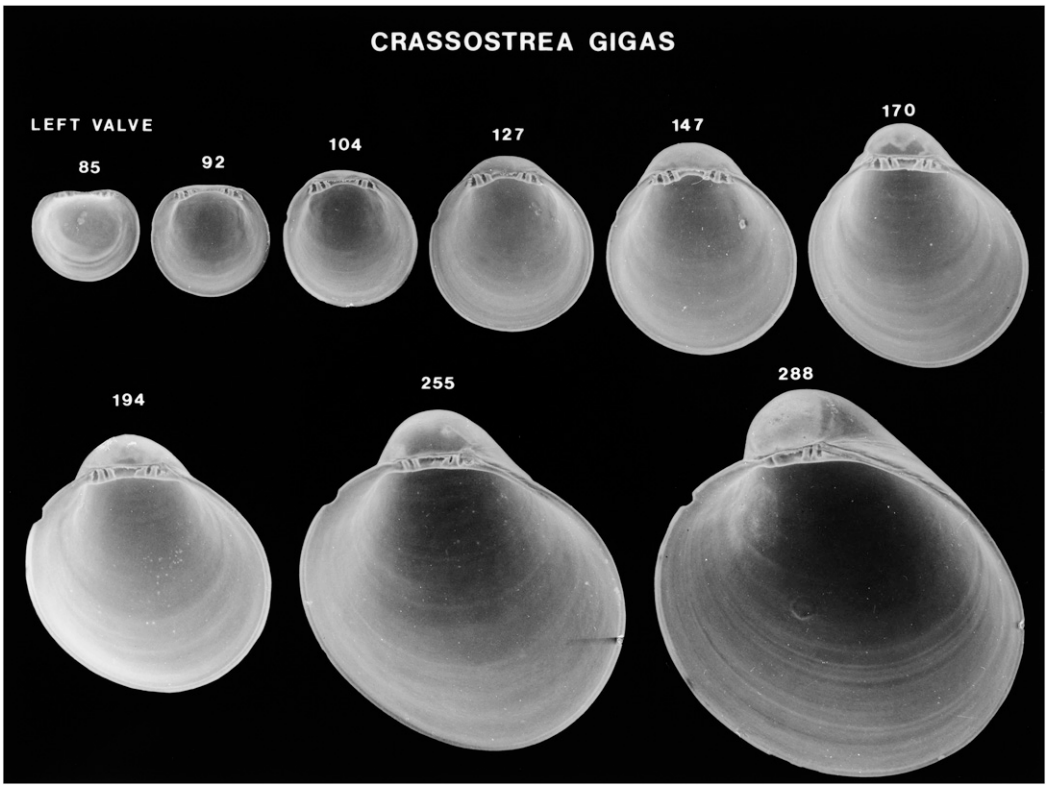

Figure 105. Scanning electron micrographs of disarticulated left shell valves of *Crassostrea gigas* larvae. Numbers indicate the maximum linear shell dimension in micrometers. Modified from Hu et al. (1993).

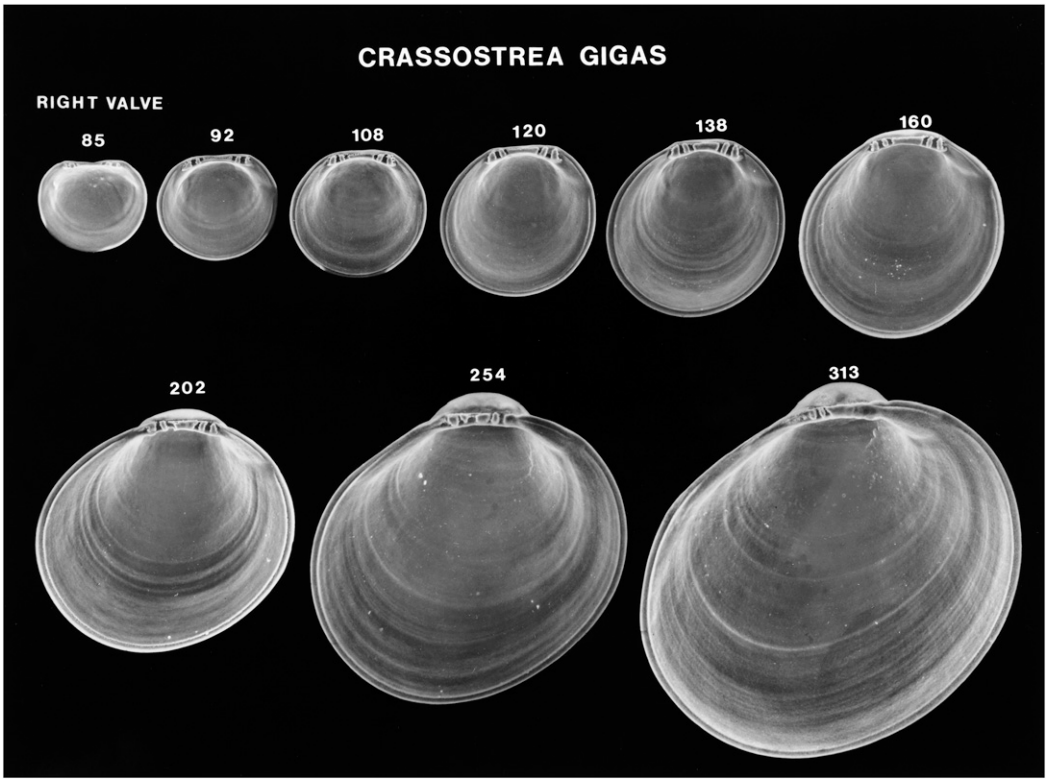

Figure 106. Scanning electron micrographs of disarticulated right shell valves of *Crassostrea gigas* larvae. Numbers indicate the maximum linear shell dimension in micrometers. Modified from Hu et al. (1993).

Downloaded From: https://bioone.org/journals/Journal-of-Shellfish-Research on 25 Feb 2020
Terms of Use: https://bioone.org/terms-of-use Access provided by IFREMER

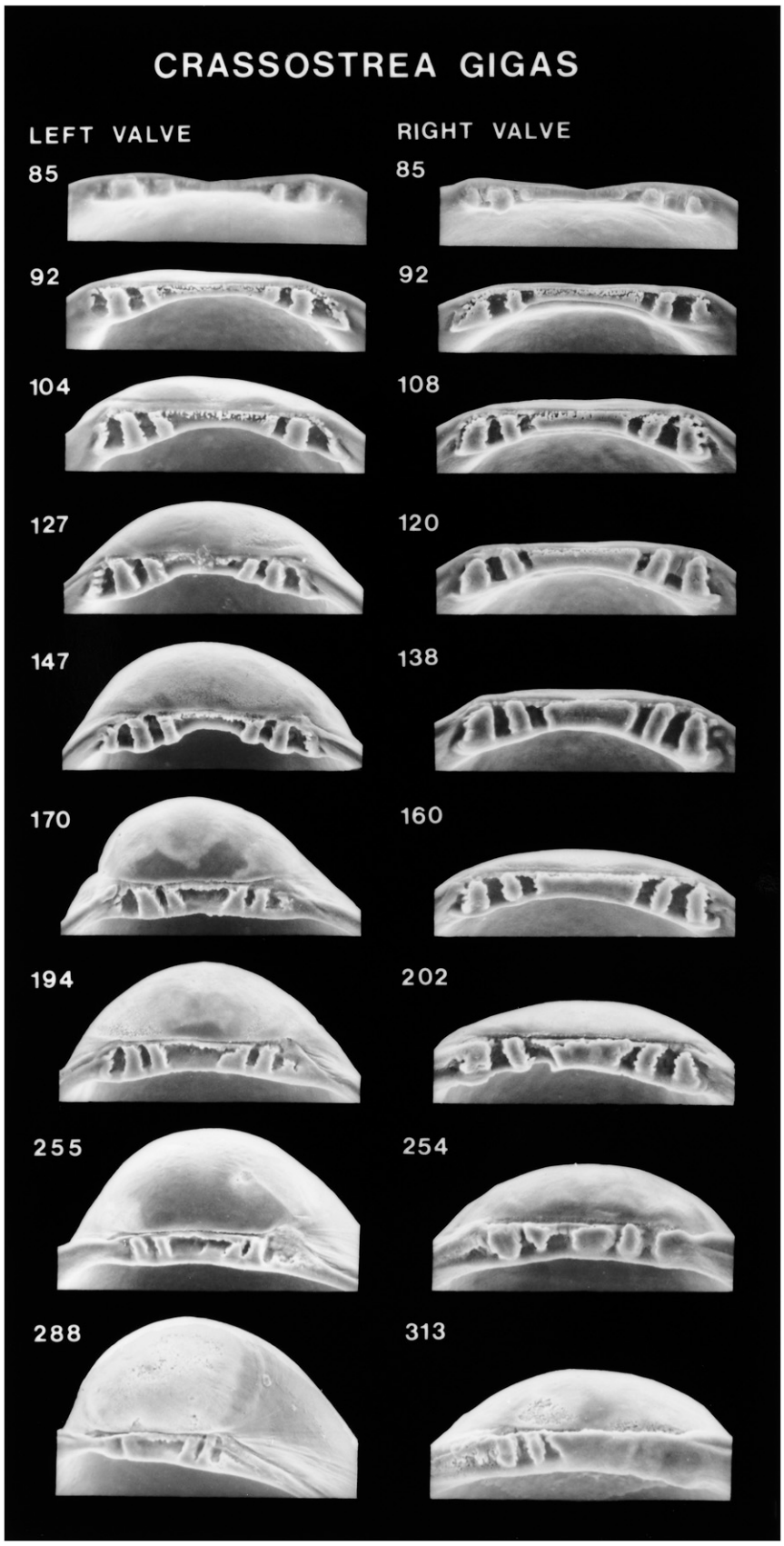

Figure 107. Scanning electron micrographs of the hinge of disarticulated shell valves of *Crassostrea gigas* larvae seen in Figures 105 and 106. Numbers indicate the maximum linear shell dimension in micrometers. Modified from Hu et al. (1993).

Downloaded From: https://bioone.org/journals/Journal-of-Shellfish-Research on 25 Feb 2020
Terms of Use: https://bioone.org/terms-of-use Access provided by IFREMER

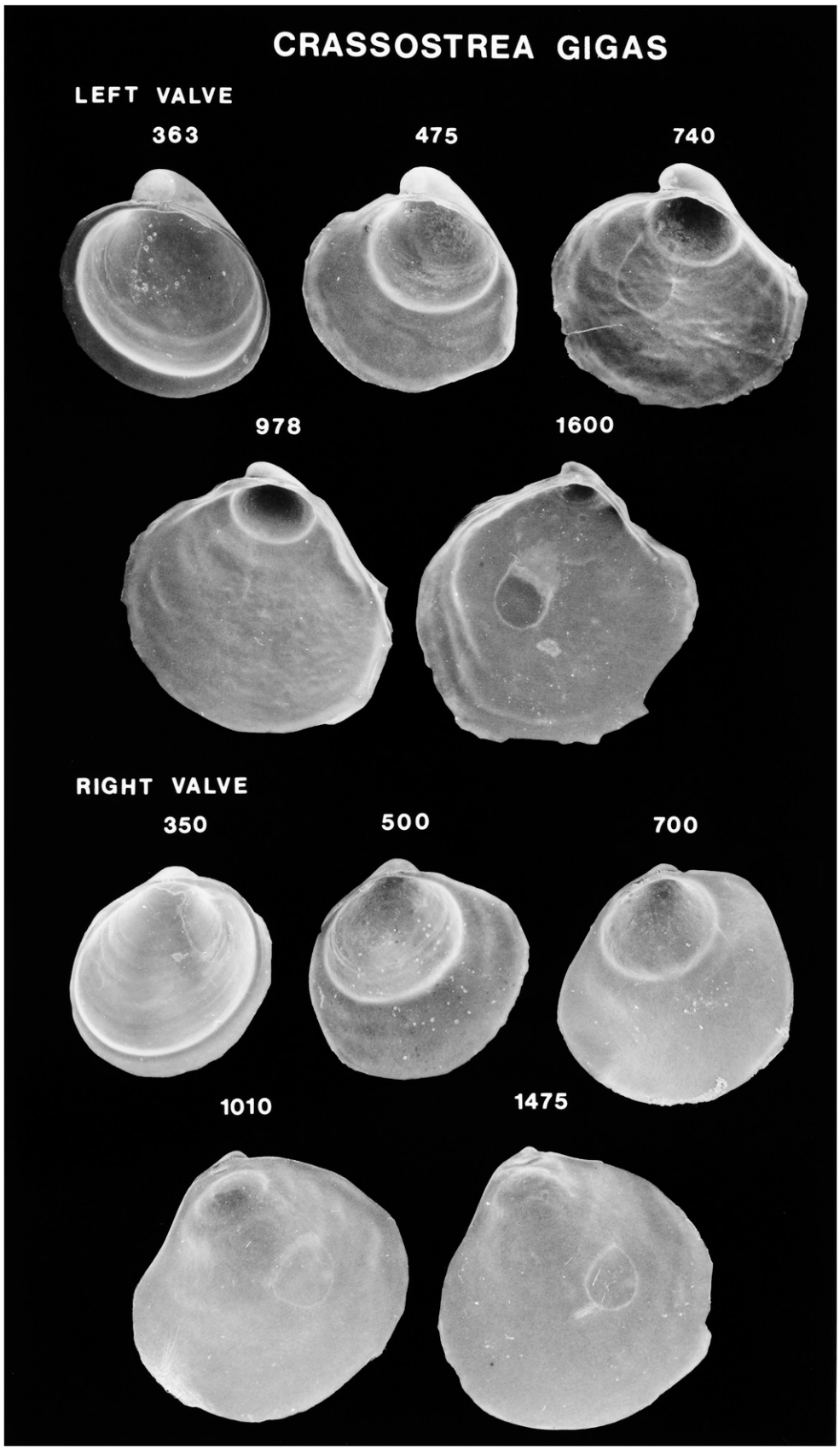

Figure 108. Scanning electron micrographs of disarticulated shell valves of *Crassostrea gigas* postlarvae. Numbers indicate the maximum linear shell dimension in micrometers. Modified from Hu et al. (1993).

Downloaded From: https://bioone.org/journals/Journal-of-Shellfish-Research on 25 Feb 2020
Terms of Use: https://bioone.org/terms-of-use Access provided by IFREMER

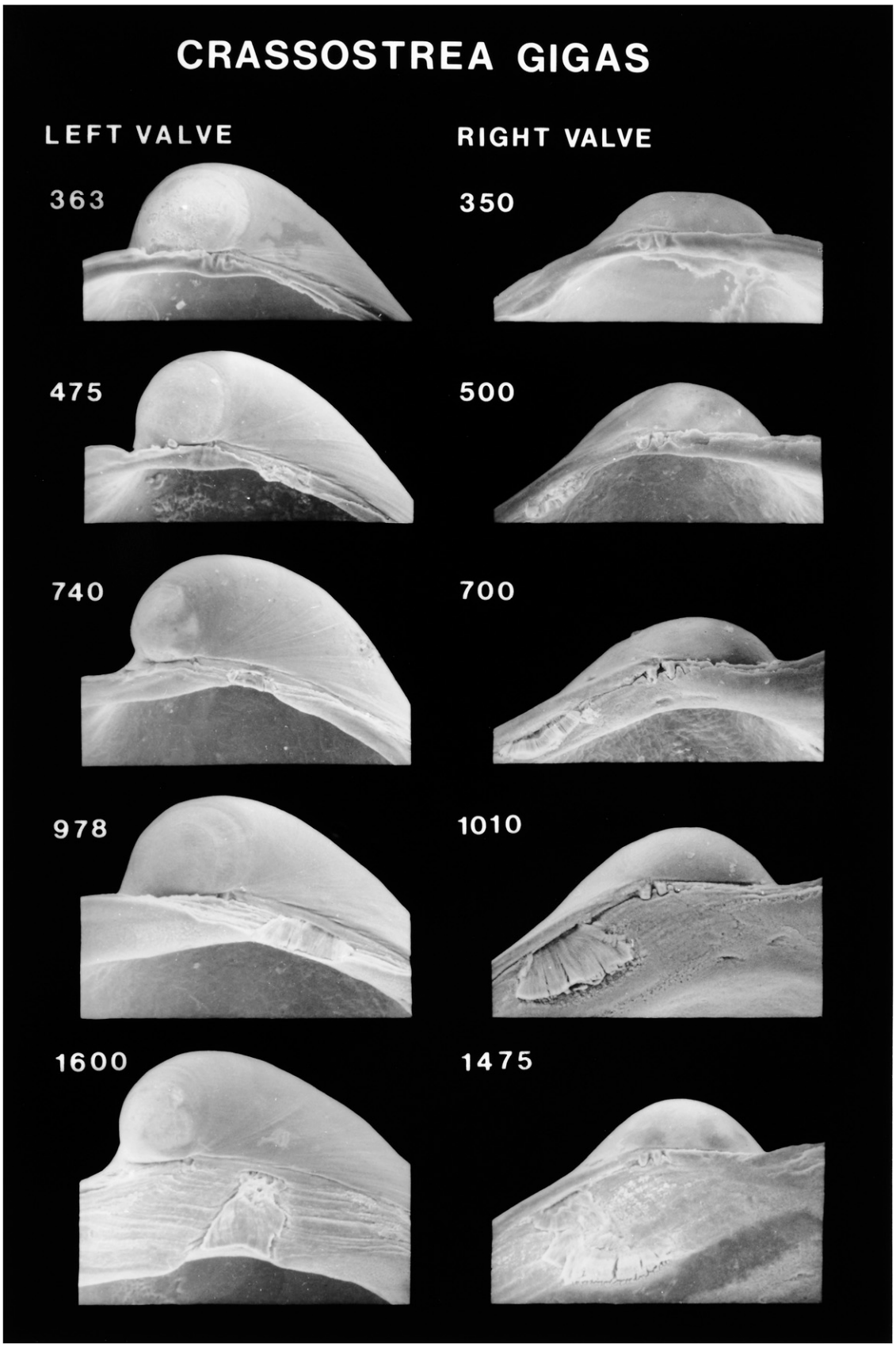

Figure 109. Scanning electron micrographs of the hinge of disarticulated shell valves of *Crassostrea gigas* postlarvae seen in Figure 108. Numbers indicate the maximum linear shell dimension in micrometers. Modified from Hu et al. (1993).

Downloaded From: https://bioone.org/journals/Journal-of-Shellfish-Research on 25 Feb 2020
Terms of Use: https://bioone.org/terms-of-use Access provided by IFREMER

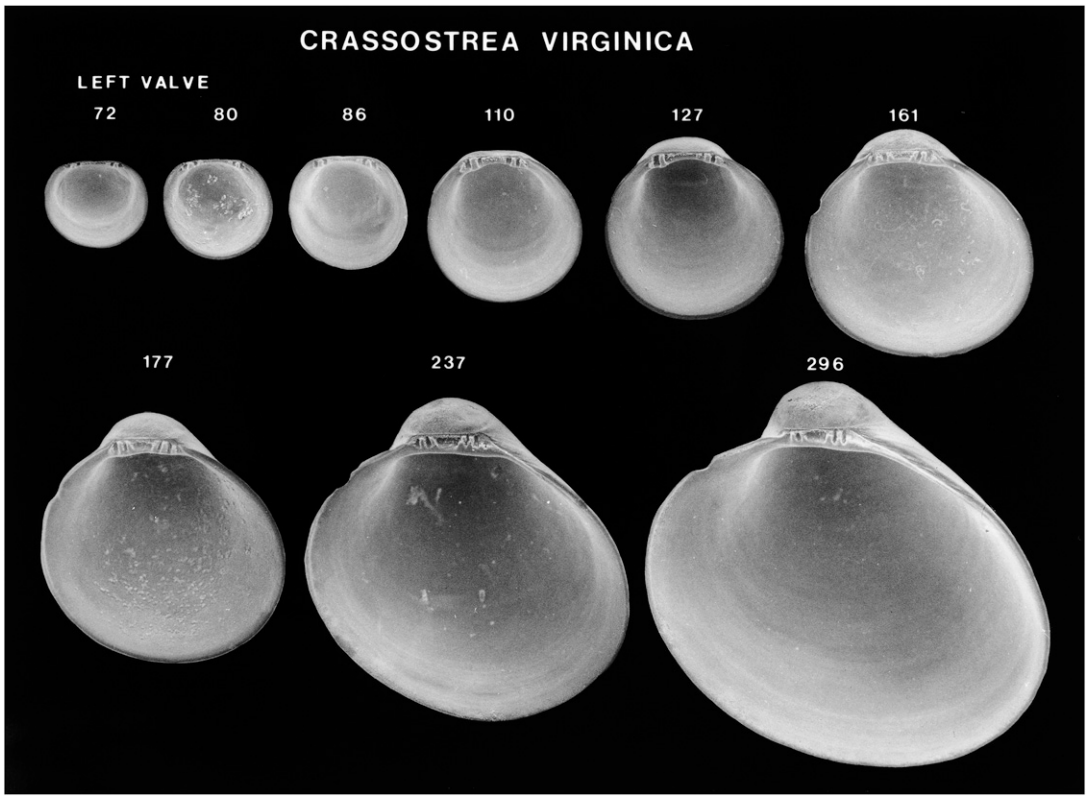

Figure 110. Scanning electron micrographs of disarticulated left shell valves of *Crassostrea virginica* larvae. Numbers indicate the maximum linear shell dimension in micrometers. Modified from Hu et al. (1993).

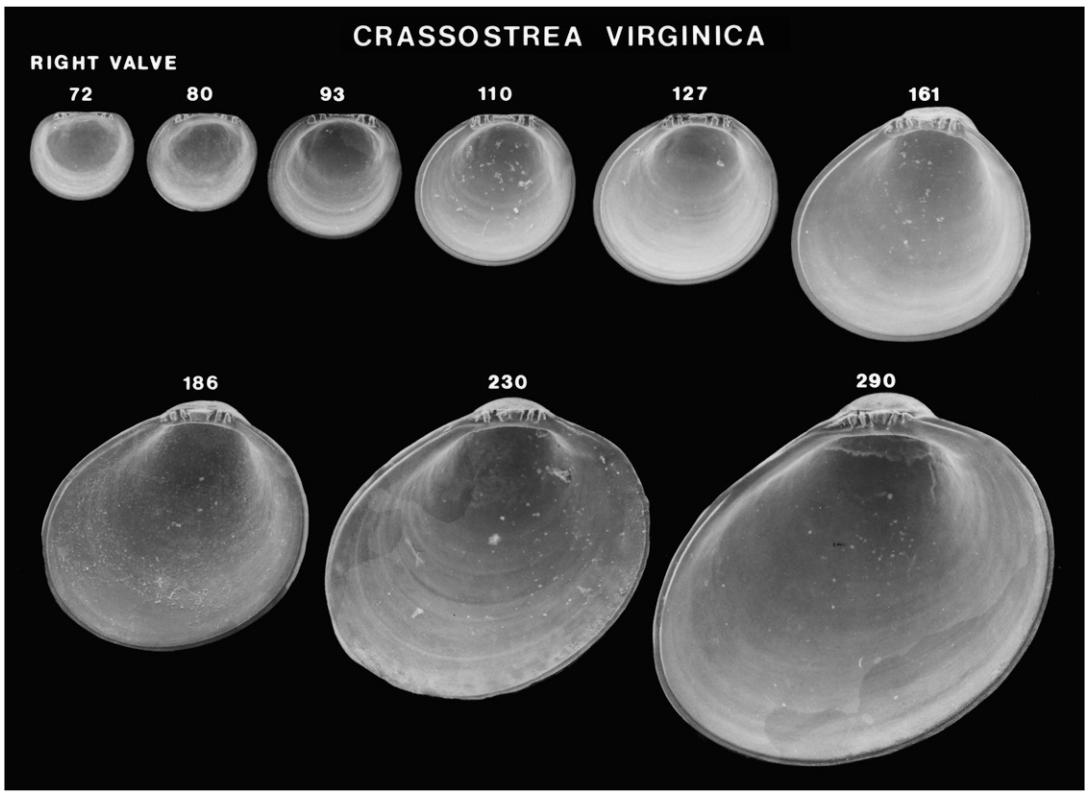

Figure 111. Scanning electron micrographs of disarticulated right shell valves of *Crassostrea virginica* larvae. Numbers indicate the maximum linear shell dimension in micrometers. Modified from Hu et al. (1993).

Downloaded From: https://bioone.org/journals/Journal-of-Shellfish-Research on 25 Feb 2020
Terms of Use: https://bioone.org/terms-of-use Access provided by IFREMER

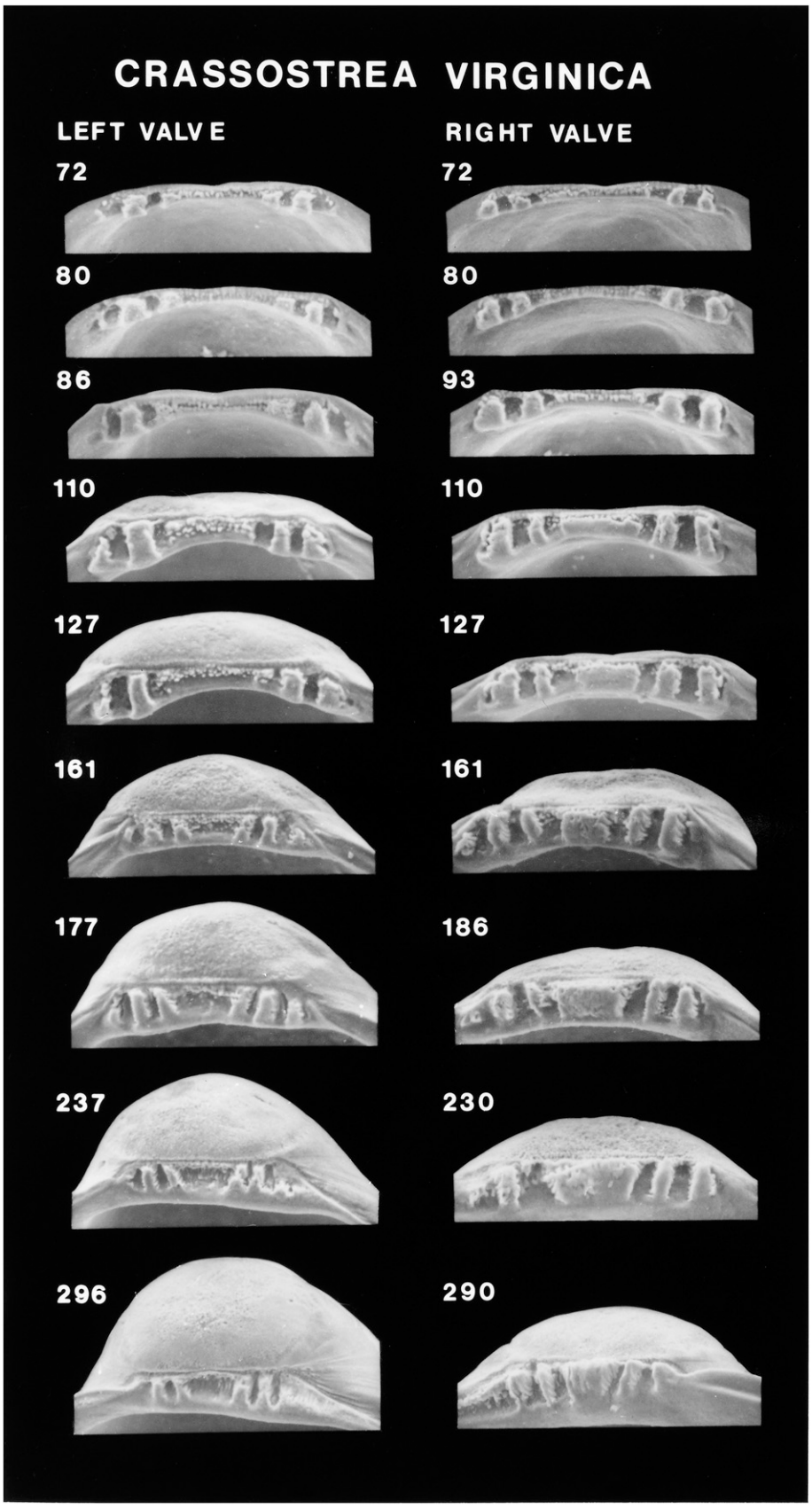

Figure 112. Scanning electron micrographs of the hinge of disarticulated shell valves of *Crassostrea virginica* larvae seen in Figures 110 and 111. Numbers indicate the maximum linear shell dimension in micrometers. Modified from Hu et al. (1993).

Downloaded From: https://bioone.org/journals/Journal-of-Shellfish-Research on 25 Feb 2020
Terms of Use: https://bioone.org/terms-of-use Access provided by IFREMER

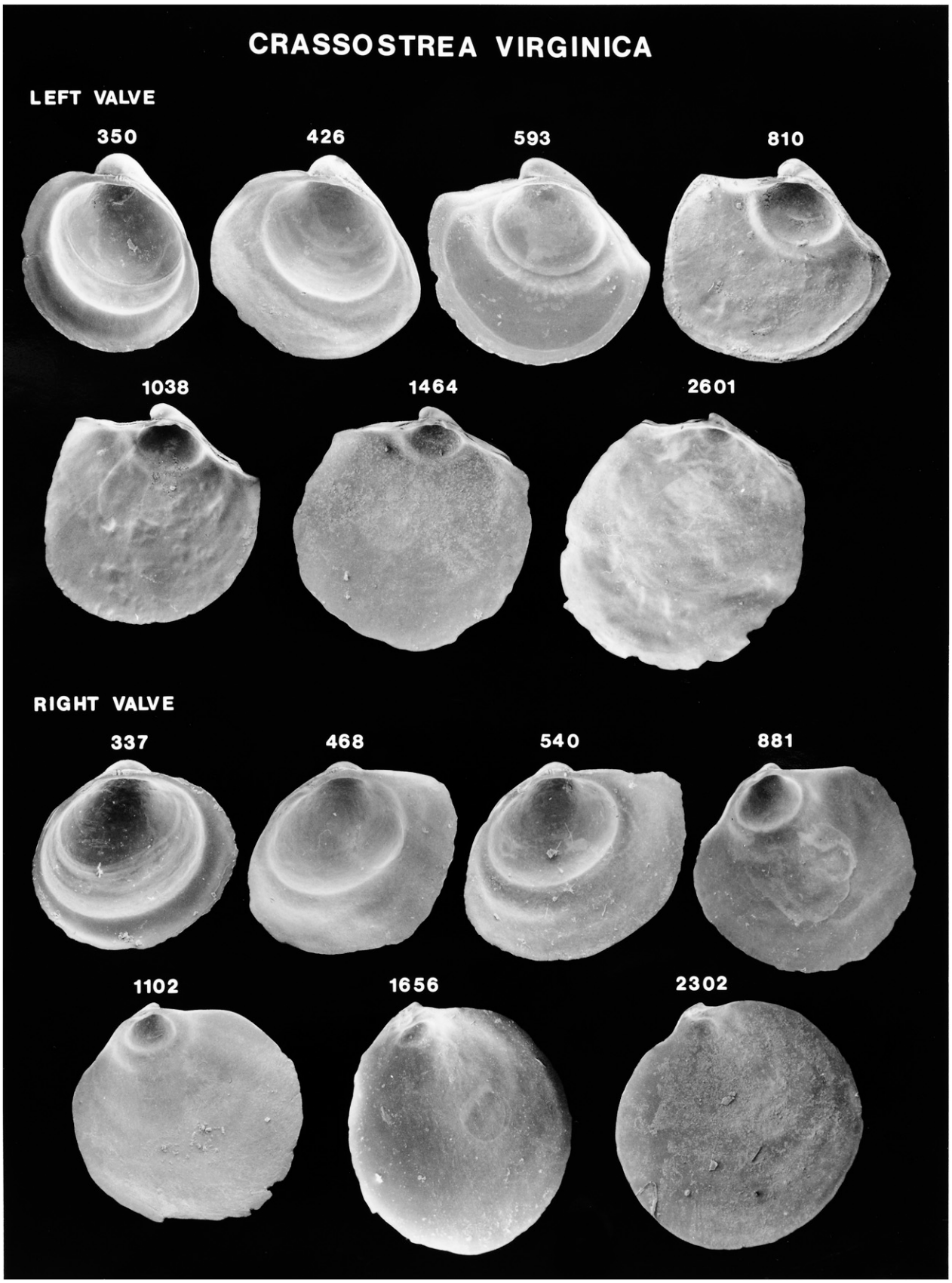

Figure 113. Scanning electron micrographs of disarticulated shell valves of *Crassostrea virginica* postlarvae. Numbers indicate the maximum linear shell dimension in micrometers. Modified from Hu et al. (1993).

Downloaded From: https://bioone.org/journals/Journal-of-Shellfish-Research on 25 Feb 2020
Terms of Use: https://bioone.org/terms-of-use Access provided by IFREMER

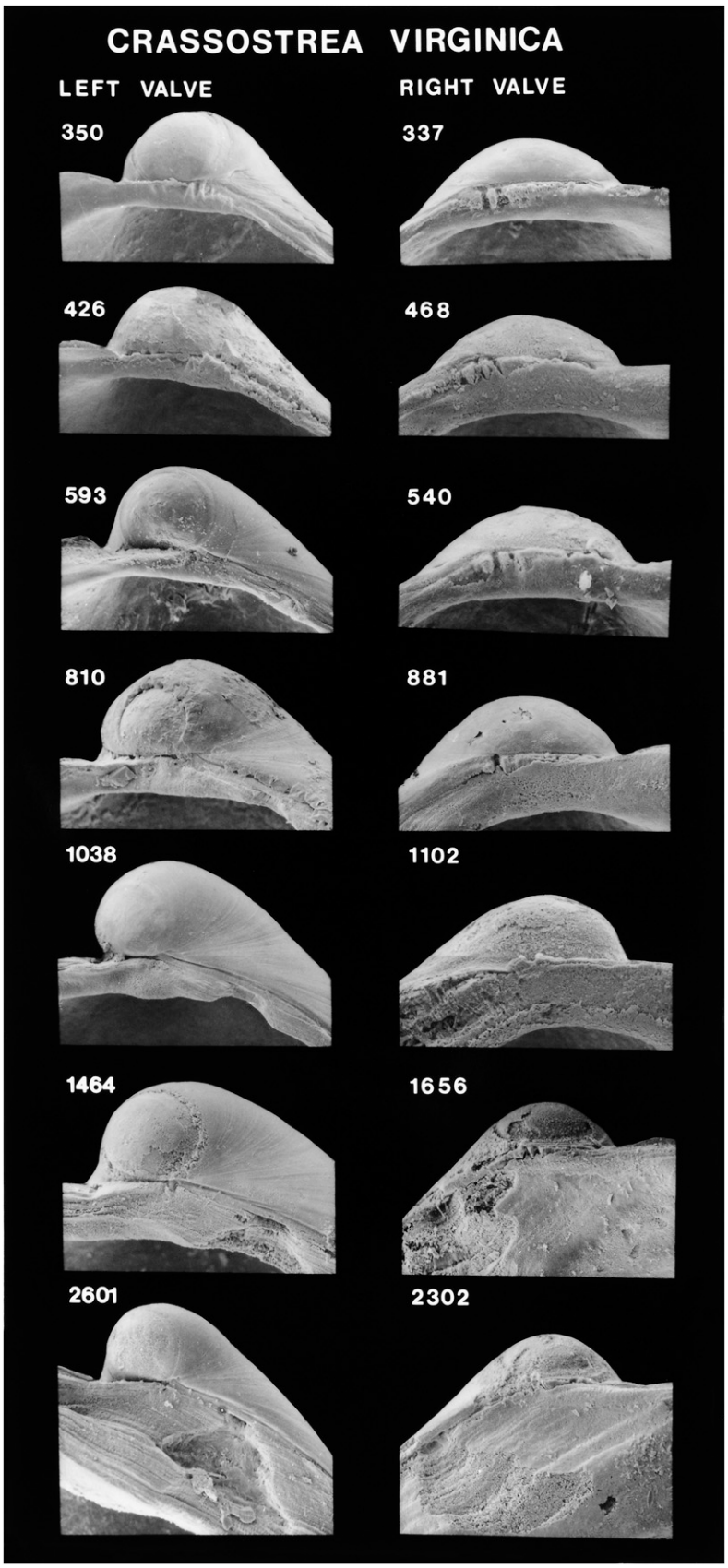

Figure 114. Scanning electron micrographs of the hinge of disarticulated shell valves of *Crassostrea virginica* postlarvae seen in Figure 113. Numbers indicate the maximum linear shell dimension in micrometers. Modified from Hu et al. (1993).

Downloaded From: https://bioone.org/journals/Journal-of-Shellfish-Research on 25 Feb 2020
Terms of Use: https://bioone.org/terms-of-use Access provided by IFREMER

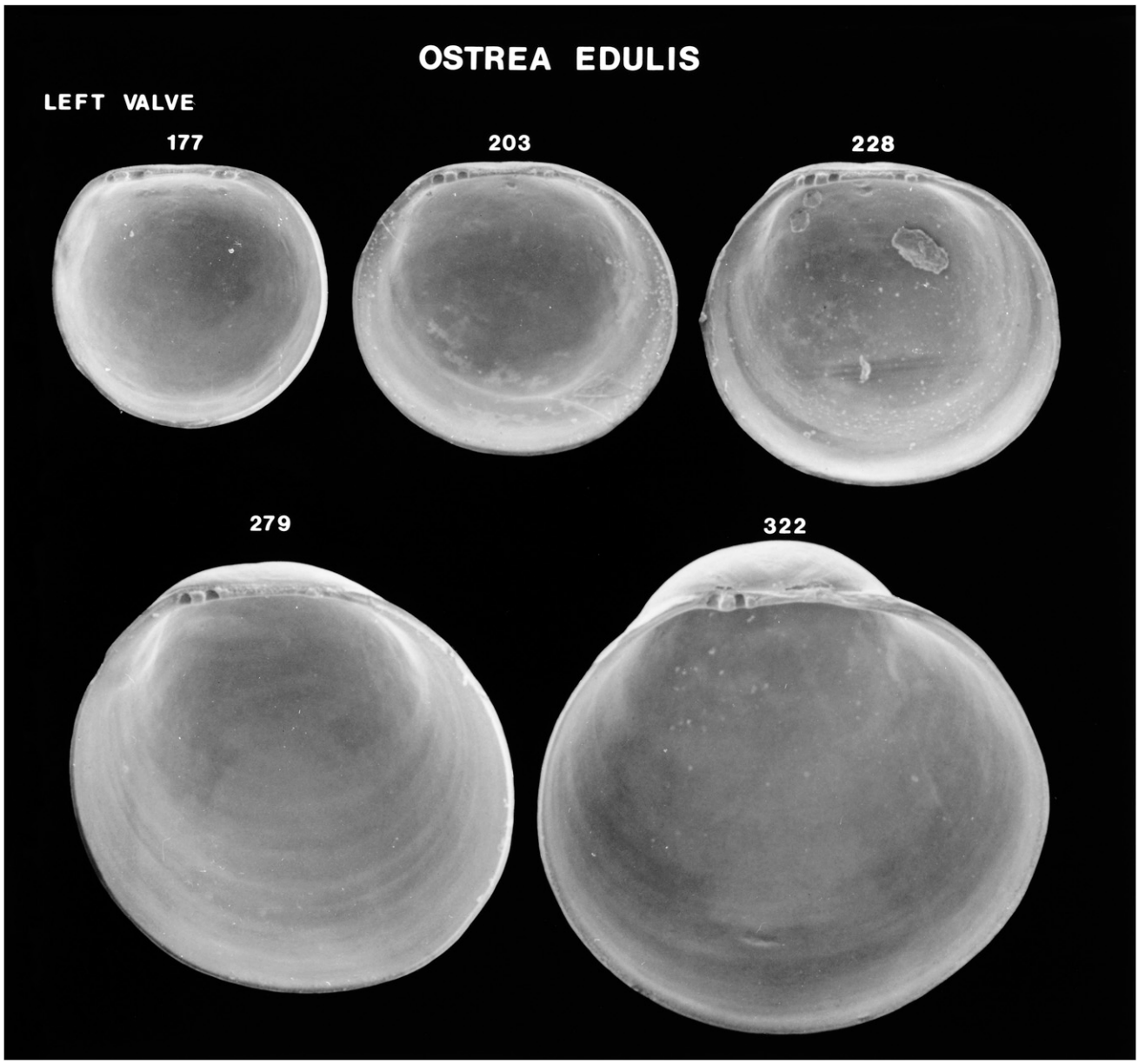

Figure 115. Scanning electron micrographs of disarticulated left shell valves of *Ostrea edulis* larvae. Numbers indicate the maximum linear shell dimension in micrometers. Modified from Hu et al. (1993).

Downloaded From: https://bioone.org/journals/Journal-of-Shellfish-Research on 25 Feb 2020
Terms of Use: https://bioone.org/terms-of-use Access provided by IFREMER

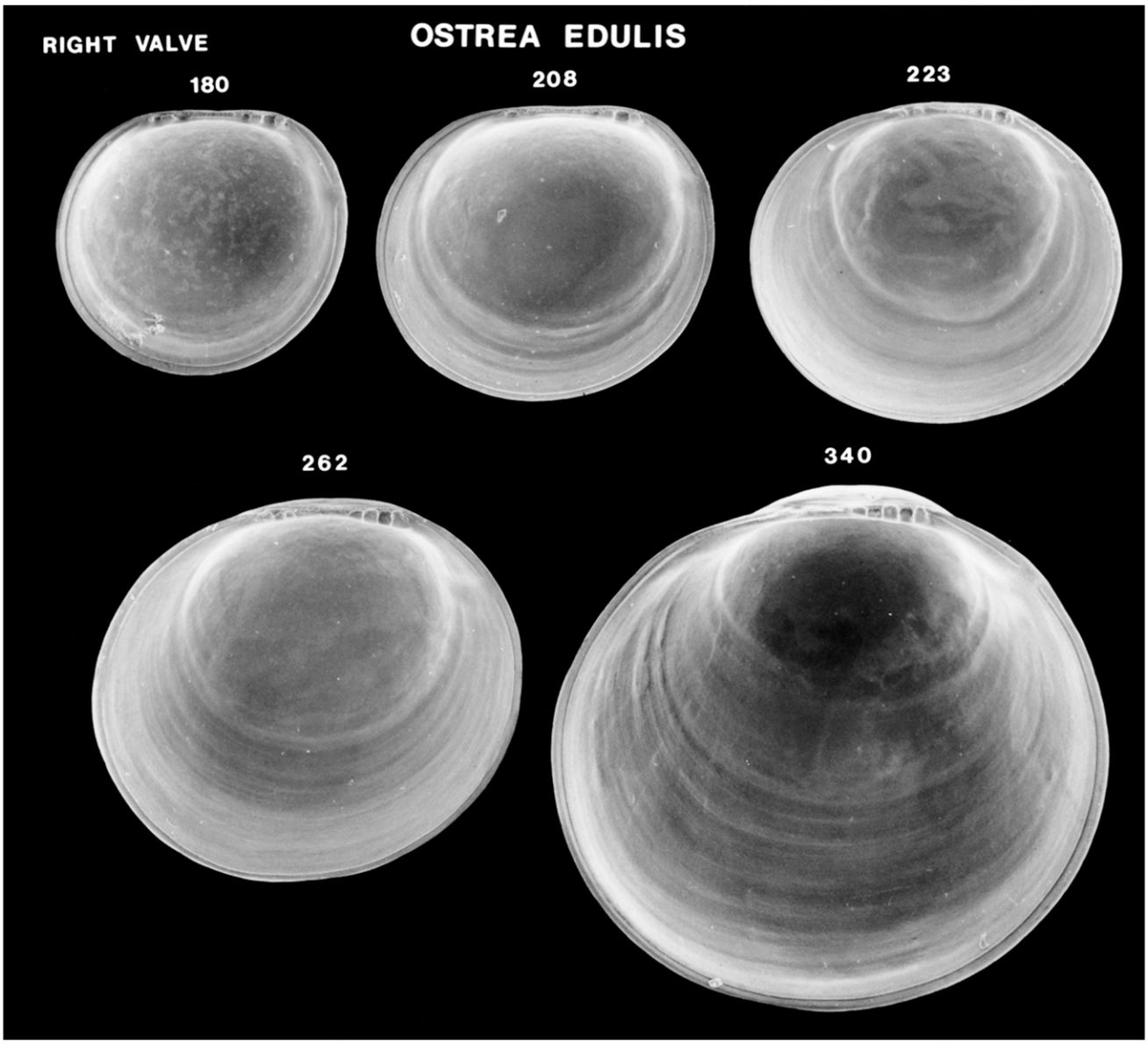

Figure 116. Scanning electron micrographs of disarticulated right shell valves of *Ostrea edulis* larvae. Numbers indicate the maximum linear shell dimension in micrometers. Modified from Hu et al. (1993).

Downloaded From: https://bioone.org/journals/Journal-of-Shellfish-Research on 25 Feb 2020
Terms of Use: https://bioone.org/terms-of-use Access provided by IFREMER

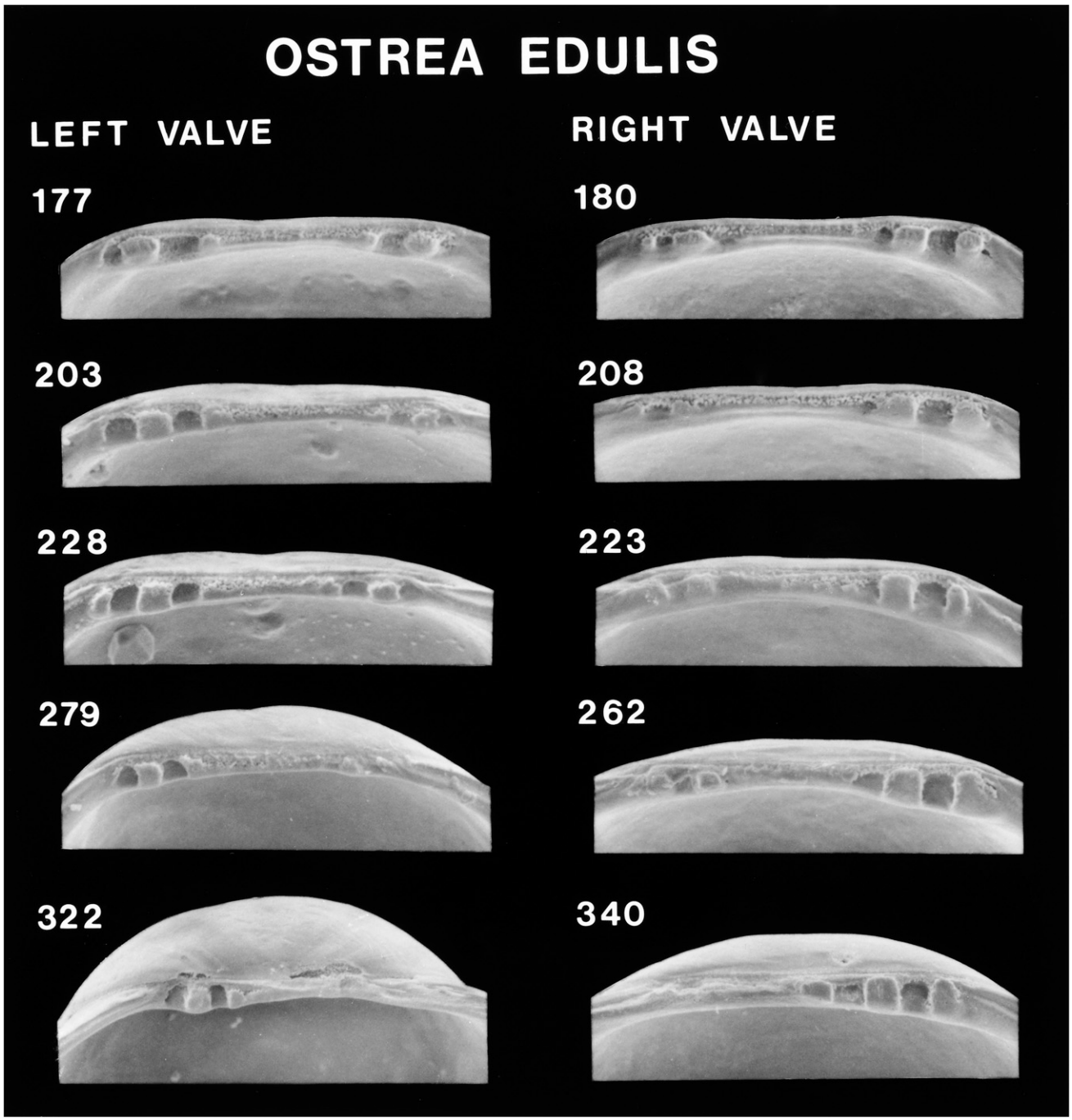

Figure 117. Scanning electron micrographs of the hinge of disarticulated shell valves of *Ostrea edulis* larvae seen in Figures 115 and 116. Numbers indicate the maximum linear shell dimension in micrometers. Modified from Hu et al. (1993).

Downloaded From: https://bioone.org/journals/Journal-of-Shellfish-Research on 25 Feb 2020
Terms of Use: https://bioone.org/terms-of-use Access provided by IFREMER

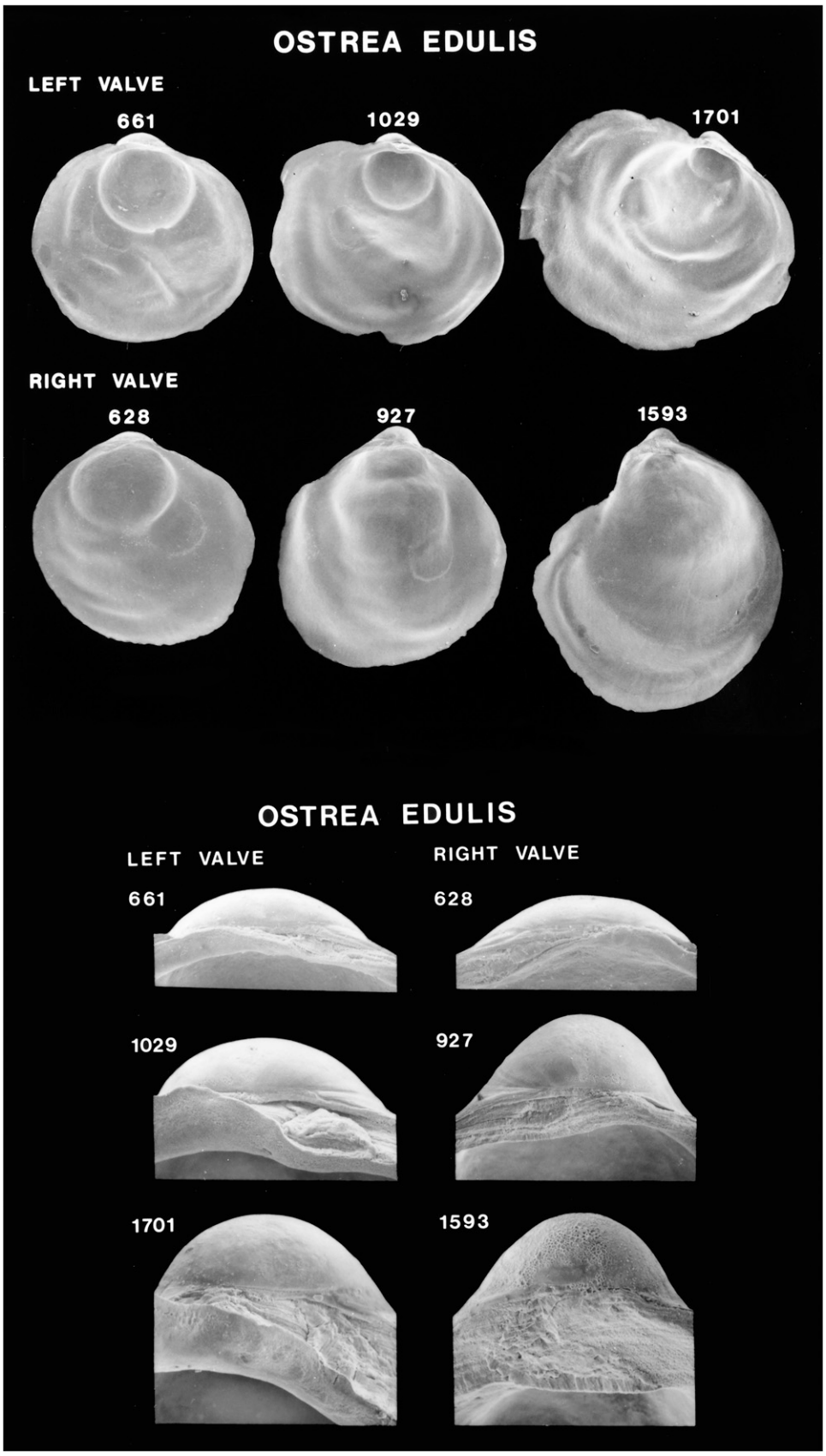

Figure 118. Scanning electron micrographs of disarticulated shell valves of *Ostrea edulis* postlarvae (top) and higher magnification scanning electron micrographs of the hinge of these shell valves (bottom). Numbers indicate the maximum linear shell dimension in micrometers. Modified from Hu et al. (1993).

Downloaded From: https://bioone.org/journals/Journal-of-Shellfish-Research on 25 Feb 2020
Terms of Use: https://bioone.org/terms-of-use Access provided by IFREMER

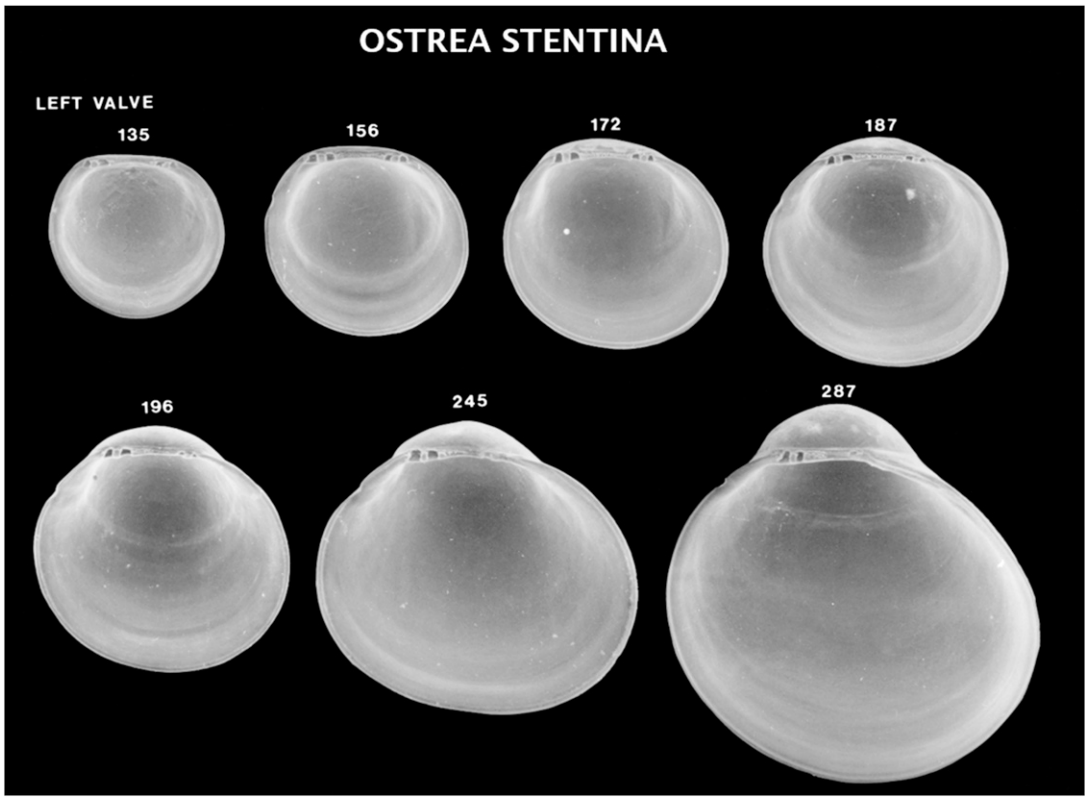

Figure 119. Scanning electron micrographs of disarticulated left shell valves of *Ostrea stentina* larvae. Numbers indicate the maximum linear shell dimension in micrometers. Modified from Hu et al. (1993).

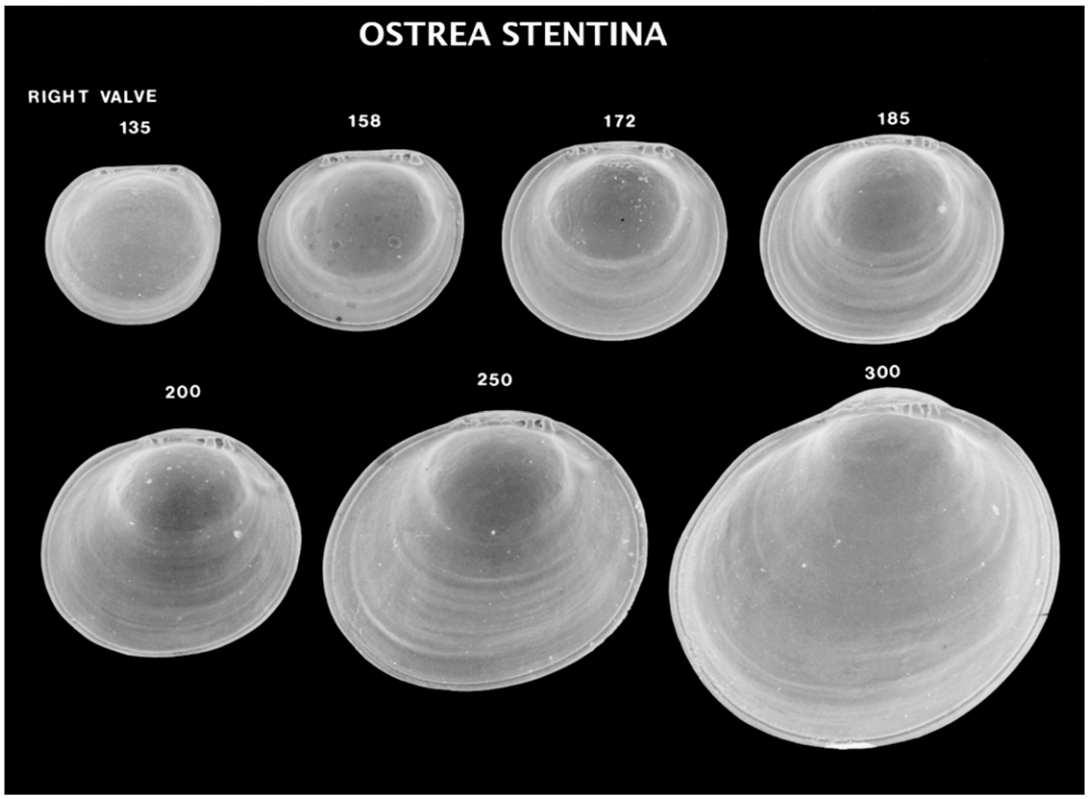

Figure 120. Scanning electron micrographs of disarticulated right shell valves of *Ostrea stentina* larvae. Numbers indicate the maximum linear shell dimension in micrometers. Modified from Hu et al. (1993).

Downloaded From: https://bioone.org/journals/Journal-of-Shellfish-Research on 25 Feb 2020
Terms of Use: https://bioone.org/terms-of-use Access provided by IFREMER

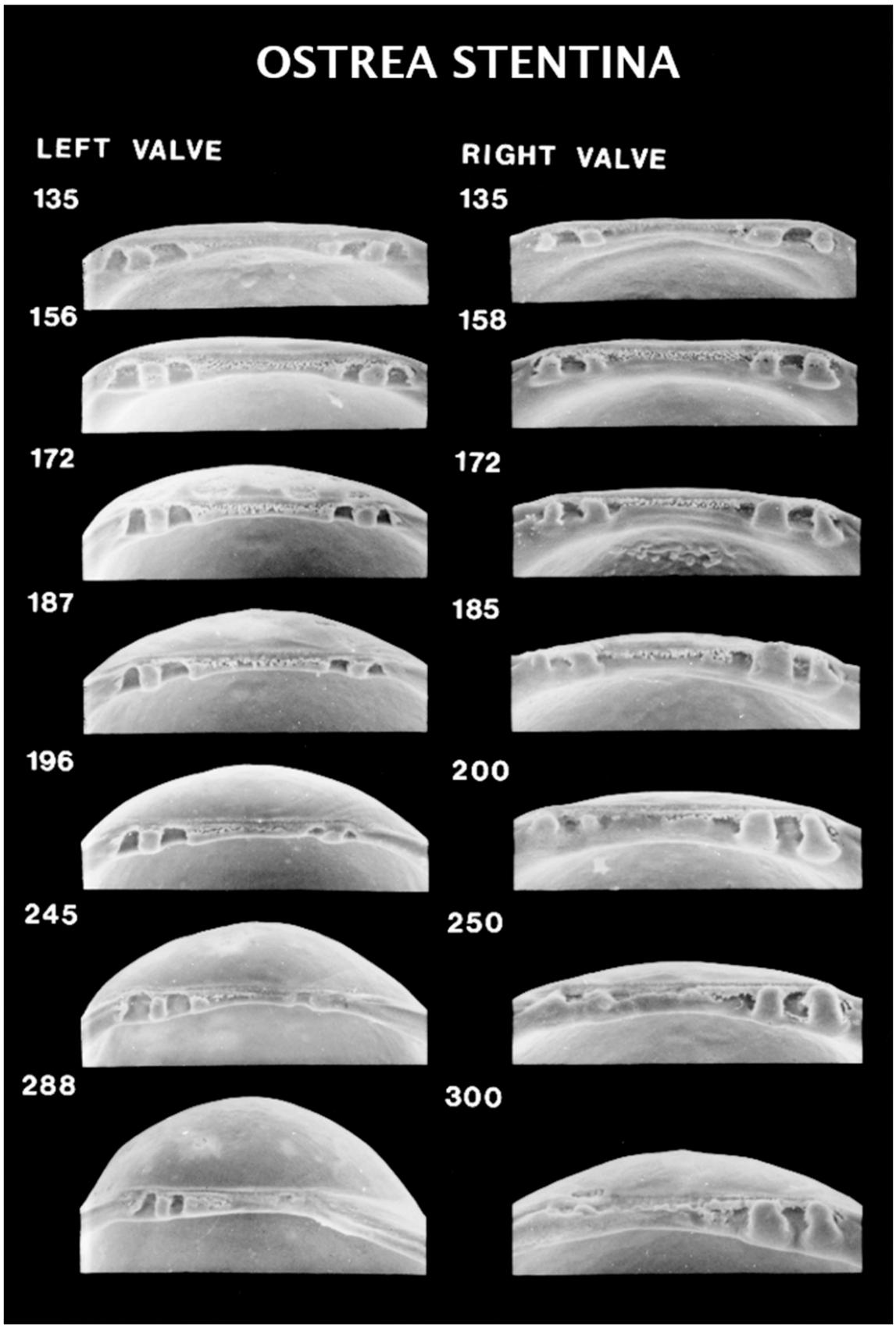

Figure 121. Scanning electron micrographs of the hinge of disarticulated shell valves of *Ostrea stentina* larvae seen in Figures 119 and 120. Numbers indicate the maximum linear shell dimension in micrometers. Modified from Hu et al. (1993).

Downloaded From: https://bioone.org/journals/Journal-of-Shellfish-Research on 25 Feb 2020
Terms of Use: https://bioone.org/terms-of-use Access provided by IFREMER

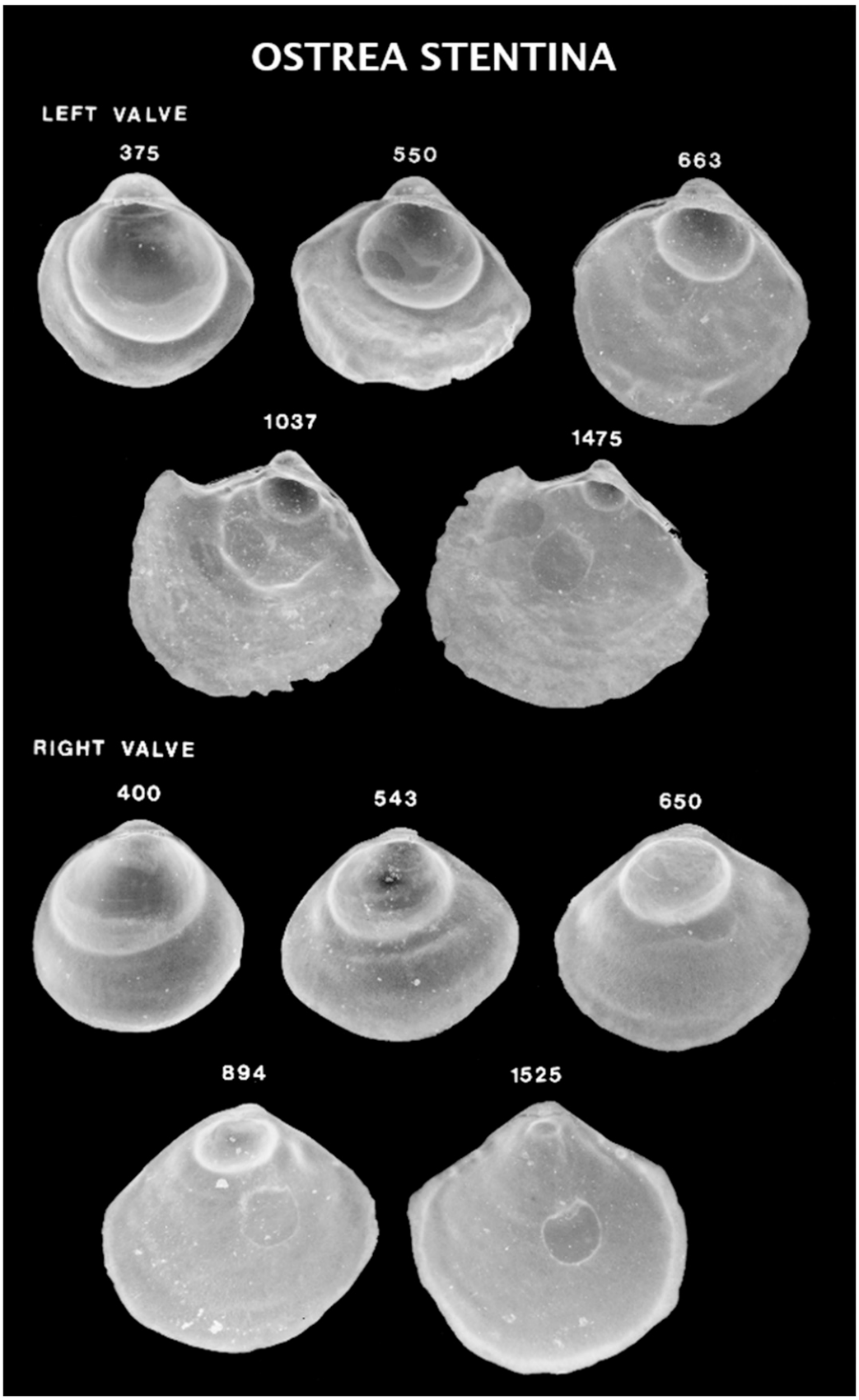

Figure 122. Scanning electron micrographs of disarticulated shell valves of *Ostrea stentina* postlarvae. Numbers indicate the maximum linear shell dimension in micrometers. Modified from Hu et al. (1993).

Downloaded From: https://bioone.org/journals/Journal-of-Shellfish-Research on 25 Feb 2020
Terms of Use: https://bioone.org/terms-of-use Access provided by IFREMER

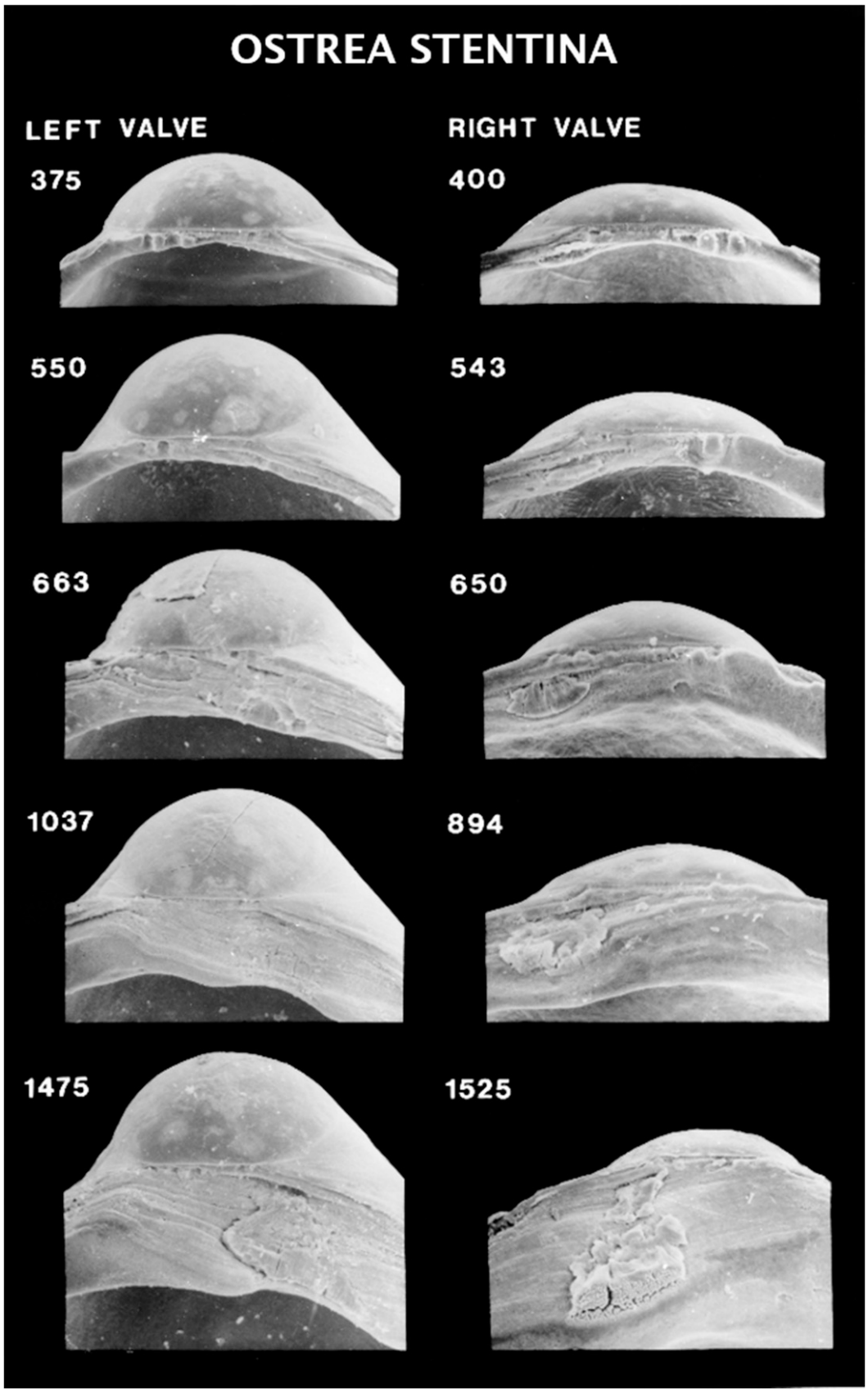

Figure 123. Scanning electron micrographs of the hinge of disarticulated shell valves of *Ostrea stentina* postlarvae seen in Figure 122. Numbers indicate the maximum linear shell dimension in micrometers. Modified from Hu et al. (1993).

Downloaded From: https://bioone.org/journals/Journal-of-Shellfish-Research on 25 Feb 2020
Terms of Use: https://bioone.org/terms-of-use Access provided by IFREMER

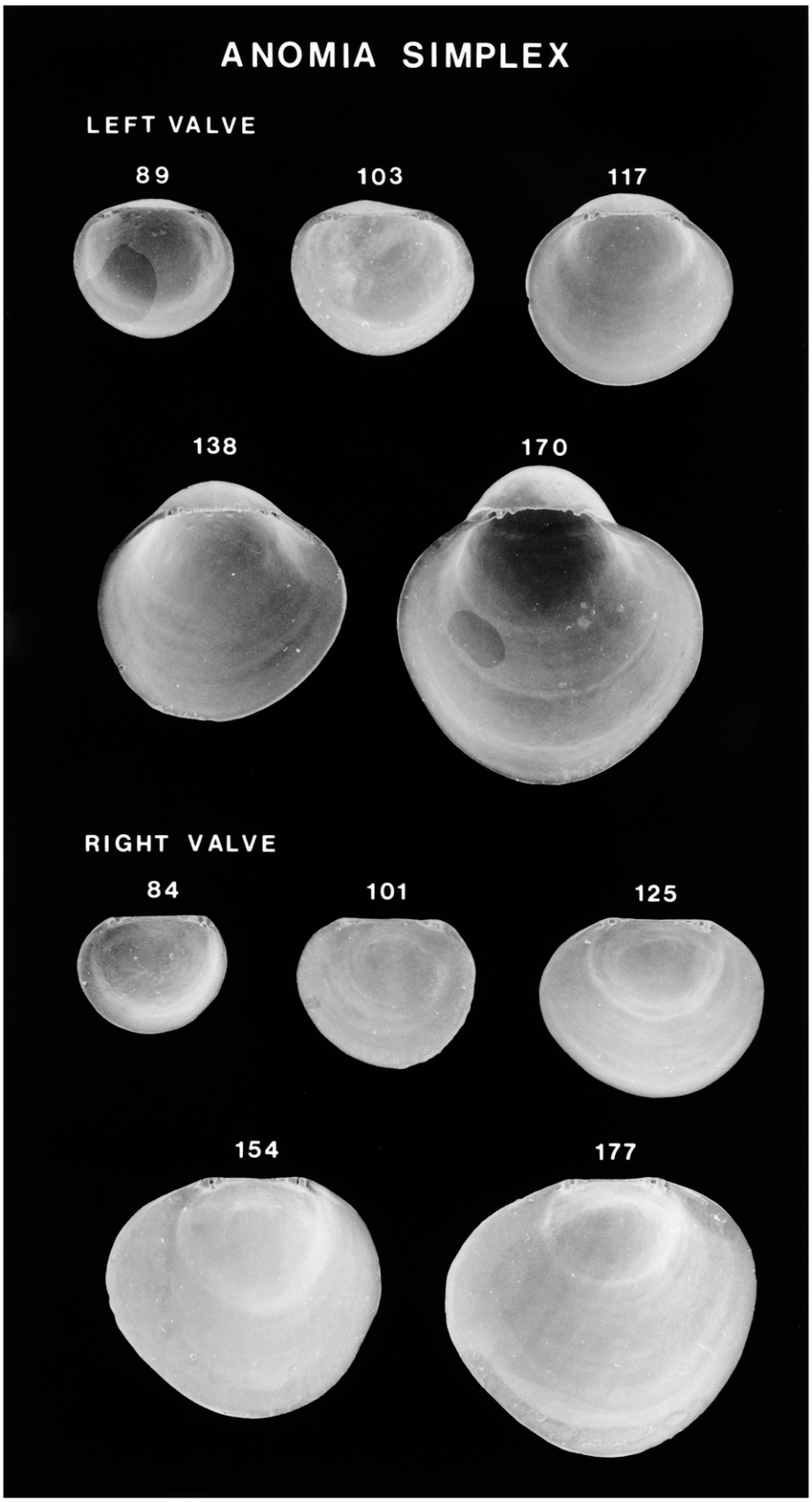

Figure 124. Scanning electron micrographs of disarticulated shell valves of *Anomia simplex* larvae. Numbers indicate the maximum linear shell dimension in micrometers.

Downloaded From: https://bioone.org/journals/Journal-of-Shellfish-Research on 25 Feb 2020
Terms of Use: https://bioone.org/terms-of-use Access provided by IFREMER

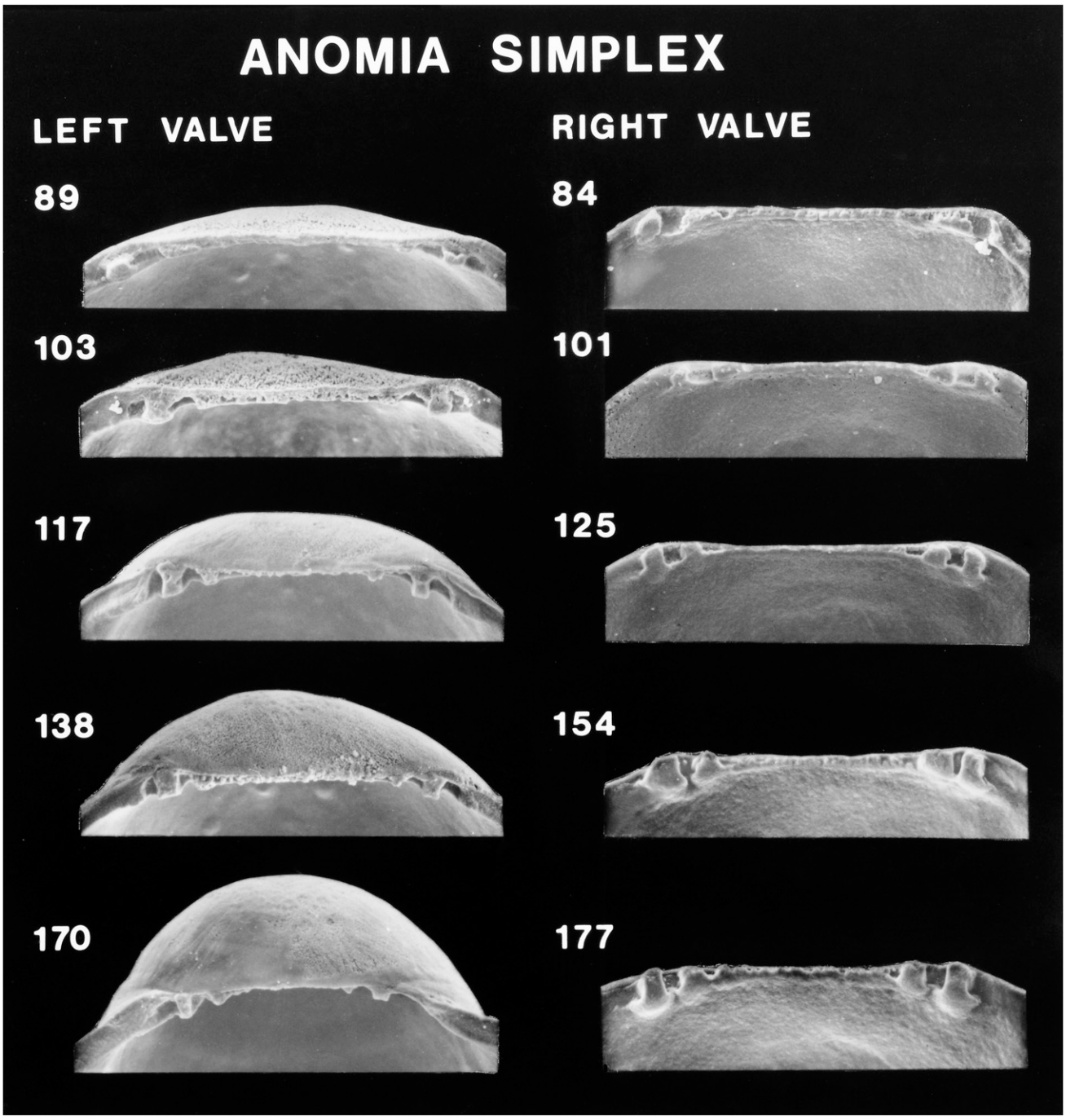

Figure 125. Scanning electron micrographs of the hinge of disarticulated shell valves of *Anomia simplex* larvae seen in Figure 124. Numbers indicate the maximum linear shell dimension in micrometers.

Downloaded From: https://bioone.org/journals/Journal-of-Shellfish-Research on 25 Feb 2020
Terms of Use: https://bioone.org/terms-of-use Access provided by IFREMER

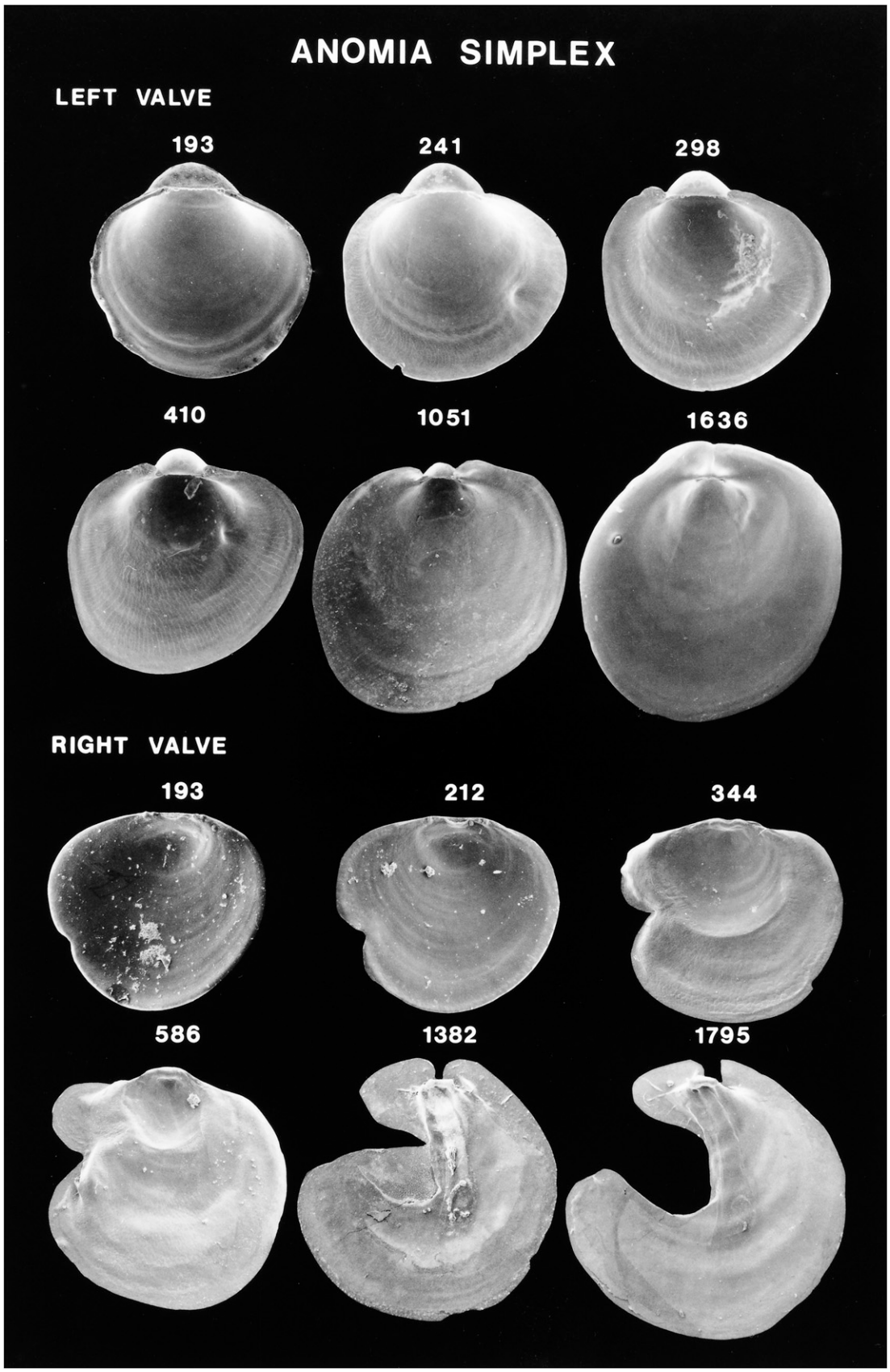

Figure 126. Scanning electron micrographs of disarticulated shell valves of *Anomia simplex* postlarvae. Numbers indicate the maximum linear shell dimension in micrometers.

Downloaded From: https://bioone.org/journals/Journal-of-Shellfish-Research on 25 Feb 2020
Terms of Use: https://bioone.org/terms-of-use Access provided by IFREMER

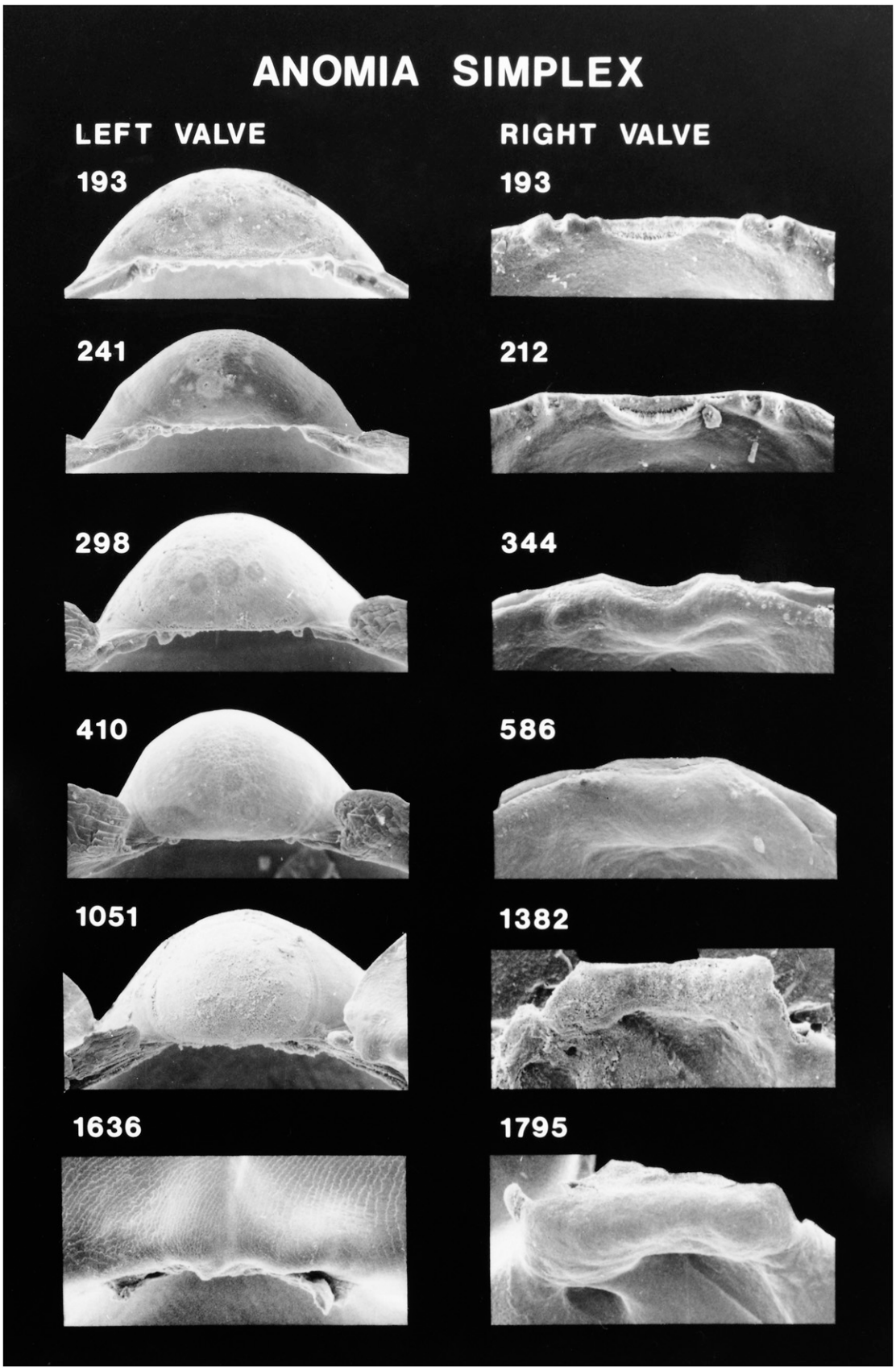

Figure 127. Scanning electron micrographs of the hinge of disarticulated shell valves of *Anomia simplex* postlarvae seen in Figure 126. Numbers indicate the maximum linear shell dimension in micrometers.

Downloaded From: https://bioone.org/journals/Journal-of-Shellfish-Research on 25 Feb 2020
Terms of Use: https://bioone.org/terms-of-use Access provided by IFREMER

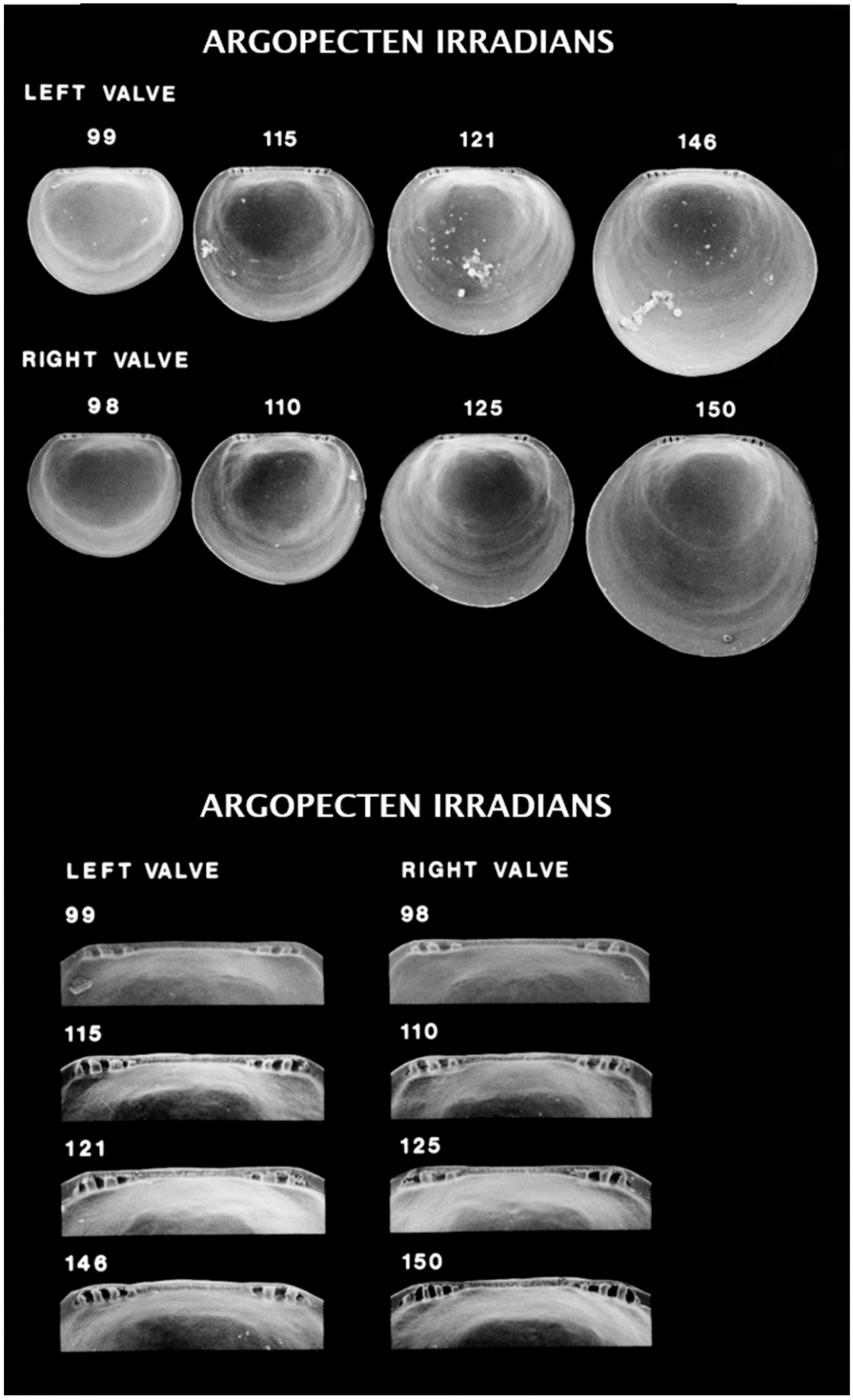

Figure 128. Scanning electron micrographs of disarticulated shell valves of *Argopecten irradians* larvae (top) and higher magnification scanning electron micrographs of the hinge of these shell valves (bottom). Numbers indicate the maximum linear shell dimension in micrometers.

Downloaded From: https://bioone.org/journals/Journal-of-Shellfish-Research on 25 Feb 2020
Terms of Use: https://bioone.org/terms-of-use Access provided by IFREMER

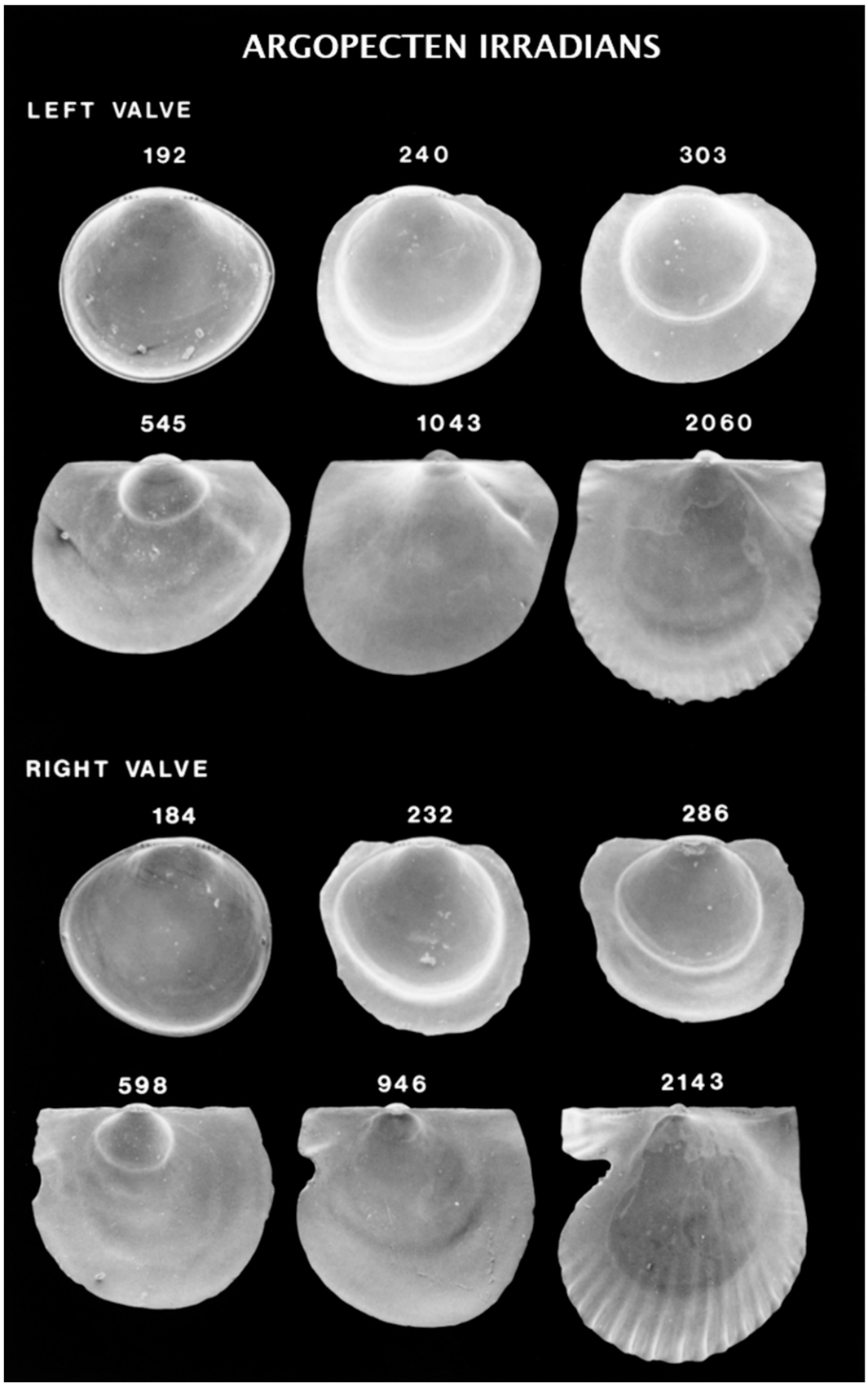

Figure 129. Scanning electron micrographs of disarticulated shell valves of *Argopecten irradians* postlarvae. Numbers indicate the maximum linear shell dimension in micrometers.

Downloaded From: https://bioone.org/journals/Journal-of-Shellfish-Research on 25 Feb 2020
Terms of Use: https://bioone.org/terms-of-use Access provided by IFREMER

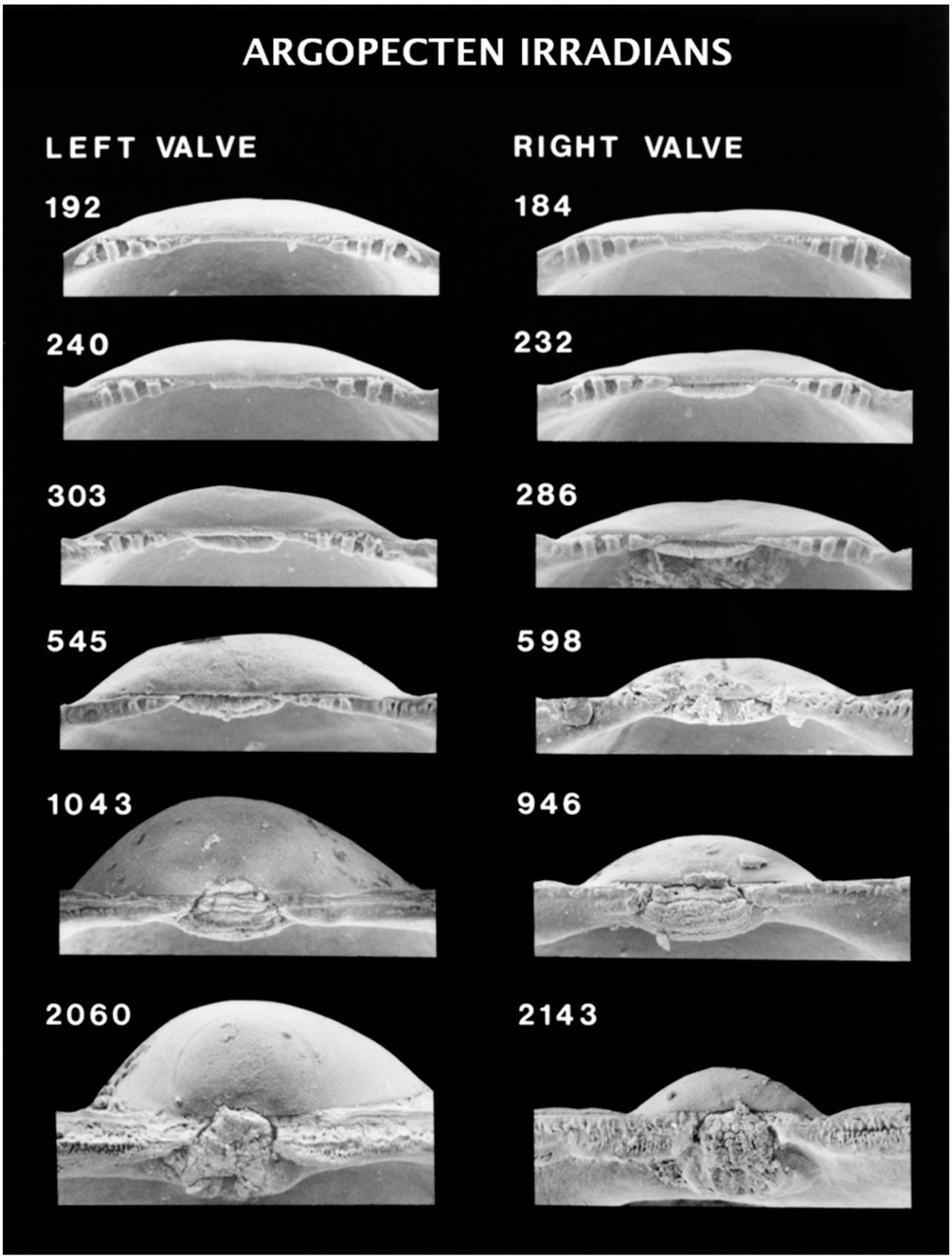

Figure 130. Scanning electron micrographs of the hinge of disarticulated shell valves of *Argopecten irradians* postlarvae seen in Figure 129. Numbers indicate the maximum linear shell dimension in micrometers.

Downloaded From: https://bioone.org/journals/Journal-of-Shellfish-Research on 25 Feb 2020
Terms of Use: https://bioone.org/terms-of-use Access provided by IFREMER

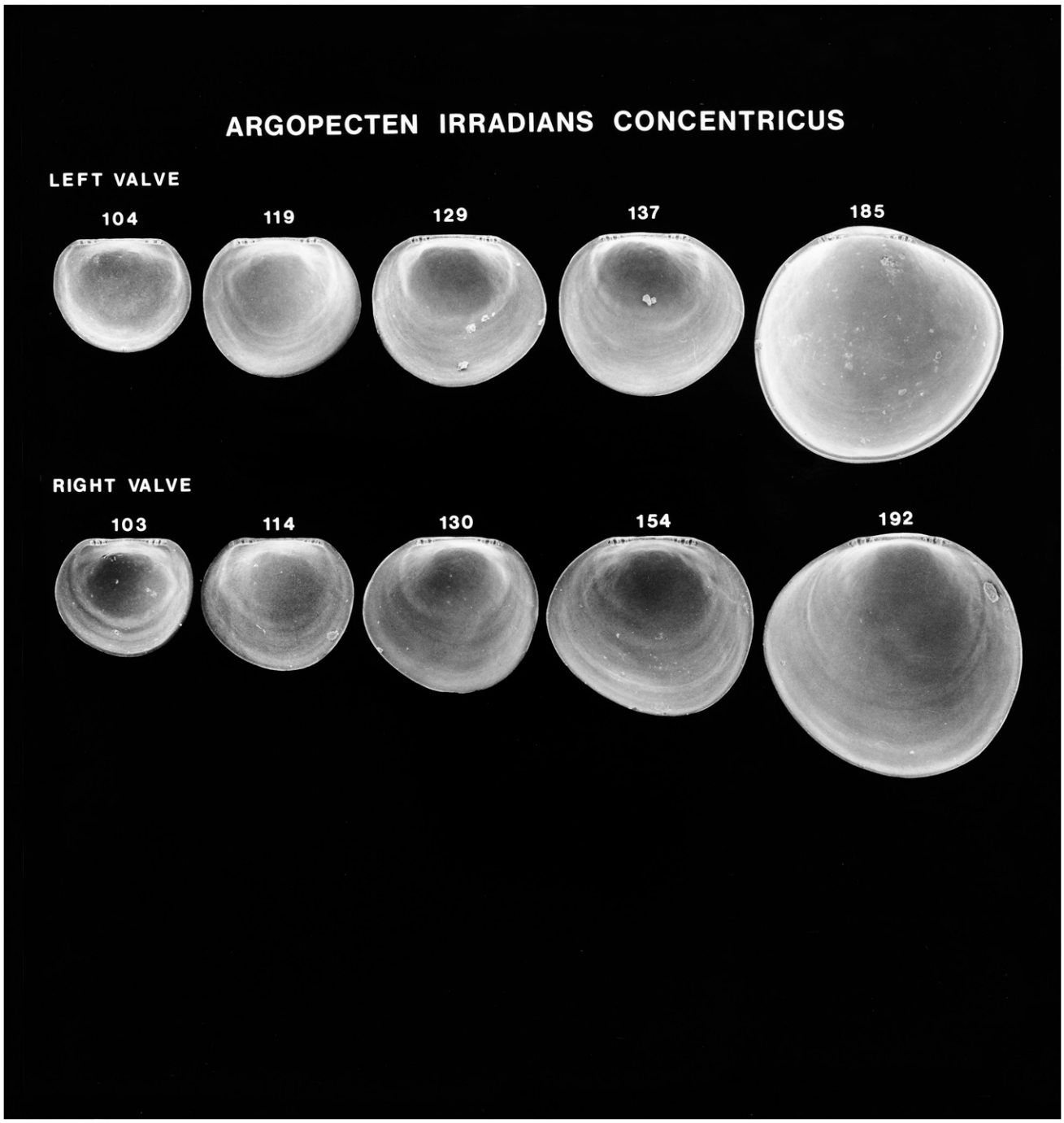

Figure 131. Scanning electron micrographs of disarticulated shell valves of *Argopecten irradians concentricus* larvae. Numbers indicate the maximum linear shell dimension in micrometers.

Downloaded From: https://bioone.org/journals/Journal-of-Shellfish-Research on 25 Feb 2020
Terms of Use: https://bioone.org/terms-of-use Access provided by IFREMER

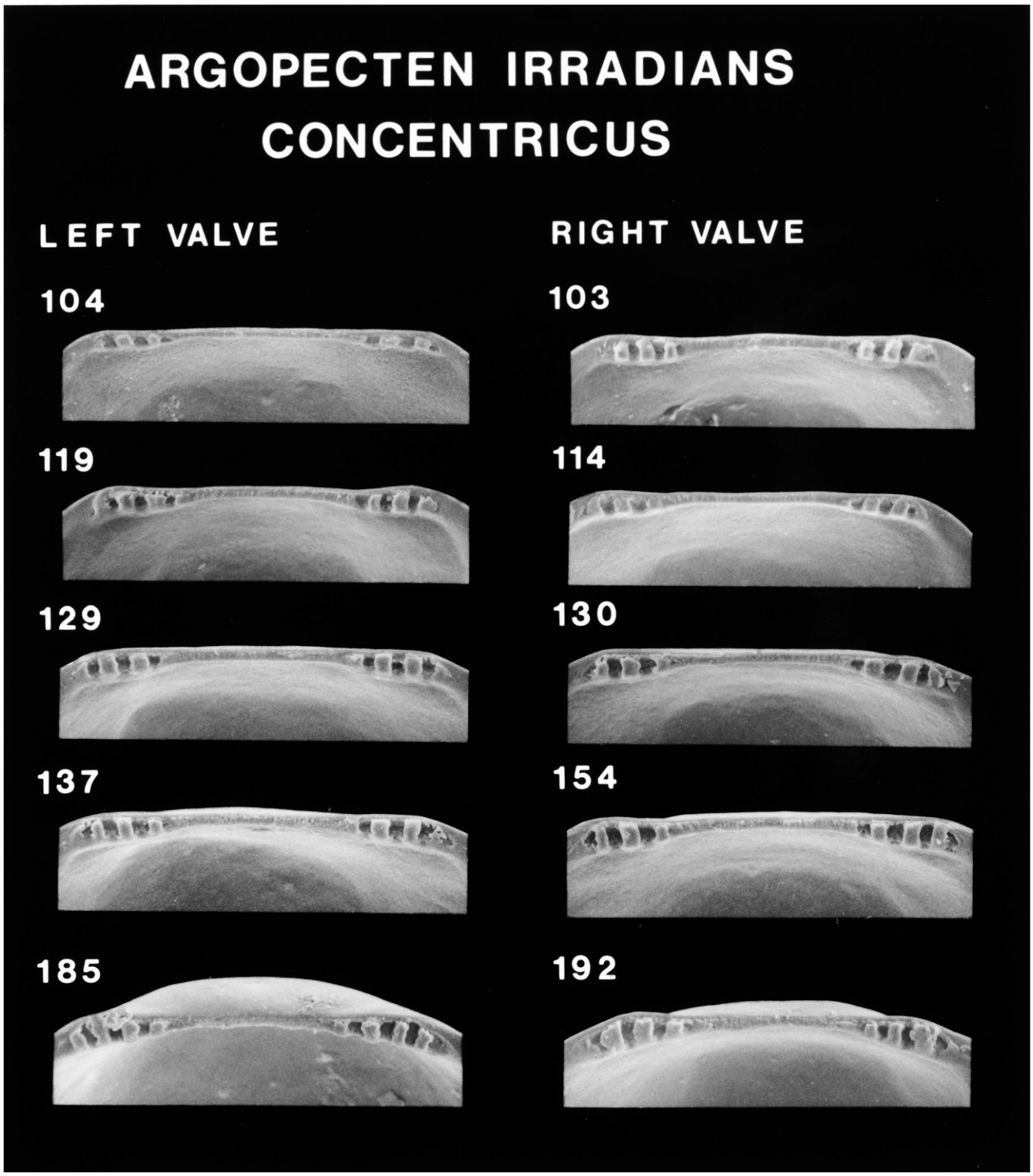

Figure 132. Scanning electron micrographs of the hinge of disarticulated shell valves of *Argopecten irradians concentricus* larvae seen in Figure 131. Numbers indicate the maximum linear shell dimension in micrometers.

Downloaded From: https://bioone.org/journals/Journal-of-Shellfish-Research on 25 Feb 2020
Terms of Use: https://bioone.org/terms-of-use Access provided by IFREMER

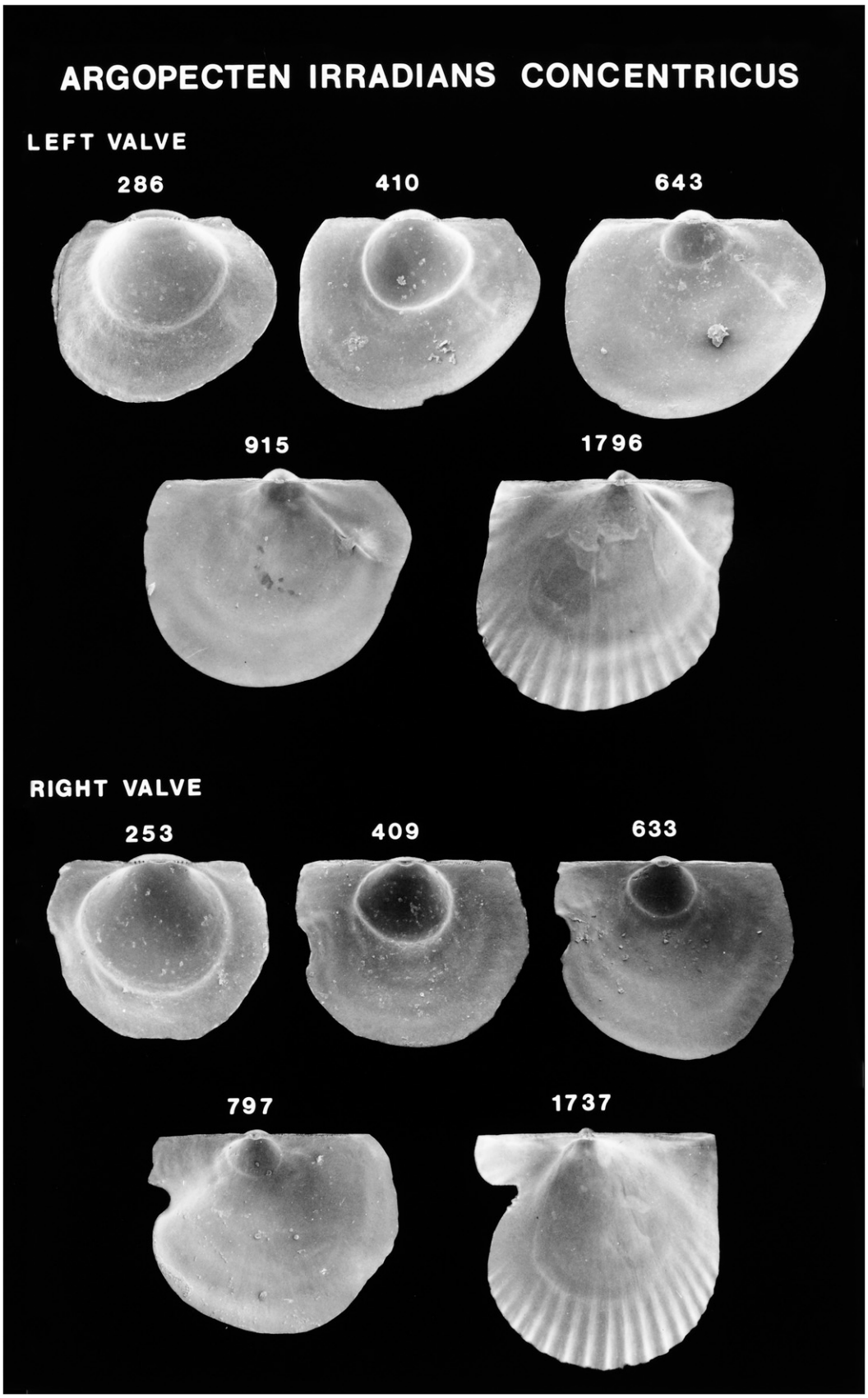

Figure 133. Scanning electron micrographs of disarticulated shell valves of *Argopecten irradians concentricus* postlarvae. Numbers indicate the maximum linear shell dimension in micrometers.

Downloaded From: https://bioone.org/journals/Journal-of-Shellfish-Research on 25 Feb 2020
Terms of Use: https://bioone.org/terms-of-use Access provided by IFREMER

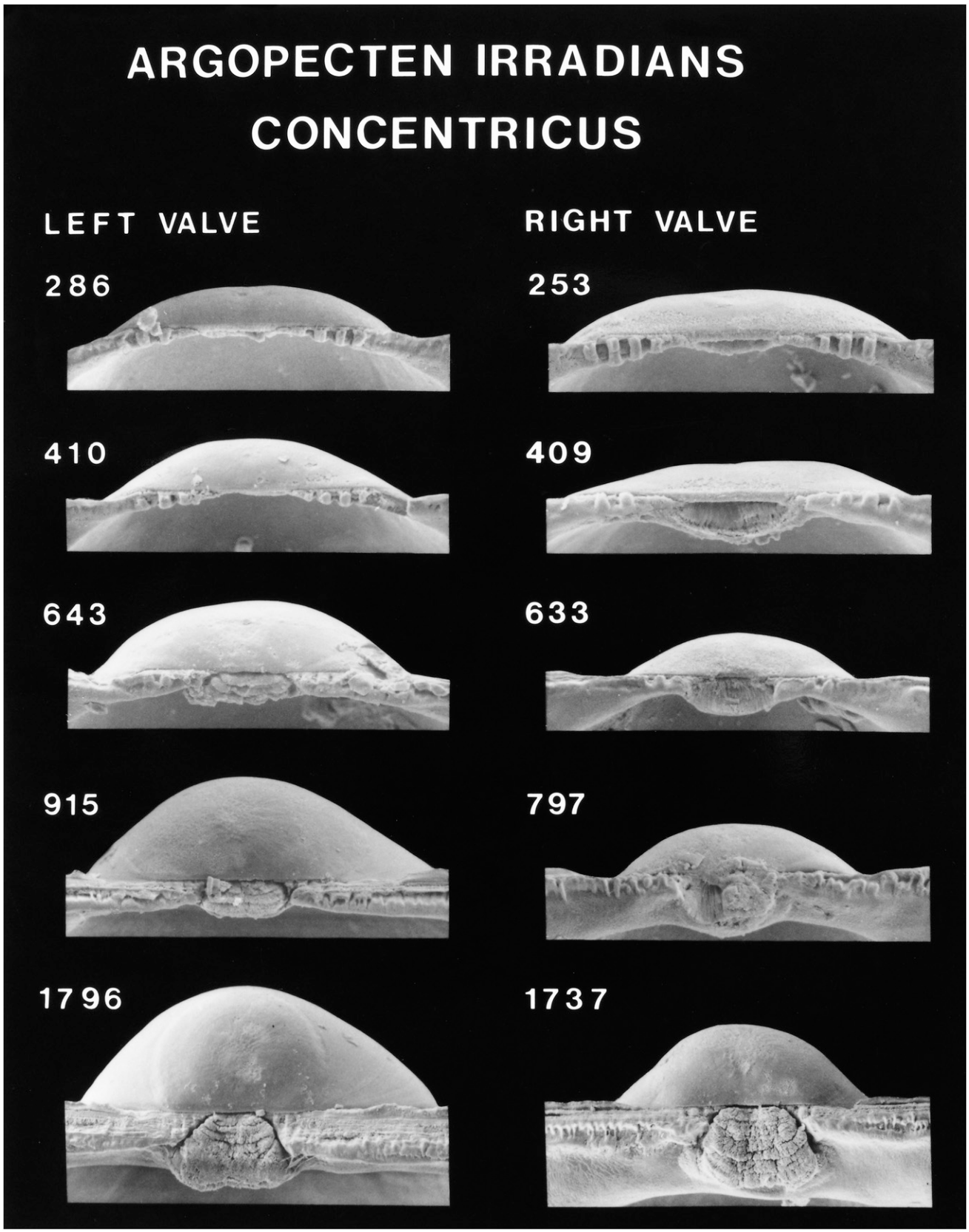

Figure 134. Scanning electron micrographs of the hinge of disarticulated shell valves of *Argopecten irradians concentricus* postlarvae seen in Figure 133. Numbers indicate the maximum linear shell dimension in micrometers.

Downloaded From: https://bioone.org/journals/Journal-of-Shellfish-Research on 25 Feb 2020
Terms of Use: https://bioone.org/terms-of-use Access provided by IFREMER

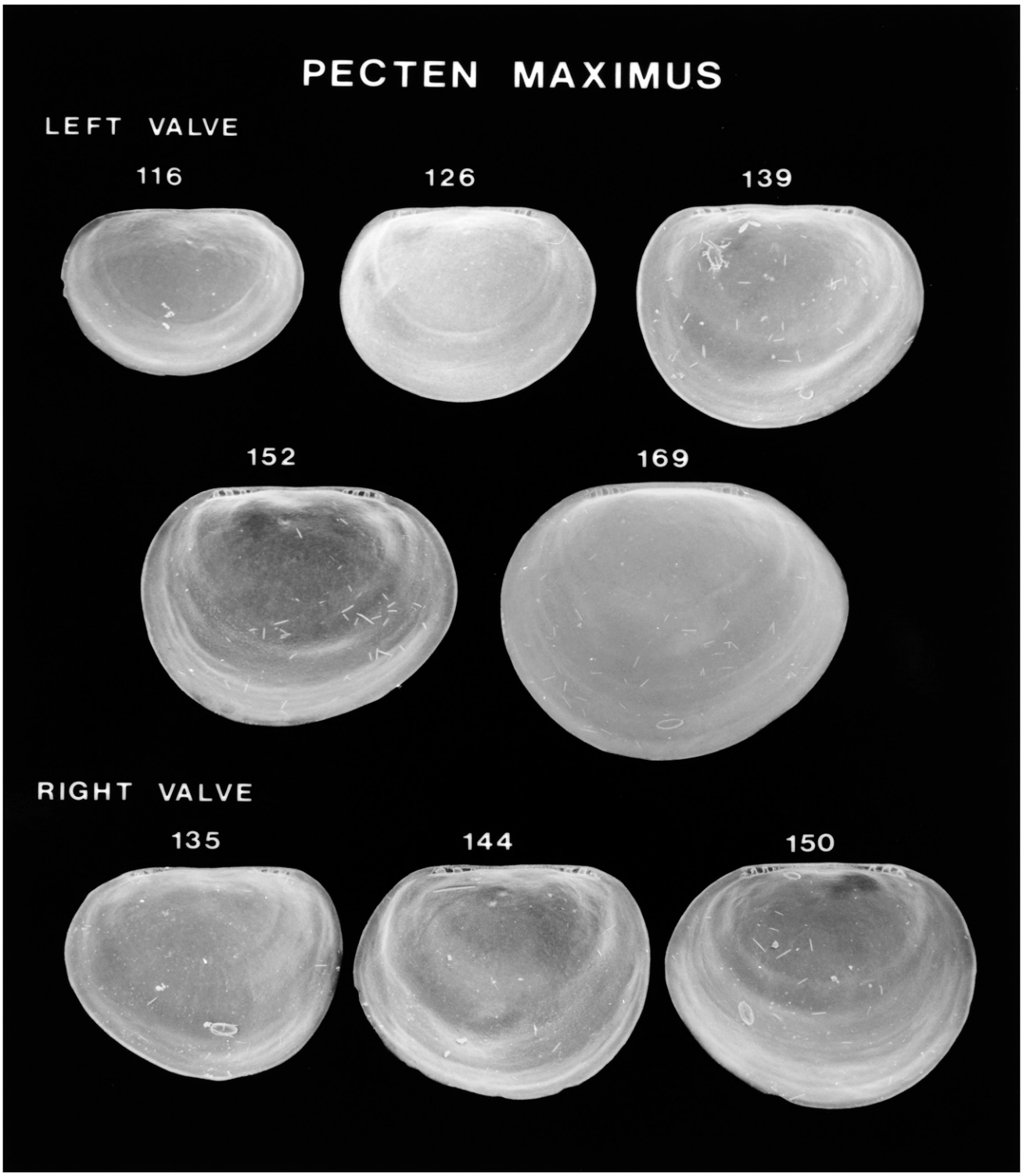

Figure 135. Scanning electron micrographs of disarticulated shell valves of *Pecten maximus* larvae. Numbers indicate the maximum linear shell dimension in micrometers.

Downloaded From: https://bioone.org/journals/Journal-of-Shellfish-Research on 25 Feb 2020
Terms of Use: https://bioone.org/terms-of-use Access provided by IFREMER

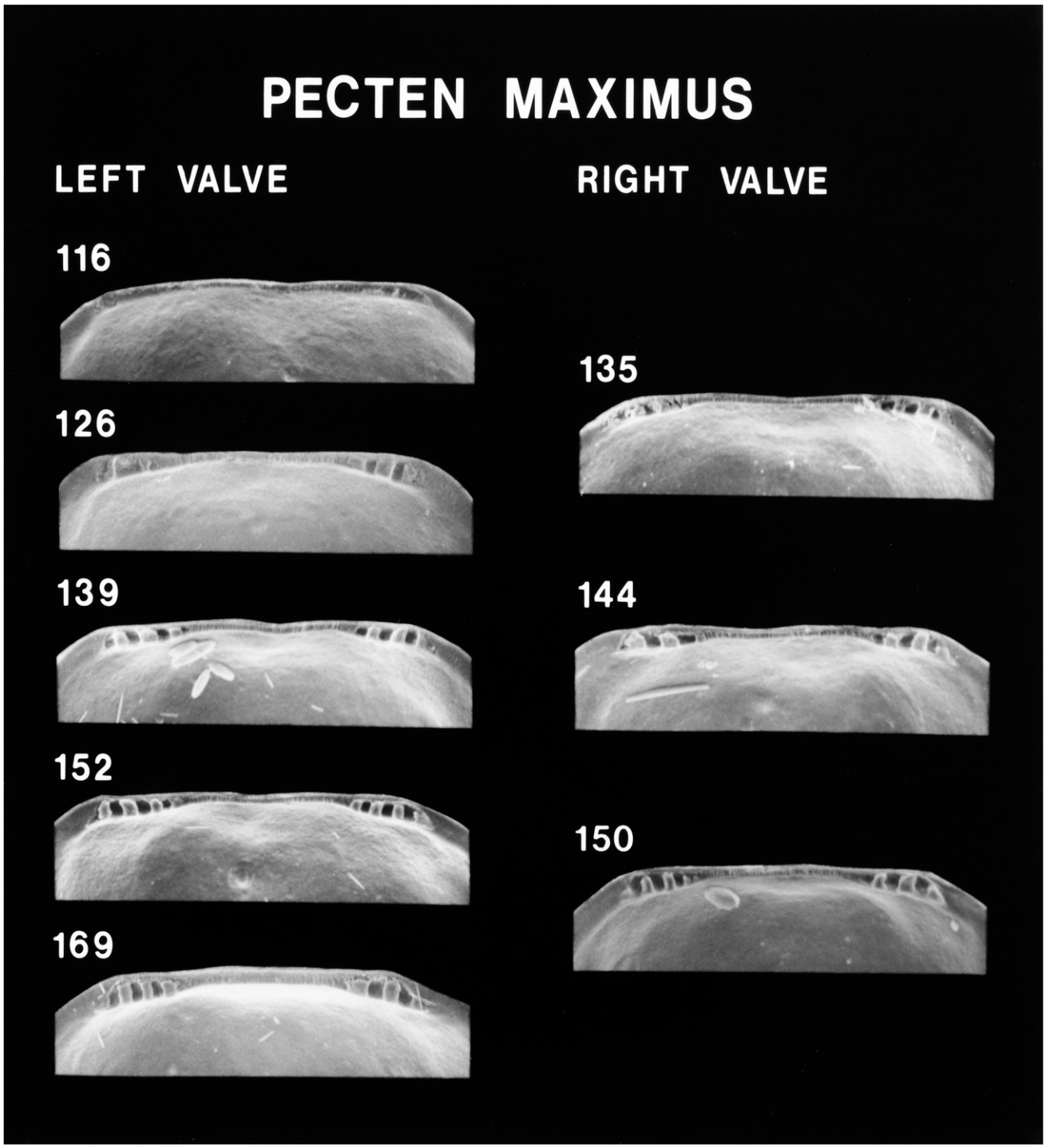

Figure 136. Scanning electron micrographs of the hinge of disarticulated shell valves of *Pecten maximus* larvae seen in Figure 135. Numbers indicate the maximum linear shell dimension in micrometers.

Downloaded From: https://bioone.org/journals/Journal-of-Shellfish-Research on 25 Feb 2020
Terms of Use: https://bioone.org/terms-of-use Access provided by IFREMER

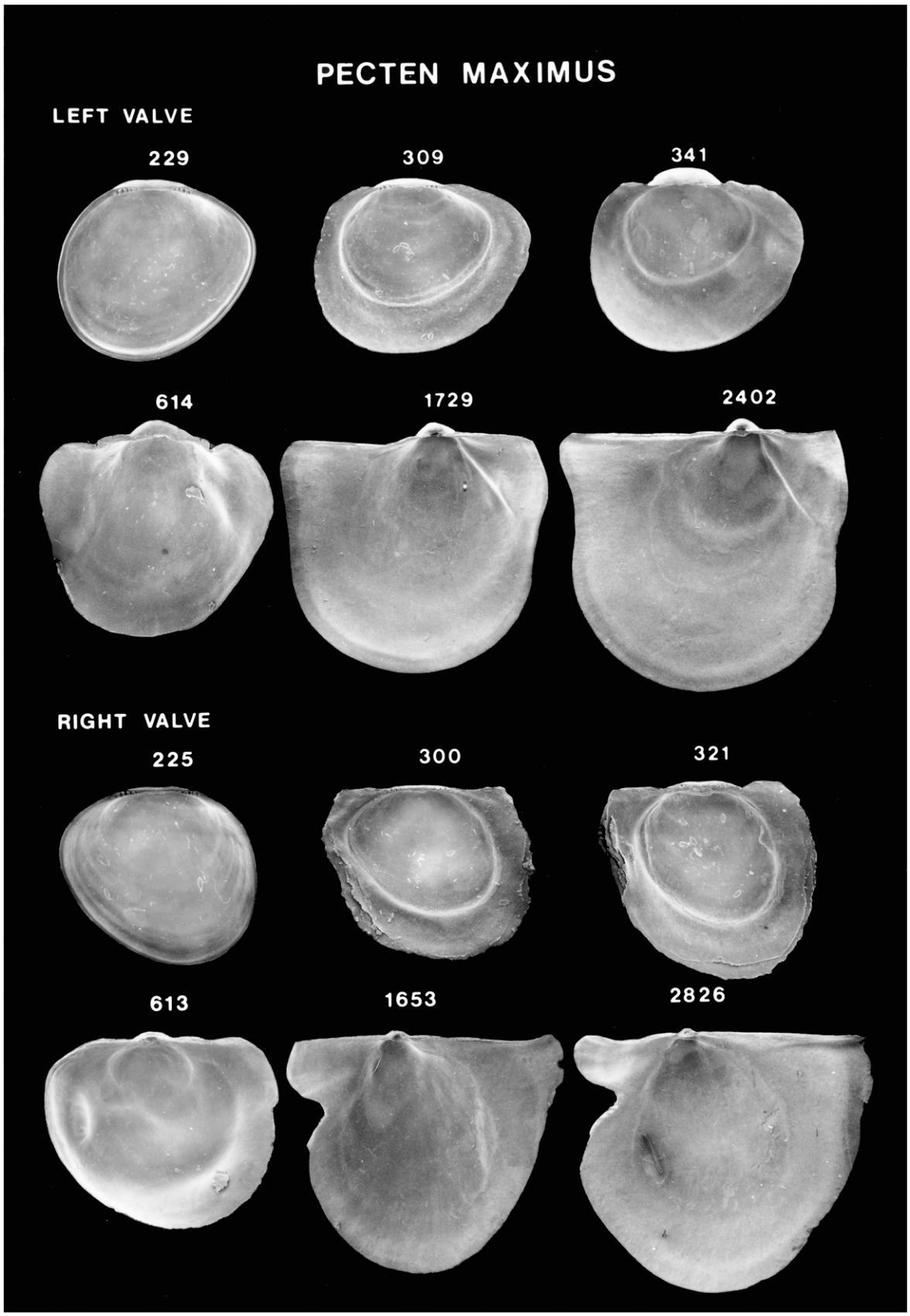

Figure 137. Scanning electron micrographs of disarticulated shell valves of *Pecten maximus* postlarvae. Numbers indicate the maximum linear shell dimension in micrometers.

Downloaded From: https://bioone.org/journals/Journal-of-Shellfish-Research on 25 Feb 2020
Terms of Use: https://bioone.org/terms-of-use Access provided by IFREMER

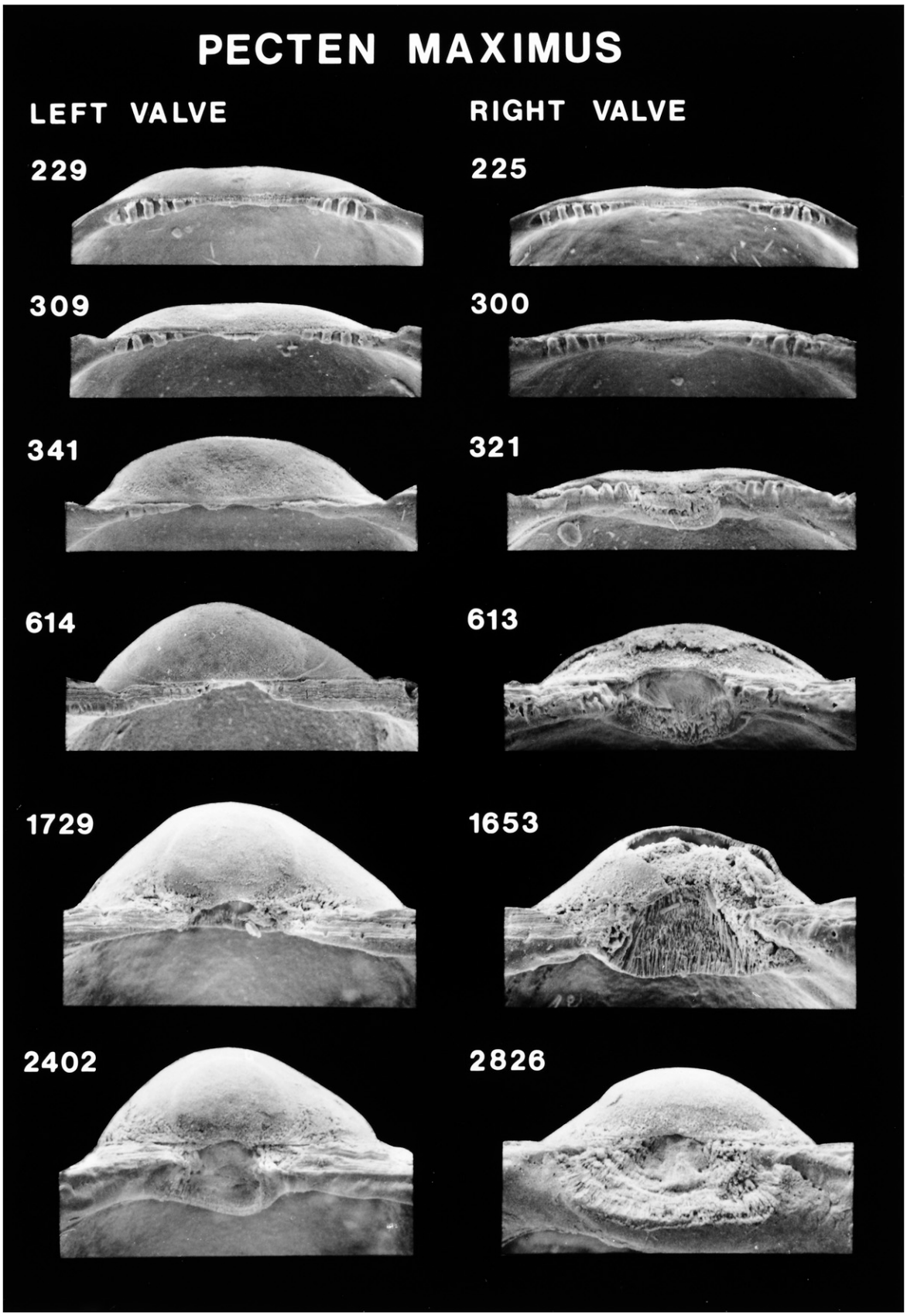

Figure 138. Scanning electron micrographs of the hinge of disarticulated shell valves of *Pecten maximus* postlarvae seen in Figure 137. Numbers indicate the maximum linear shell dimension in micrometers.

Downloaded From: https://bioone.org/journals/Journal-of-Shellfish-Research on 25 Feb 2020
Terms of Use: https://bioone.org/terms-of-use Access provided by IFREMER

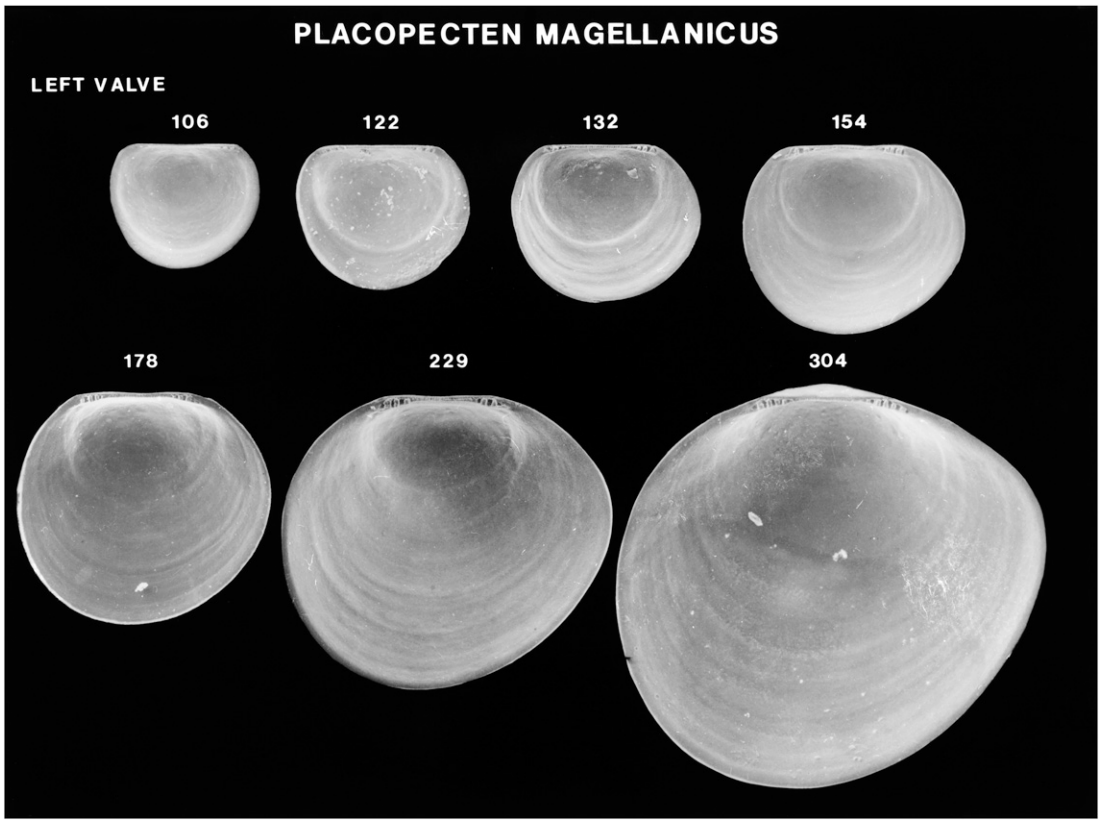

Figure 139. Scanning electron micrographs of disarticulated left shell valves of *Placopecten magellanicus* larvae. Numbers indicate the maximum linear shell dimension in micrometers.

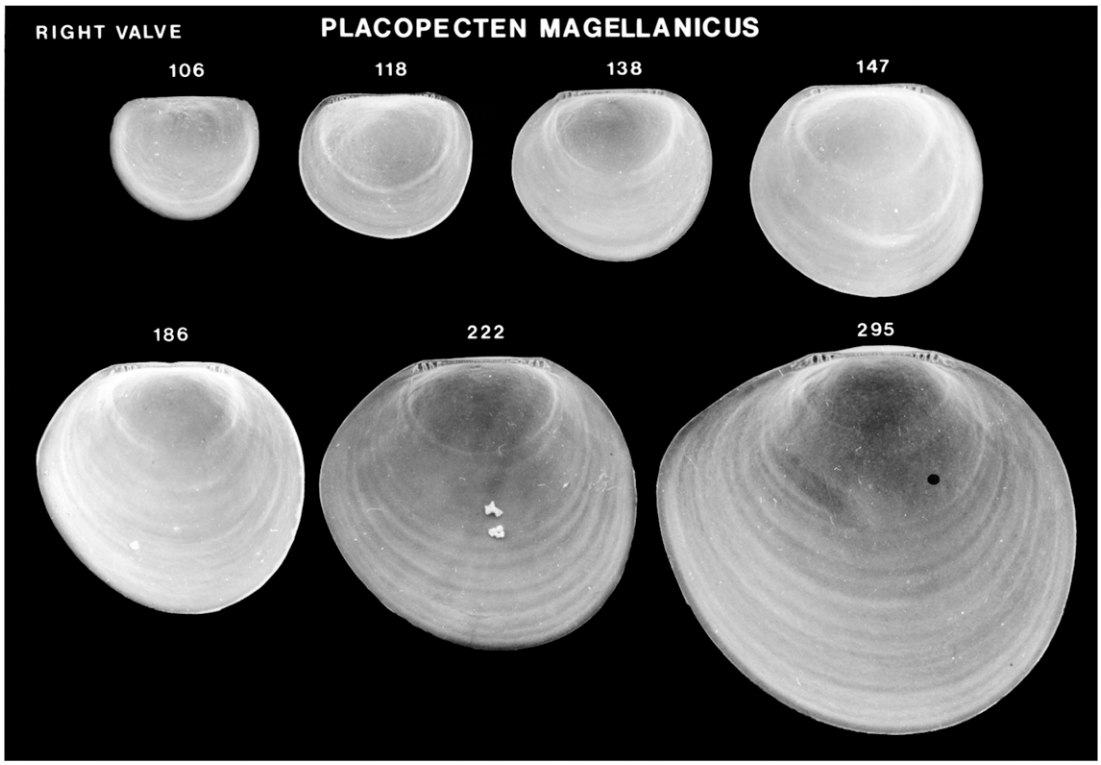

Figure 140. Scanning electron micrographs of disarticulated right shell valves of *Placopecten magellanicus* larvae. Numbers indicate the maximum linear shell dimension in micrometers.

Downloaded From: https://bioone.org/journals/Journal-of-Shellfish-Research on 25 Feb 2020
Terms of Use: https://bioone.org/terms-of-use Access provided by IFREMER

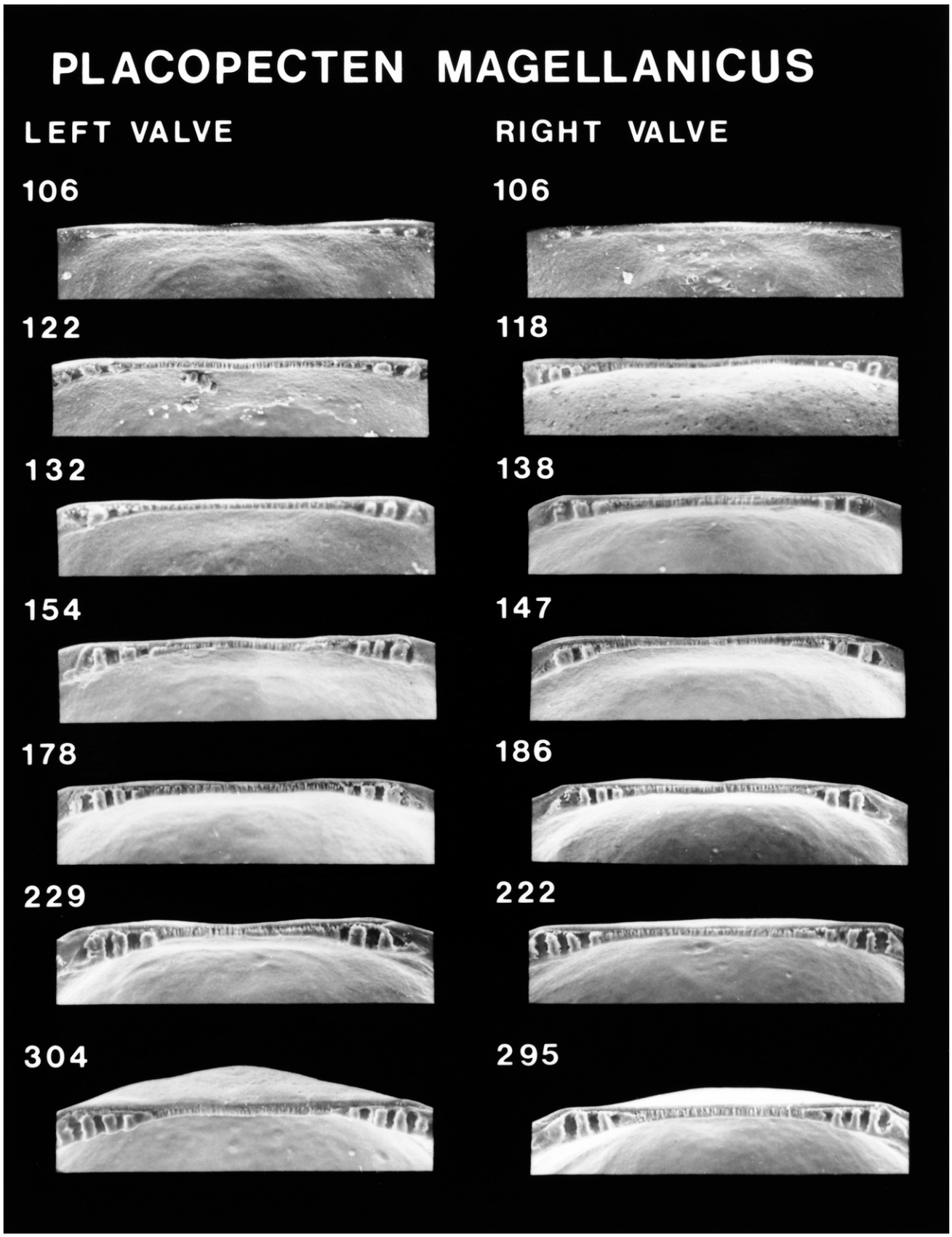

Figure 141. Scanning electron micrographs of the hinge of disarticulated shell valves of *Placopecten magellanicus* larvae seen in Figures 139 and 140. Numbers indicate the maximum linear shell dimension in micrometers.

Downloaded From: https://bioone.org/journals/Journal-of-Shellfish-Research on 25 Feb 2020
Terms of Use: https://bioone.org/terms-of-use Access provided by IFREMER

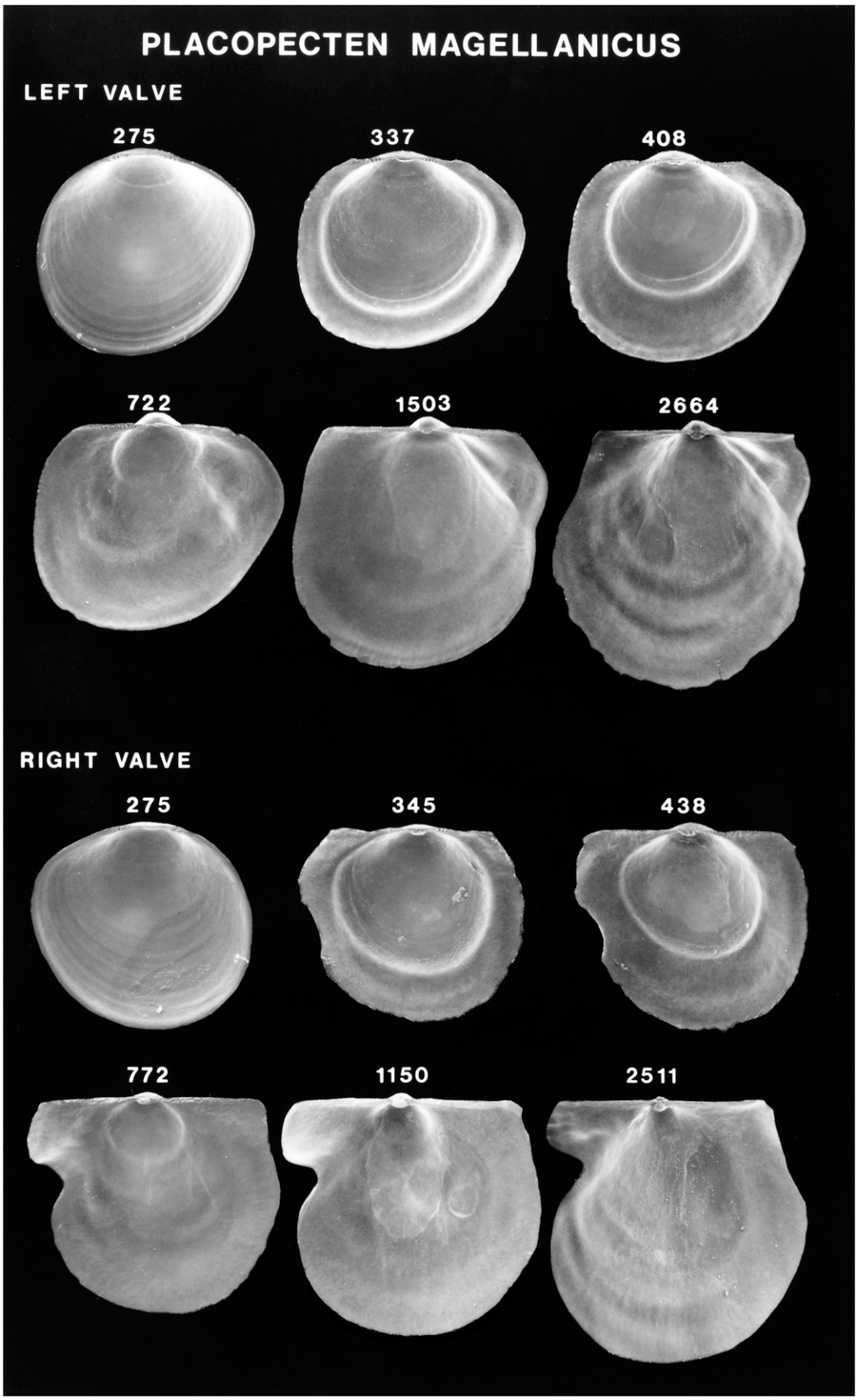

Figure 142. Scanning electron micrographs of disarticulated shell valves of *Placopecten magellanicus* postlarvae. Numbers indicate the maximum linear shell dimension in micrometers.

Downloaded From: https://bioone.org/journals/Journal-of-Shellfish-Research on 25 Feb 2020
Terms of Use: https://bioone.org/terms-of-use Access provided by IFREMER

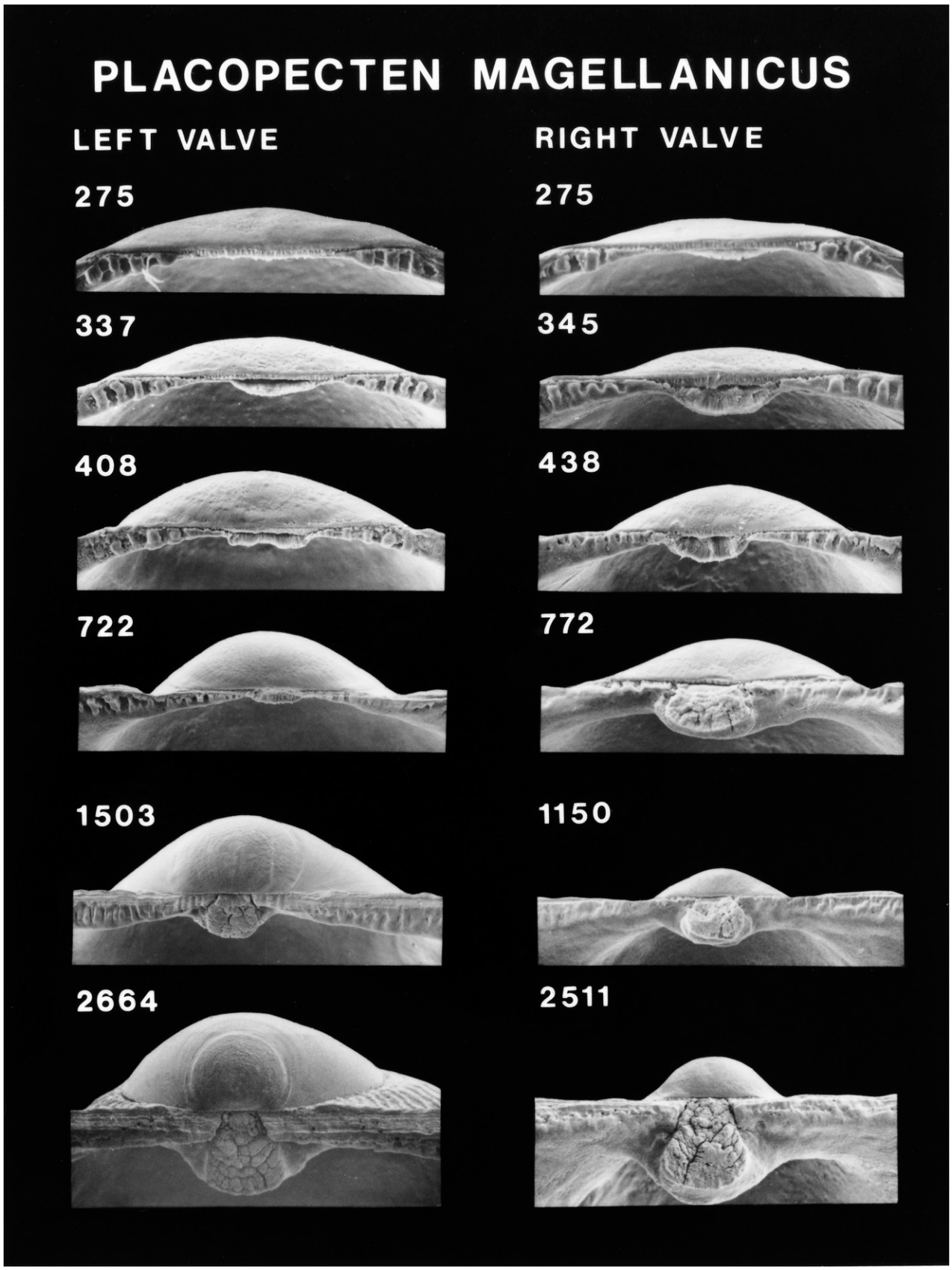

Figure 143. Scanning electron micrographs of the hinge of disarticulated shell valves of *Placopecten magellanicus* postlarvae seen in Figure 142. Numbers indicate the maximum linear shell dimension in micrometers.

Downloaded From: https://bioone.org/journals/Journal-of-Shellfish-Research on 25 Feb 2020
Terms of Use: https://bioone.org/terms-of-use Access provided by IFREMER

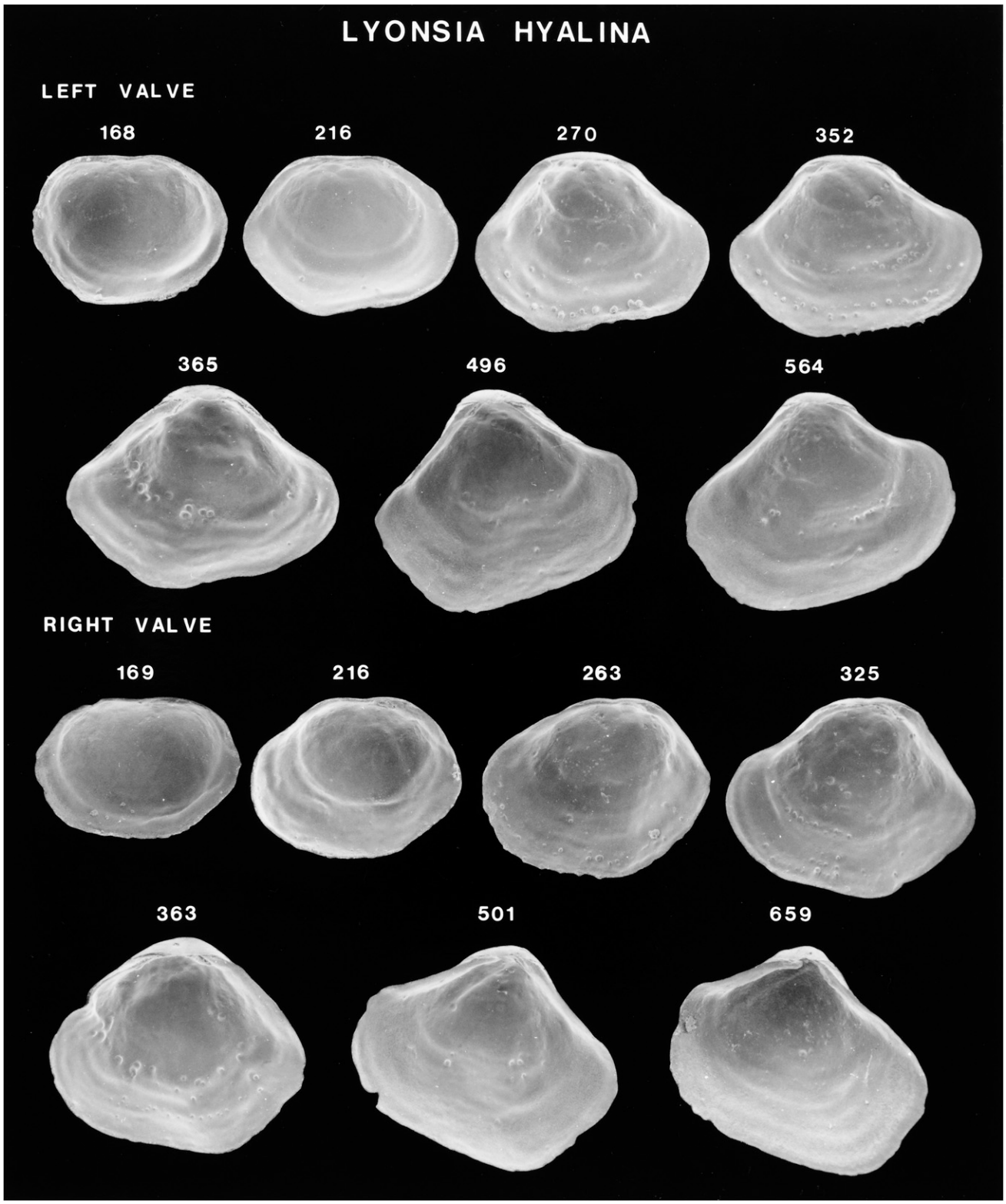

Figure 144. Scanning electron micrographs of disarticulated shell valves of *Lyonsia hyalina* postlarvae. Numbers indicate the maximum linear shell dimension in micrometers.

Downloaded From: https://bioone.org/journals/Journal-of-Shellfish-Research on 25 Feb 2020
Terms of Use: https://bioone.org/terms-of-use Access provided by IFREMER

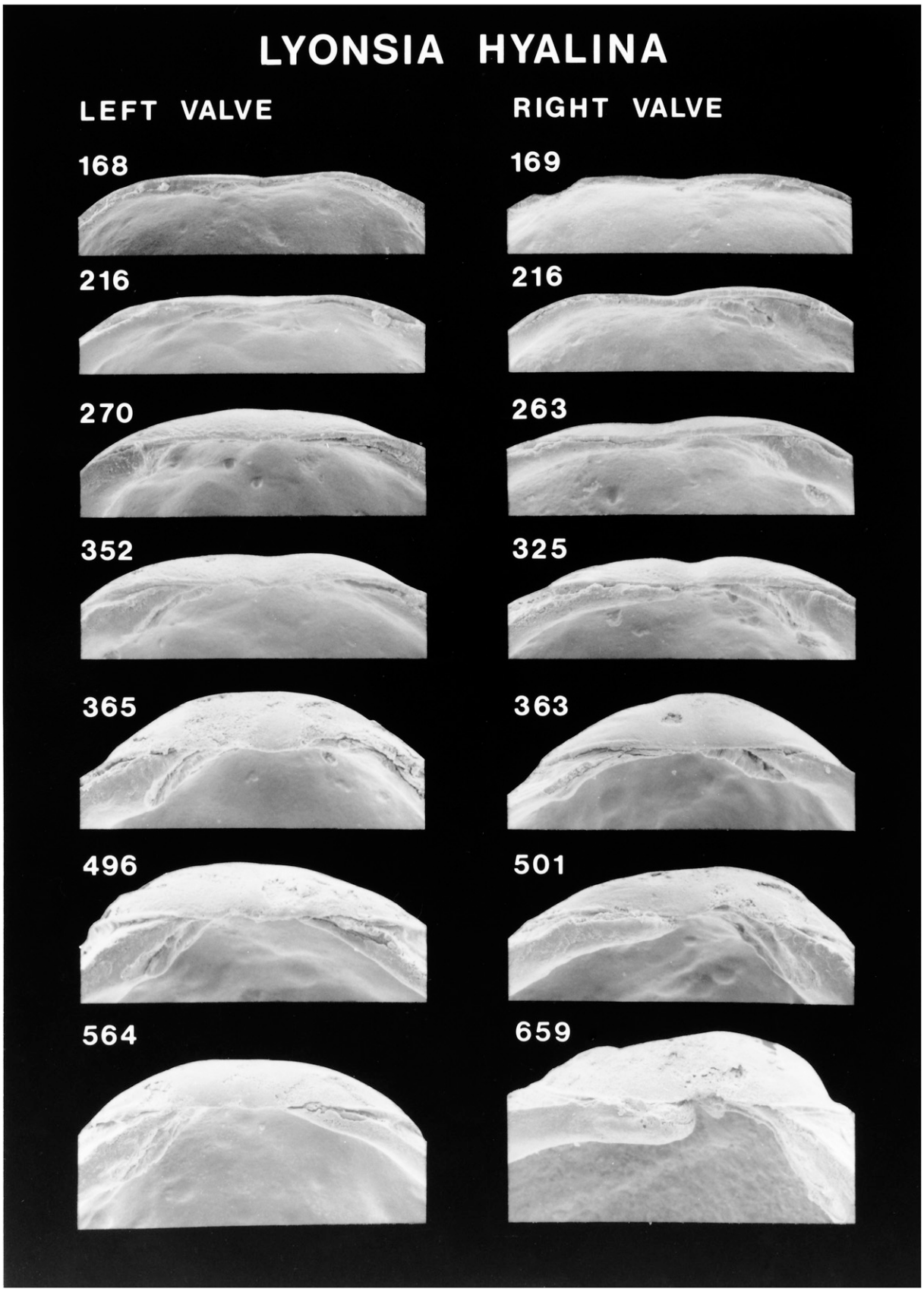

Figure 145. Scanning electron micrographs of the hinge of disarticulated shell valves of *Lyonsia hyalina* postlarvae seen in Figure 144. Numbers indicate the maximum linear shell dimension in micrometers.

Downloaded From: https://bioone.org/journals/Journal-of-Shellfish-Research on 25 Feb 2020
Terms of Use: https://bioone.org/terms-of-use Access provided by IFREMER

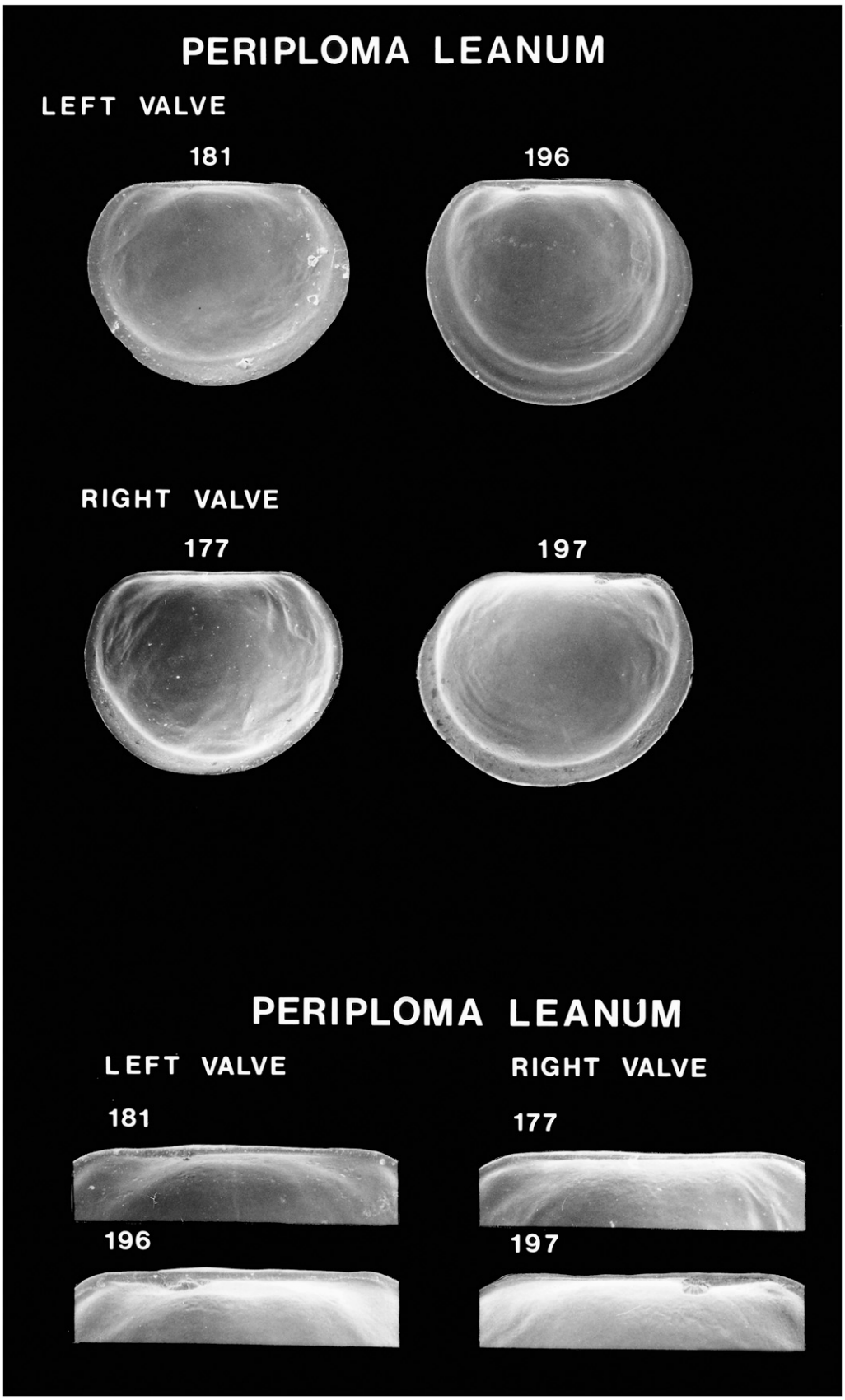

Figure 146. Scanning electron micrographs of disarticulated shell valves of *Periploma leanum* postlarvae (top) and higher magnification scanning electron micrographs of the hinge of these shell valves (bottom). Numbers indicate the maximum linear shell dimension in micrometers.

Downloaded From: https://bioone.org/journals/Journal-of-Shellfish-Research on 25 Feb 2020
Terms of Use: https://bioone.org/terms-of-use Access provided by IFREMER

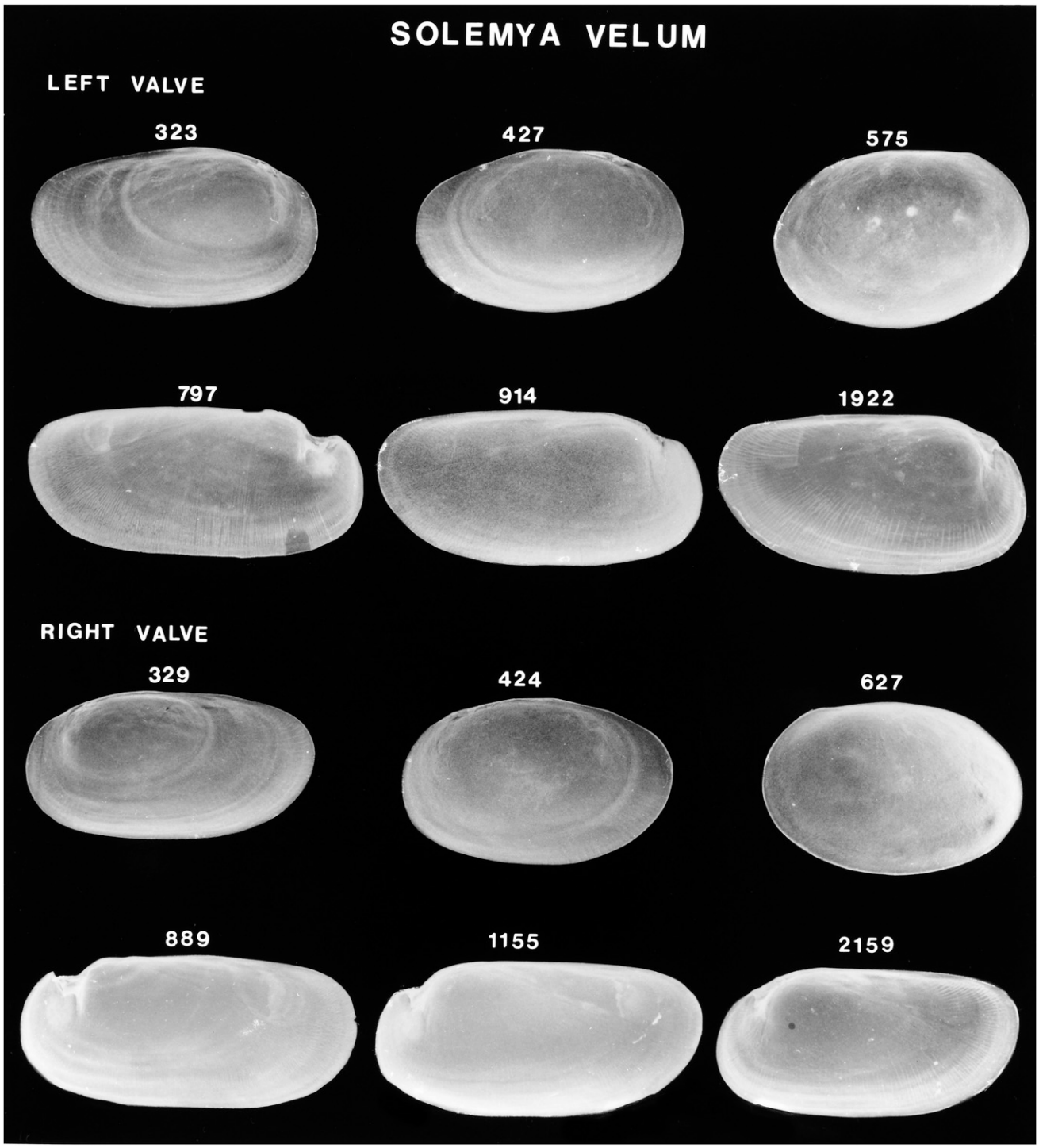

Figure 147. Scanning electron micrographs of disarticulated shell valves of *Solemya velum* postlarvae. Numbers indicate the maximum linear shell dimension in micrometers. Modified from Gustafson and Lutz (1992).

Downloaded From: https://bioone.org/journals/Journal-of-Shellfish-Research on 25 Feb 2020
Terms of Use: https://bioone.org/terms-of-use Access provided by IFREMER

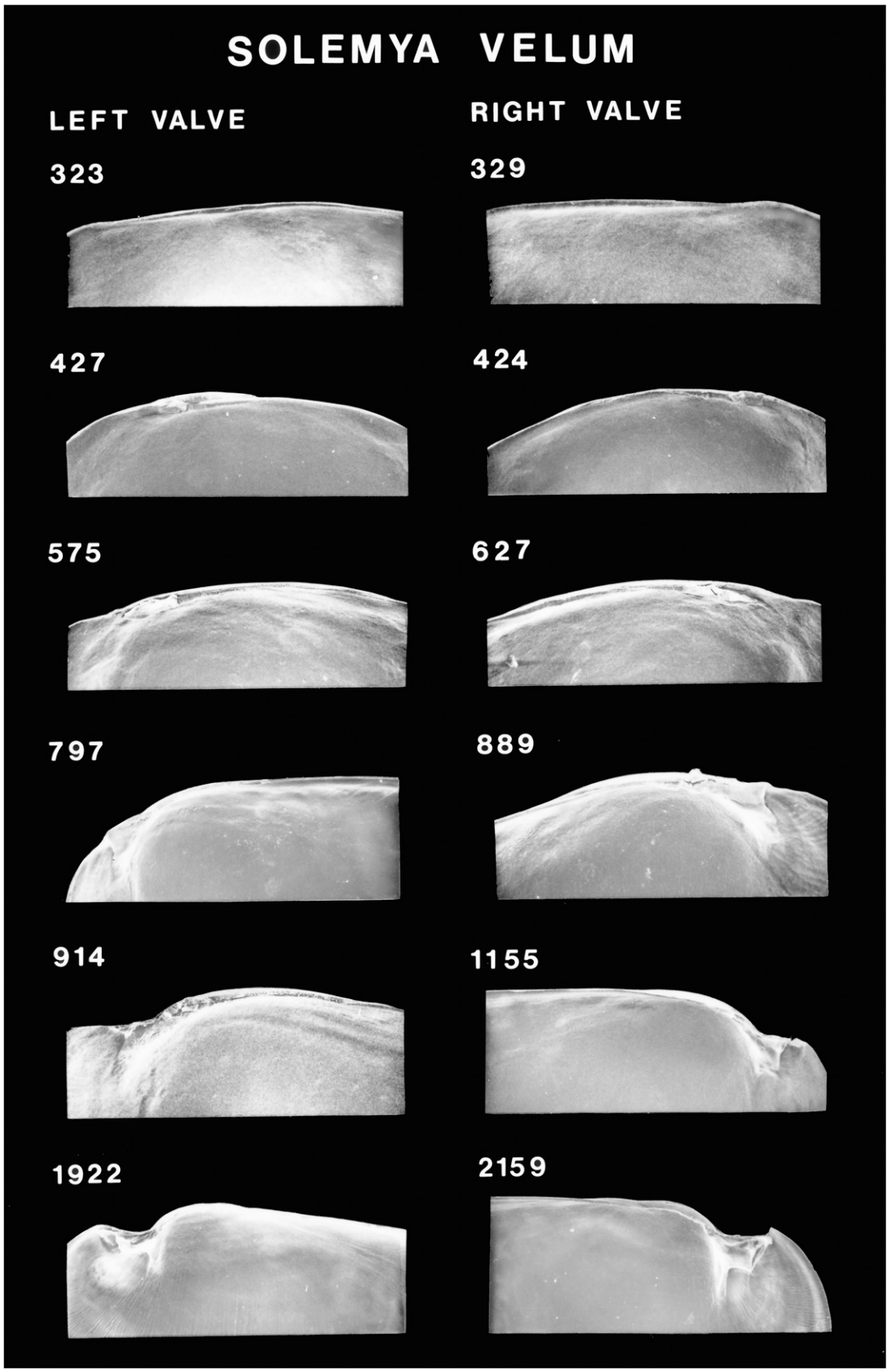

Figure 148. Scanning electron micrographs of the hinge of disarticulated shell valves of *Solemya velum* postlarvae seen in Figure 147. Numbers indicate the maximum linear shell dimension in micrometers. Modified from Gustafson and Lutz (1992).

Downloaded From: https://bioone.org/journals/Journal-of-Shellfish-Research on 25 Feb 2020
Terms of Use: https://bioone.org/terms-of-use Access provided by IFREMER

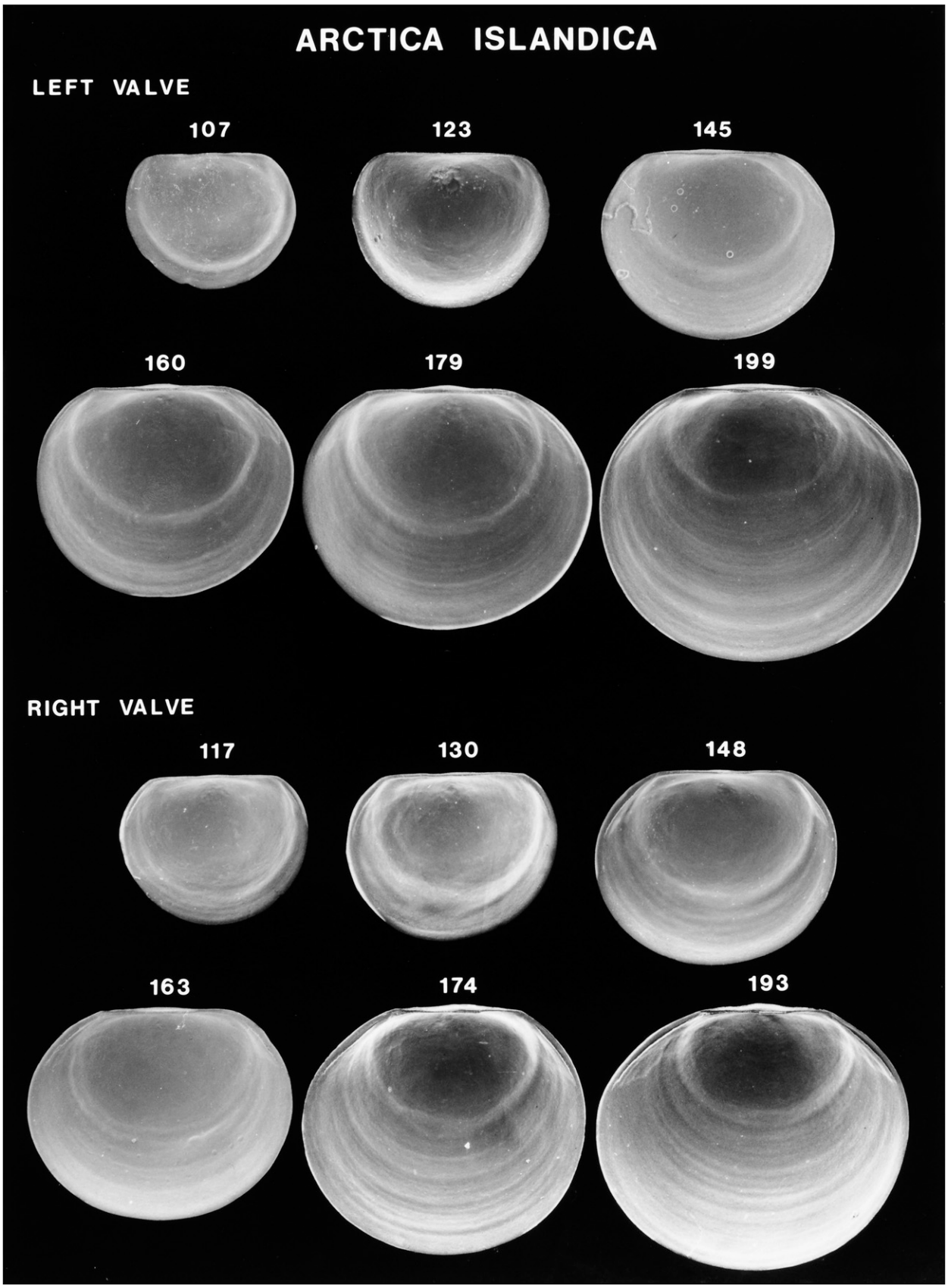

Figure 149. Scanning electron micrographs of disarticulated shell valves of *Arctica islandica* larvae. Numbers indicate the maximum linear shell dimension in micrometers. Modified from Lutz et al. (1982).

Downloaded From: https://bioone.org/journals/Journal-of-Shellfish-Research on 25 Feb 2020
Terms of Use: https://bioone.org/terms-of-use Access provided by IFREMER

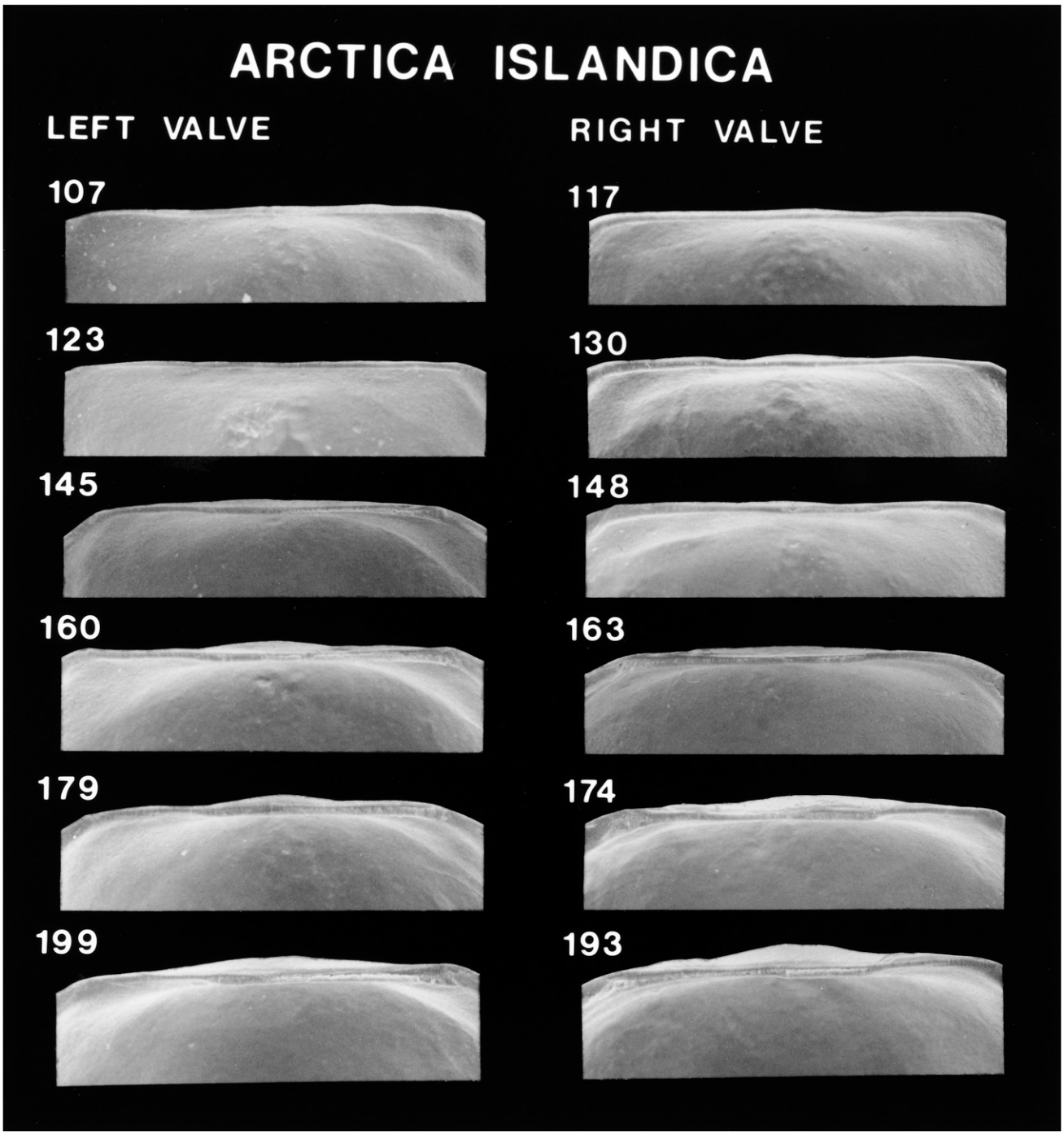

Figure 150. Scanning electron micrographs of the hinge of disarticulated shell valves of *Arctica islandica* larvae seen in Figure 149. Numbers indicate the maximum linear shell dimension in micrometers. Modified from Lutz et al. (1982).

Downloaded From: https://bioone.org/journals/Journal-of-Shellfish-Research on 25 Feb 2020
Terms of Use: https://bioone.org/terms-of-use Access provided by IFREMER

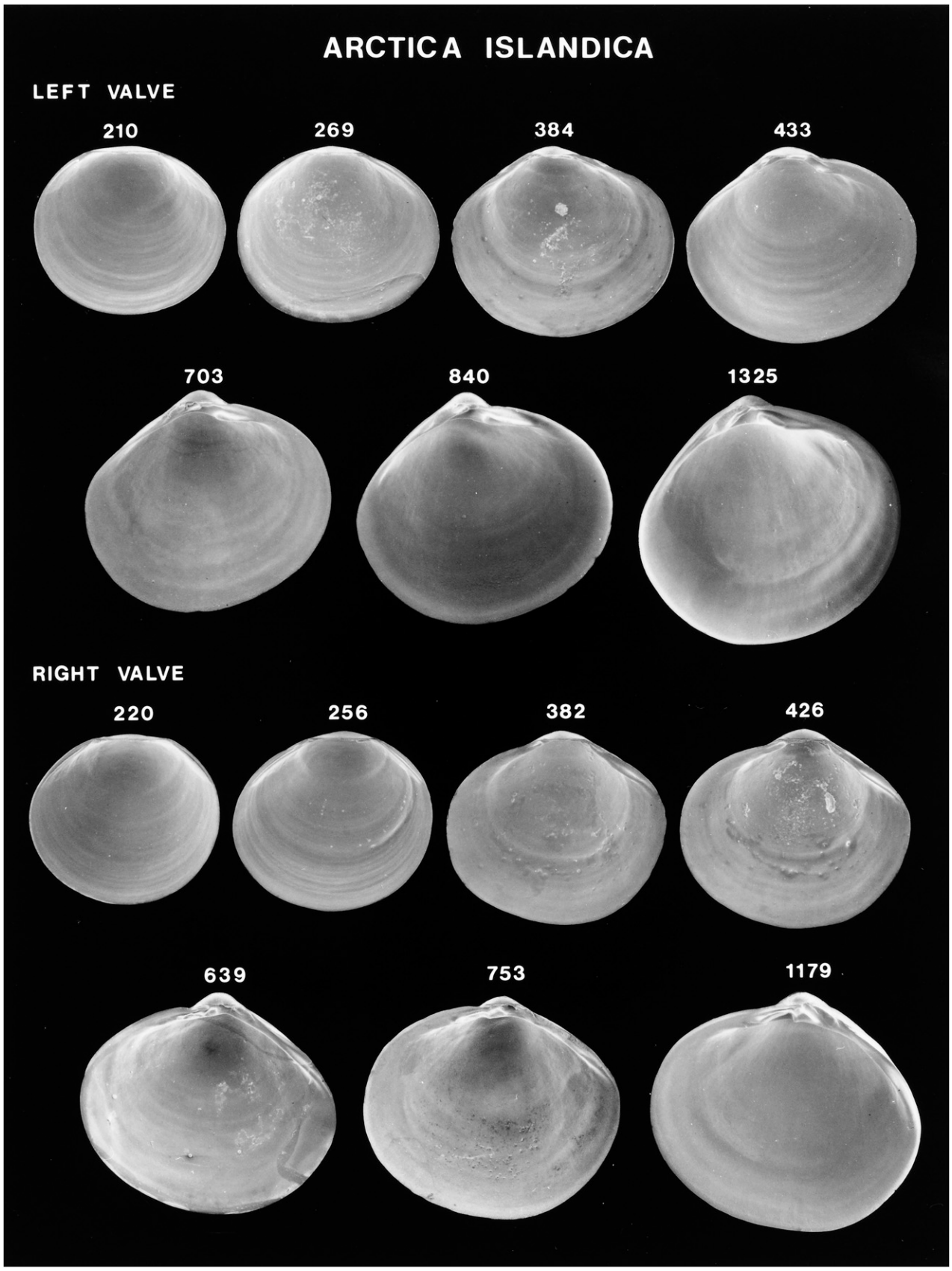

Figure 151. Scanning electron micrographs of disarticulated shell valves of *Arctica islandica* postlarvae. Numbers indicate the maximum linear shell dimension in micrometers. Modified from Lutz et al. (1982).

Downloaded From: https://bioone.org/journals/Journal-of-Shellfish-Research on 25 Feb 2020
Terms of Use: https://bioone.org/terms-of-use Access provided by IFREMER

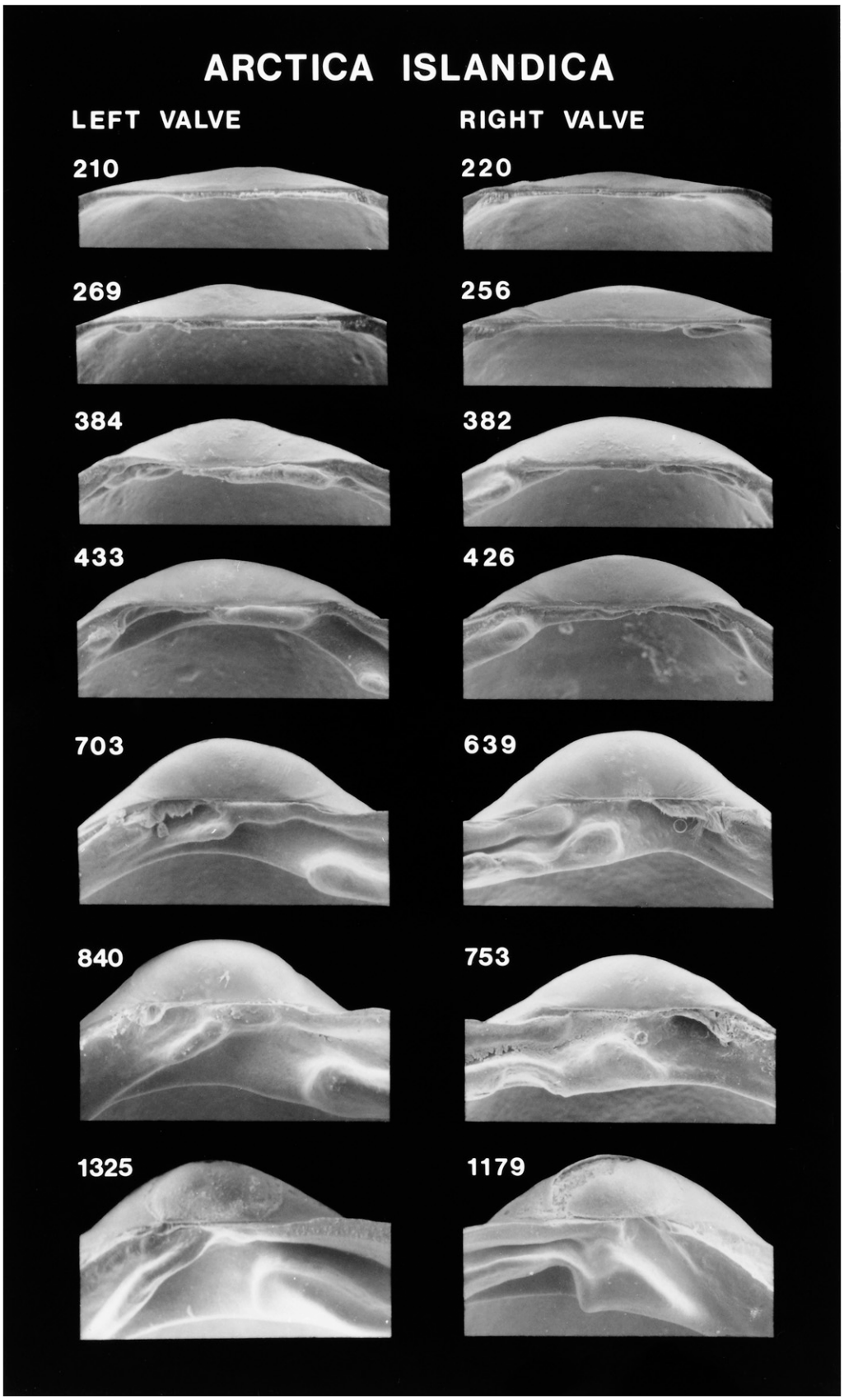

Figure 152. Scanning electron micrographs of the hinge of disarticulated shell valves of *Arctica islandica* postlarvae seen in Figure 151. Numbers indicate the maximum linear shell dimension in micrometers. Modified from Lutz et al. (1982).

Downloaded From: https://bioone.org/journals/Journal-of-Shellfish-Research on 25 Feb 2020
Terms of Use: https://bioone.org/terms-of-use Access provided by IFREMER

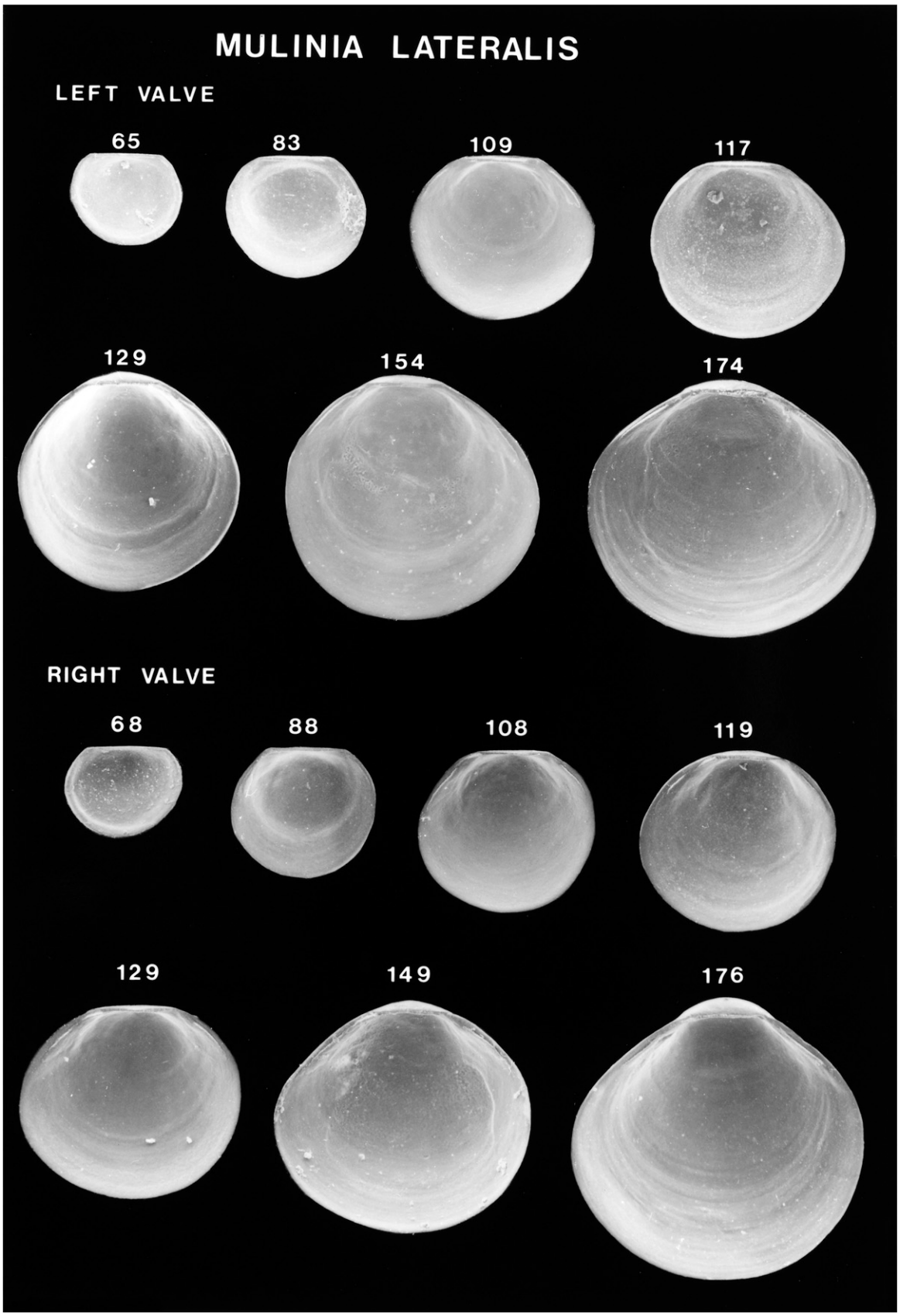

Figure 153. Scanning electron micrographs of disarticulated shell valves of *Mulinia lateralis* larvae. Numbers indicate the maximum linear shell dimension in micrometers.

Downloaded From: https://bioone.org/journals/Journal-of-Shellfish-Research on 25 Feb 2020
Terms of Use: https://bioone.org/terms-of-use Access provided by IFREMER

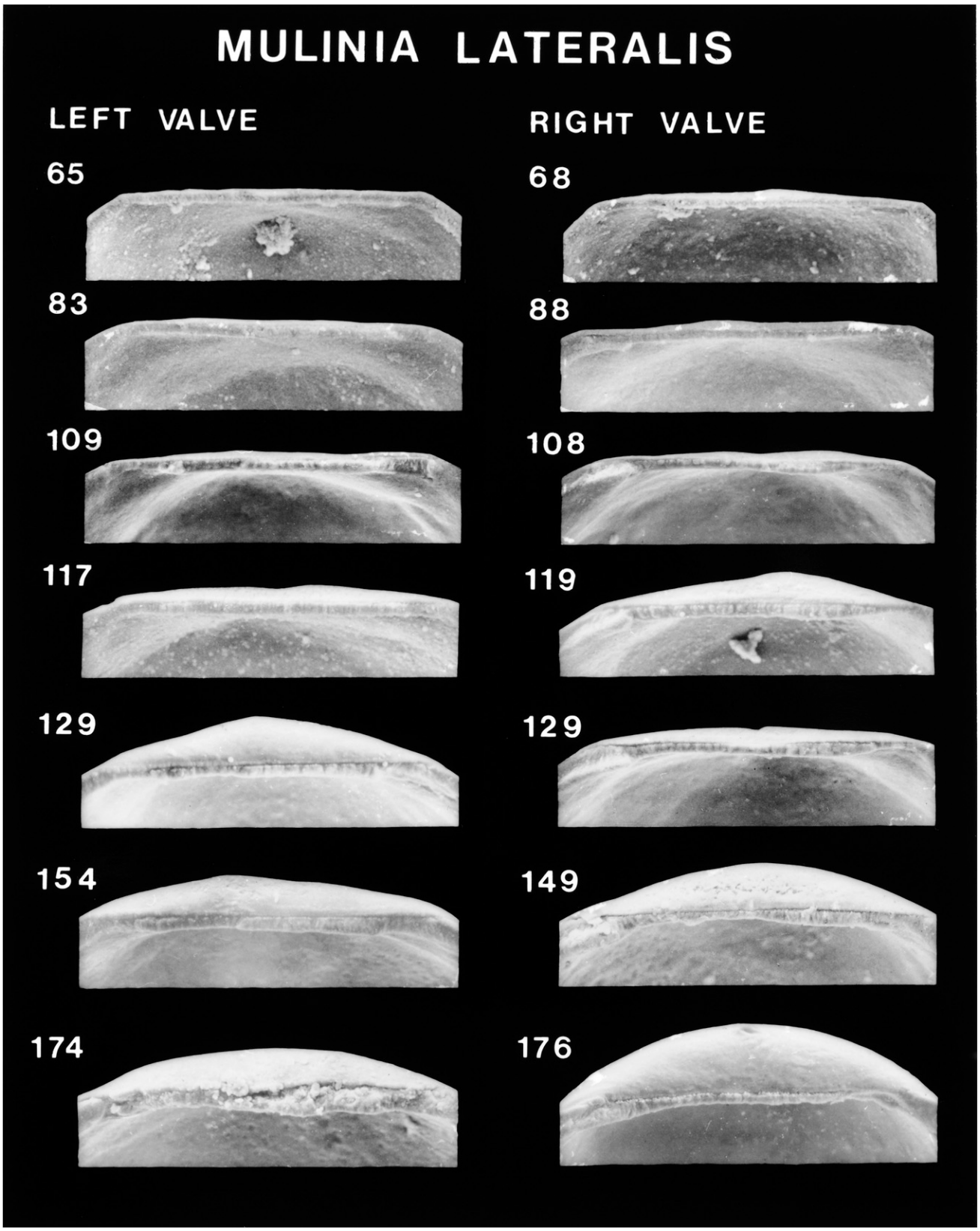

Figure 154. Scanning electron micrographs of the hinge of disarticulated shell valves of *Mulinia lateralis* larvae seen in Figure 153. Numbers indicate the maximum linear shell dimension in micrometers.

Downloaded From: https://bioone.org/journals/Journal-of-Shellfish-Research on 25 Feb 2020
Terms of Use: https://bioone.org/terms-of-use Access provided by IFREMER

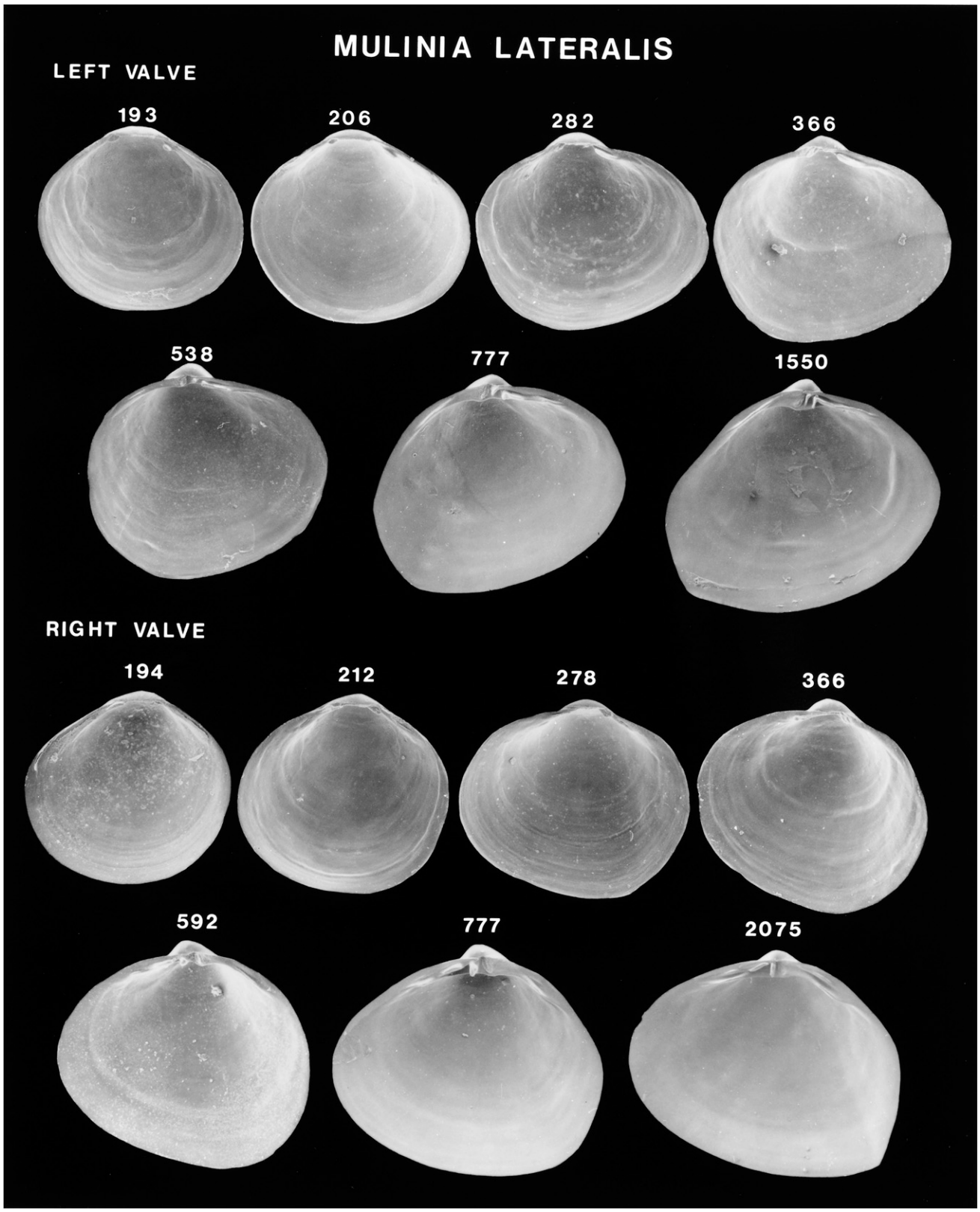

Figure 155. Scanning electron micrographs of disarticulated shell valves of *Mulinia lateralis* postlarvae. Numbers indicate the maximum linear shell dimension in micrometers.

Downloaded From: https://bioone.org/journals/Journal-of-Shellfish-Research on 25 Feb 2020
Terms of Use: https://bioone.org/terms-of-use Access provided by IFREMER

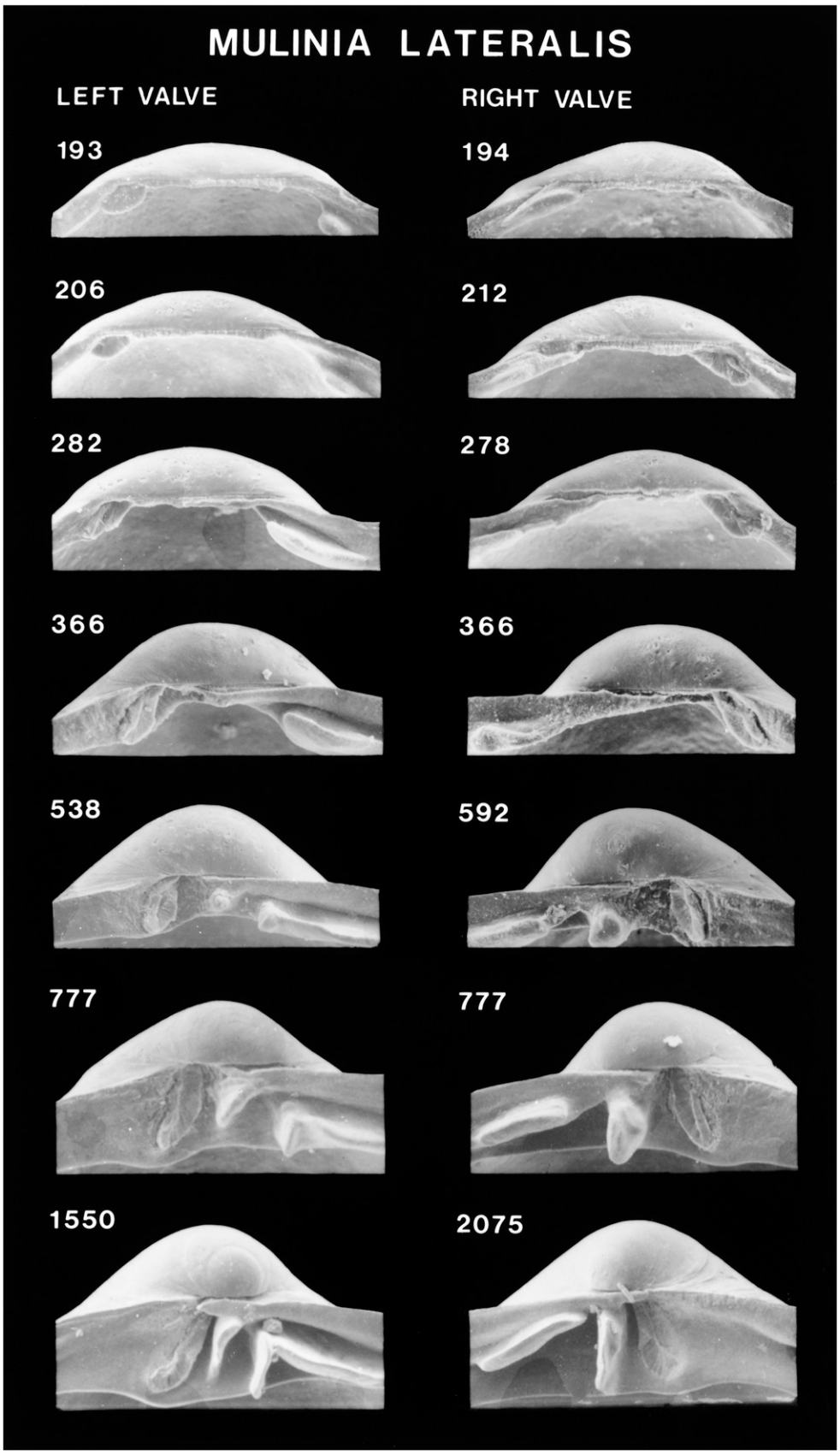

Figure 156. Scanning electron micrographs of the hinge of disarticulated shell valves of *Mulinia lateralis* postlarvae seen in Figure 155. Numbers indicate the maximum linear shell dimension in micrometers.

Downloaded From: https://bioone.org/journals/Journal-of-Shellfish-Research on 25 Feb 2020
Terms of Use: https://bioone.org/terms-of-use Access provided by IFREMER

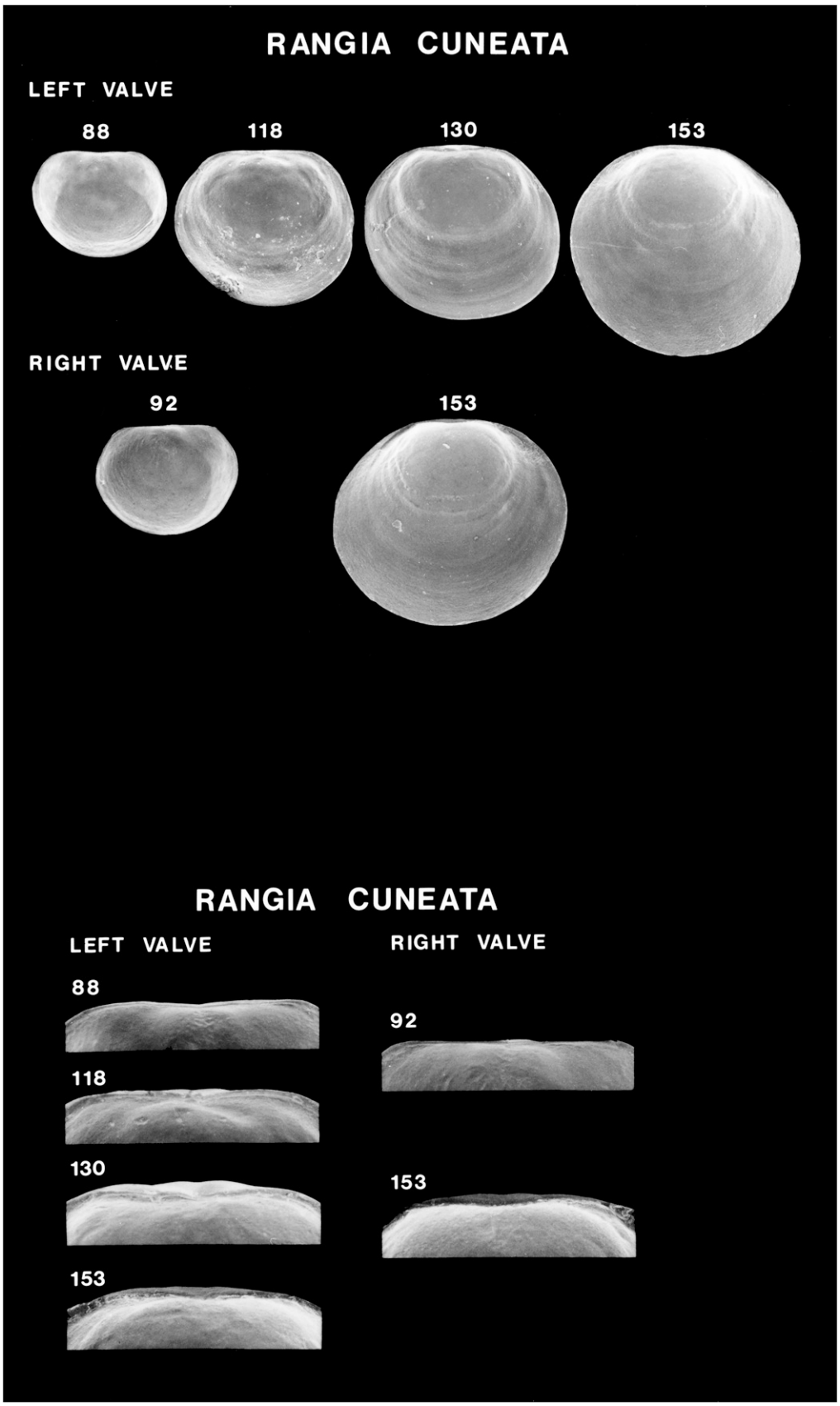

Figure 157. Scanning electron micrographs of disarticulated shell valves of *Rangia cuneata* larvae (top) and higher magnification scanning electron micrographs of the hinge of these shell valves (bottom). Numbers indicate the maximum linear shell dimension in micrometers.

Downloaded From: https://bioone.org/journals/Journal-of-Shellfish-Research on 25 Feb 2020
Terms of Use: https://bioone.org/terms-of-use Access provided by IFREMER

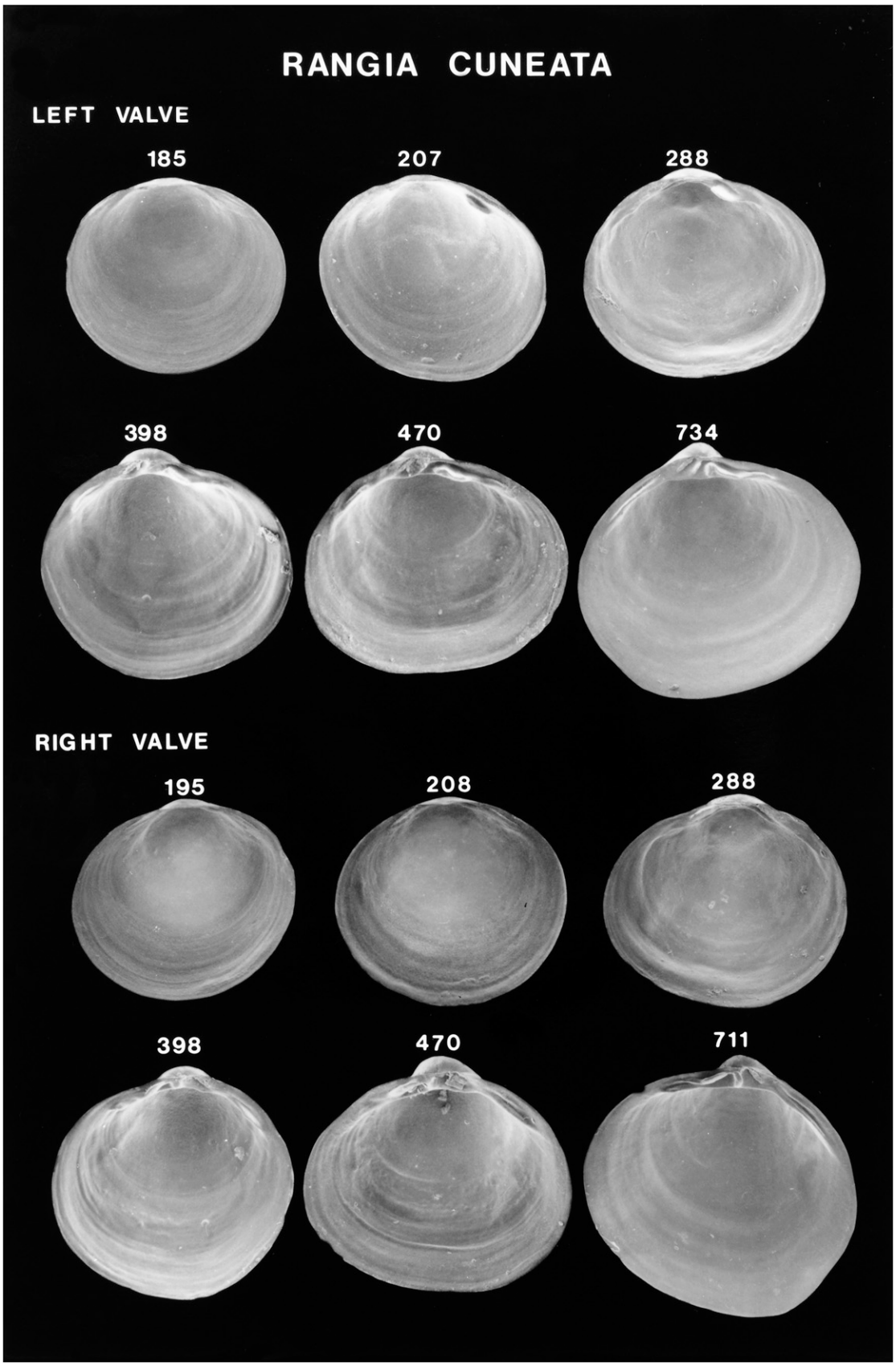

Figure 158. Scanning electron micrographs of disarticulated shell valves of *Rangia cuneata* postlarvae. Numbers indicate the maximum linear shell dimension in micrometers.

Downloaded From: https://bioone.org/journals/Journal-of-Shellfish-Research on 25 Feb 2020
Terms of Use: https://bioone.org/terms-of-use Access provided by IFREMER

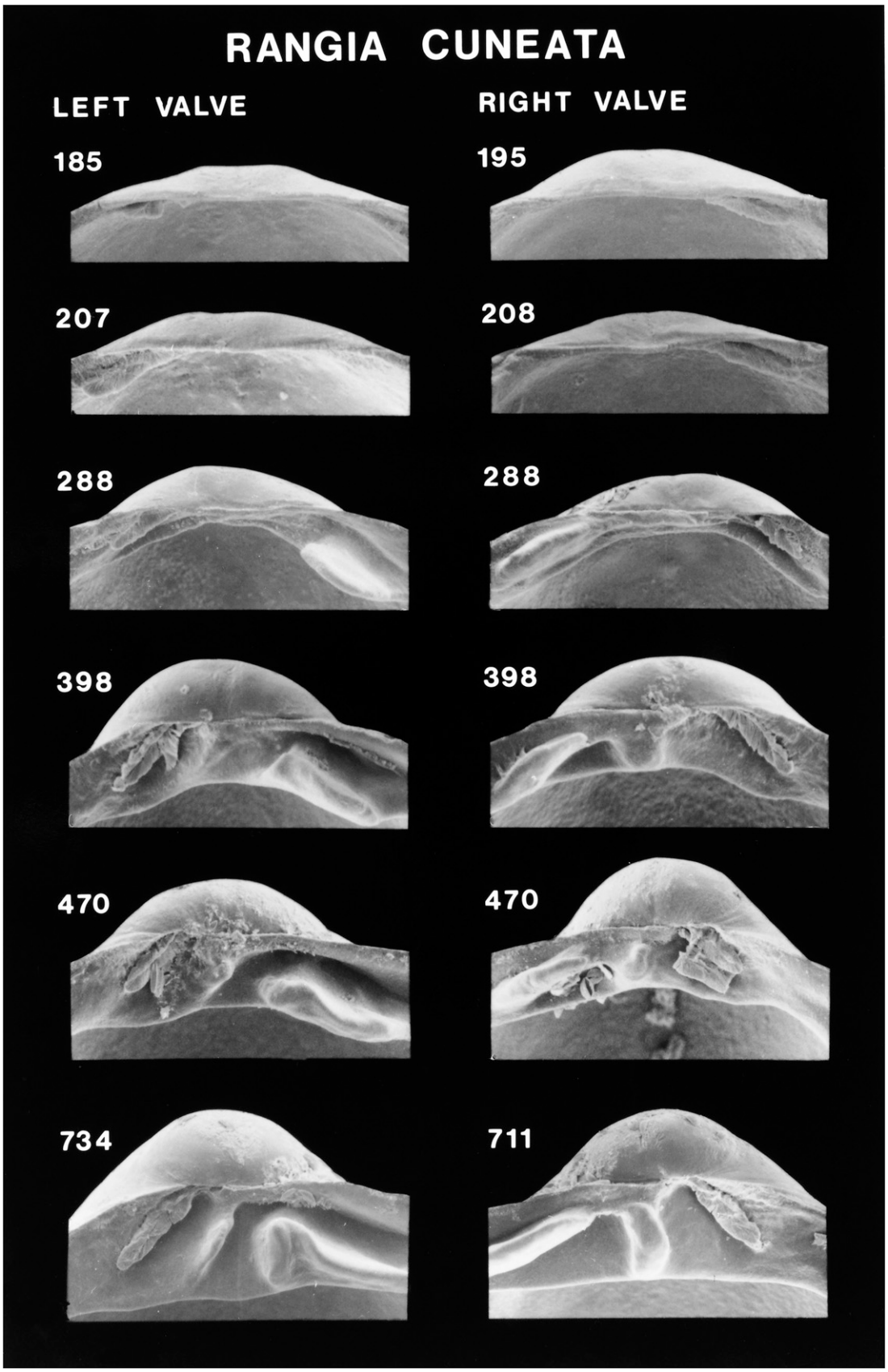

Figure 159. Scanning electron micrographs of the hinge of disarticulated shell valves of *Rangia cuneata* postlarvae seen in Figure 158. Numbers indicate the maximum linear shell dimension in micrometers.

Downloaded From: https://bioone.org/journals/Journal-of-Shellfish-Research on 25 Feb 2020
Terms of Use: https://bioone.org/terms-of-use Access provided by IFREMER

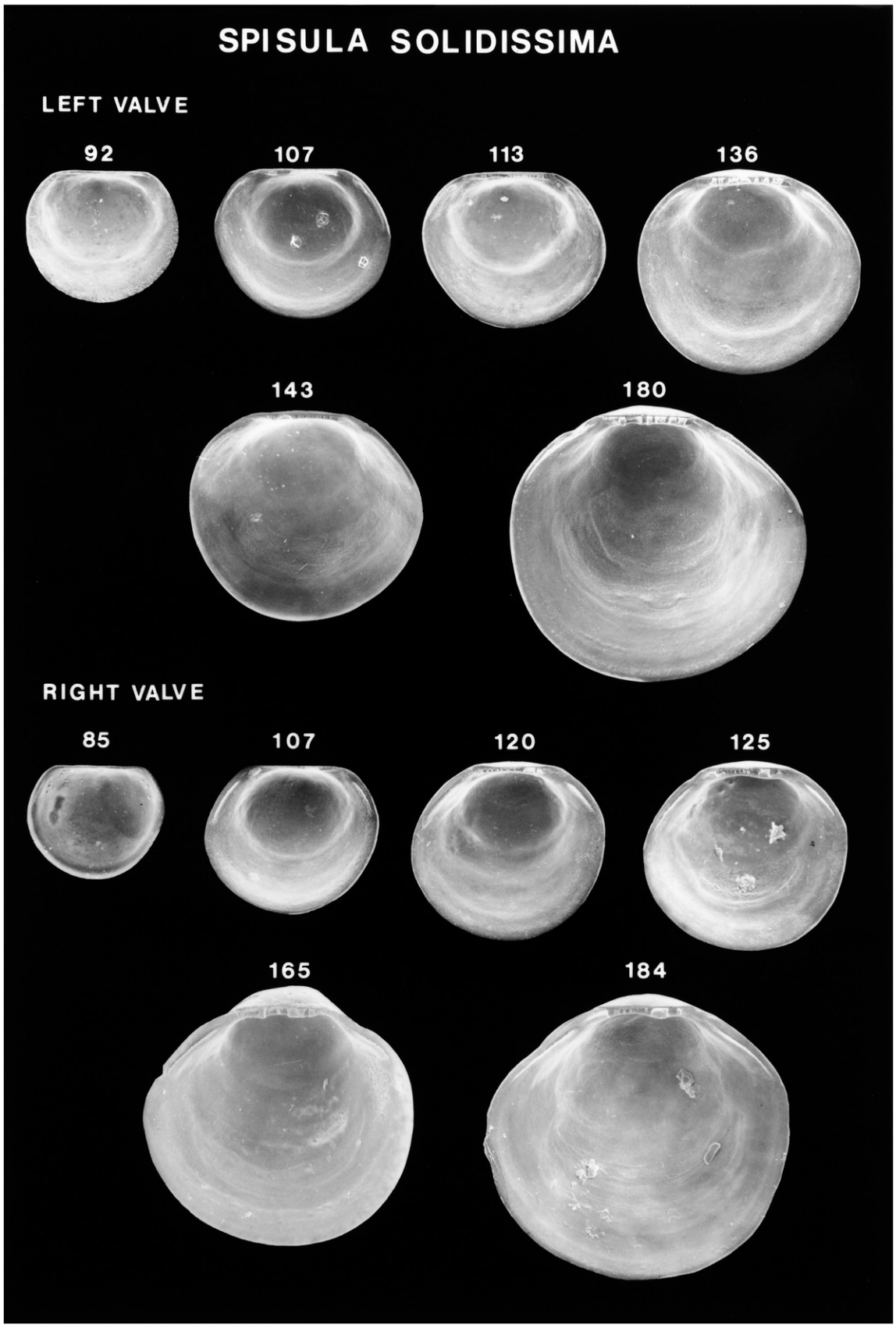

Figure 160. Scanning electron micrographs of disarticulated shell valves of *Spisula solidissima* larvae. Numbers indicate the maximum linear shell dimension in micrometers.

Downloaded From: https://bioone.org/journals/Journal-of-Shellfish-Research on 25 Feb 2020
Terms of Use: https://bioone.org/terms-of-use Access provided by IFREMER

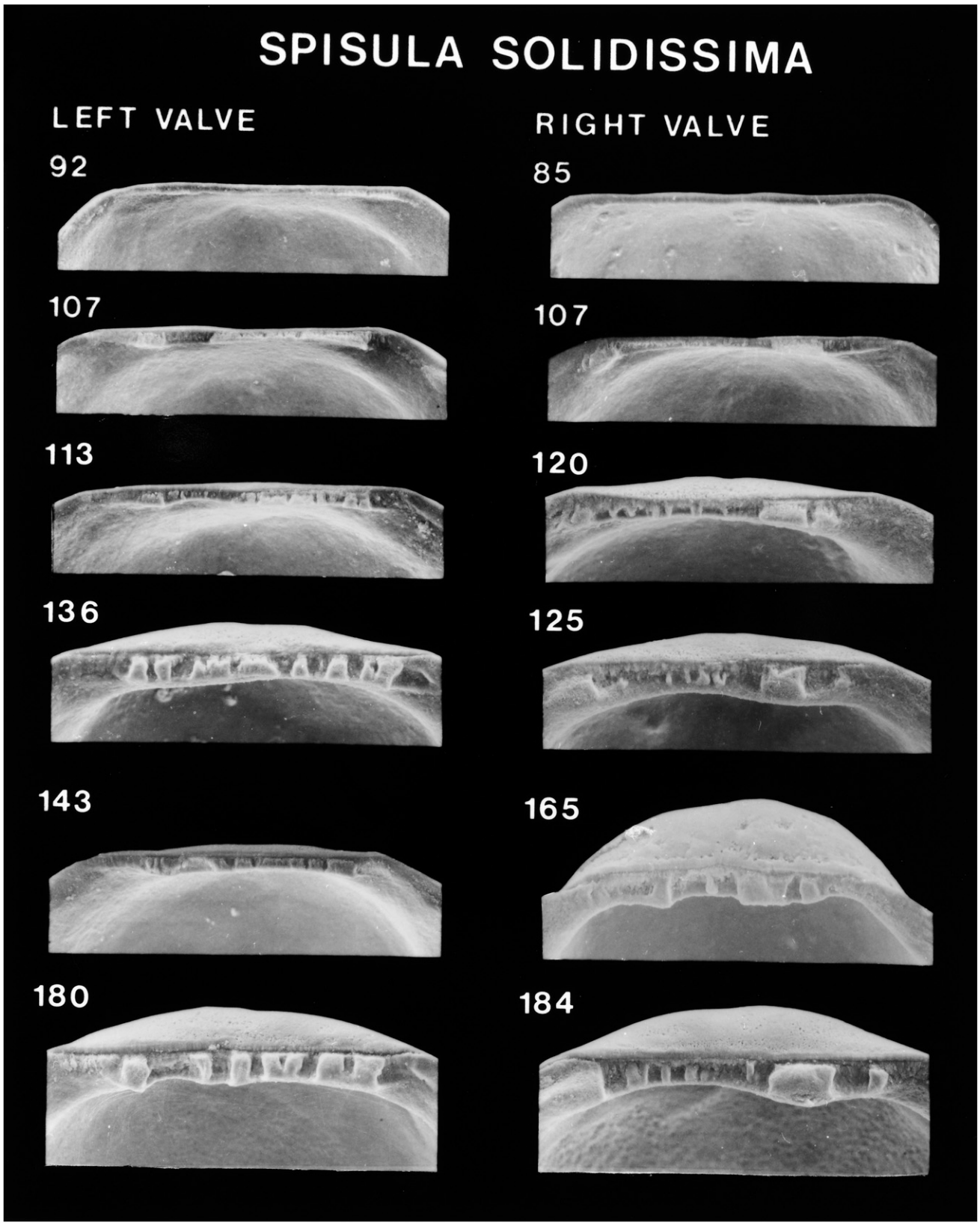

Figure 161. Scanning electron micrographs of the hinge of disarticulated shell valves of *Spisula solidissima* larvae seen in Figure 160. Numbers indicate the maximum linear shell dimension in micrometers.

Downloaded From: https://bioone.org/journals/Journal-of-Shellfish-Research on 25 Feb 2020
Terms of Use: https://bioone.org/terms-of-use Access provided by IFREMER

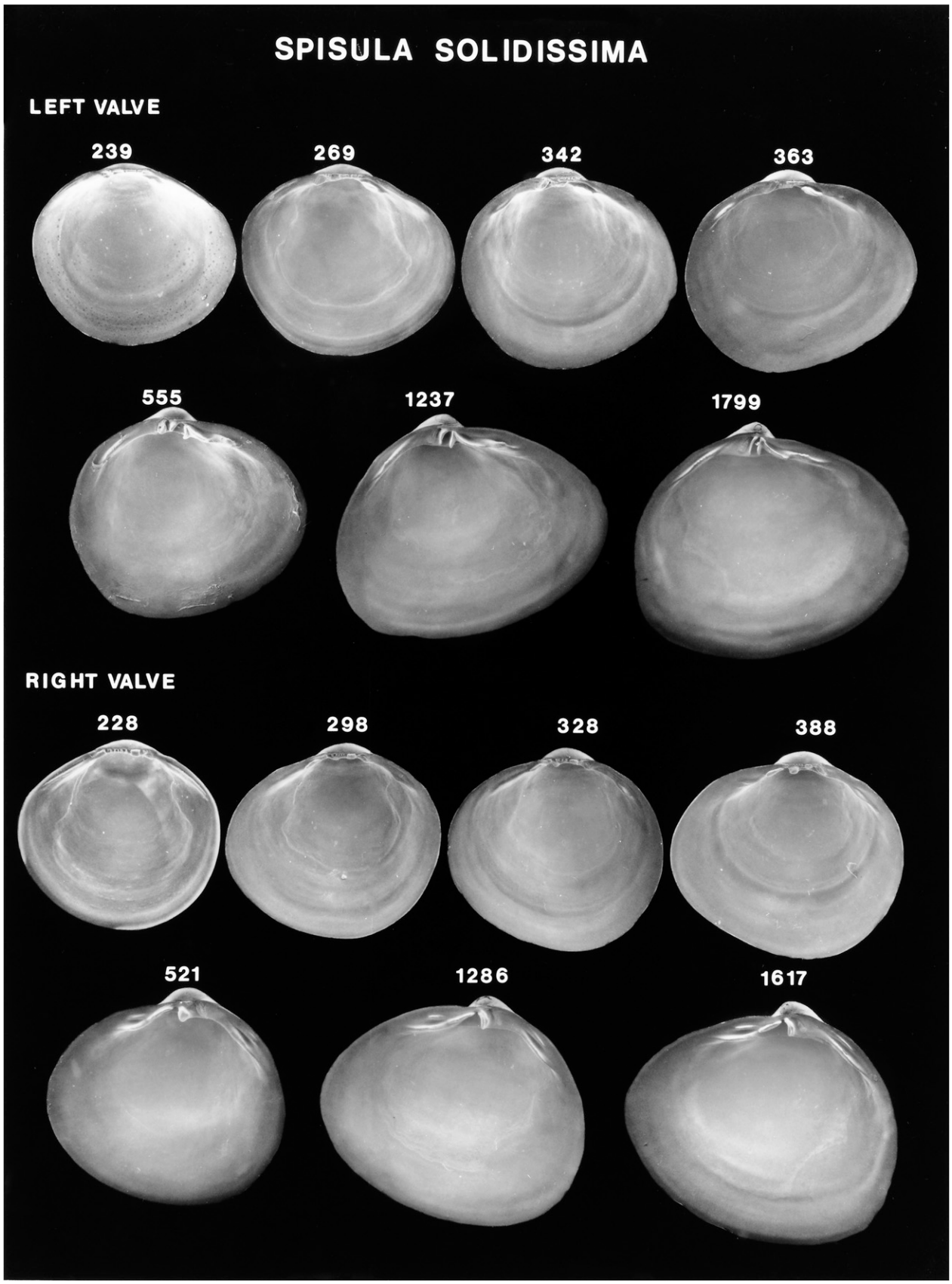

Figure 162. Scanning electron micrographs of disarticulated shell valves of *Spisula solidissima* postlarvae. Numbers indicate the maximum linear shell dimension in micrometers.

Downloaded From: https://bioone.org/journals/Journal-of-Shellfish-Research on 25 Feb 2020
Terms of Use: https://bioone.org/terms-of-use Access provided by IFREMER

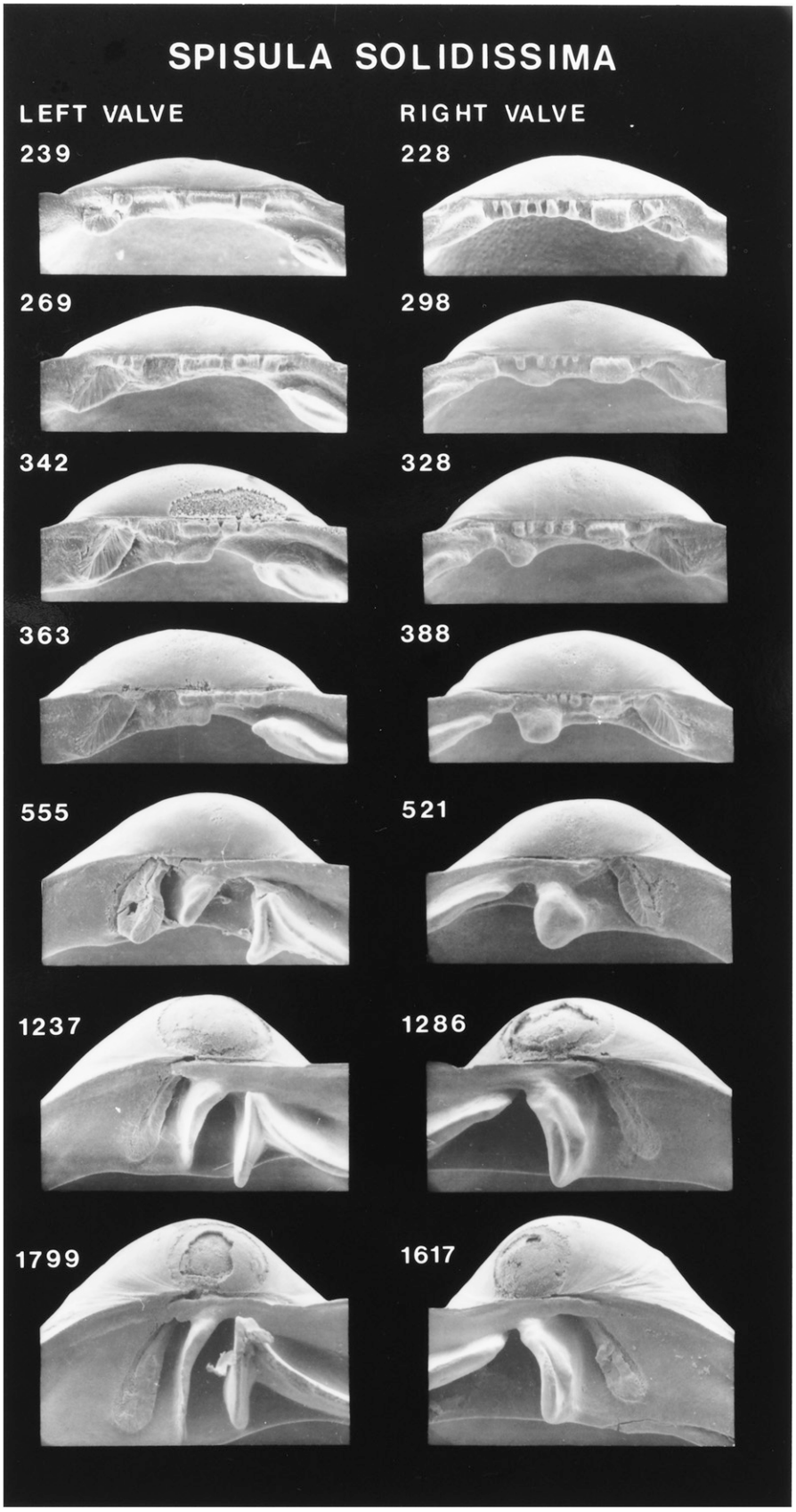

Figure 163. Scanning electron micrographs of the hinge of disarticulated shell valves of *Spisula solidissima* postlarvae seen in Figure 162. Numbers indicate the maximum linear shell dimension in micrometers.

Downloaded From: https://bioone.org/journals/Journal-of-Shellfish-Research on 25 Feb 2020
Terms of Use: https://bioone.org/terms-of-use Access provided by IFREMER

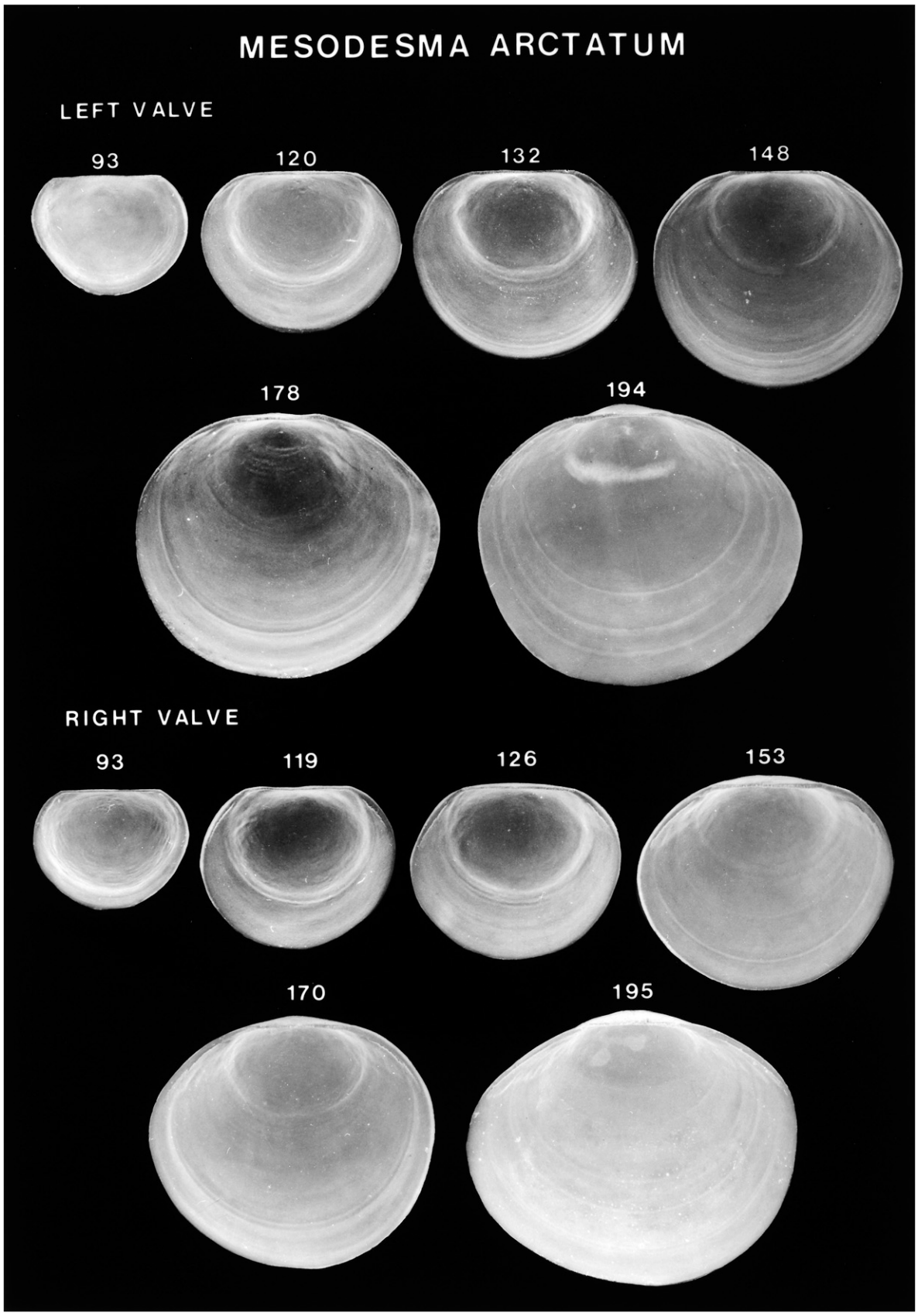

Figure 164. Scanning electron micrographs of disarticulated shell valves of *Mesodesma arctatum* larvae. Numbers indicate the maximum linear shell dimension in micrometers.

Downloaded From: https://bioone.org/journals/Journal-of-Shellfish-Research on 25 Feb 2020
Terms of Use: https://bioone.org/terms-of-use Access provided by IFREMER

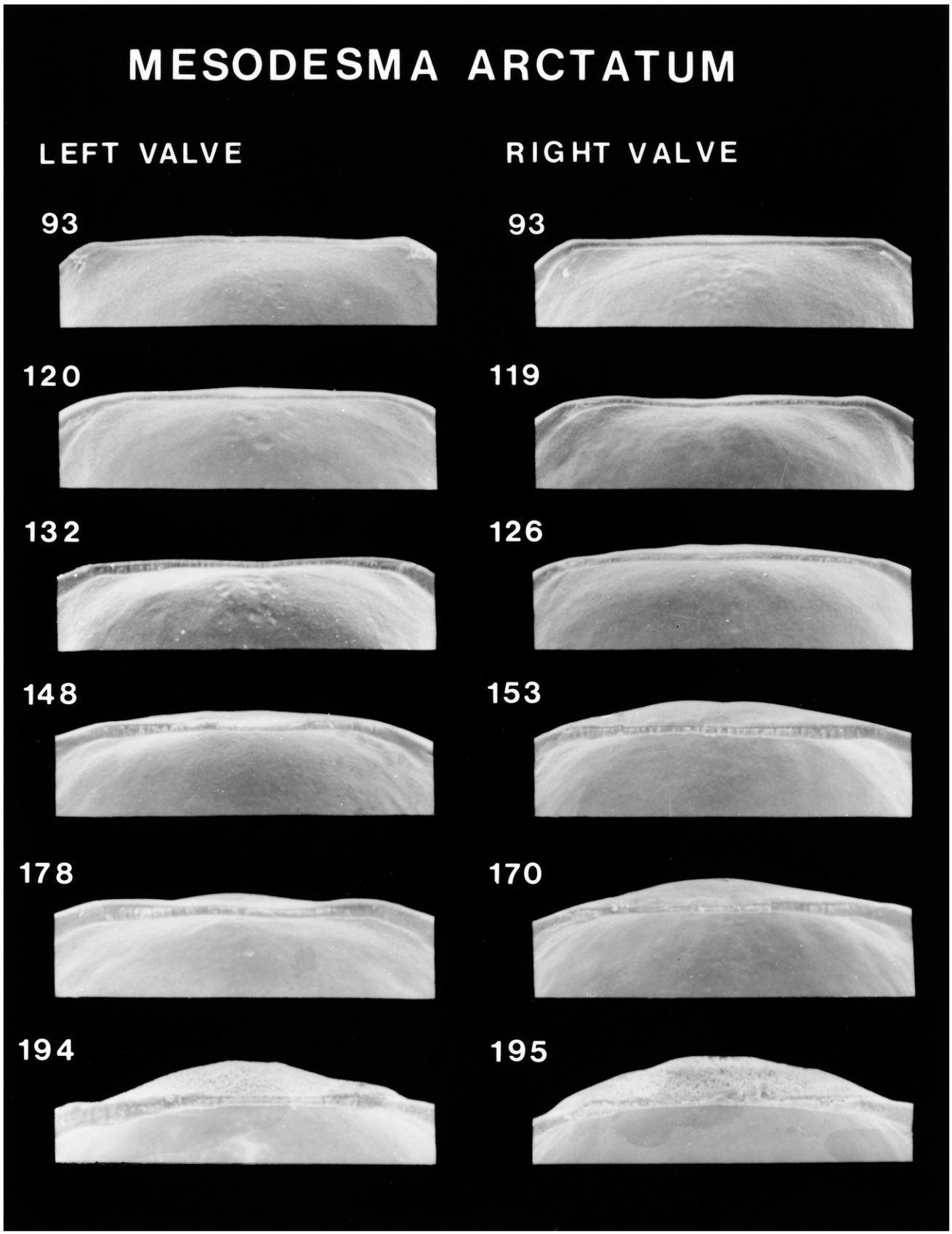

Figure 165. Scanning electron micrographs of the hinge of disarticulated shell valves of *Mesodesma arctatum* larvae seen in Figure 164. Numbers indicate the maximum linear shell dimension in micrometers.

Downloaded From: https://bioone.org/journals/Journal-of-Shellfish-Research on 25 Feb 2020
Terms of Use: https://bioone.org/terms-of-use Access provided by IFREMER

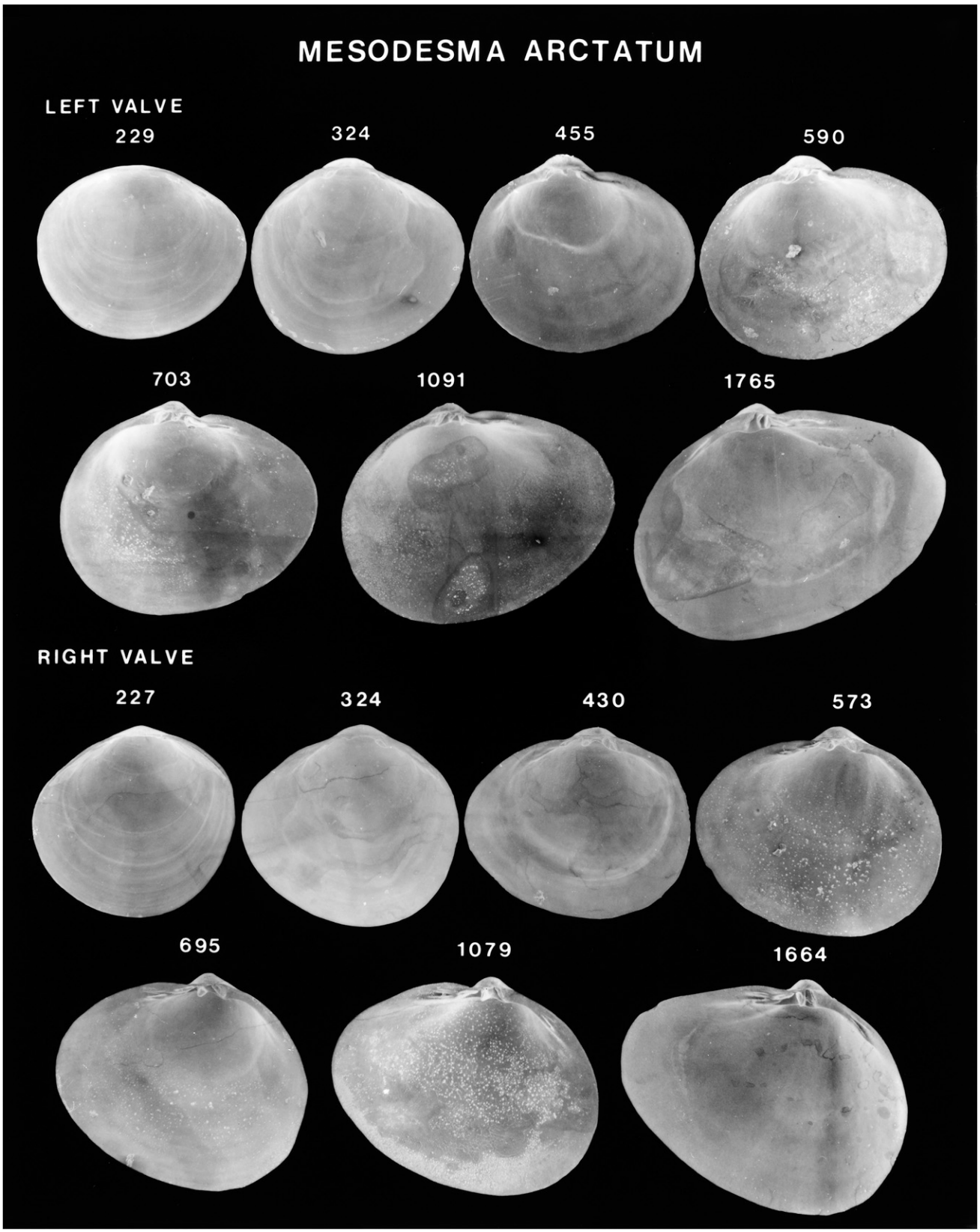

Figure 166. Scanning electron micrographs of disarticulated shell valves of *Mesodesma arctatum* postlarvae. Numbers indicate the maximum linear shell dimension in micrometers.

Downloaded From: https://bioone.org/journals/Journal-of-Shellfish-Research on 25 Feb 2020
Terms of Use: https://bioone.org/terms-of-use Access provided by IFREMER

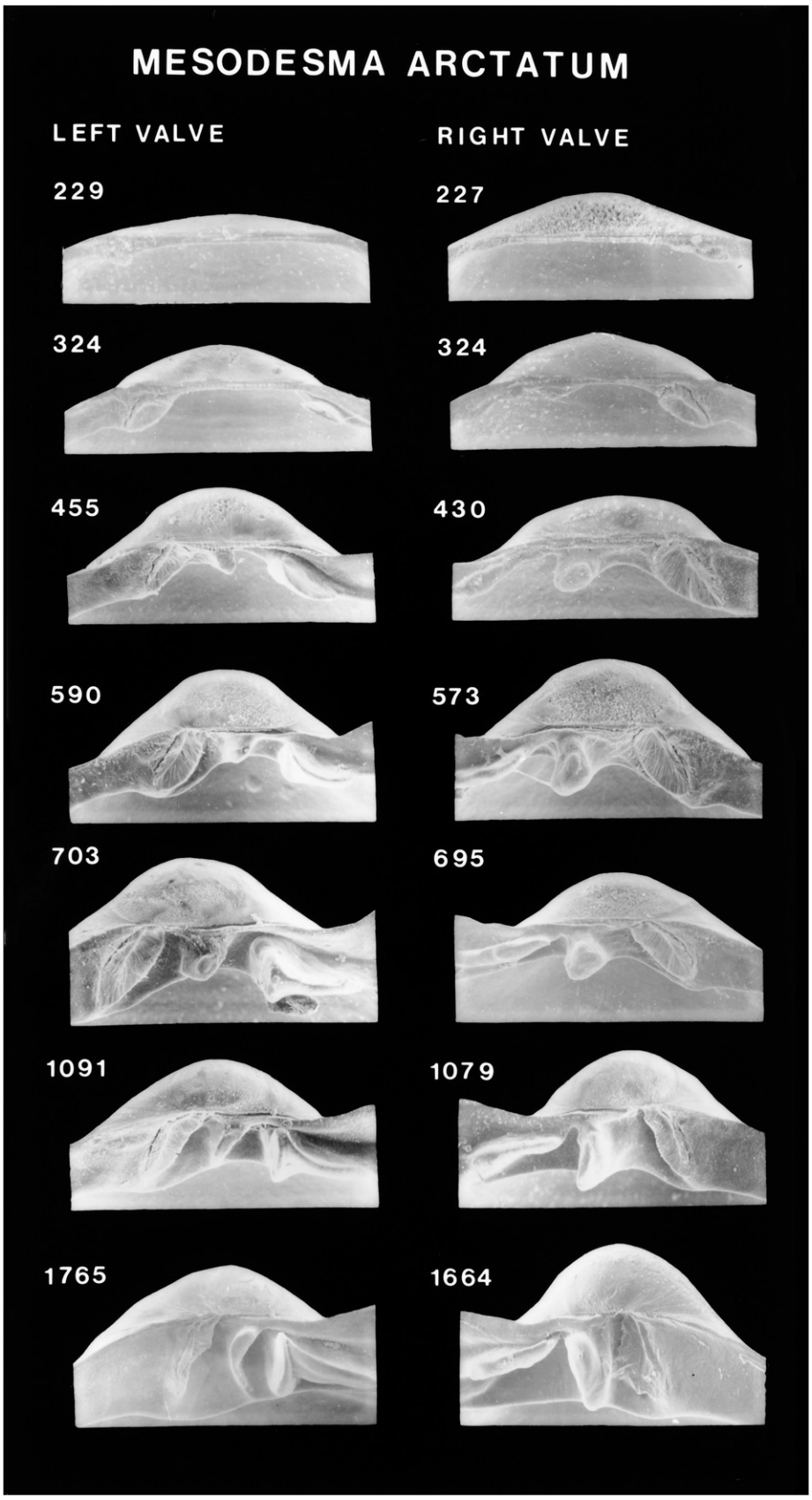

Figure 167. Scanning electron micrographs of the hinge of disarticulated shell valves of *Mesodesma arctatum* postlarvae seen in Figure 166. Numbers indicate the maximum linear shell dimension in micrometers.

Downloaded From: https://bioone.org/journals/Journal-of-Shellfish-Research on 25 Feb 2020
Terms of Use: https://bioone.org/terms-of-use Access provided by IFREMER

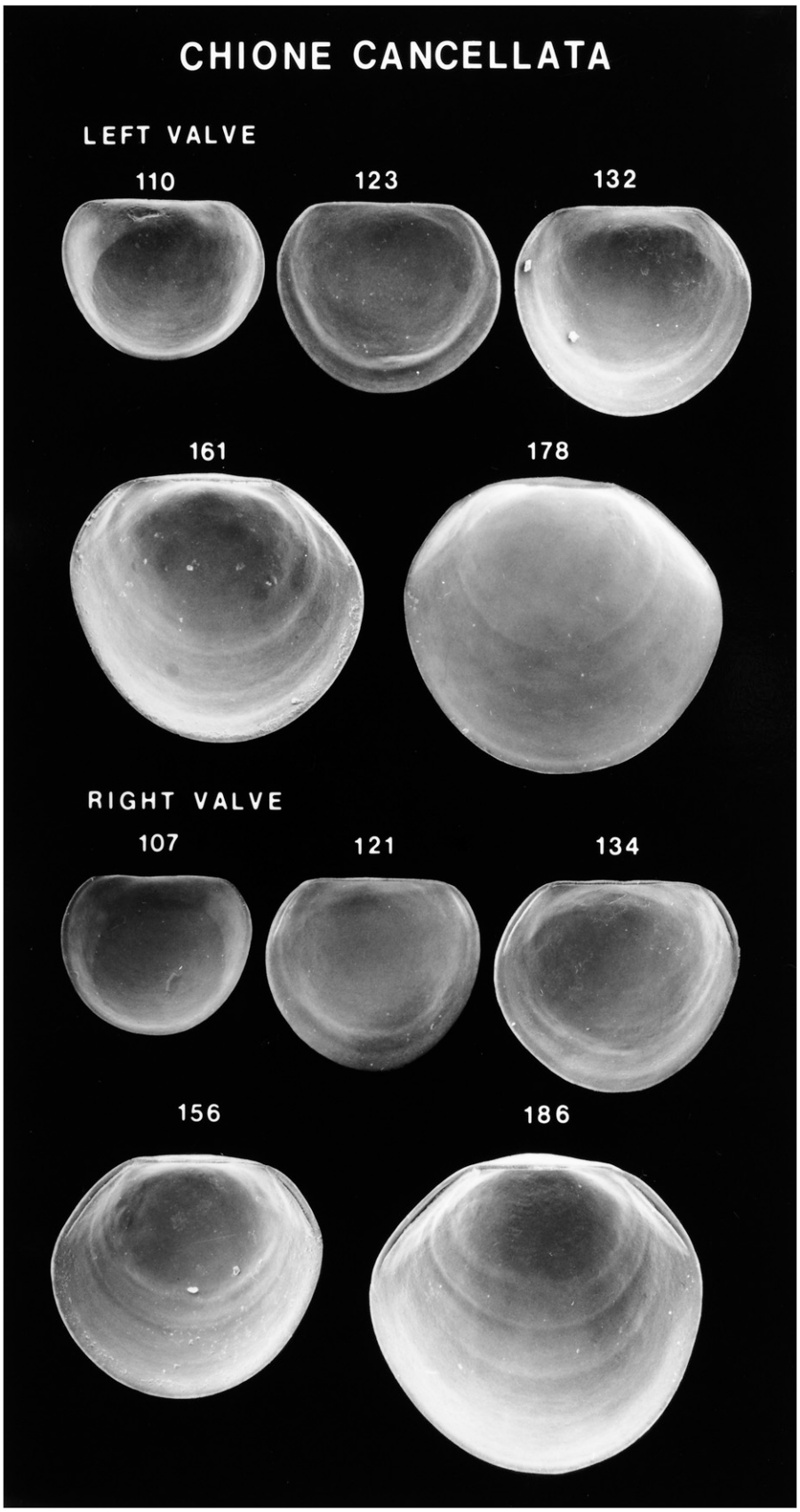

Figure 168. Scanning electron micrographs of disarticulated shell valves of *Chione cancellata* larvae. Numbers indicate the maximum linear shell dimension in micrometers. Modified from Goodsell et al. (1992).

Downloaded From: https://bioone.org/journals/Journal-of-Shellfish-Research on 25 Feb 2020
Terms of Use: https://bioone.org/terms-of-use Access provided by IFREMER

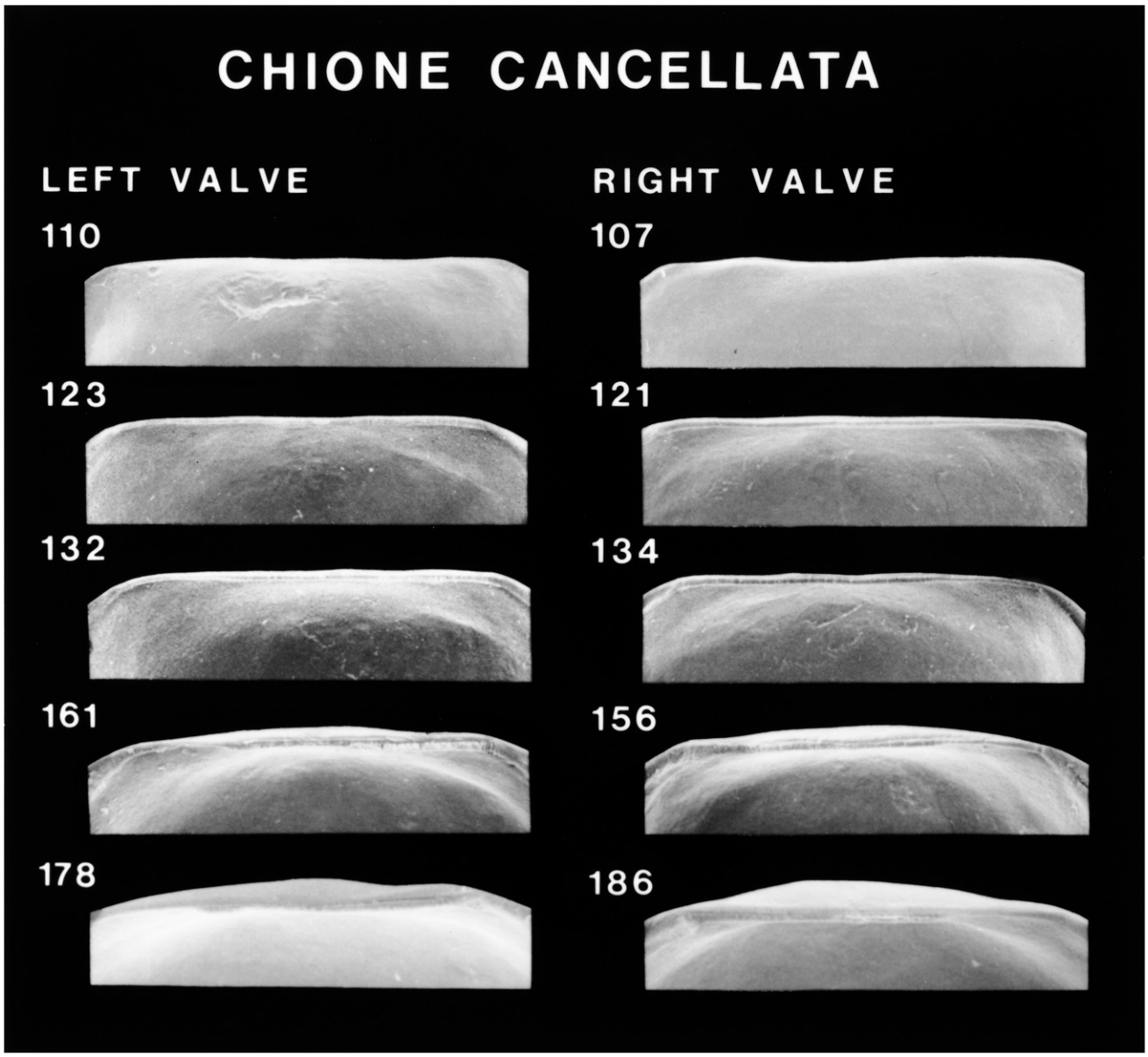

Figure 169. Scanning electron micrographs of the hinge of disarticulated shell valves of *Chione cancellata* larvae seen in Figure 168. Numbers indicate the maximum linear shell dimension in micrometers. Modified from Goodsell et al. (1992).

Downloaded From: https://bioone.org/journals/Journal-of-Shellfish-Research on 25 Feb 2020
Terms of Use: https://bioone.org/terms-of-use Access provided by IFREMER

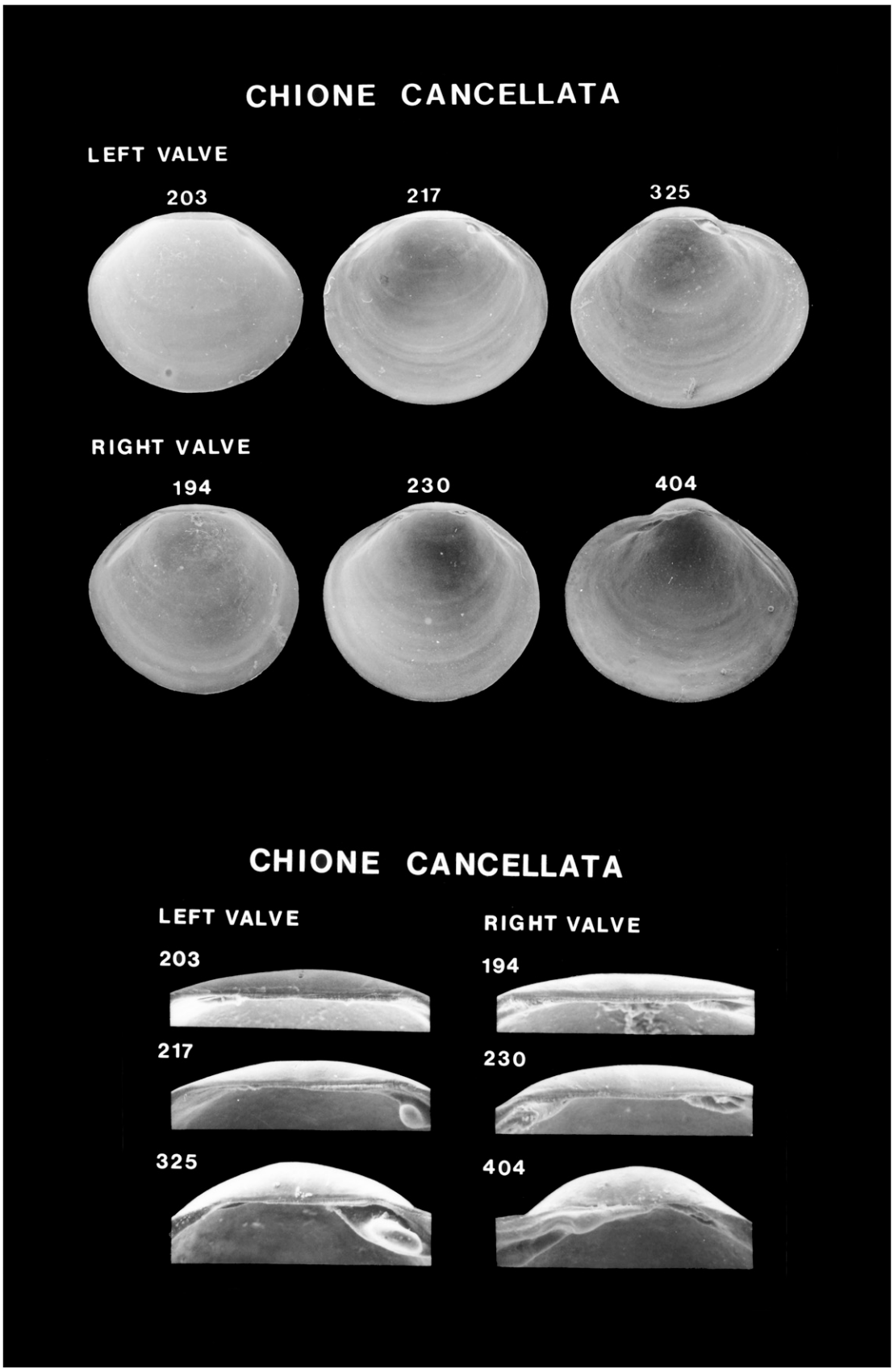

Figure 170. Scanning electron micrographs of disarticulated shell valves of *Chione cancellata* postlarvae (top) and higher magnification scanning electron micrographs of the hinge of these shell valves (bottom). Numbers indicate the maximum linear shell dimension in micrometers. Modified from Goodsell et al. (1992).

Downloaded From: https://bioone.org/journals/Journal-of-Shellfish-Research on 25 Feb 2020
Terms of Use: https://bioone.org/terms-of-use Access provided by IFREMER

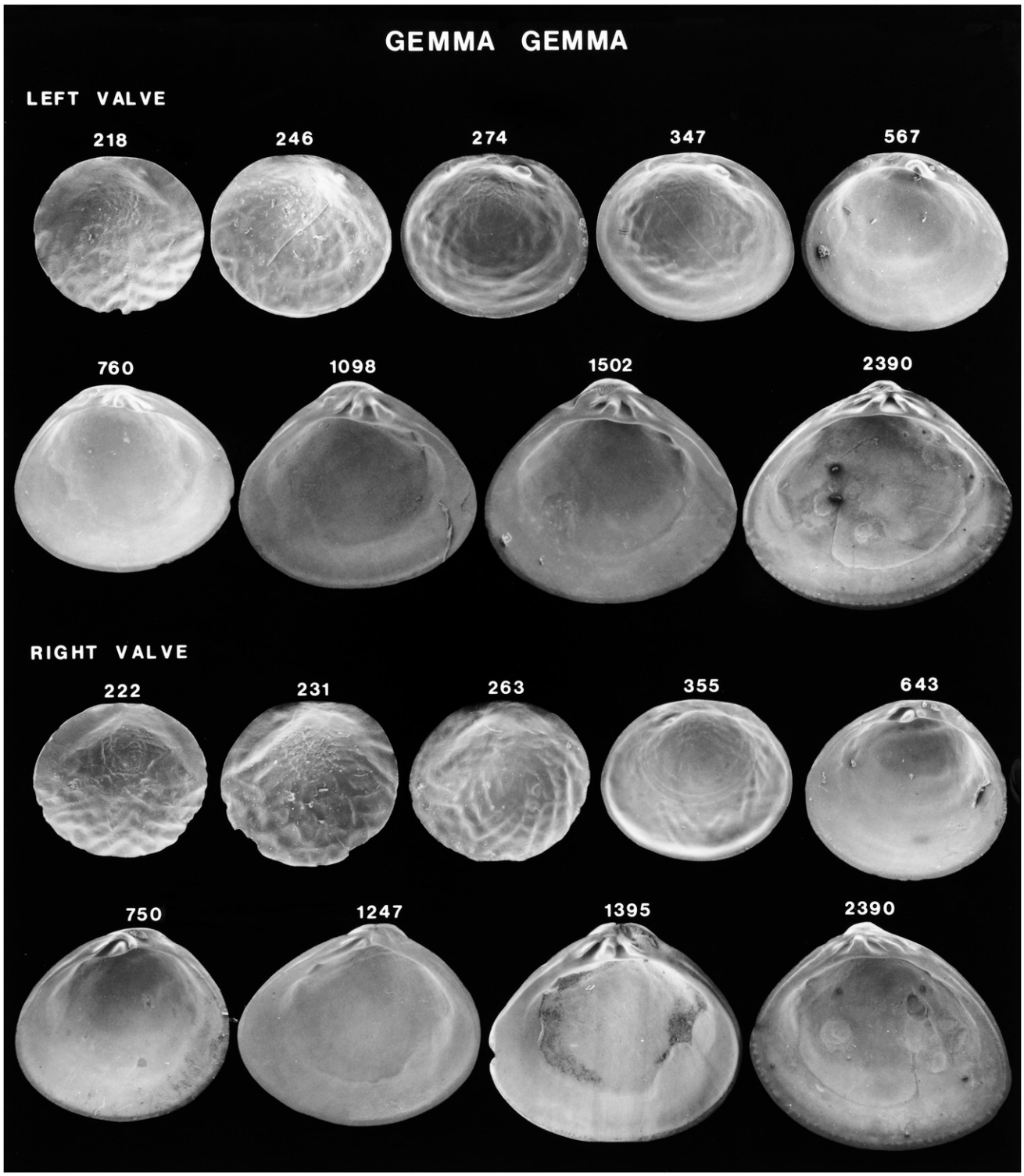

Figure 171. Scanning electron micrographs of disarticulated shell valves of *Gemma gemma* postlarvae. Numbers indicate the maximum linear shell dimension in micrometers.

Downloaded From: https://bioone.org/journals/Journal-of-Shellfish-Research on 25 Feb 2020
Terms of Use: https://bioone.org/terms-of-use Access provided by IFREMER

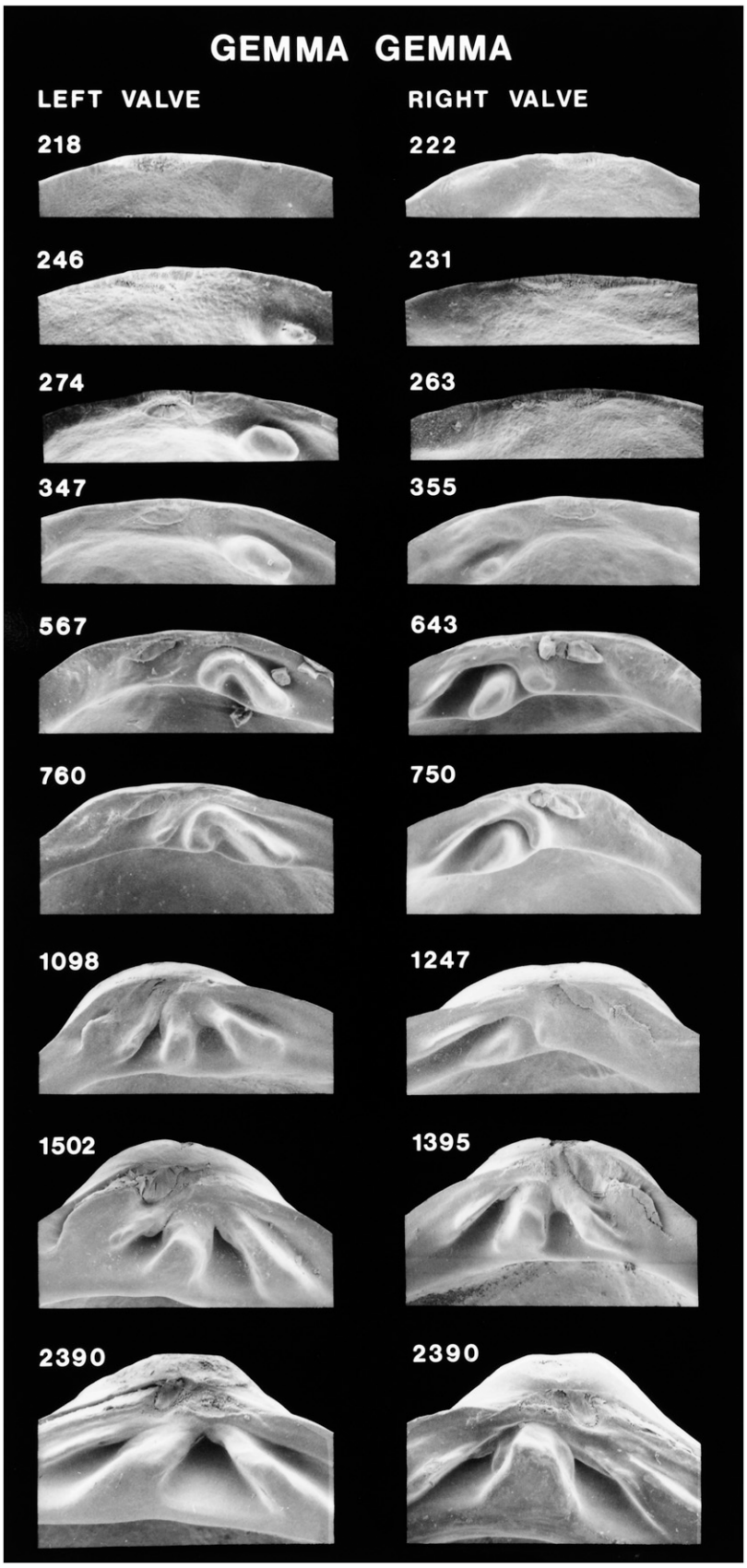

Figure 172. Scanning electron micrographs of the hinge of disarticulated shell valves of *Gemma gemma* postlarvae seen in Figure 171. Numbers indicate the maximum linear shell dimension in micrometers.

Downloaded From: https://bioone.org/journals/Journal-of-Shellfish-Research on 25 Feb 2020
Terms of Use: https://bioone.org/terms-of-use Access provided by IFREMER

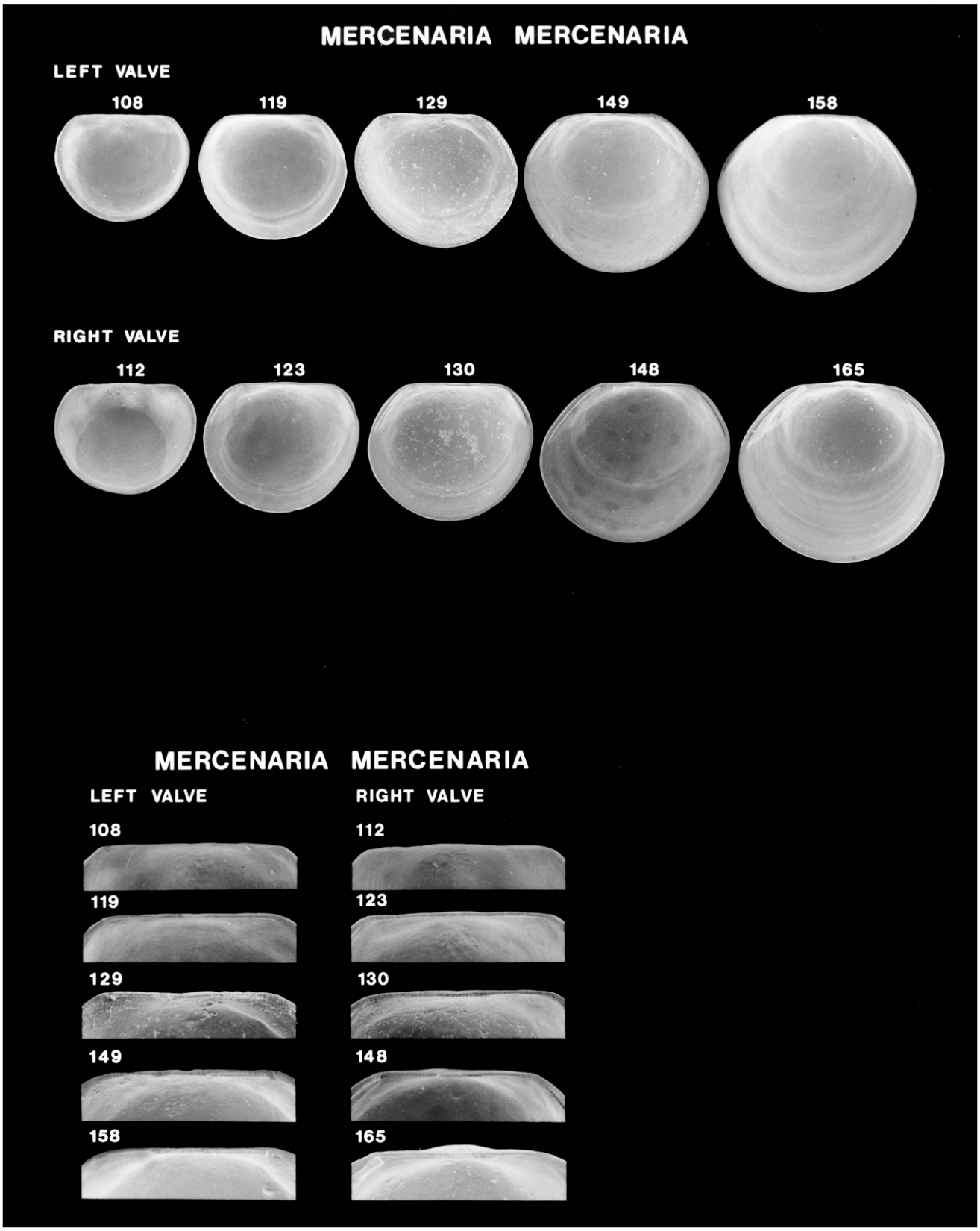

Figure 173. Scanning electron micrographs of disarticulated shell valves of *Mercenaria mercenaria* larvae (top) and higher magnification scanning electron micrographs of the hinge of these shell valves (bottom). Numbers indicate the maximum linear shell dimension in micrometers. Modified from Goodsell et al. (1992).

Downloaded From: https://bioone.org/journals/Journal-of-Shellfish-Research on 25 Feb 2020
Terms of Use: https://bioone.org/terms-of-use Access provided by IFREMER

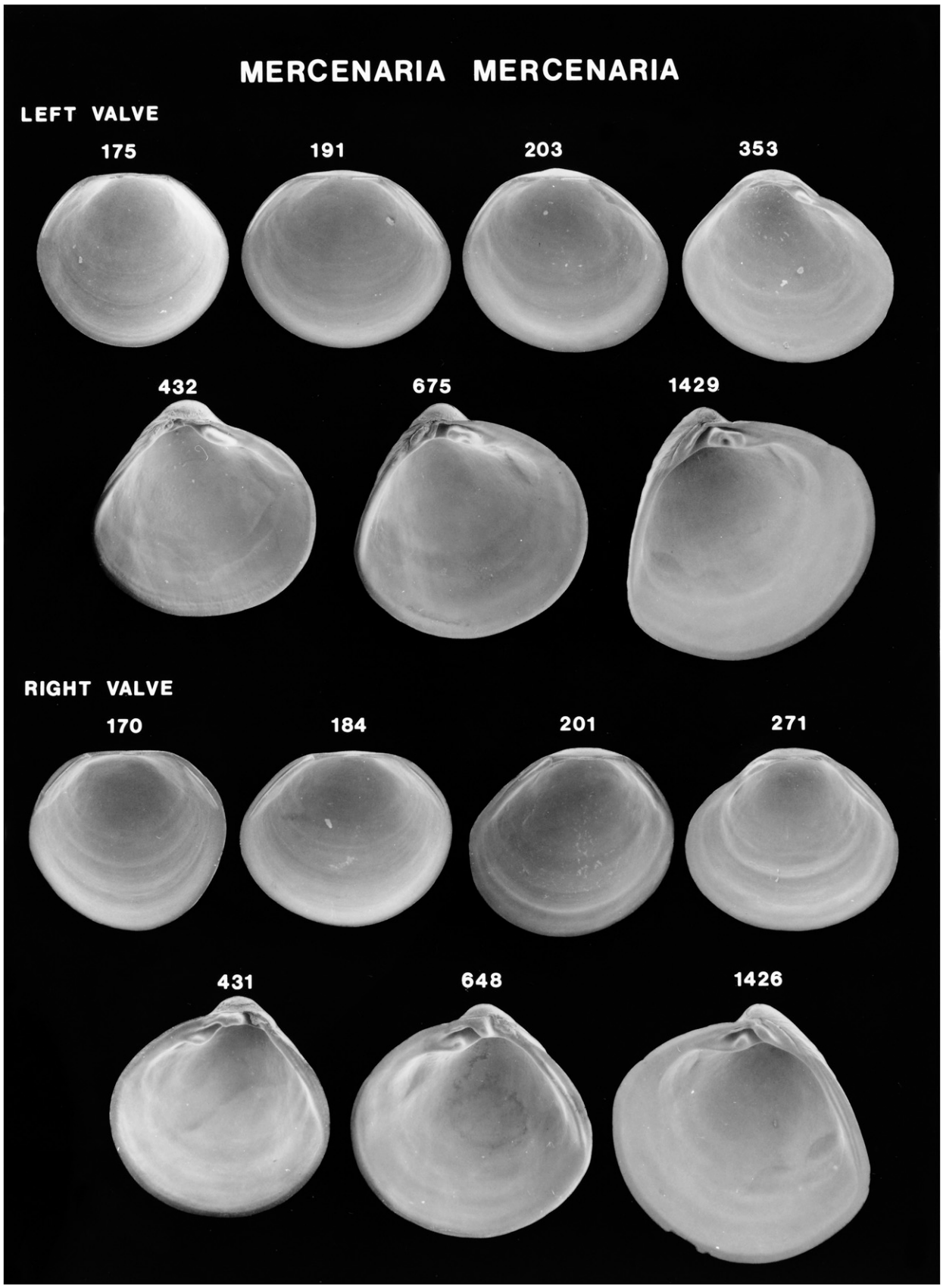

Figure 174. Scanning electron micrographs of disarticulated shell valves of *Mercenaria mercenaria* postlarvae. Numbers indicate the maximum linear shell dimension in micrometers. Modified from Goodsell et al. (1992).

Downloaded From: https://bioone.org/journals/Journal-of-Shellfish-Research on 25 Feb 2020
Terms of Use: https://bioone.org/terms-of-use Access provided by IFREMER

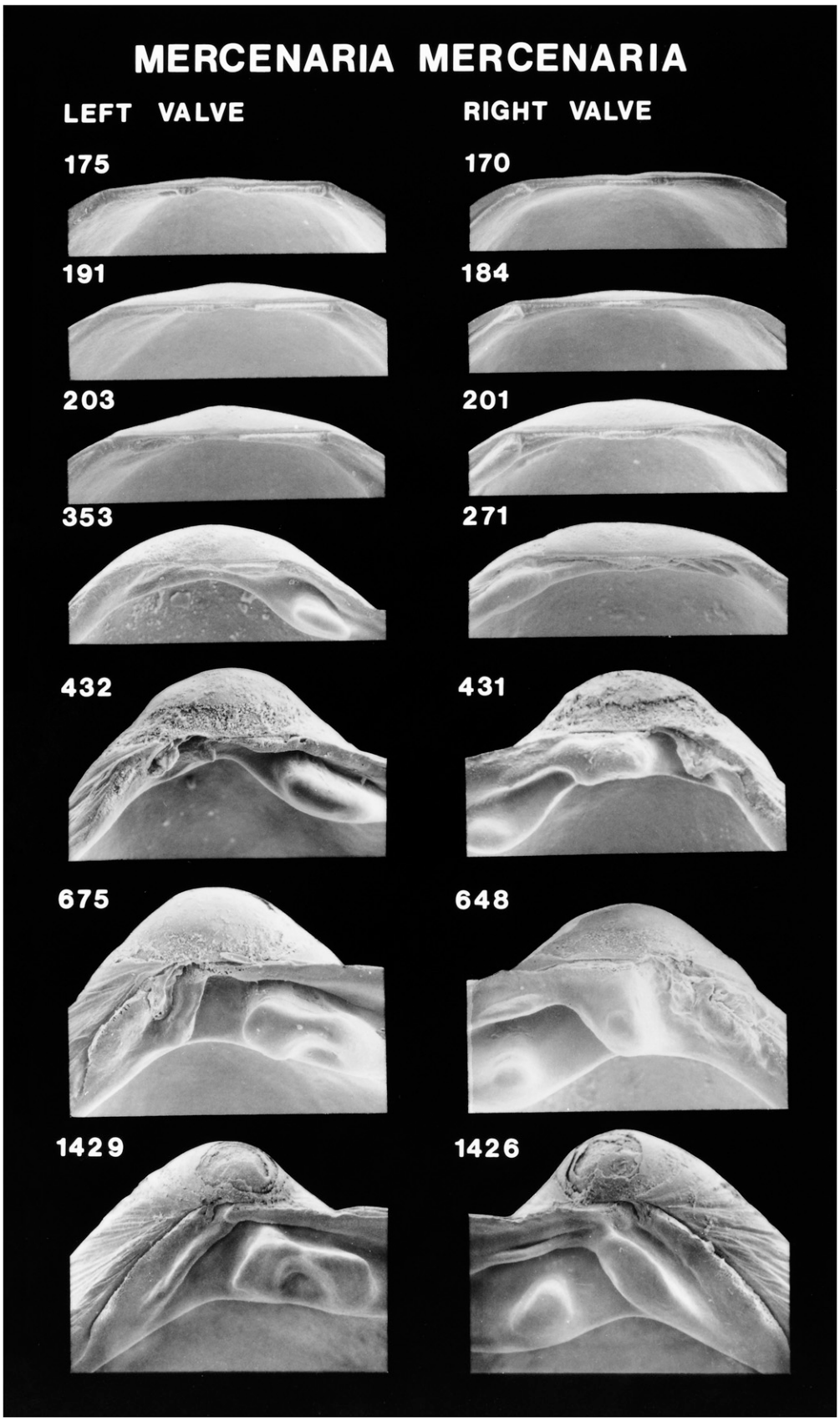

Figure 175. Scanning electron micrographs of the hinge of disarticulated shell valves of *Mercenaria mercenaria* postlarvae seen in Figure 174. Numbers indicate the maximum linear shell dimension in micrometers. Modified from Goodsell et al. (1992).

Downloaded From: https://bioone.org/journals/Journal-of-Shellfish-Research on 25 Feb 2020
Terms of Use: https://bioone.org/terms-of-use Access provided by IFREMER

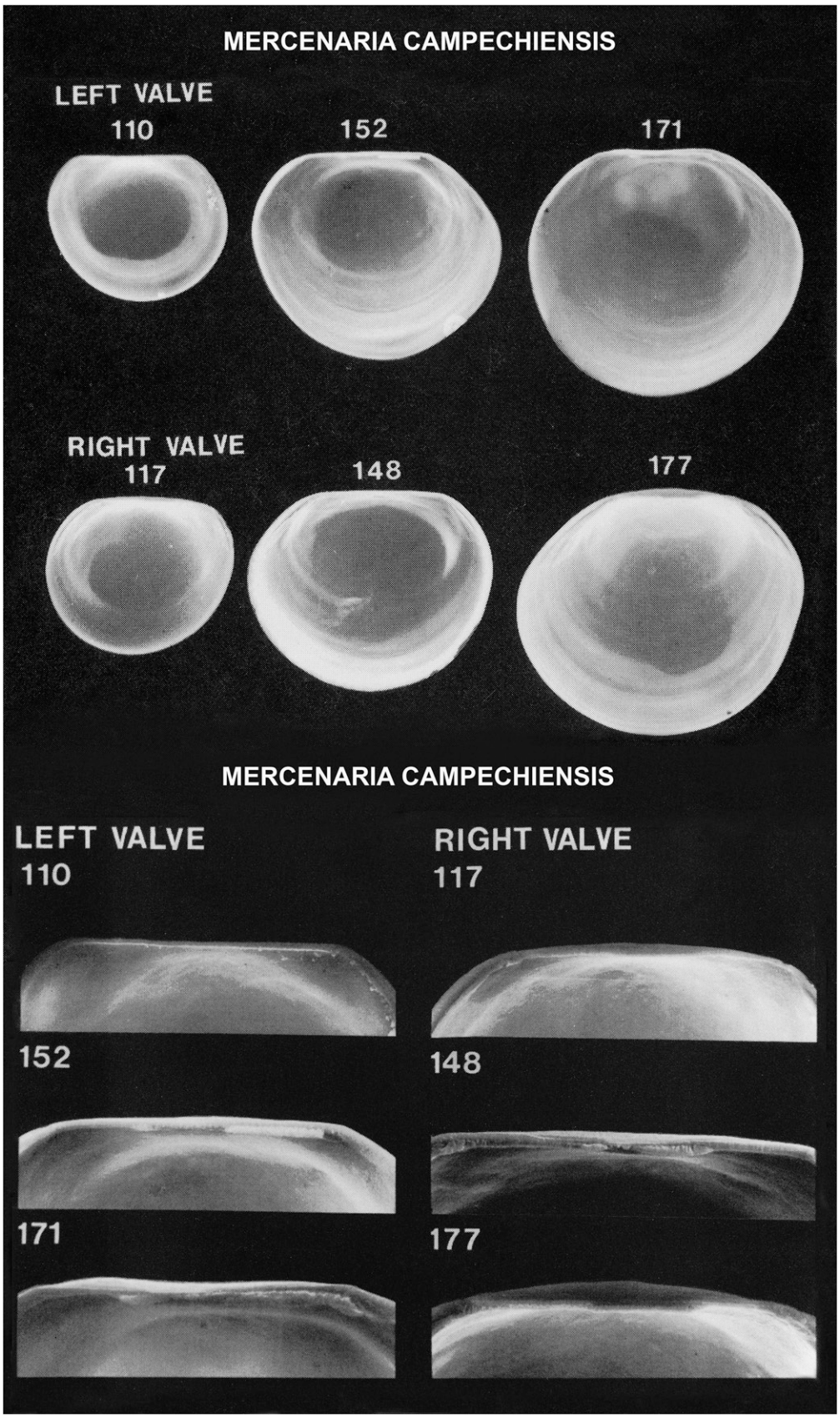

Figure 176. Scanning electron micrographs of disarticulated shell valves of *Mercenaria campechiensis* larvae (top) and higher magnification scanning electron micrographs of the hinge of these shell valves (bottom). Numbers indicate the maximum linear shell dimension in micrometers. Modified from Goodsell et al. (1992).

Downloaded From: https://bioone.org/journals/Journal-of-Shellfish-Research on 25 Feb 2020
Terms of Use: https://bioone.org/terms-of-use Access provided by IFREMER

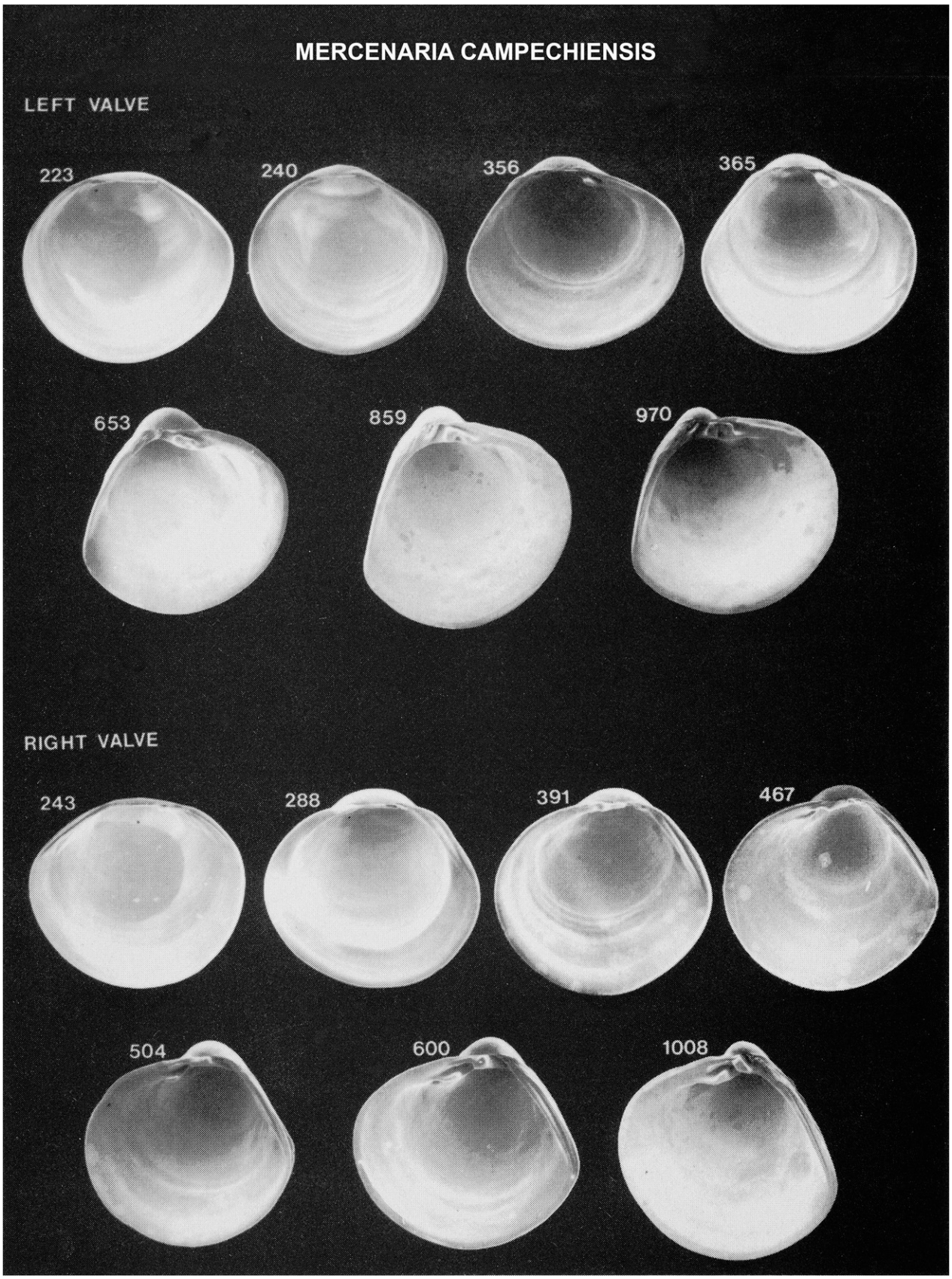

Figure 177. Scanning electron micrographs of disarticulated shell valves of *Mercenaria campechiensis* postlarvae. Numbers indicate the maximum linear shell dimension in micrometers. Modified from Goodsell et al. (1992).

Downloaded From: https://bioone.org/journals/Journal-of-Shellfish-Research on 25 Feb 2020
Terms of Use: https://bioone.org/terms-of-use Access provided by IFREMER

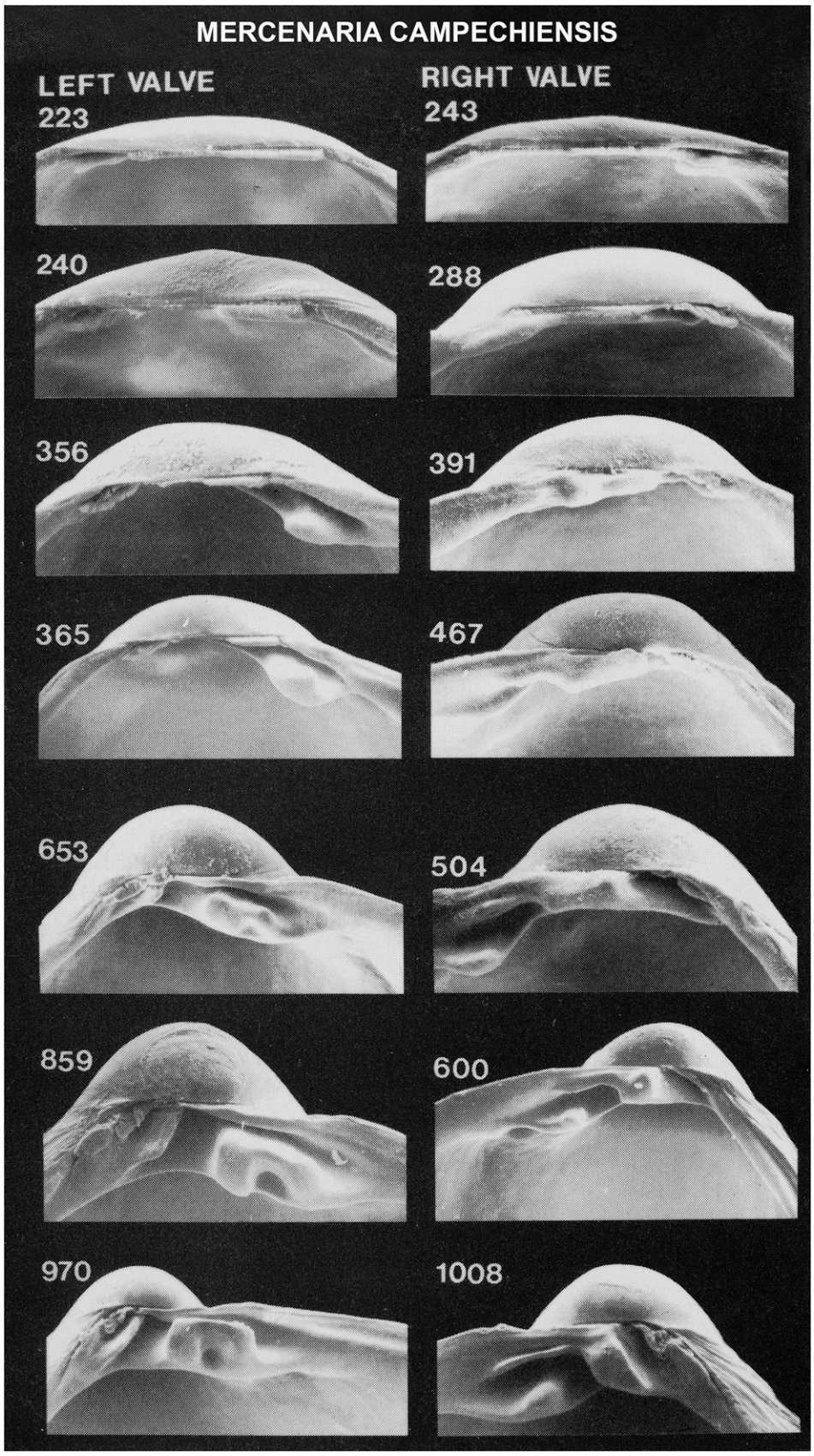

Figure 178. Scanning electron micrographs of the hinge of disarticulated shell valves of *Mercenaria campechiensis* postlarvae seen in Figure 177. Numbers indicate the maximum linear shell dimension in micrometers. Modified from Goodsell et al. (1992).

Downloaded From: https://bioone.org/journals/Journal-of-Shellfish-Research on 25 Feb 2020
Terms of Use: https://bioone.org/terms-of-use Access provided by IFREMER

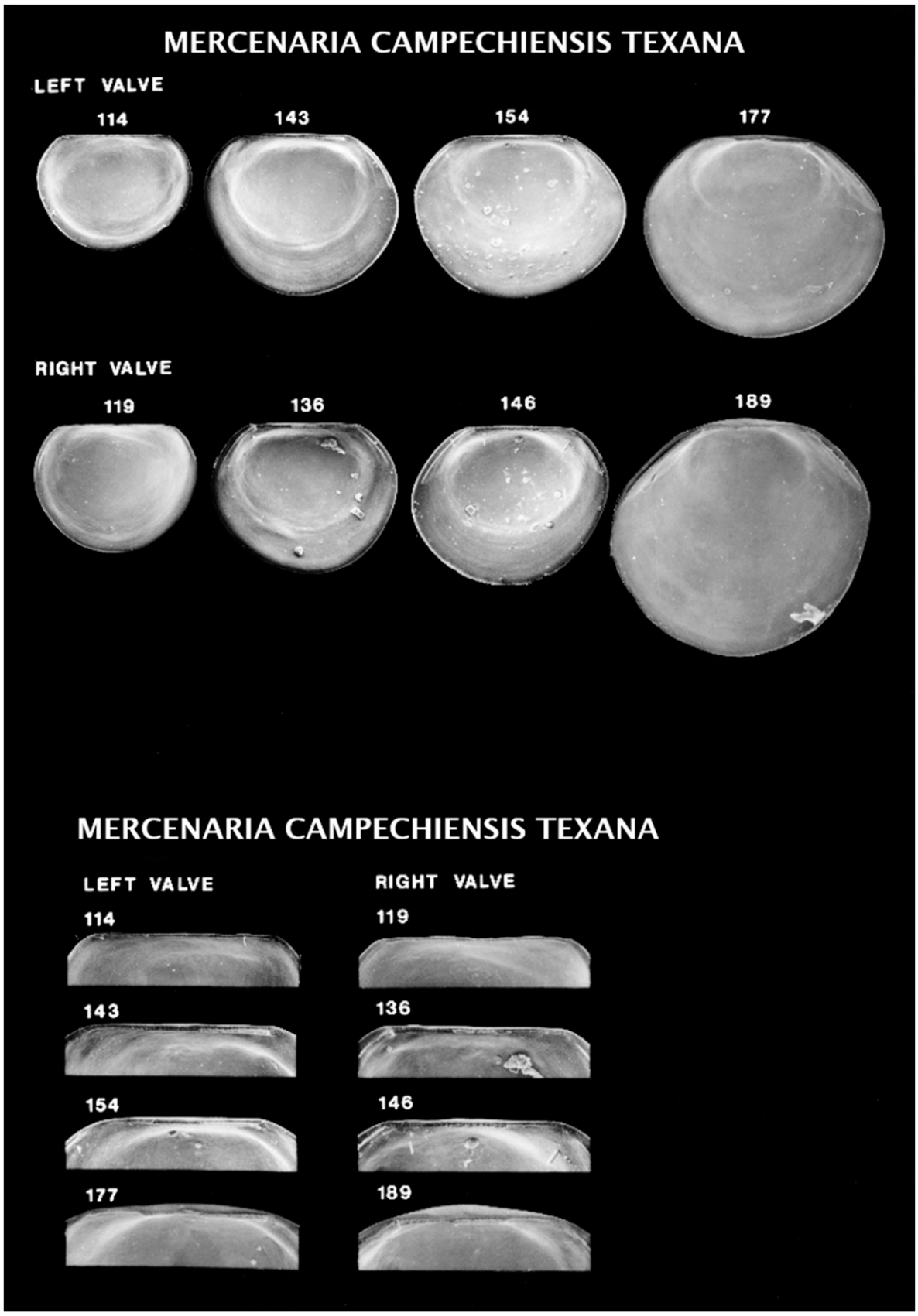

Figure 179. Scanning electron micrographs of disarticulated shell valves of *Mercenaria campechiensis texana* larvae (top) and higher magnification scanning electron micrographs of the hinge of these shell valves (bottom). Numbers indicate the maximum linear shell dimension in micrometers. Modified from Goodsell et al. (1992).

Downloaded From: https://bioone.org/journals/Journal-of-Shellfish-Research on 25 Feb 2020
Terms of Use: https://bioone.org/terms-of-use Access provided by IFREMER

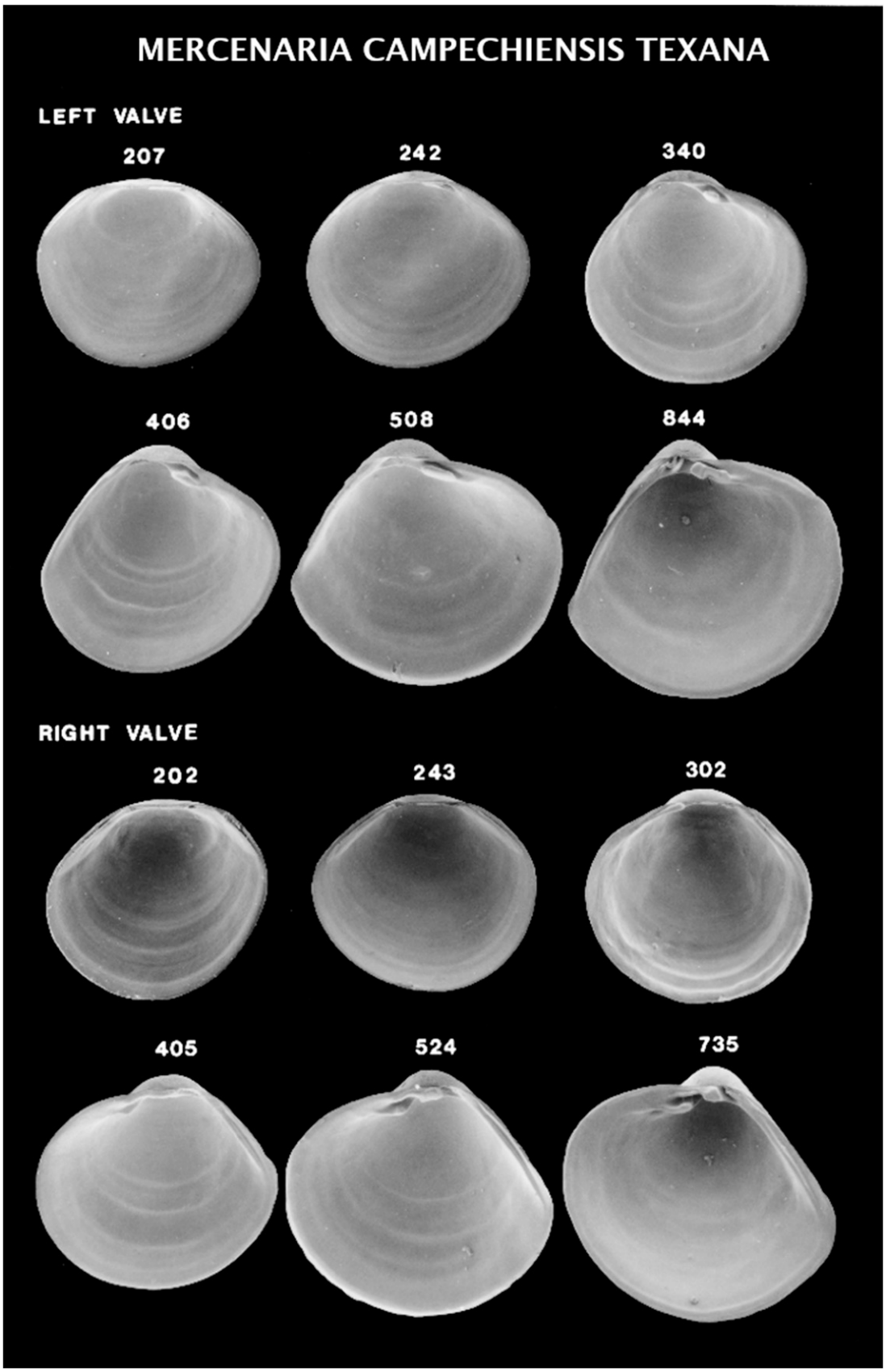

Figure 180. Scanning electron micrographs of disarticulated shell valves of *Mercenaria campechiensis texana* postlarvae. Numbers indicate the maximum linear shell dimension in micrometers. Modified from Goodsell et al. (1992).

Downloaded From: https://bioone.org/journals/Journal-of-Shellfish-Research on 25 Feb 2020
Terms of Use: https://bioone.org/terms-of-use Access provided by IFREMER

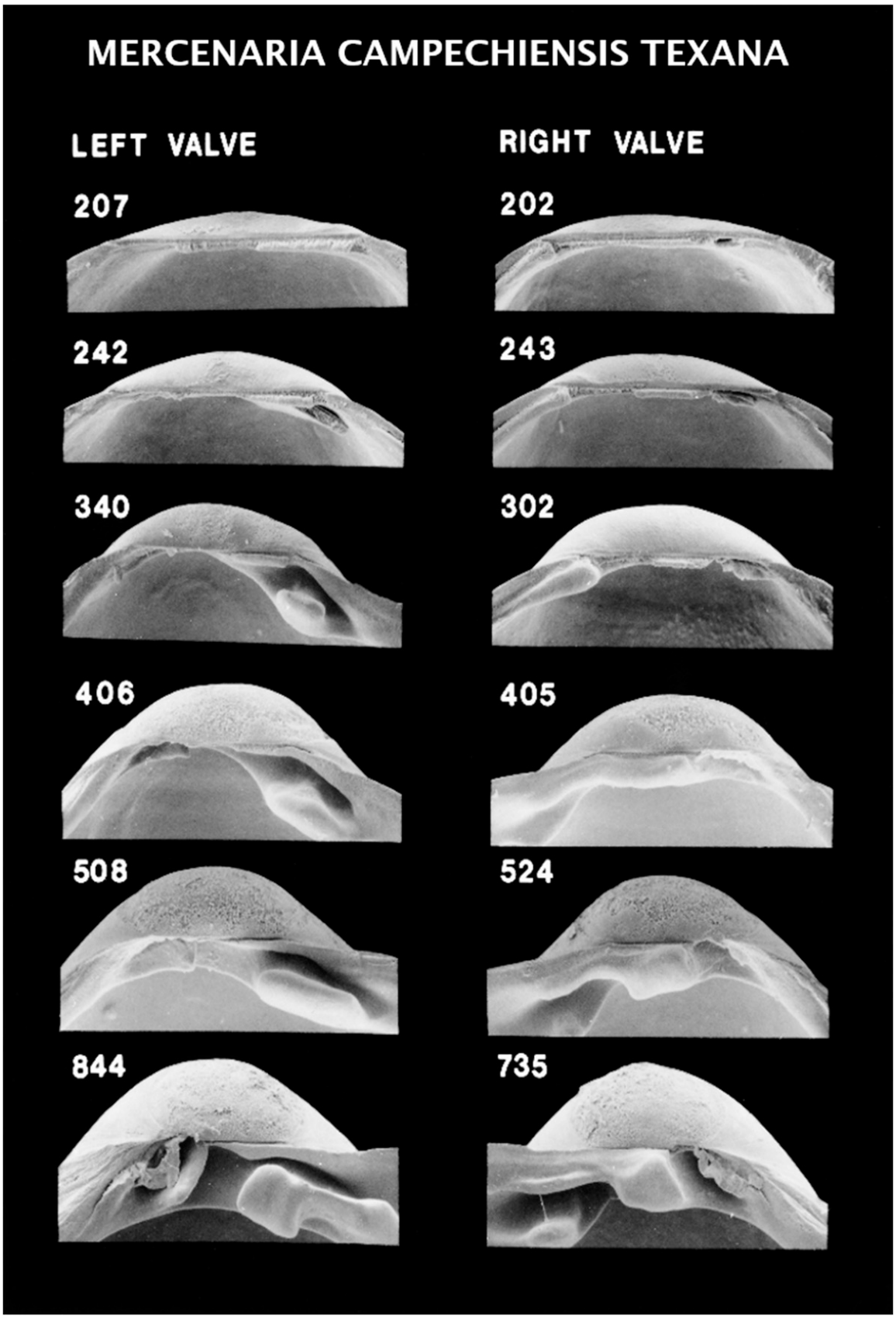

Figure 181. Scanning electron micrographs of the hinge of disarticulated shell valves of *Mercenaria campechiensis texana* postlarvae seen in Figure 180. Numbers indicate the maximum linear shell dimension in micrometers. Modified from Goodsell et al. (1992).

Downloaded From: https://bioone.org/journals/Journal-of-Shellfish-Research on 25 Feb 2020
Terms of Use: https://bioone.org/terms-of-use Access provided by IFREMER

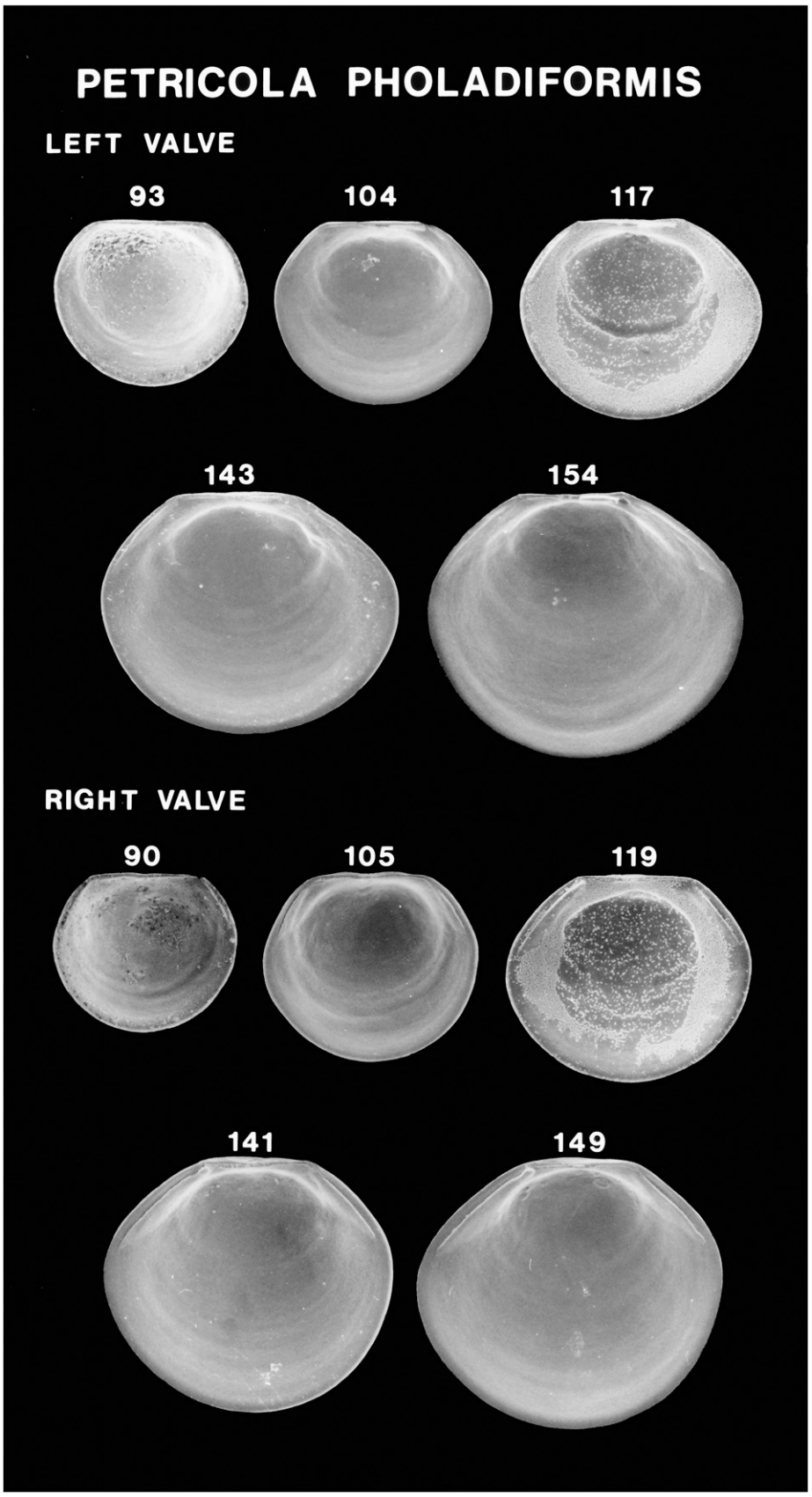

Figure 182. Scanning electron micrographs of disarticulated shell valves of *Petricola pholadiformis* larvae. Numbers indicate the maximum linear shell dimension in micrometers.

Downloaded From: https://bioone.org/journals/Journal-of-Shellfish-Research on 25 Feb 2020
Terms of Use: https://bioone.org/terms-of-use Access provided by IFREMER

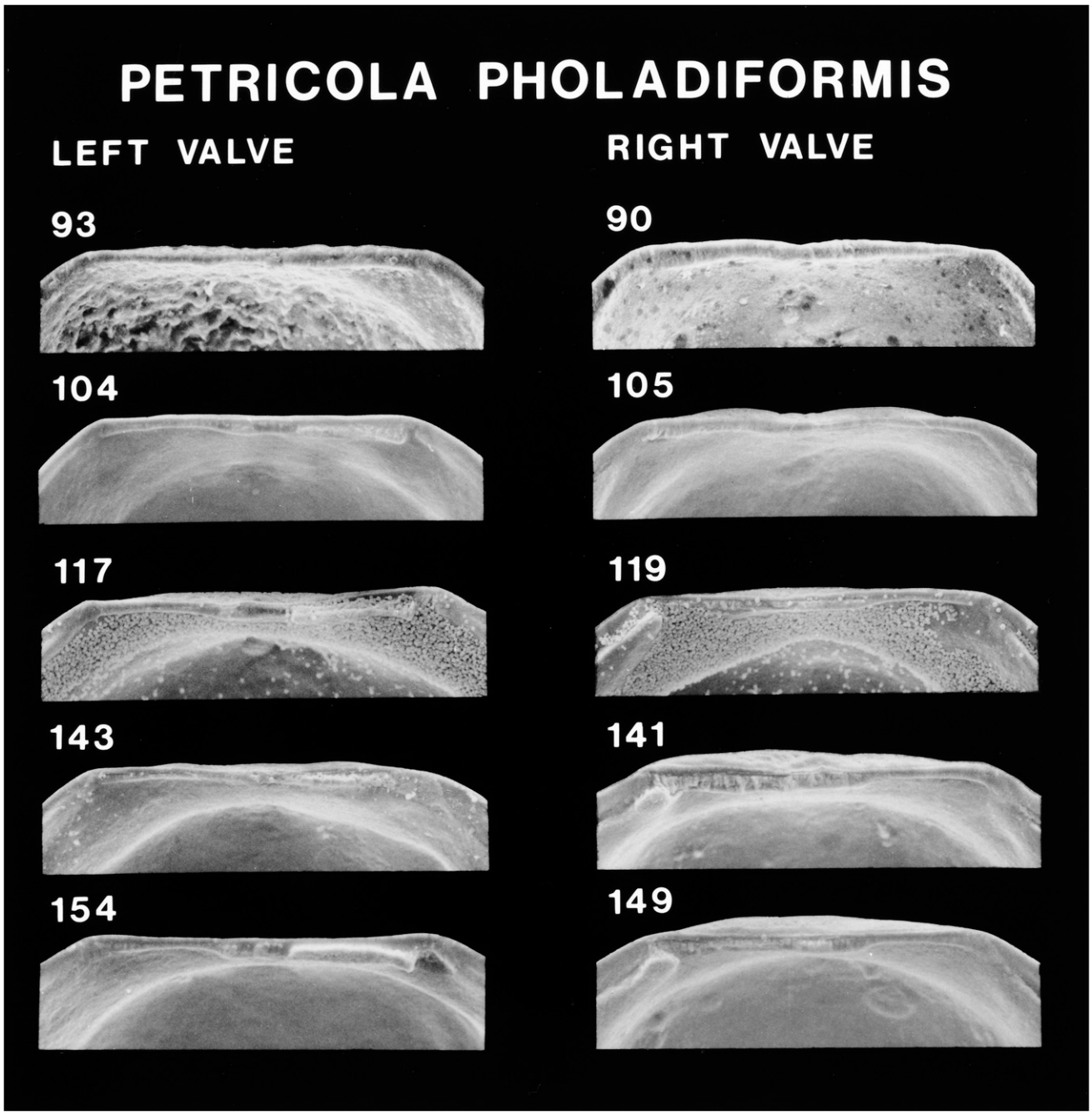

Figure 183. Scanning electron micrographs of the hinge of disarticulated shell valves of *Petricola pholadiformis* larvae seen in Figure 182. Numbers indicate the maximum linear shell dimension in micrometers.

Downloaded From: https://bioone.org/journals/Journal-of-Shellfish-Research on 25 Feb 2020
Terms of Use: https://bioone.org/terms-of-use Access provided by IFREMER

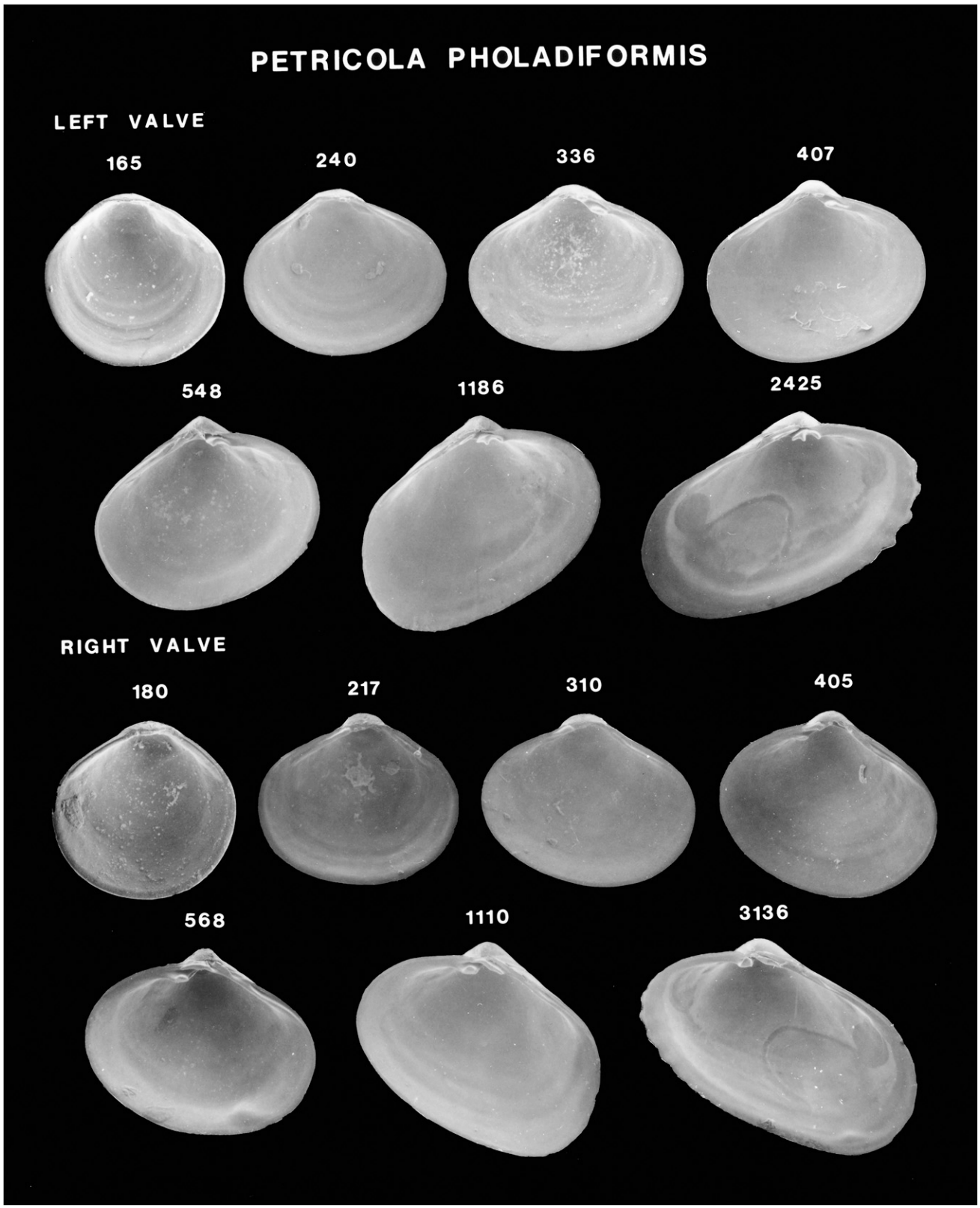

Figure 184. Scanning electron micrographs of disarticulated shell valves of *Petricola pholadiformis* postlarvae. Numbers indicate the maximum linear shell dimension in micrometers.

Downloaded From: https://bioone.org/journals/Journal-of-Shellfish-Research on 25 Feb 2020
Terms of Use: https://bioone.org/terms-of-use Access provided by IFREMER

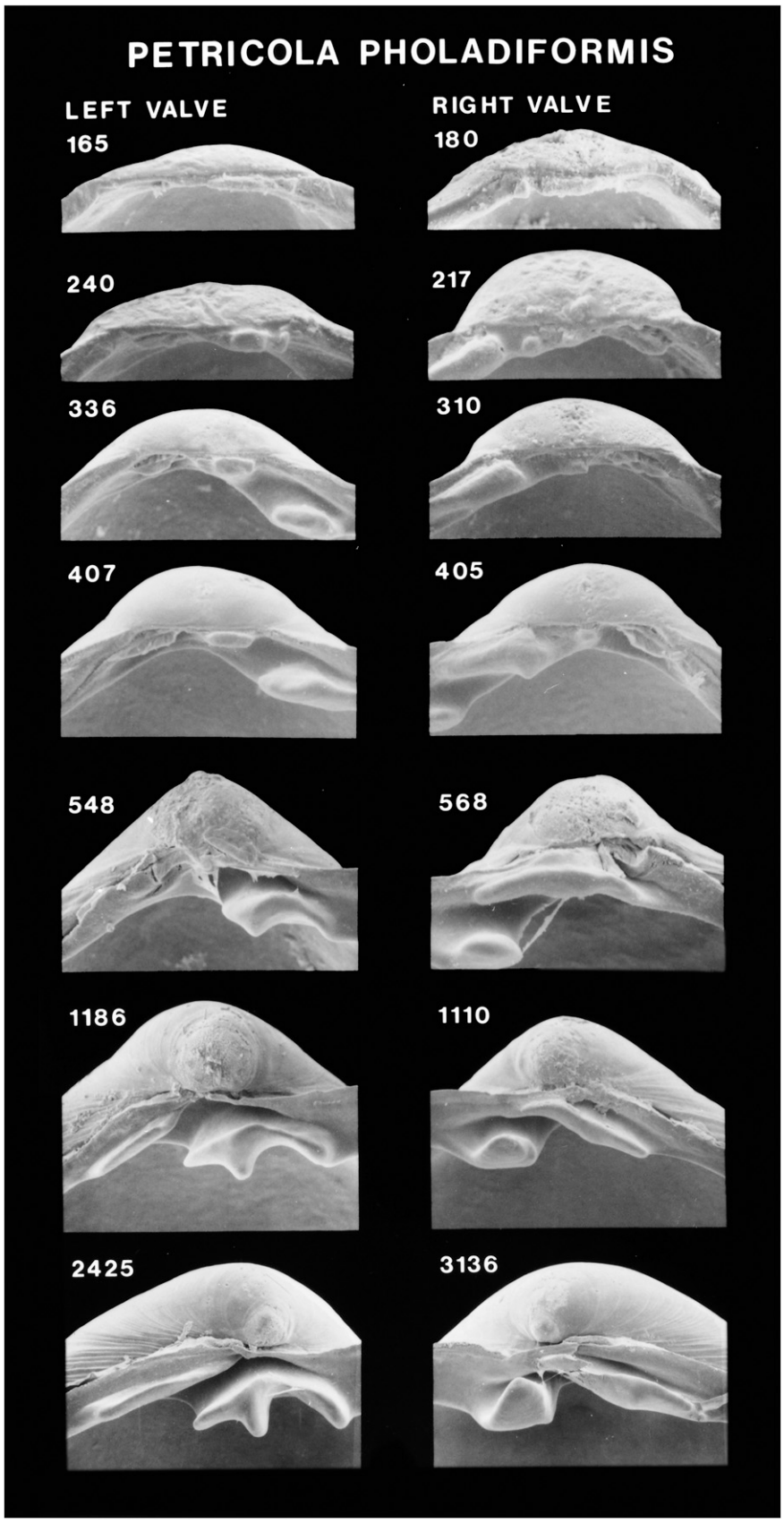

Figure 185. Scanning electron micrographs of the hinge of disarticulated shell valves of *Petricola pholadiformis* postlarvae seen in Figure 184. Numbers indicate the maximum linear shell dimension in micrometers.

Downloaded From: https://bioone.org/journals/Journal-of-Shellfish-Research on 25 Feb 2020
Terms of Use: https://bioone.org/terms-of-use Access provided by IFREMER

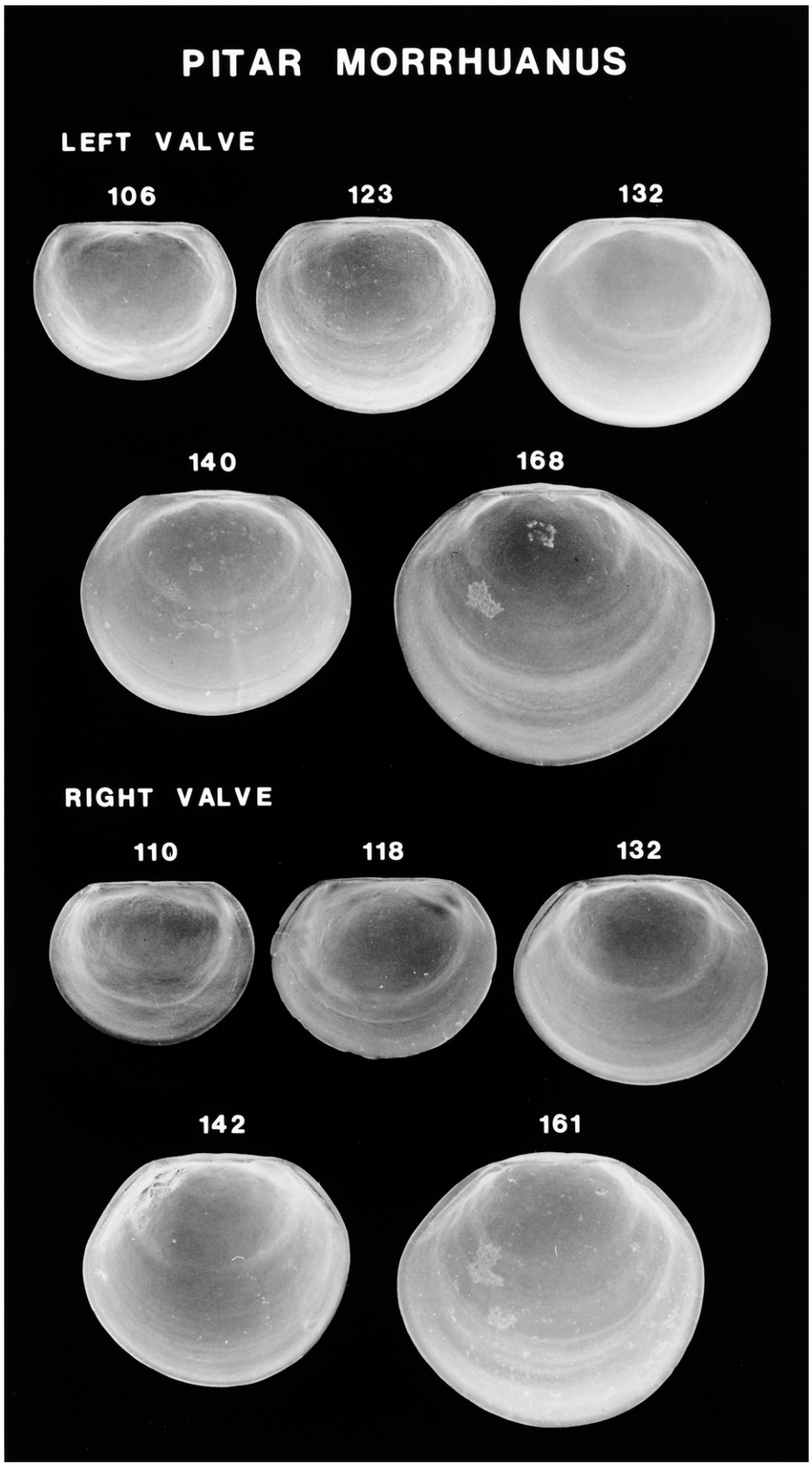

Figure 186. Scanning electron micrographs of disarticulated shell valves of *Pitar morrhuanus* larvae. Numbers indicate the maximum linear shell dimension in micrometers. Modified from Goodsell et al. (1992).

Downloaded From: https://bioone.org/journals/Journal-of-Shellfish-Research on 25 Feb 2020
Terms of Use: https://bioone.org/terms-of-use Access provided by IFREMER

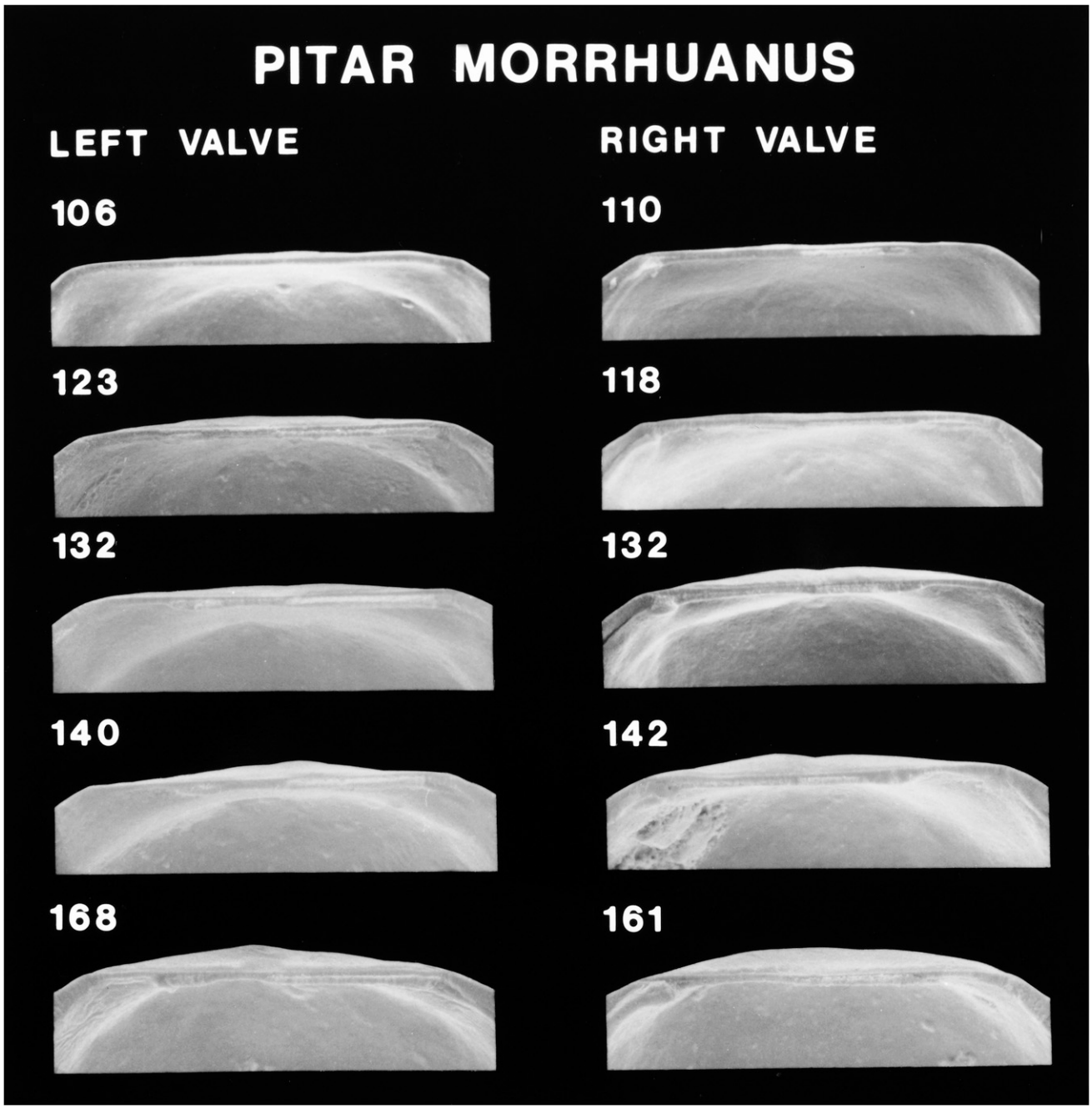

Figure 187. Scanning electron micrographs of the hinge of disarticulated shell valves of *Pitar morrhuanus* larvae seen in Figure 186. Numbers indicate the maximum linear shell dimension in micrometers. Modified from Goodsell et al. (1992).

Downloaded From: https://bioone.org/journals/Journal-of-Shellfish-Research on 25 Feb 2020
Terms of Use: https://bioone.org/terms-of-use Access provided by IFREMER

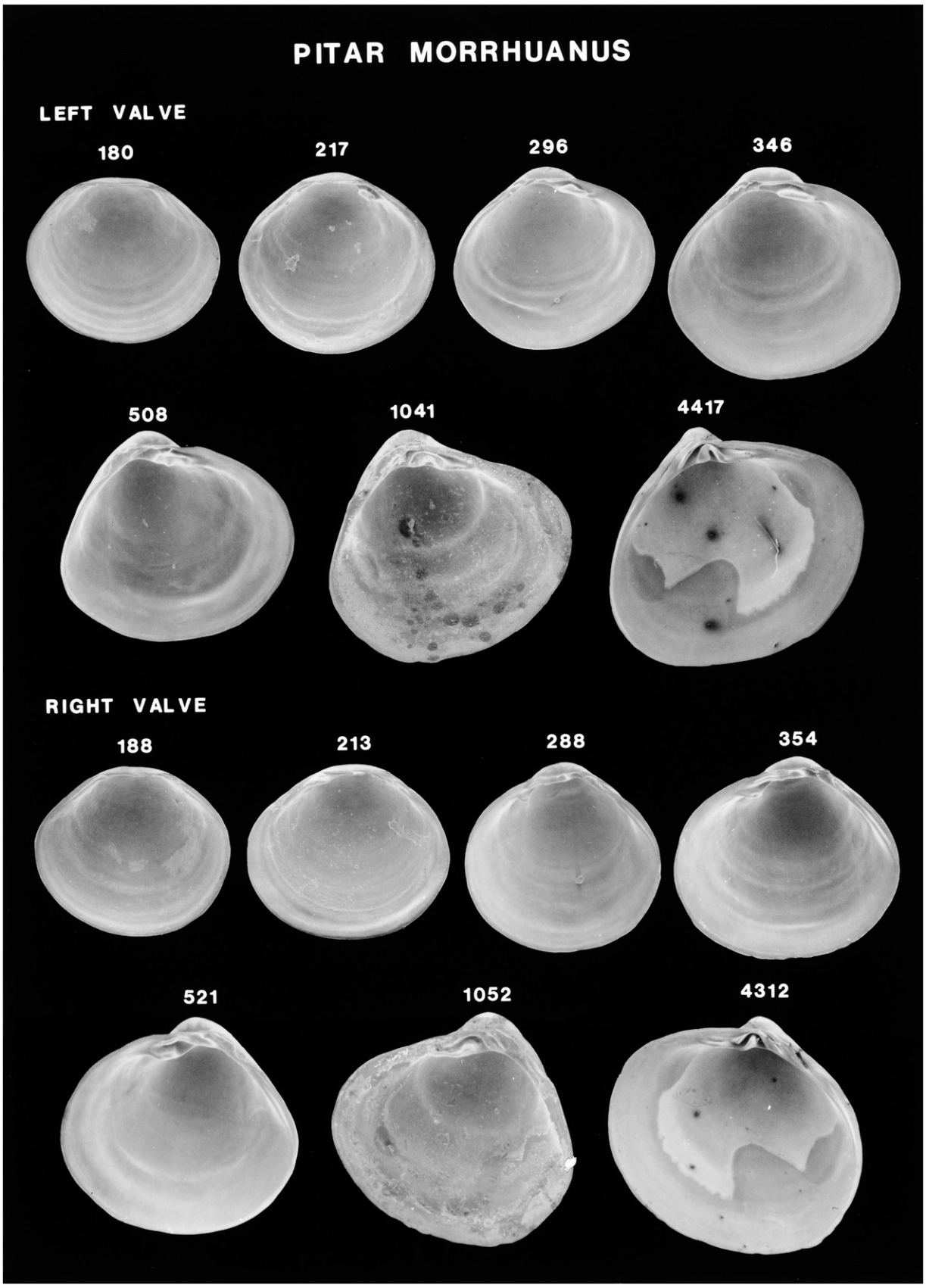

Figure 188. Scanning electron micrographs of disarticulated shell valves of *Pitar morrhuanus* postlarvae. Numbers indicate the maximum linear shell dimension in micrometers. Modified from Goodsell et al. (1992).

Downloaded From: https://bioone.org/journals/Journal-of-Shellfish-Research on 25 Feb 2020
Terms of Use: https://bioone.org/terms-of-use Access provided by IFREMER

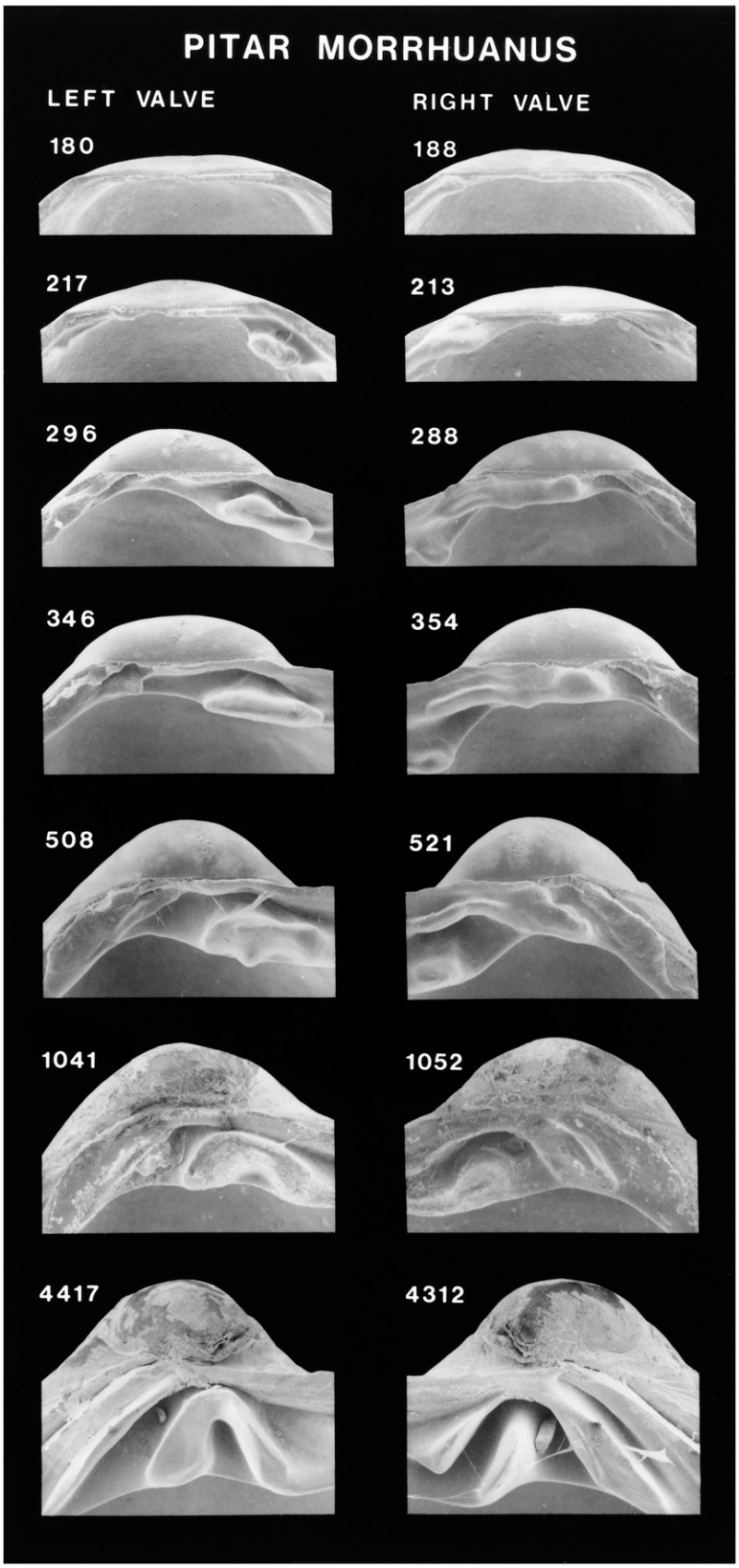

Figure 189. Scanning electron micrographs of the hinge of disarticulated shell valves of *Pitar morrhuanus* postlarvae seen in Figure 188. Numbers indicate the maximum linear shell dimension in micrometers. Modified from Goodsell et al. (1992).

Downloaded From: https://bioone.org/journals/Journal-of-Shellfish-Research on 25 Feb 2020
Terms of Use: https://bioone.org/terms-of-use Access provided by IFREMER

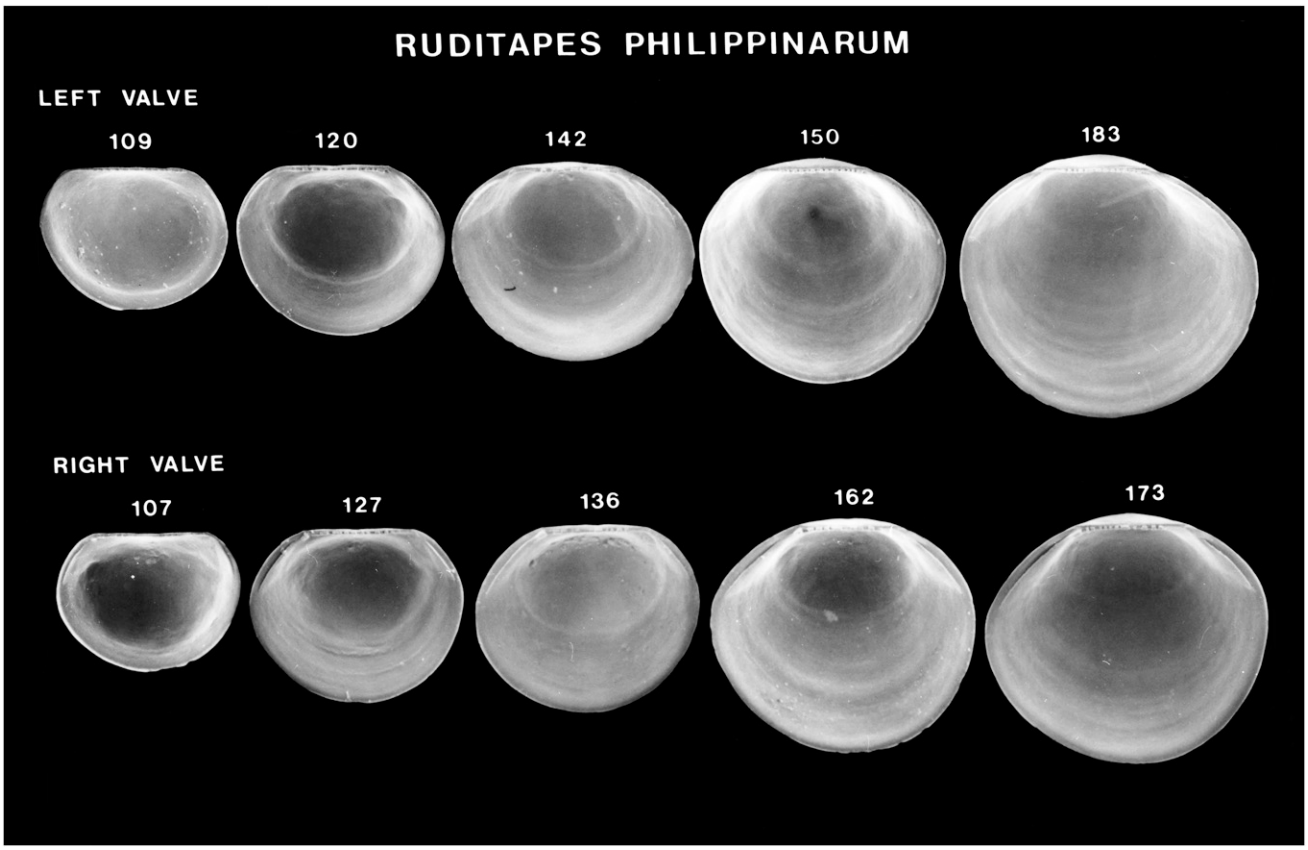

Figure 190. Scanning electron micrographs of disarticulated shell valves of *Ruditapes philippinarum* larvae. Numbers indicate the maximum linear shell dimension in micrometers.

Downloaded From: https://bioone.org/journals/Journal-of-Shellfish-Research on 25 Feb 2020
Terms of Use: https://bioone.org/terms-of-use Access provided by IFREMER

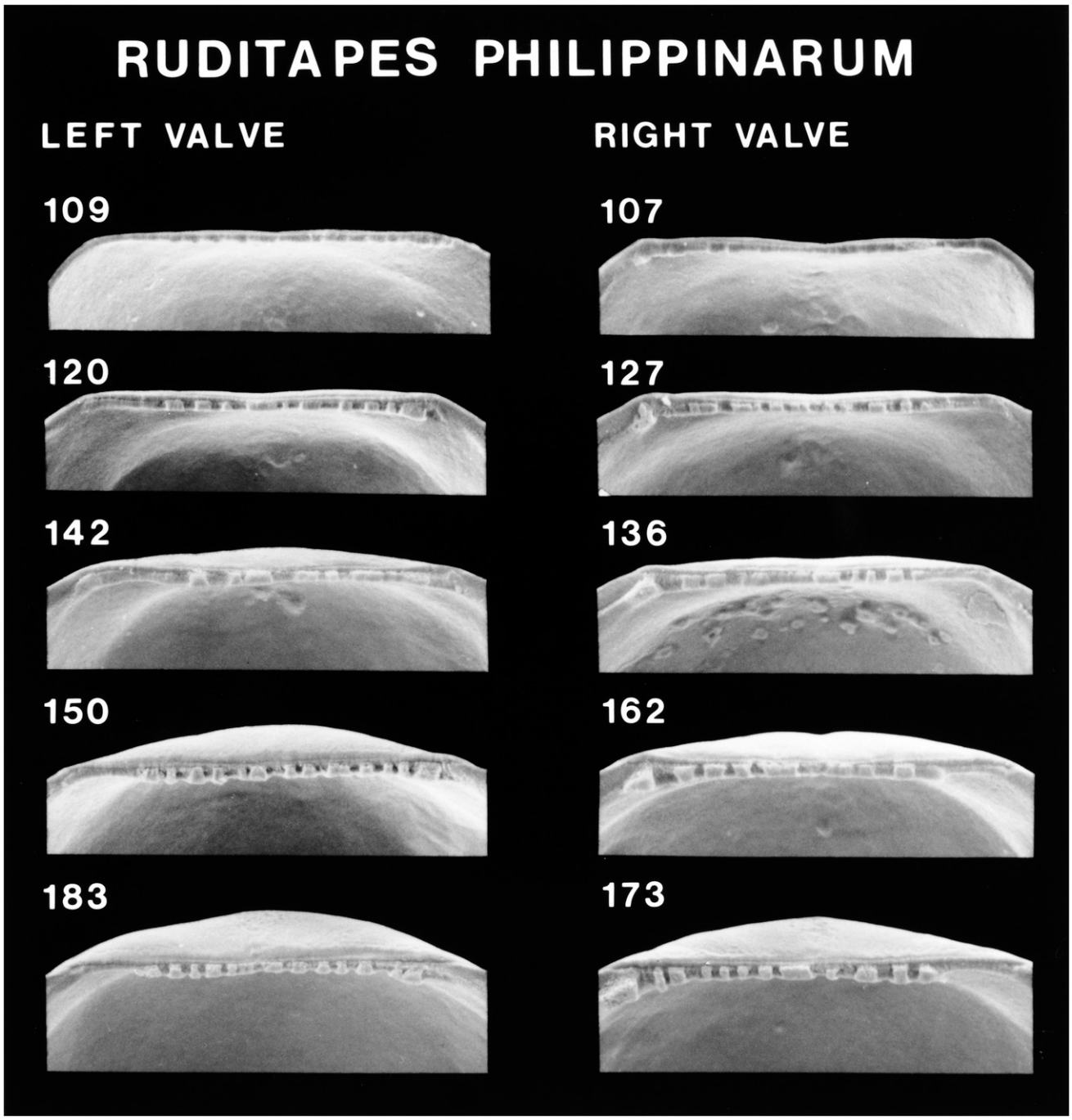

Figure 191. Scanning electron micrographs of the hinge of disarticulated shell valves of *Ruditapes philippinarum* larvae seen in Figure 190. Numbers indicate the maximum linear shell dimension in micrometers.

Downloaded From: https://bioone.org/journals/Journal-of-Shellfish-Research on 25 Feb 2020
Terms of Use: https://bioone.org/terms-of-use Access provided by IFREMER

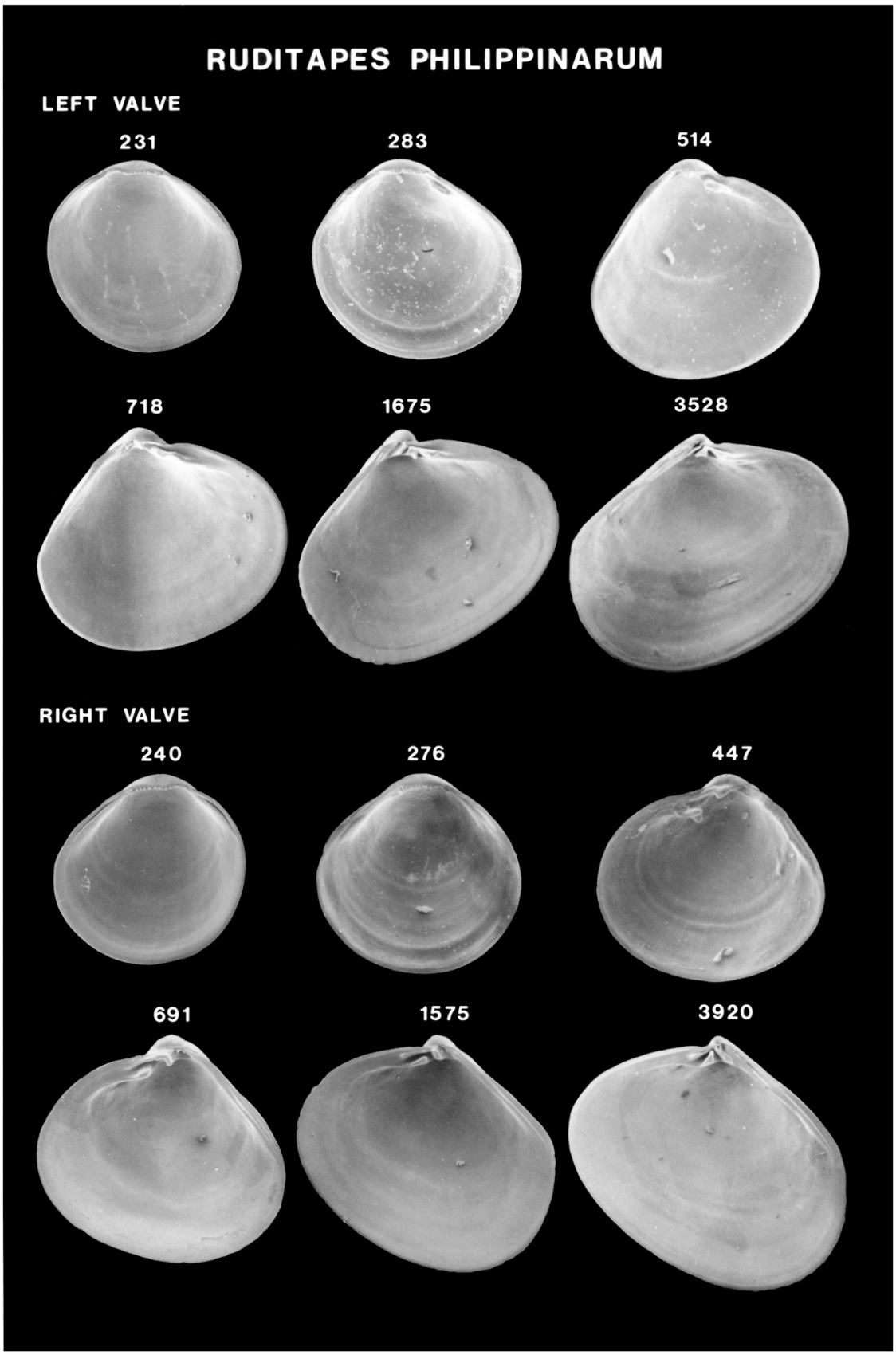

Figure 192. Scanning electron micrographs of disarticulated shell valves of *Ruditapes philippinarum* postlarvae. Numbers indicate the maximum linear shell dimension in micrometers.

Downloaded From: https://bioone.org/journals/Journal-of-Shellfish-Research on 25 Feb 2020
Terms of Use: https://bioone.org/terms-of-use Access provided by IFREMER

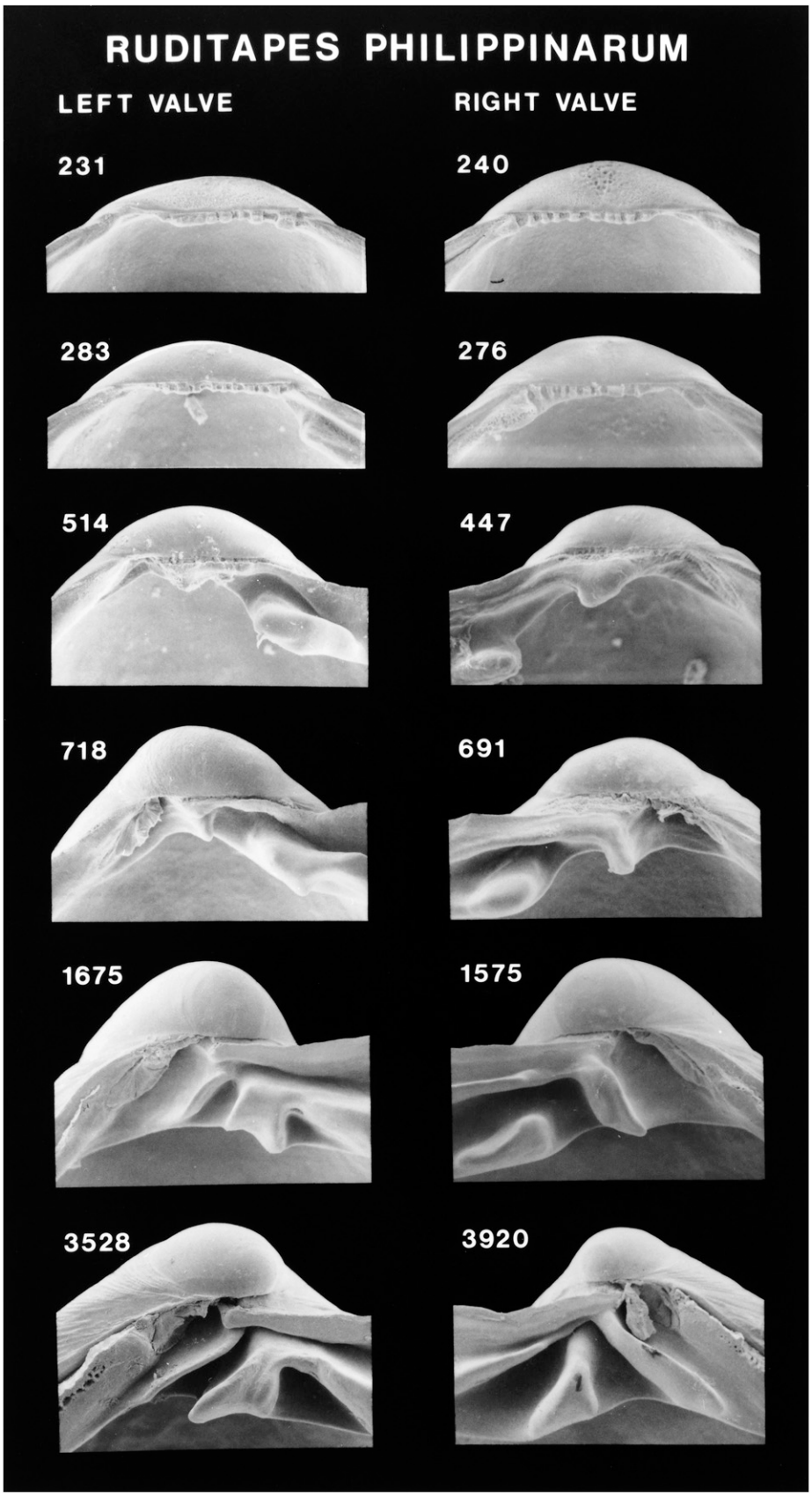

Figure 193. Scanning electron micrographs of the hinge of disarticulated shell valves of *Ruditapes philippinarum* postlarvae seen in Figure 192. Numbers indicate the maximum linear shell dimension in micrometers.

Downloaded From: https://bioone.org/journals/Journal-of-Shellfish-Research on 25 Feb 2020
Terms of Use: https://bioone.org/terms-of-use Access provided by IFREMER

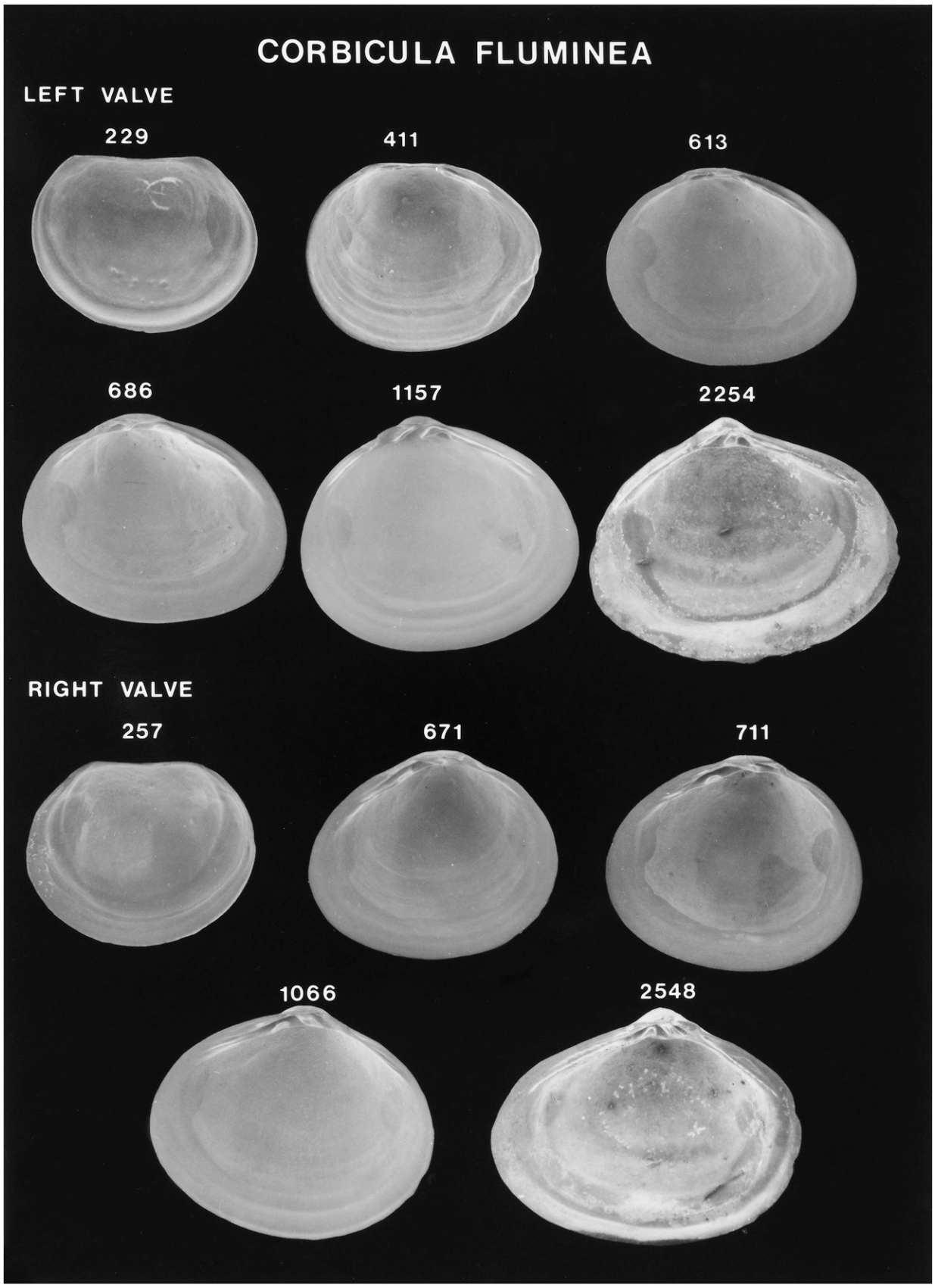

Figure 194. Scanning electron micrographs of disarticulated shell valves of *Corbicula fluminea* postlarvae. Numbers indicate the maximum linear shell dimension in micrometers. Modified from Kennedy et al. (1991).

Downloaded From: https://bioone.org/journals/Journal-of-Shellfish-Research on 25 Feb 2020
Terms of Use: https://bioone.org/terms-of-use Access provided by IFREMER

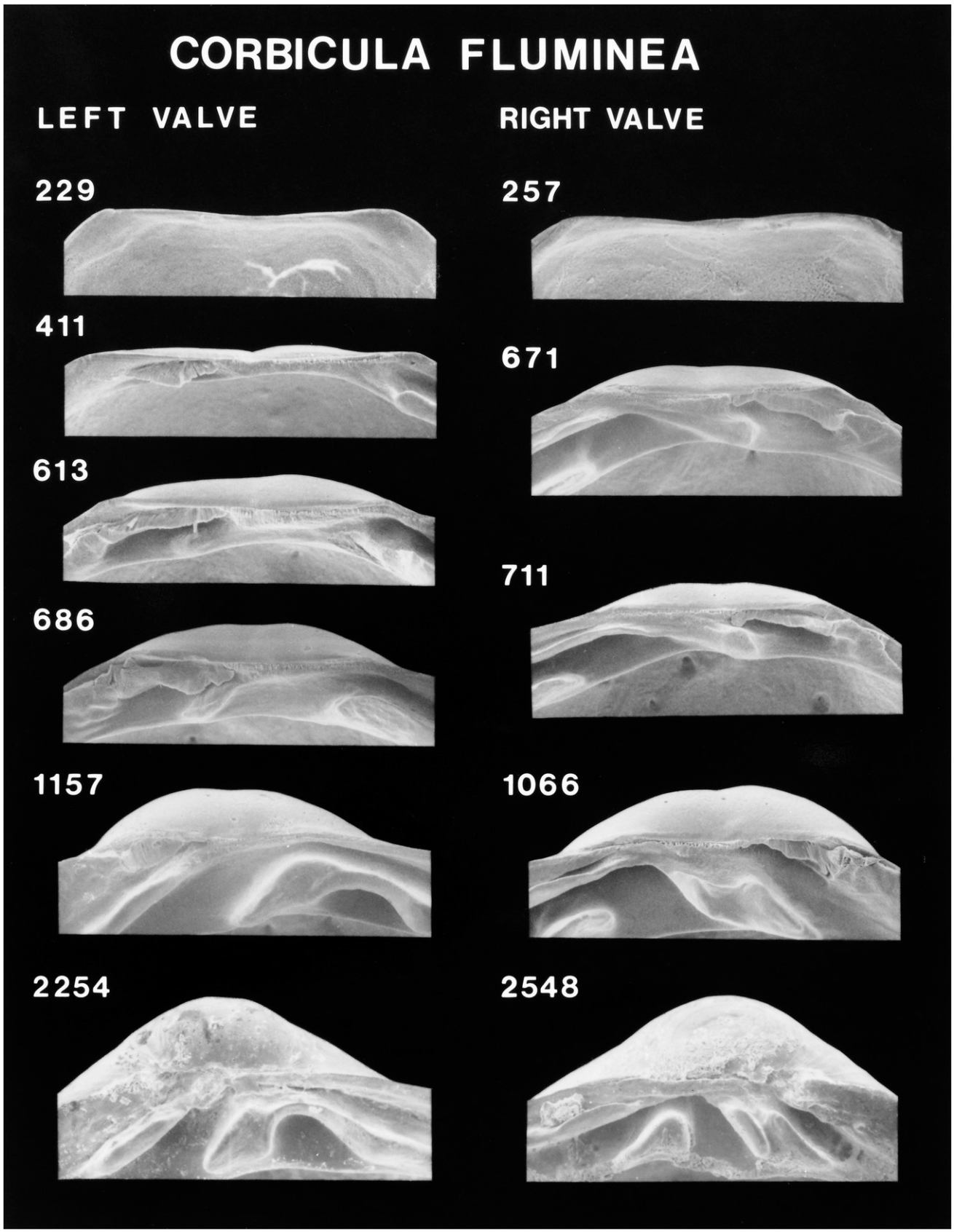

Figure 195. Scanning electron micrographs of the hinge of disarticulated shell valves of *Corbicula fluminea* postlarvae seen in Figure 194. Numbers indicate the maximum linear shell dimension in micrometers. Modified from Kennedy et al. (1991).

Downloaded From: https://bioone.org/journals/Journal-of-Shellfish-Research on 25 Feb 2020
Terms of Use: https://bioone.org/terms-of-use Access provided by IFREMER